VRIJE UNIVERSITEIT BRUSSEL

FAKULTEIT WETENSCHAPPEN

EENHEID ANALYTISCHE SCHEIKUNDE

DISCRETE SUSPENDED PARTICLES OF BARITE AND THE BARIUM CYCLE IN THE OPEN OCEAN

Proefschrift voorgelegd met het oog op het behalen van de graad van Doctor in de Wetenschappen

Promotor: I. ELSKENS

TOME I : TEXT

OKTOBER 1979

DEHAIRS FRANK

VRIJE UNIVERSITEIT BRUSSEL

FAKULTEIT WETENSCHAPPEN

EENHEID ANALYTISCHE SCHEIKUNDE

DISCRETE SUSPENDED PARTICLES OF BARITE AND THE BARIUM CYCLE IN THE OPEN OCEAN

Proefschrift voorgelegd met het oog op het behalen van de graad van Doctor in de Wetenschappen

Promotor: I. ELSKENS

TOME I : TEXT

OKTOBER 1979

DEHAIRS FRANK

..."Want diegenen die in geleerde trant schrijven naar de smaak van een handjevol deskundigen, en die noch Persius, noch Laelius als beoordelaars afwijzen, die komen mij eerder beklagenswaardig dan gelukzalig voor. Zij martelen zich immers voortdurend af; ze voegen toe, veranderen, strepen door, schrijven het toch weer, beginnen opnieuw, werken om, laten het lezen, leggen voor jaren in de la, en nooit is het hun naar de zin. Zo betalen zij voor hun onbeduidende beloning, d.w.z. een lofprijzing (maar dan van heel weinigen) zo'n hoge tol: zoveel nachtwerk, het aanzienlijke verlies aan dromen — het heerlijkste dat er bestaat — zoveel zweet, zoveel martelingen! Tel daar nog bij op het verlies aan gezondheid, de aantasting van het uiterlijk voorkomen, oogziekte of zelfs blindheid, armoede, nijd, het gemis aan plezier, voortijdige ouderdom, een vroege dood en wat dies meer zij. Zoveel ellende meent die wijze te moeten betalen om (...) te worden gewaardeerd."

Uit "Laus Stultitiae", Erasmus (1508)
vertaald door A.J.Hiensch; Prisma n° 1359.

DANKWOORD:

In de eerste plaats wens ik de professoren R.Chesselet en J.Jedwab te bedanken voor het feit dat zij deze kennismaking met de bijzonder boeiende domeinen der geochemie en der oceanografie mogelijk gemaakt hebben, alsook voor hun voortdurende begeleiding bij het tot stand komen van dit werk. Professor R.Wollast weze van harte bedankt voor zijn voortdurende interesse in dit werk, die geuit werd in meerdere vruchtbare diskussies en terechtzettingen. De Professoren I.Elskens and P.Polk wezen eveneens zeer hartelijk bedankt voor hun voortdurende blijk van interesse alsook voor hun regelmatige aansporingen dit werk binnen de vastgestelde tijdslimiet de beëindigen.

Zonder de hulp van C.E.Lambert, die mij de geheimen der neutronen aktivatie bijbracht, zonder de menige diskussies samen gevoerd en vooral zonder de gastvrijheid genoten tijdens de talrijke verblijven te Gif-sur-Yvette, had dit werk heel wat moeizamer en ongetwijfeld saaier verlopen. De hele werkgroep te Gif-sur-Yvette weze bedankt voor zijn sympathie en gastvrijheid. In het bijzonder wens ik hier P.Buat-Menard, C.Jehanno, M.Arnold, O.Aubey, P. Auger en J.Rancher te bedanken voor gevoerde diskussies en direkte praktische hulp bij de neutronen aktivatie en elektronen mikroskopische analyses.

Zonder J.C.Brun-Cottan's hulp en suggesties, en het bestaan van diens eigen doktoraatswerk ware men waarschijnlijk niet zover kunnen doordringen in de interpretatie der

granulometrische gegevens. T.Church die de goedheid had het thesis-plan,alsook de aan dit werk verwante publikatie te willen korrigeren en beoordelen, en wiens eigen doktoraats-werk als leidraad en referentiepaal diende, weze hiervoor bijzonder bedankt. J.Klossa's bijdrage met betrekking op de elektronen-diffraktie opnamen is van bijzonder groot belang geweest tijdens dit werk; hij weze hiervoor zeer hartelijk bedankt.

A.Herbosch wens ik bijzonder te bedanken voor de vele suggesties geleverd en voor de hulp verleend bij het toe-passen van de faktor analyses. P.Kummert's hulp bij het oplossen der problemen i.v.m. de komputer programmatie zijn van onschatbare waarde geweest, alsook het ter onzer beschikking stellen door de Professoren Lemonne en Sacton van scanningstafels uitgerust met koordinatografen.

De medewerkers van Prof. Jedwab, in het bijzonder G.Delvaux en D.Bourse zijn van harte bedankt voor allerhande praktische hulp geleverd tijdens de elektronen mikroskopische analyses aan de Université Libre de Bruxelles. D.Losman die het geduld heeft gehad een eerste versie van deze thesis door te nemen en talrijke belangrijke suggesties leverde, weze hiervoor, alsook voor haar kontinue morele en ideologische steun zeer hartelijk bedankt.

De waarde van allerhande logistieke steun bekomen van R.Linckx en M.Romain, tijdens het leggen van de laatste hand aan deze thesis, is niet te schatten. Zij zijn hiervoor dan ook bijzonder hartelijk bedankt.

Tenslotte nog een dankwoord aan de naaste familieleden

voor het jarenlange geduld dat ze hebben uitgeoefend bij het uitkijken naar de dag dat dit werk zou worden beëindigd. Dit werk weze dan ook een bewijs voor hen, dat mijn talrijke verblijven te Parijs en te Gif-sur-Yvette, die met enige achterdocht werden aanvaard, inderdaad een wetenschappelijk karakter hadden.

TABLE OF CONTENTS

ABSTRACT

Several facts stress the necessity of a more detailed knowledge of the barium cycle in the ocean. Indeed, although estimations of the overall cycle of barium in the ocean exist, only little information is available on the intermediary stages of the pathway; the generally accepted gross pathway being: —— incorporation of dissolved Ba by organisms in the SiO_2, $CaCO_3$ and organic matter fraction, —— partly redissolution of these biogenic materials at depth and release of Ba, —— sedimentation of the residual fraction. Further, discussion exists concerning the exact source of the Ba that is accumulating in the sediments: in litterature, settling of Ba-enriched biogenic matter is opposed to hydrothermal processes.

In this work we have studied some of these problems by analyzing the role of the suspended matter which, up to recently, has been but poorly investigated. Some data were available before starting our research: 1) from measurements of Ba and Al in suspended matter it was deduced that more than 90% of the particulate Ba can be concentrated in phases other than aluminosilicates (i.e. continental material) ; 2) preliminary investigations, in our laboratory, of suspended matter samples with a scanning electron microscope and electron microprobe (SEM-EMP equipment) revealed the presence of discrete barium- and sulphur-rich particles.

We have analyzed suspended matter samples, collected with 30 litre Niskin bottles during GEOSECS and other cruises in the Atlantic and Pacific Oceans, both by SEM-EMP, allowing the study of individual micron-sized particles, and by neutron activation analysis (INAA) for global, quantitative data on element concentrations. The geometric mean of all our INAA measurements of particulate barium amounts to 20 ng/Kg sea water. Our SEM-EMP investigations revealed the

ubiquity of Ba- and S-rich particles in suspension, and this throughout the watercolumn. These particles have an average diameter of 1 µm and were identified as barite crystals. They contain minor amounts of K and Sr. Especially in surface water, they occur together with discrete $SrSO_4$ particles which can contain various amounts of Ba. This suggests the existence, in surface water, of a solid solution series with $BaSO_4$ and $SrSO_4$ as end members.

Barite particle size, volume analysis with the SEM, and INAA measurement of total particulate Ba upon the same suspended matter samples revealed that, for intermediate and deep water, barite is the most important carrier of Ba in suspension with up to 90% and more of total particulate Ba carried by this mineral. Other carriers are $CaCO_3$ and SiO_2 skeletons, particulate organic matter and aluminosilicates. Their contribution appears to be important in surface water, with 50% of total particulate Ba carried by biogenic components and in bottom water, with 20% carried by aluminosilicates.

The origin of suspended barite is clearly biological. This is emphasized by the positive relationship between productivity and the total particulate barium content in the first 1000 m of the watercolumn and by the occurrence in surface water of $(Ba,Sr)SO_4$ solid solutions of variable composition. Further, we observed barite crystals inside small organic pellets, which may represent decaying organic matter. These observations suggest two possible processes of barite formation: 1) Direct secretion of barite granules by organisms. This is known to occur in the benthic Xenophyophoria (Rhizopoda). Collosphaerid and acantharid Radiolaria are known to secrete $SrSO_4$ crystals and it can be assumed that these organisms produce as well $(Sr,Ba)SO_4$ solid solutions and $BaSO_4$ crystals ; 2) Another possible process is the precipitation of barite inside sulphate rich organic microenvironments, such as fecal material.

Suspended barite dissolves in the watercolumn, which is known to be undersaturated with respect to $BaSO_4$. Application of a Stokes settling and dissolution rate model to our barite size distribution data enabled us to deduce a barite dissolution rate constant in sea water, and to compute the dissolution rate, J_{Ba}, of barite in the watercolumn. This latter value (0.4 $\mu g.cm^{-2}.yr^{-1}$) is as large as the J_{Ba} term which is deduced from estimated dissolution rates of SiO_2 and $CaCO_3$ tests (0.5 $\mu g.cm^{-2}.yr^{-1}$). The total J_{Ba} (0.9 $\mu g.cm^{-2}.yr^{-1}$) is important when compared with the mean river input of dissolved barium (min. 0.6 $\mu g.cm^{-2}.yr^{-1}$), and emphasizes the important recycling of Ba in the watercolumn. Further, the estimated productions of particulate Ba (1.35 $\mu g.cm^{-2}.yr^{-1}$) (i.e. incorporation of Ba in SiO_2 and $CaCO_3$ skeletons and production of barite; the latter value is deduced by considering barite to be produced during decomposition of organic matter in the surface waters) equilibrates the input of dissolved Ba (1.5 $\mu g.cm^{-2}.yr^{-1}$). The residual flux of suspended barite and of the estimated flux of Ba associated with fecal material towards the sediments is sufficient to account for known accumulation rates of Ba (0.5 to 1.0 $\mu g.cm^{-2}.yr^{-1}$ in the Atlantic, with suspended barite contributing for a maximum of 0.4 $\mu g.cm^{-2}.yr^{-1}$.

To conclude, our work has shown that barite crystals occur in suspended matter in the World Ocean. This barite is formed by biological activity and constitutes the main carrier of barium in suspended matter. The dissolution of this barite at depth is as important as the dissolution of other biogenic components of suspended matter carrying only trace amounts of Ba but which dissolve more rapidly than the barite phase. Part of the suspended barite can survive dissolution and can constitute an important fraction of the Ba that is accumulating in the sediments.

2. INTRODUCTION

2.1. Bibliography

Geochemists studying the marine environment have always granted considerable attention to barium. Its apparent unrelatedness towards the detritic, terrigenic components and its occurrence in common authigenic minerals in the sediments, such as barite, zeolite and manganese nodules enhance the geochemical value of this element, especially for those who study chemical processes operating in the watercolumn and on the ocean floor.

A survey is given hereunder of those studies that contributed directly to a comprehension of the geochemical pathway of Ba in the ocean. It is tried to separate as much as possible the two basically different approaches, defined by Cronan (1974), as "two schools of thought". In the first approach sedimentary Ba is supposed to be supplied by submarine volcanic activity, while in the second one, biological processes are invoked.

A. Volcanic processes as a source of sedimentary Ba

Revelle and Emery (1951) analyzed barite concretions from the sea floor off California. In their final conclusiions they consider this sedimentary to be formed by interaction of ascending hot chloride- and barium-rich solutions with

sulphate-rich interstitial water. The hypothesis of hydrothermal formation is thought to be supported by the presence, in the vicinity of the sampling place, of a fault through which barium-rich solutions may have escaped from the magma. Revelle and Emery discuss also biological processes, when attempting to explain the presence of these concretions; this will be discussed below (point B). Later, however, Goldberg et al. (1969) clearly demonstrated, from the Th and U content, the Sr^{87}/Sr^{86} ratio and the δS^{34} values, that these barite concretions have similar characteristics as barite occurring as crystal aggregates and veins on the continent.

Arrhenius and Bonatti find evidence of volcanic barite formation in that an important accumulation of sedimentary barite in the South Pacific (up to 9% on a $CaCO_3$ free basis), coincides with the Easter Island Rise. The latter region is characterized by the presence of active magma reservoirs and does not extend below an area of high organic productivity. Hydrothermal transport, besides hydration and cation exchange with effusive lava and vulcanites on the ocean floor, is considered as one of the possible mechanisms responsible for the input of Ba in the sediments. This Ba is thought to be partitioned between solution in sea water, in which it crystallizes rapidly to form barite, and the authigenic zeolite harmotome, which becomes overgrown at a later stage by phillipsite. Barite is believed to enclose the major fraction of this volcanic Ba. Arrhenius and Bonatti also

discuss the role of planktonic organisms in the accumulation of barite in the sediments. To explain the intermediary barite accumulation observed at the equator, it is suggested that slowly moving deep waters carries the residual Ba away from the Easter Island Rise. In the highly productive equatorial region this Ba could be extracted by marine organisms and precipitated as barite in their protoplasm. After death, sedimentation of their remains could account for the accumulation of barite crystals in the sediments underneath the equator. Arrhenius and Bonatti further report the occurrence of barite-celestite solid solutions in manganese nodules and the presence of Ba in a manganese oxide phase. For these phases volcanic as well as continental origins are considered. They suggest that the analysis of certain[☆] trace elements should allow a discrimination between " barite and harmotome crystallized near the source of barium-rich, acidic vulcanites and the same minerals formed from continental solution with passage through the biosphere". Isotopes of sulphur, oxygen and thorium were shown to be efficient tools to trace the origins of marine barite (see below). Recently Guichard et al. (1979) showed that the analysis of the rare earth element series allows a clear distinction to be made between barites of deep-sea and of continental origin.

Further studies in the East Pacific Ocean (Boström and

[☆] The tracer should be ideally imperfect, by which it is meant that although it incorporates well in the host structure, it fractionates differently in different geochemical environments.

Peterson, 1966; Boström et al., 1972;1973; Heath and Dymond, 1977) show the Ba distribution in this region to be related with the presence of the active ridge, although this relationship seems less clear than for Fe, Mn, Cu, Cr, Ni, Pb. Boström and Peterson (1966) observed that Ba and Sr accumulate on the flanks of the Rise and the covariation between both elements is attributed to their occurrence as celestobarite.

More direct evidence of the effective role of hydrothermal solutions is given by Bertine and Keene (1975). These authors studied the oxygen and sulphur composition of individual barite crystals confined in a barite-opal rock recovered from a possible fraction zone (Lau Basin) in the Pacific Ocean NE of Australia. Similarity of the sulphur isotopic composition with that of sea water and differences in oxygen isotopic composition between the barite sulphate fraction and that of sea water, indicate that such barites can have precipitated from sea water at high temperatures (> 100°C). The authors propose barite and opal to have been precipitated by contact of hydrothermal solutions with the cooler ocean waters: a perfect illustration of the utility of the ideally imperfect tracer principle of Arrhenius and Bonatti (1965).

Direct exhalation of micron sized barite crystals should be considered as a possible source of sedimentary and possibly of suspended barite. Indeed, barite was identified in continental fumarole incrustations original from the valley of the 10,000 smokes, Alaska (Stoiber and Rose, 1974).

Further, scanning electron microscope and electron microprobe analysis of volcanic sublimates of the Nyamuragira volcano (Zaïre), revealed the presence of well crystallized mono-crystals of barite, with a tabular habit and ranging from 4 to 5 μm in size (Bernard, 1976). The high levels of chlorine they contain are believed to result from a volatilisation process at high temperatures (~ 1400°C). This same author observed that Ba occurs only as barite and is a minor composite of volcanic sublimates.

B. The accumulation of barium in the biogenic phase as a possible source of sedimentary barium.

The biological production of barite is one of the possible ways Ba can be concentrated in marine organisms. Today this is known to occur in several species of the benthic Xenophyophoria (Rhizopoda classis) (Schulze und Thierfelder, 1905; Arrhenius and Bonatti, 1965; Tendal, 1972; Lowenstam, 1974). The possibility of the contribution of barite granules, excreted by the Xenophyophoria, to sedimentary barite was considered by Revelle and Emery (1951).

Analysis of sediments collected along a meridional section across the equator, in the Pacific (Goldberg and Arrhenius, 1958) shows the accumulation rate of Ba to be more than twenty times higher in the sediments underlying the highly productive Equatorial Divergences. Although high Ba accumulations are found in association with both siliceous and calcareous deposits (see also Goldberg, 1958), it is observed by particle analysis, that the largest Ba

Further, scanning electron microscope and electron microprobe analysis of volcanic sublimates of the Nyamuragira volcano (Zaïre), revealed the presence of well crystallized mono-crystals of barite, with a tabular habit and ranging from 4 to 5 µm in size (Bernard, 1976). The high levels of chlorine they contain are believed to result from a volatilisation process at high temperatures (~ 1400°C). This same author observed that Ba occurs only as barite and is a minor composite of volcanic sublimates.

B. The accumulation of barium in the biogenic phase as a possible source of sedimentary barium.

The biological production of barite is one of the possible ways Ba can be concentrated in marine organisms. Today this is known to occur in several species of the benthic Xenophyophoria (Rhizopoda classis) (Schulze und Thierfelder, 1905; Arrhenius and Bonatti, 1965; Tendal, 1972; Lowenstam, 1974). The possibility of the contribution of barite granules, excreted by the Xenophyophoria, to sedimentary barite was considered by Revelle and Emery (1951).

Analysis of sediments collected along a meridional section across the equator, in the Pacific (Goldberg and Arrhenius, 1958) shows the accumulation rate of Ba to be more than twenty times higher in the sediments underlying the highly productive Equatorial Divergences. Although high Ba accumulations are found in association with both siliceous and calcareous deposits (see also Goldberg, 1958), it is observed by particle analysis, that the largest Ba

concentrations are confined to phillipsite crystals and to yellow aggregates (5-15 μm). In the latter Ba seems associated with highly refractive micro-crystals believed to be barite. The matrix itself is considered to represent the excretion product of benthic organisms. It is further shown that the calcareous fraction of the sediments, mainly consisting of coccoliths, has practically no importance as a Ba carrier. Thompson and Bowen (1969) came to the same conclusion, after analysis of a coccolith ooze from the tropical Atlantic. Hanor (1972), also observes an increase in the Ba accumulation (correlated with the biogenic silica accumulation) in the sediments underlying the equatorial zone of high productivity in the East Pacific. Ba accumulation rates up to 3.5 $mg.cm^{-2}. 10^{-3}$ years, are found near the equator, as compared to 0.3 $mg.cm^{-2}.10^{-3}$ years more to the north. It is suggested that it is the carbonate dissolution that causes the release and precipitation of Ba, associated with the carbonate fraction. In the Atlantic Ocean as well, regions of high Ba accumulation are observed to extend under surface waters characterized by a high organic productivity and a high dissolved phosphate content (Turekian and Tausch, 1964).

Arrhenius (1963), proposes the planktonic community to act as a conveyor mechanism. This mechanism consists in the concentration of a whole series of elements, such as Si, N, P, Ra, Ba in the surface waters and in their

subsequent transport to the deep-sea. Spines of acantharid Radiolaria are shown to contain Ba, up to 5400 ppm of ash and Foraminifera skeletons some 700 ppm. Near the bottom these elements are released and are responsible for the observed increase in concentrations of the dissolved elements. Part of the fraction that is released may become incorporated in a suitable host structure, through a crystallization process at the sediment-water interface. For Ba, Sr and Pb, the partitioning between harmotome-type zeolites, manganese oxide minerals and crystalline solid solutions of celestite, barite and anglesite is considered.

Another interpretation of the observed Ba distribution in the sediments is given by Arrhenius and Bonatti (1965). Biogenic barite granules with $BaSO_4$ partly substituted by $SrSO_4$ could dissolve more rapidly than the calcite skeletons in the sediments. The Ba accumulation would therefore be high in regions where the exposure time of the barite granules to the corroding sea water is short. These are regions with a high rate of carbonate deposition such as occurring under the highly productive equatorial surface waters, or regions where carbonate is preserved from dissolution such as in the shallow waters above the Easter Island Rise.

In his extensive contribution to the study of marine barite, Church (1970) observes the barite containing cores to be rich in carbonate or silica tests, but also in manganese and iron phases. Small barite crystals (< 5 μm) are the most abundant;

the larger crystals (up to 100 μm) are rare and often associated with the manganese phases. Geographically, barite-rich sediments in the East Pacific correspond with areas predominantly consisting of carbonate and radiolarian oozes. Church's model for marine barite formation is similar to the one described Arrhenius (1963). Once released from biogenic phases in the deep ocean, Ba is precipitated as barium sulphate in the deep or interstitial waters, due to the existence of saturation conditions. This assumption is supported by the observation that sedimentary barite exhibits Io/Th^{232} and Th^{228}/Th^{232} isotopic ratios, characteristic of deep-sea authigenic minerals ($Io = Th^{230}$). Io/Th^{232} ratios in sedimentary barite are lower than in the bulk sediment. The reason for this lays in the difference of this ratio, for the dissolved Th species, between deep and surface waters. Surface waters, from where the bulk of the sediments are supposed to derive their Io/Th ratio, have a higher ratio than deep waters, due to the biological transport of Th^{232}, derived from continental runoff, to the deep sea. Ionium is produced uniformly in the watercolumn from its parent U^{234} which occurs in a dissolved state in sea water. The authigenic, deep sea origin of sedimentary barite is emphasized further by its Th^{228} / Th^{232} ratio. In sedimentary barite Th^{228}/Th^{232} ratios are higher than unity, pointing towards a radioactive disequilibrium. Th^{228} derives from Ra^{228} which is a highly mobile isotope in the sediments that preferentially incorporates in authigenic

minerals such as phillipsite and barite . Church further observes a striking relationship between organic carbon content and barite occurrence in the sediments of an East Pacific region that includes Arrhenius and Bonatti's (Arrhenius and Bonatti, 1965) high barium containing Easter Island Rise; but he does not confirm their high Ba values. It is proposed that Ba accumulation is not only favored in areas underlying productive surface waters, but also in environments where biological remains are well preserved and may accumulate. Shallow depth regions atop of the oceanic ridge systems may be such Places. In regions of high carbonate accumulation ($CaCO_3$ fraction = 90 %) the barium input in the sediments is shown to be entirely accounted for by the Ba contribution of sedimenting $CaCO_3$, clay and organic matter, volcanic and hydrothermal activity are not invoked. Elemental composition and geographical distribution of two different Xenophyophoria families, allow Church to consider these organisms as unlikely contributors of marine barite.

Turekian (1968) does not succeed in explaining the relatively high Ba accumulation (0.5 $mg.cm^{-2}.10^{-3}yr$) in a core from the Mid-Atlantic Ridge by the Ba input from rivers alone (both dissolved and particulate Ba are considered). It is assumed that this continental supply accumulated inhomogenously in the sediments. In a mass balance calculation the removal of Ba from the surface waters through the biological

formation of barium sulphate crystals, their subsequent sinking and relatively quick dissolution , is considered. As a result, $BaSO_4$ would only accumulate in relatively shallow depths such as the ridge areas. The sea floor depth in abyssal plains on the contrary, would allow complete dissolution of the crystals before they reach the sediments. In the latter case only sediments underlying highly productive areas, such as the Antarctic (Turekian and Johnson, 1966), are likely to accumulate considerable quantities of Ba.It is further stated that the dissolution of the barium sulphate crystals may give rise to the observed increase in dissolved barium in deep waters characterized by slow circulation rates, such as the deep Pacific. In several later studies however, (Wolgemuth and Broecker; 1970; Li et al., 1973; Chan et al., 1976), a mean river supply of 0.6mg . $cm^{-2}.10^{-3}$ yrs Ba is used as working hypothesis. This is about four times more than suggested by Turekian (1968).). As a result it appears that the river supply of barium, in most cases, fully satisfies the sedimentary demand, exception made of the equatorial regions of high Ba accumulation. Besides its possible role as a source of sedimentary Ba, particulate biogenic matter, enriched in Ba, is invoked also to explain the distribution of dissolved Ba in the watercolumn.

C. The dissolution of Ba-carrying biogenic particulates as a source of dissolved Ba in the watercolumn

Chow and Goldberg's contribution (1960) is of major importance in that for the first time a dissolved Ba profile is measured. The similarity between the profile of dissolved Ba and those of the main nutrients suggests a close relation between Ba and the biochemical cycles in the sea. It is proposed that during the oxidation of detrital

organic matter, in which high levels of sulphate are assumed to become available, barium sulphate precipitates. Subsequent oxidation of this organic microenvironment liberates the barium sulphate phase, which may then dissolve in the water-column . In addition, the direct transfer of Ba by organisms is considered. Chow and Goldberg discuss further the supply of Ba from the ocean floor. The latter process could occur after decomposition of Ba-carrying organic matter on the sea floor. Experimental evidence that such a process can also occur for sedimentary barite is given by Bolze et al. (1974), who show that sulphate reducing bacteria grown under anaerobic conditions in the presence of powdered barite, as sole sulphate source, mobilize barium.

Today, dissolved barium profiles from most oceans have been measured (Chow and Patterson, 1966; Turekian and Johnson, 1966; Wolgemuth and Broecker, 1970; Bender et al., 1972; Li et al.,1973; Chan et al., 1976;1977). From this spectrum of measurements it is evident that deep waters are enriched in dissolved barium as compared to surface waters. Concentration of Ba by biogenic particles in the surface water and subsequent release in the deep, after decomposition or dissolution of the carrier, is the pattern generally considered to explain the dissolved Ba profiles.

Material balance calculations by Wolgemuth and Broecker (1970) and Li et al.(1973) assign an important role to the particulate Ba fraction formed in the surface mixed layer. Besides the dissolved Ba amount transported out of the surface layer by downwelling waters, the sinking of par-

ticulate Ba compensates for the dissolved Ba introduced in the surface layer by upwelling and river input. Since steady state conditions are assumed a fraction of this particulate Ba, equal to the amount introduced by rivers, is assumed to be buried in the sediments; the rest of the sinking particulate Ba redissolves in the deep waters creating the observed excess.

The observation of a positive relationship between dissolved barium and silicon has led several authors to consider diatom skeletons as possible barium carriers (Ku et al., 1970; Edmond, 1970; Bacon and Edmond, 1972; Li et al., 1973). The sinking and dissolution of these skeletal structures are thought to govern the observed dissolved barium and silicon profiles. Heavy support for this assumption was found in the data of Vinogradova and Kovals'kiy (1962) showing high Ba concentrations (several thousand ppm of ash) in two Black Sea diatom species, and in the recapitulative survey on the role of diatoms as Ba carriers by Brongersma-Sanders (1966). Wolgemuth and Broecker (1970) stated that if Ba is indeed carried by the silica fraction, the Ba/Si ratio in their siliceous frustules should equal the ratio of excess Ba/excess Si in the deep sea waters (excess = excess concentration in the deep-sea as compared to the surface waters). Relatively few data exist in literature concerning the Ba content of marine phytoplankton. However, data of Martin and Knauer (1973) and Riley and Roth (1970) do not confirm

the high Ba accumulations in plankton as originally suggested from generalization of Vinogradova and Kovals'kiy's (op.cit.) experimental data.

Evidence exists that a more slowly dissloving phase than silica actually functions as the Ba-carrier (Broecker, 1974; Chan et al.,1976; 1977). In the Pacific, deep waters are more enriched in dissolved Ba with respect to surface waters as compared to the Atlantic. The same pattern is observed for dissolved carbon, phosphorus and silicon. However, the enrichment factor is larger for Ba (7 X); than for Si (4 X) and C, P (2 X), (Broecker, 1974). It is assumed that the net transport of Atlantic deep water to the Pacific and the return of empoverished Pacific surface water, inside a steady state system,account for the observed discrepancies (see also Wolgemuth and Broecker, 1970 ; Berger, 1970). Further, the faster recycling of C, P and Si, after dead of the organisms, allow these elements to be retained more efficiently in the Atlantic (Broecker, 1974). As a result, Ba could be carried by a more slowly dissolving phase, such as barite, instead of being associated with the organic and/or silica fraction (Broecker, 1974). In recent studies (Chan et al., 1976; 1977) the silica-barium relation theory is shown to be more complex than previously thought. Besides silicon, alkalinity as well, shows a close similarity with the Ba profile, making the identification of the carrier phase more difficult. It is concluded that the closer similarity of the Ba profiles with

those of silicon and alkalinity, than with those of nitrate and phosphate, points towards a more slowly dissolving phase as the effective Ba-carrier, instead of the more labile tissue and protoplasm; opal, calcium carbonate and barite are considered as possible candidates.

Although the biogenic particulate matter is constantly invoked in order to explain the accumulation of Ba in the sediments as well as the distribution of dissolved Ba in the watercolumn, it appears that the suspended matter itself, as an important field of the marine environment has been poorly studied experimentally. Practically no data exist about particulate Ba in suspension. The systematic analysis of particulate Ba in suspended matter will contribute to the elucidation of the geochemical pathway of Ba in the oceans.

To our knowledge, the first measurements on particulate Ba content of suspended matter in sea water were performed by Darcourt (1973), on samples collected during the R/V Jean Charcot, Harmatan expedition in 1971. It is shown that Ba, for its major part (more than 90%), is not associated with the aluminosilicate fraction, and therefore that an important non-terrigenic Ba phase indeed exists in suspension. Subsequent analysis of some Harmatan suspended matter samples with a combined scanning electron microscope and electron mircroprobe equipment, by prof. J. Jedwab at the Université Libre de Bruxelles (Belgium), revealed the presence of small discrete Ba- and S-rich particles which were assumed to be barium sulphate particles.

These two observations have incited us to start the present work.

2.2 Purpose of the present study

Two main objectives are aimed at:

1º-The verification of the observation by Darcourt (1973) that Ba in suspended matter is present in excess over the quantities that are associated with continental, detritic matter.

-The verification if this excess Ba is an ubiquitous component of oceanic suspended matter.

-The identification of the carriers of Ba in suspended matter and the evaluation of their relative contributions to the total amount of particulate Ba.

-The ascertaining of the origins of the particulate Ba that is not associated with terrigenic matter

2º-The evaluation of the role of Ba-carriers in suspended matter as a possible source of dissolved Ba in the deep-sea and of sedimentary Ba.

This study was made possible as a result of our participation to GEOSECS, an international program on oceanographical research, and was carried out at the Laboratoire de Géochimie, Université Libre de Bruxelles, Belgium, and at the Centre des Faibles Radioactivités (CFR-CNRS), Gif-sur-Yvette, France.

This work has been preceded by the following of our publications: Chesselet et al. (1976); Dehairs (1977); Dehairs et al. (1979)

PART I

METHODOLOGY

INTRODUCTION

In order to settle the problem of ubiquity of particulate Ba in the ocean, suspended matter samples from the main oceans were analyzed. This was made possible by our participation to GEOSECS, an international research program in oceanography (see below) which was conducted on the scale of the World Ocean.

Suspended matter samples from the Atlantic, Antarctic and Pacific Ocean were analyzed. Since total suspended matter occurs only in very small quantities (from 5 to 300 µg/Kg sea water; Brewer et al.,1976) and since only about 10 litres of sea water were filtered, a very sensitive method of analysis had to be used. Further, risks of contamination had to be kept as small as possible. This required handling and eventual pre-analytical treatment of the samples to be avoided or to be kept as limited as possible. Non destructive instrumental neutron activation analysis (INAA) emerged as the optimal technique for quantitative analysis. The method is very sensitive and, in this specific case,required no preliminary treatment of the samples before irradiation.

A preliminary step leading to the identification of the Ba carriers in suspended matter consisted in the study of the inter-element relations between Ba and Sr,Ca which are elements that can be considered as typical for the biogenic fraction, and between Ba and Al, which is

considered as a tracer of the continental, detritic fraction. This multi-elemental analysis can be fulfilled easily by the method that was chosen for quantitative analysis. Indeed, INAA allows the quantitative analysis of several elements in a single run, which represents a considerable saving of time.

The definitive identification of the Ba-carriers in suspension requires an analysis of the elemental composition of single particles. A detailed morphological analysis of the particles, which are selected on the basis of their chemical composition, is further required to trace back their origin and history. Therefore, we have used the scanning electron microscope equipped with an electron microprobe (SEM-EMP equipment). In addition crystallographic analyses were performed on selected particles in order to establish their degree of crystallinity and to deduce their mineralogy. This was done with the high voltage electron microscope equipped with micro-diffraction facilities. Such types of analyses require the complete mastering of all problems concerning the transfer of micro-particles to substrates suitable for each analyzing device.

Once the different Ba-carriers identified, their relative contribution to the total particulate Ba content, measured by INAA, must be deduced. As concerns the barium-sulphate particles, the Ba weight was estimated from their particle size, volume measurements. In order to compare this Ba weight with the total particulate Ba amount, both,

the neutron activation analysis and the size distribution analysis were performed on subsamples of the same original samples. Other potential barium carriers in suspended matter are: silicate and carbonate skeletons, particulate organic matter and aluminosilicates, which together form the main constituents of suspended matter. The contribution of siliceous frustules to total particulate Ba was estimated from our experimental results concerning the in vitro uptake of Ba by two diatom species, common in the open ocean. The contribution of carbonate skeletons was deduced from our own data and from other CFR-GEOSECS data on the particulate Ca concentration in the World Ocean and from literature data on the Ba content of carbonate skeletons. The role of particulate organic matter was estimated from literature data. The concentration of aluminosilicates in suspended matter was deduced from our own data and from other CFR-GEOSECS data on the the particulate Al content in the World Ocean and their role as barium carriers was estimated from literature data on the Ba content of shales, whose composition is close to the one of aluminosilicates in oceanic suspended matter.

CHAPTER I

THE SAMPLING AT SEA

1.1 THE GEOSECS PROGRAM (from Craig, 1972)

GEOSECS is an international research program, founded during the International Decade of Ocean Exploration (IDOE). It is the purpose of this research program to contribute to the understanding of the movement, dispersion and mixing of oceanic water masses. As a result the participating scientists are particularly interested in the measurement of chemical and radiochemical parameters characterized by important variations, as well vertically in the watercolumn, as horizontally and which may be considered as tracers. Great interest exists for the study of particulate matter in suspension as a potential carrier of certain of these tracers, which for this reason can not be considered as conservative parameters.

Great effort was made to measure as many parameters as possible aboard the ship. A salinity - temperature - depth sensor, a dissolved oxygen probe and a nephelometer allowed a continuous recording of T,sal.,O_2 and particulate matter profiles, which are displayed on monitors. A direct study of these profiles enabled to choose the depths at which water samples were to be taken. Salinity measurements, gas chromatogrphy of Ar, dissolved N_2 and total CO_2, alkalinity titrations, analysis of nutrients (PO_4, NO_3, sil.) were performed on shipboard by the GEOSECS crew. All these data are treated by computer and displayed on the spot.

Before starting the Atlantic and Pacific campaigns five intercalibration and testing stations were occupied in the North Pacific and Atlantic and in the South Pacific.

1.2 GEOGRAPHICAL POSITION OF THE SAMPLING STATIONS

Most of the station were visited during the GEOSECS Atlantic and Pacific Ocean campaigns, which were respectively undertaken from July 18, 1972 to April 4, 1973 aboard R.V. Knorr (Woodshole Oceanographical Institution) and from August 22, 1973 to June 10, 1974, aboard R.V. Melville (Scripps Institution of Oceanography). We also studied several stations visited during cruises in the Atlantic Ocean, aboard R.V. Jean Charcot, under the responsability of the CFR: HARMATAN 1971; MIDLANTE 1974; TRANSAT 1975. Included in this study are also two stations of the ATLANTIS II expedition in the Atlantic, during which several GEOSECS stations were re-occupied. The position of all these stations is given in Table I.1 and Figure I.1.

TABLE I.1: Geographical position of stations and investigated depth intervals

Stations		Positions	Investigated depth interval, in m		
Atlantic Ocean					
GEOSECS ST	17	74°56'N-01°07'W	from 992	to 3439	■ ♦
	5	56°54'N-42°47'W	363	2464 m	■
	3	51°01'N-43°01'W	28	3660	■ ♦
	27	42°00'N-41°59'W	1441	4858	■
	120	33°15'N-56°34'W	900	3187	♦
	115	28°04'N-25°54'W	1145	3732	♦
	31	27°00'N-53°31'W	1	5500	♦
	37	12°01'N-51°00'W	949	1940	♦
	58	27°02'S-37°00'W	197	4422	■ ♦
	67	44°58'S-51°10'W	40	5580	■ ♦
	91	49°36'S-11°37'E	486	3074	■
	82	56°15'S-57°38'W	1	5202	■ ♦
ATLANTIS II					
ST	715	52°56'N-36°13'W	2000		■
	2111	33°41'N-57°38'W	954	2195	■ ♦
HARMATAN 1971					
ST	6	04°30'N-19°35'W	2000	3000	■
	15	00°00' -05°30'W	1000	4000	■ ♦
MIDLANTE 1974					
ST	Madcap	28°40'N-25°25'W	1075	5043	♦
	9	24°03'N-28°56'W	910	2265	♦
	50	34°43'N-29°34'W	985	3510	♦
TRANSAT 1975					
ST	17	34°06'N-61°17'W	5	4380	♦
	37	14°48'N-74°12'W	1000		♦
Pacific Ocean					
GEOSECS ST	257	10°10'S-170°00'W	1263	5182	■ ♦
	263	16°36'S-167°05'W	676		■
	269	23°59'S-174°26'W	1253	6348	■ ♦
	310	26°55'S-157°11'W	1557	4789	■ ♦
	282	57°35'S-169°36'E	2131	5187	■ ♦

■ Inspected for $BaSO_4$ presence by SEM-EMP.
♦ Analysed for total Ba_p by INAA.

Figure I.1,A

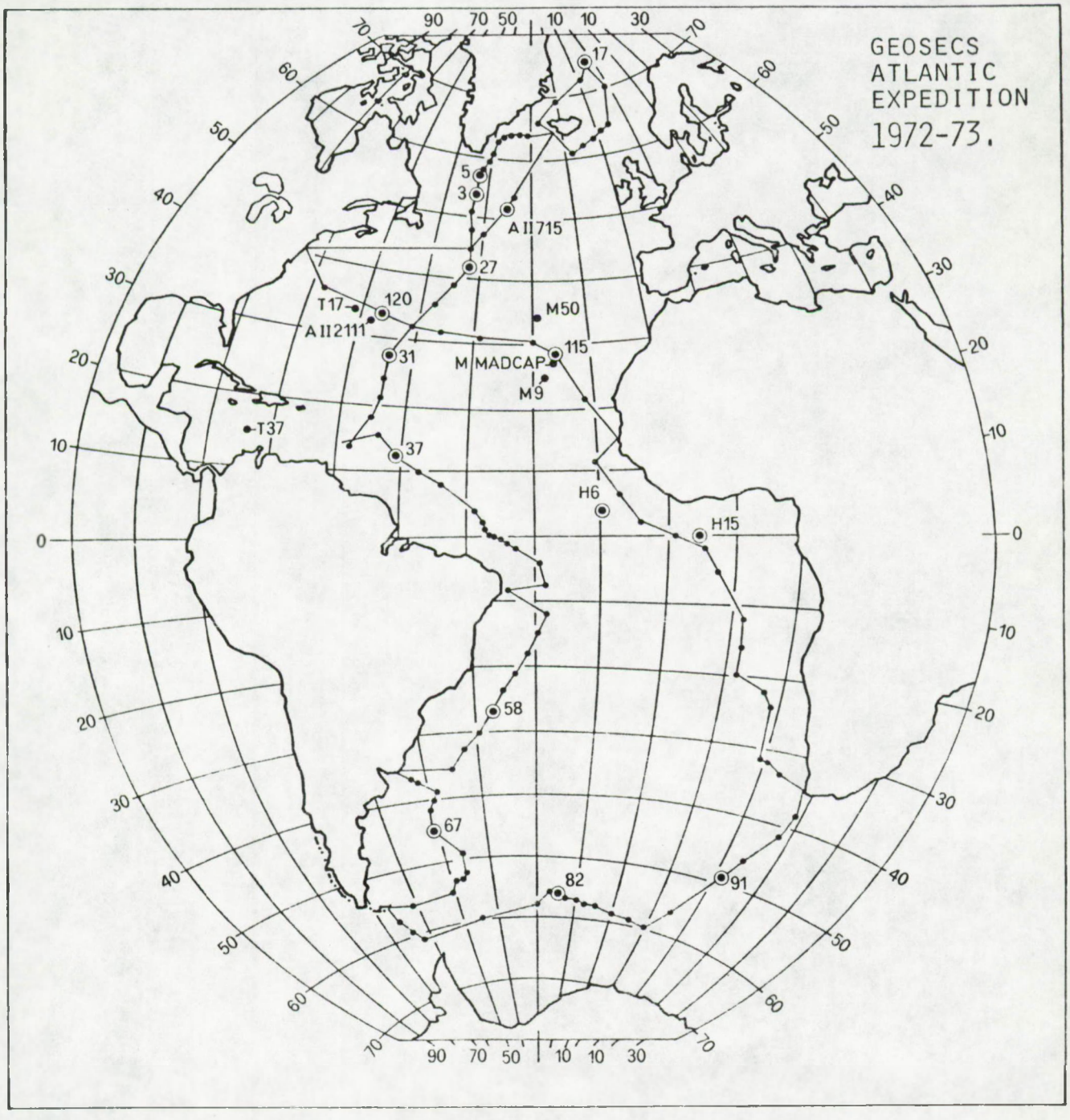

Geographical location of the analyzed profiles in the Atlantic Ocean. Station numbers which are not preceded by a letter, refer to GEOSECS stations. Station numbers preceded by:

AII = ATLANTIS II stations

M = MIDLANTE "

T = TRANSAT "

H = HARMATAN "

Figure I.1,B

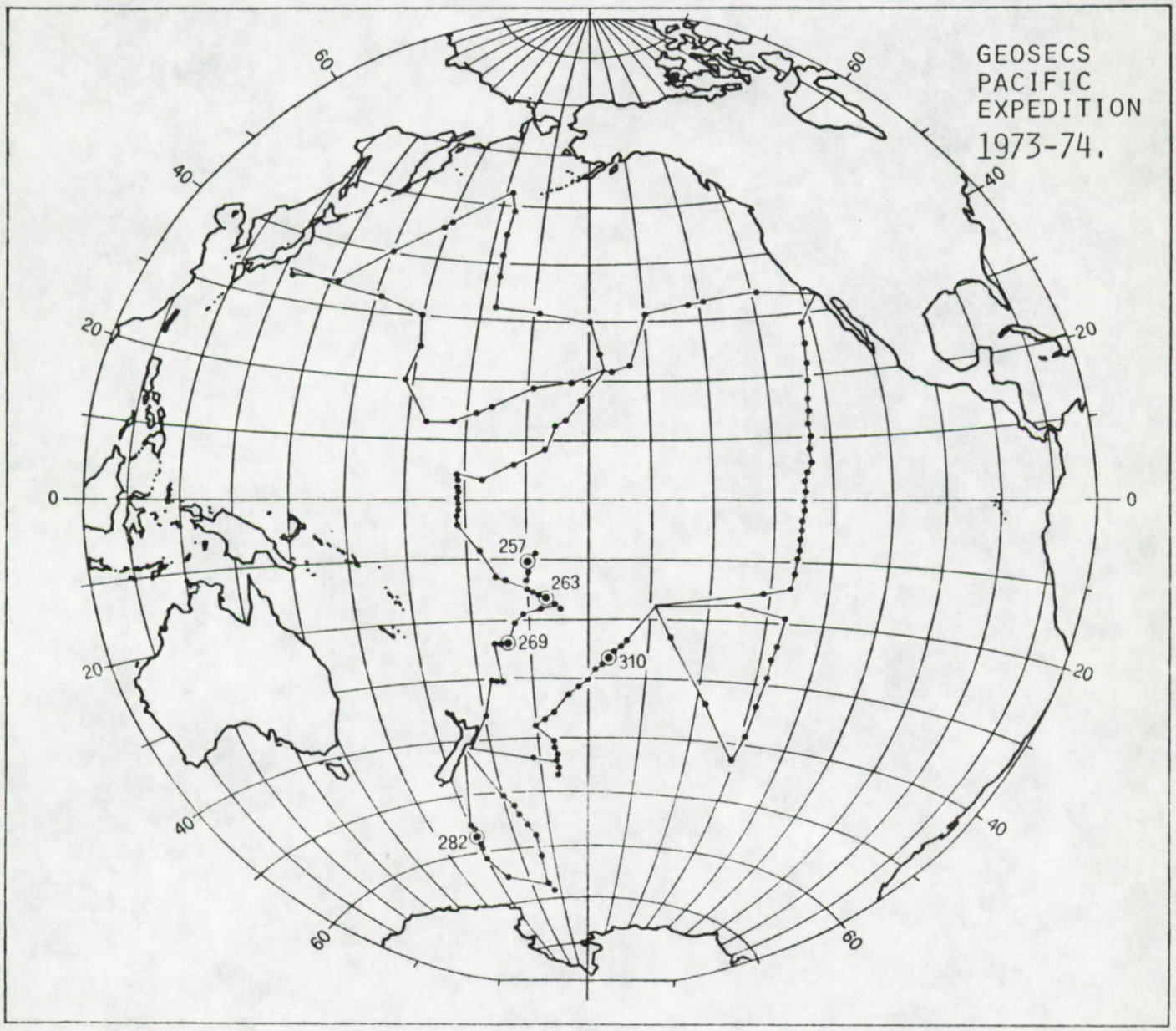

Positions of analyzed profiles in the Pacific Ocean. All numbers refer to GEOSECS stations.

CHAPTER 2

EXPERIMENTAL TECHNIQUES

2.1 Sampling and weighing of suspended particulate matter

2.1.1 Shipboard sampling technique

During the GEOSECS cruises samples were collected with 30 litre PVC Niskin bottles, mounted on a rosette sampler, attached to a stainless steel cable. On shipboard, part of this sea water sample is transfered into clean 10 litre polyethylene containers, which were thoroughly rinsed with one litre of the collected sea water. In the shipboard laboratory this sea water is filtered under pressure. The incoming prefiltered air, forces the water through a pre-weighed, 37 mm Ø Nuclepore membrane with a pore size of 0.4 µm. The Nuclepore membrane is contained in a plexiglass holder. Filtered water is recuperated in polyethylene containers for weighing, in order to determine its amount, and for later chemical analysis by other GEOSECS participants. Depending on the particle load, 4 to 10 litres are filtered. At the end of each filtration the membranes are rinsed under suction with distilled, deionised water to remove residual sea salt. Thereafter, each filter is stocked in a clean plastic box. At the Woods Hole Oceanographic Institution, filters were weighed with a Mettler micro-balance (model M 5), after a several day lasting equilibration period in the weighing room. These weighed filters arrived at our laboratories in sealed plastic boxes.

During the cruises which were not conducted in the

GEOSECS framework, a similar sampling method was used.

2.1.2 Validity of the particulate matter weight measurements (from Brewer et al., 1976)

Repeated weighings of filter sets over periods of days and even years showed that a precision is achieved which is better than ± 5 µg. In the case of 10 litre samples this corresponds to a precision of 0.5 µg/Kg sea water. The concentration of total suspended matter ranged between 5 and 300 µg/Kg SW in the Atlantic Ocean.

24 duplicate and 1 triplicate sample were obtained during the GEOSECS Atlantic campaign. Weighing of these samples yielded a standard deviation value of 5.2 µg/Kg sea water.

Further, GEOSECS station 120 (33°15'N-56°33'W) occupied on march 27, 1973, was re-occupied on september 20, 1974, as Atlantis II station 2111 (33°40'N-57°36'W). Both profiles of suspended particulate matter amounts are compared in Figure I.2, as taken from Brewer et al. (op.cit.). The concordance is very good for mid-water samples. The larger divergences observed in the nepheloïd layer are due to different bottom topographies and to the fact that the watercolumn at station 2111 is 700 m shallower than at station 120.

Figure I.2: Comparison of the total suspended matter profiles of two North Atlantic stations in close vicinity, but sampled with a time interval of 17 months (data from Brewer et al.,1976).

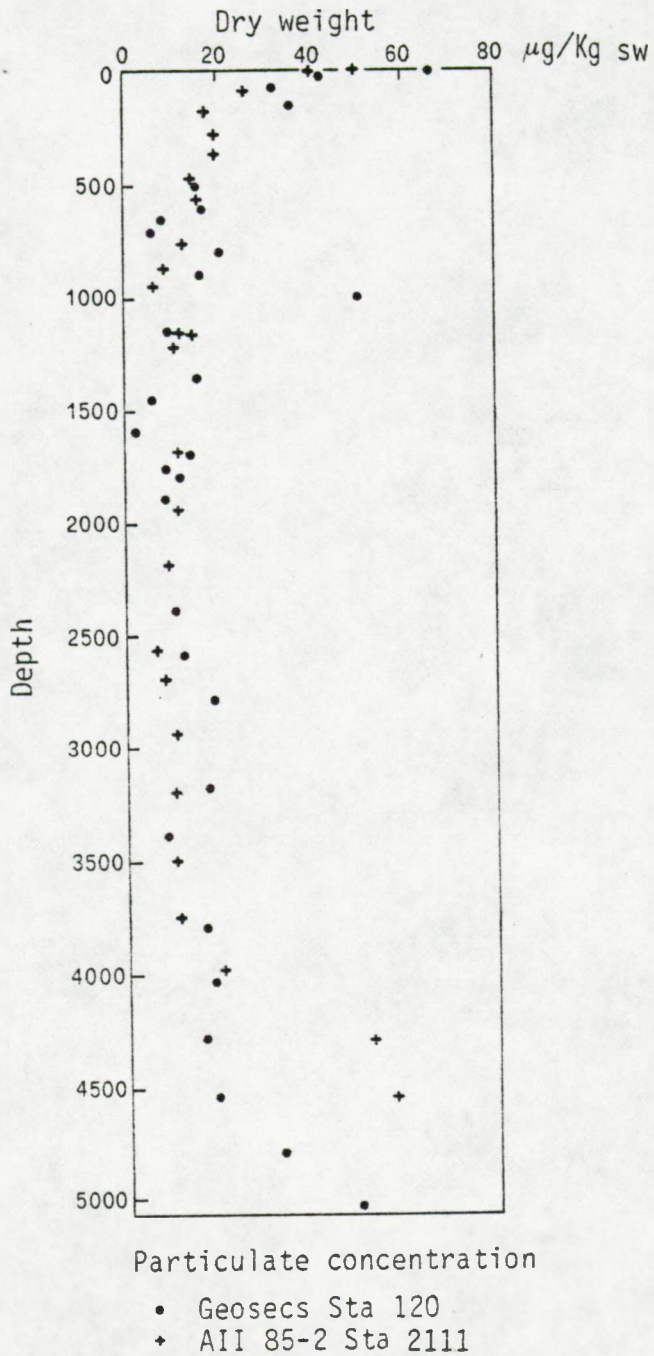

2.1.3 Filtration efficiency of the Nuclepore membranes

In order to assess the collection efficiency of the Nuclepore membrane filters for particles having sizes inferior to the pore size, P.Buat-Menard, working at the CFR, filtered sea water on a consecutive series of filters, with decreasing pore size. During this experiment filtrations were performed successively on 3 Nuclepore membranes having a pore size of 0.4, 0.2 and 0.1 µm. Gravimetric analysis showed the collection efficiency of the 0.4 µm membranes to be superior to 98% (by weight).

2.2 Instrumental neutron activation analysis.

2.2.1. Theoretical: (From Schulze, 1962; Lenihan and Thomson, 1965; P. Buat-Menard, CFR-CNRS, course on neutron activation analysis)

Neutron activation is the only non-destructive method capable to analyse heterogenous solid samples available only in minimal amounts, such as oceanic suspended matter. Atomic absorption and mass spectrometry attain the same sensitivity, but require a chemical extraction of the elements of interest which may result in contamination of the sample. Neutron activation analysis, in this case, is performed directly on the membrane sample without any chemical treatment.

The applied neutron activation technique consists in the bombardment of the sample with thermal neutrons that are produced by U^{235} chain fission inside a reactor.

The activation process occurs at the level of the nuclei of the target atoms and as a result the molecular context in which the atoms of the analyzed species occur is unimportant.

The probability for the nuclei of the target atoms to capture a neutron is expressed by their cross section σ, being the ratio of the number of neutron captions per nucleus, to the number of incoming neutrons per cm^2 and per second. This

capture probability is inversely proportional to the speed, or energy of incoming neutrons. It is assimilated to a surface value and expressed in barns (1 barn = 10^{-24} cm^2).

Several characteristics both of the stable parent isotope and the radioactive daughter isotope must be considered carefully before deciding which radioactive isotope is to be measured; they are: the abundancy of the stable parent isotope; the half-life of the produced radioactive isotope; the emission efficiency; the energies of the produced γ-rays and the yield of the detector.

Maximum activity is attained only after an infinite irradiation time. An irradiation lasting one period of the produced radioactive isotope results in 50% of the saturation activity. Generally the irradiation time is less than one period. By measuring this induced amount of radioactivity, it is possible to estimate the amount of radioisotopes responsible for this activity and therefore the amount of stable atoms. It is evident that this supposes a constant production rate of radionuclides, or in other words, a constant flux of neutrons.The induced activity at a time t_1 after the end of the irradiation is written:

$$A_{t_1} = \Phi \cdot \sigma \cdot \frac{m.\theta}{M} (1-e^{-\lambda t}) \cdot N \cdot e^{\lambda t_1} \qquad (1.1)$$

with:

N = Avagadro's number = 6.02×10^{23}

Φ = neutron flux in number of neutrons.cm^{-2}.sec^{-1}

σ = cross section in barns ($10^{-24} cm^2$)

m = mass of the element in g , present in the sample

M = atomic weight in g , of the element from which the radioisotope results

Θ = isotopic abundancy of the activated isotope

λ = radioactive constant, in sec.

t = irradiation time in sec.

t_1 = decay time in sec. between the end of the irradiation and the start of the activity measurement.

m, the concentration in g of the element in the sample is derived from (1.1):

$$m = \frac{A_{t1} \cdot M \cdot e^{-\lambda t1}}{\Phi.\sigma.\Theta\ (1-e^{-\lambda t}).N} \qquad (1.2)$$

Thus in principle the direct measurement of the mass of an element is possible. In practice,however σ , the cross section , is usually not known with sufficient precision and the neutron flux is not constant enough during the irradiation. Therefore,in general, monitors or standards are processed that are activated simultaneously with the samples and counted in the same conditions.

The mass m of an element is then easily obtained by solving

$$m_{sample} = m_{standard} \cdot \frac{activity_{sample}}{activity_{stand.}} \qquad (1.3)$$

both activities being activities at time t_o, at the end of the irradiation.

A_{t_o}, the activity at the end of the irradiation is obtained as follows:

1°) for counting times $t_c > 1/2\ T$

$$A_{t_o} = \frac{A_{t1} \cdot e^{(0.693/T).\Delta} \cdot (0.693/T).t_r}{1 - e^{-(0.693/T).t_r}} \qquad (1.4)$$

2°) for counting times $t_c < 1/2T$

$$A_{t_o} = A_{t1} \cdot e^{(0.693/T).(\Delta + 1/2.t_r)} \qquad (1.5)$$

with Δ = time elapsed between end of irradiation and start of γ-ray counting operation

t_r = real counting time (= with dead time correction)

t_c = counting time without dead time correction

T = period of the radioactive isotope measured

2.2.2. Method:

The only sample preparation, prior to irradiation, consisted in pelletizing the filter membranes. Therefore samples, monitors and blanks were carefully folded and pelletized in a stainless steel press into small (~ 4 mm^2) tablets. These were packed into alcohol cleaned plastic envelopes. The compact form of these samples, enabled a fast transfer to new, "cold" envelopes, immediately after irradiation and before γ-spectrometry. This yielded optimal counting geometrics.

Neutron activation analyses were performed at the "Laboratoire d'Analyse par Activation, Perre Süe", at the "Centre d'Etudes Nucléaires" , Saclay (France), in collaboration with and under the direction of the "Centre des Faibles Radioactivités" at Gif sur Yvette (France). The activation laboratory is equipped with a pneumatic conveyor system, guiding the samples from the reactor (EL 3) to the counting room. Different irradiation channels, characterized by different neutron fluxes were used. In general however the flux of thermal neutrons was of the order of 2×10^{13} neutrons $cm^{-2}.sec^{-1}$.

γ-spectrometry was performed with a SEIN Ge-Li diode detector[☆], coupled to a photo-multiplier and amplifier and a DIDAC 440 Intertechnique multichannel analyser. The Ge-Li diode has a resolution of about 1 Kev per channel. Calibration of the multi-channel analyser was performed with the 1332 KeV and 122 KeV photopeaks emitted by a Co^{60} source (half-life: 5.27 years).

In order to satisfy the requirements of counting statistics and to realize an optimal occupation of available machine-time, irradiation and γ-spectrometry conditions were carefully chosen in function of the neutron flux intensity,

---

☆ Characteristics of Ge-Li diode:
resolution: Co^{60}-1332 KeV photopeak: FWHM width : 3 KeV
- 122 KeV " " " 1.5 KeV
yield : 1 % for the Co^{60} 1332 KeV photopeak.

the characteristics of target nuclei and produced radioisotopes, and the detector yield. It was further checked if chosen irradiation conditions would not result in breeding a too high total activity that would saturate the detector. Preliminary investigations of marine suspended matter samples showed that Na, if not sufficiently eliminated pior to activation, will give rise to an important activity of Na^{24} (half life: 14.96 hours). Although an important part of the particulate Na originally present on the filters, is eliminated during the shipboard rinsing (§ 2.1.1), the remaining Na concentration still may amount to 1,000 and 10,000 ppm of total dry matter, as shown by early measurements on suspended matter from the Atlantic by Darcourt (1973).

A first short irradiation, lasting one minute and followed by γ-spectrometry within 7 minutes, allowed to analyse for Al, Cu, V, Ca, while a second irradiation of 10 to 15 minutes, followed by γ-spectrometry withing 120 minutes, allowed to analyse for Ba, Sr, Mn. The characteristics of the measured radioisotopes and stable parent isotopes are listed, in Table I.2; data are from Lederer et al. (1968).

Elemental concentrations were determined by comparing sample activity with a standard activity. Standards consisted of a mixture of ultra-pure A.R. grade solutions. Of this mixture 50 µl was pipetted on a Nuclepore membrane or Whatman 41 filter and allowed to dry out in a laminary flow hood.

Table I.2: Characteristics of measured radio isotopes, from Lederer et al. (1968). Duration of irradiation and counting periods are also indicated.

Element	Radio-isotope	Principal means of production	isotopic abundancy in %	cross section for thermal neutrons in barns	half-life min.	Energy of analyzed photopeak in KeV	Radiation intensity in %	Duration of irradiation in min.	Duration of counting period in min.
Al	Al 28	Al 27(n,γ)	100	0.235	2.3	1780	100	1	3-5
Cu	Cu 66	Cu 65(n,γ)	30.9	2.3	5.1	1039	9	1	3-5
V	V 52	V 51(n,γ)	99.75	4.9	3.7	1434	100	1	3-5
Ca	Ca 49	Ca 48(n,γ)	0.185	1.1	8.8	3100	89	1	3-5
Ba	Ba 139	Ba 138(n,γ)	71.66	0.4	82.9	166	23	10-15	5-10
Sr	Sr 85m	Sr 84(n,γ)	0.56	0.65	70	231	85	10-15	5-10
Mn	Mn 56	Mn 55(n,γ)	100	13.3	154.8	847	99	10-15	5-10
Mg	Mg 27	Mg 26(n,γ)	11.17	0.03	9.5	1013	30	1-3	3-10
S	S 37	S 36(n,γ)	.014	.14	5.07	3090	90	10	3-5

Per 50 µl, the utilized standard solutions contained:

a) Cu: 5.065 µg
   V: 0.261 µg
   Al: 44.12 µg
   Ca: 51.1 µg
   S: 65.2 µg

b) Ba: 10 µg
   Sr: 10 µg
   Mn: 0.08 µg

The utilized multi-element solutions were checked by atomic absorption spectrometry , and at regular intervals they were compared with a standard rock powder (W_1) of the National Bureau of Standards (Buat-Menard, 1979).

During the one minute irradiation, samples were irradiated one at a time and each fourth to fifth sample was accompanied by a standard. As concerns the irradiations which lasted 10 to 15 min. (to analyse for Ba, Sr, Mn), they were performed on two to three samples at a time, always accompanied by a standard. Stripping of the spectra was performed manually.

Blanks of the different filter types used were analyzed by Buat-Menard (1979) at the CFR. These values are given in Table I.2, together with the estimated detection limits.

Table I.3: Blank filters: mean values for impurities in Whatman 41 filters and Nuclepore (0.45 µm) membrane filters and INAA detection limits for oceanic suspended matter.

Element	Whatman 41 ng/cm^2	Nuclepore 0.45 µm ng/cm^2	Detection limit* ng/Kg sw	Average particulate load in sea water ng/Kg sw
				(this study)
Al	40 ± 20	8 ± 4	4	110
Ca	100 ± 50	22 ± 10	11	600
V	0.1 ± 0.05	4×10^{-2} $\pm1.5.10^{-2}$	2×10^{-2}	0.4
Mn	0.4 ± 0.2	0.2 ± 0.1	0.1	4.8
Ba	<10	<0.4	1.0	20
Cu	< 2	<2	0.4	3
Sr	<10	<0.4	1.0	16

*As calculated for 30 litre of sea water, filtered on a Nuclepore membrane of 37 mm in diameter, with a pore size of 0.45 µm , and of which 1/4 is analyzed by INAA.

Accuracy of the INAA measurements: The 2σ confidence limits which is given for every INAA data, does not take into account the uncertainties on the volume of filtered water. This 2σ value takes account only of the stochastic fluctuations during the counting of γ-photons and is given by:

$$2\sigma = \frac{2\sqrt{N_1 + N_2}}{N_1 - N_2} \qquad (1.6)$$

with N_1= integrated counts of the photo-peak

N_2= integrated counts of the background spectrum

2.2.3. Validity of the neutron activation data for Ba

The validity of the INAA particulate Ba data was checked by analyzing duplicate samples and by analyzing samples collected during the re-occupation of a same location by different expeditions.

i) Duplicate sampling. On a few occasions duplicate samples were taken at the same station. Results are presented in Table I.4.a

Table I.4.a : Validity of the INAA data: comparison of particulate Ba data for duplicate samples

Depth in m	Ba_p	
	ng/Kg sw	2σ %
ATLANTIS II station 2111		
954	17.8	9
954	16.8	15
2195	5.4	18
2195	3.5	68
GEOSECS station 67		
10+	12.8	51
10+	13.8	59
42+	20.6	54
42+	18.3	76
445	50.5	11
445	56.4	3

+ Same water samples but filtered on two separate Nuclepore membranes as a result of rapid filter obstruction.

From Table I.4.a it appears that, with the exception of the duplicate Atlantis II 2195 m samples, the data agree within 13 %.

ii) Re-occupation of a station. GEOSECS Station 120 (33°15'N-56°34'W) was re-occupied after a period of 17 months by R.V. Atlantis II, as Station 2111 (33°40'N-57°36'W)(see also § 2 .1.2). Five samples taken at similar depths, were analyzed (Table I.4.b):

Table I.4.b: Validity of the INAA data: comparison of particulate Ba data of GEOSECS station 120 and ATLANTIS II station 2111.

depth in m	Particulate Ba in ng/Kg sw ATLANTIS II st. 2111	2σ %	depth in m	Particulate Ba in ng/Kg sw GEOSECS st. 120	2σ %
954	16.8☆	15	900	15.3	10
	17.8	9			
1168	13.6	26	1150	10.3	30
2195	3.5☆	68	2186	9.8	12
	5.4	18			
3199	8.2	15	3187	10.5	16

☆Duplicate samples, see Table I.4.a .

It is seen that despite the 17 month interval between the samplings and the fact that the exact location of the original station could not be re-occupied, both profiles show similar values for particulate ba concentrations.

2.3 Electron microscope and electron microprobe analysis

2.3.1. Sample preparation and SEM-EMP equipment:

Only part of each filter was kept in Brussels for analysis with the scanning electron microscope and electron microprobe (= combined SEM-EMP equipment). Subsampling on the filters was performed with an especially designed plexiglass cutting device that allowed to cut off one quart of the original filter. All these operations were performed in a laminary flow hood running at a low debit. The main part of each filter was saved for instrumental neutron activation analysis at the Centre des Faibles Radioactivités (CFR) in Gif-sur-Yvette (France).

The sample consisted of a small portion (approximately 0.8 cm^2) of the original filter, mounted with colloidal carbon (aquadag) onto an aluminium stub and vacuum coated with a conducting material, such as C, Pd, Au. In most cases carbon coating was performed.

The analytic facility at the Université Libre de Bruxelles consisted of a Cambridge Mark IV stereoscan equipped with a half-focusing Cambridge wavelength diffractive spectrometer (WDS) and a Tracor Northern NS 880 energy dispersive spectrometer (EDS), with a Si-(Li) (= lithium drifted silicon) crystal detector. At the CFR in Gif-sur-Yvette, a CAMECA stereoscan and an EDAX EDS were used.

The WDS is characterized by a higher signal/background ratio and a higher resolution. The Ba $L\alpha_{1,2}$ and Ti $K\alpha_{1,2}$ lines, which overlap when analyzing with the EDS having a resolution between 160 and 180 ev, are clearly discriminated by the available LiF_{345} [☆] crystal of the WDS. The WDS is therefore used for the "semi-automatic" detection of Ba-rich particles, which is discussed below. The WDS is however not well suited for the fast recording of complete elemental spectra, since the different spectral lines have to be searched by rotating the analyzing crystals over the 2θ domain in they function optimally. Since in most cases this operation requires the use of different crystals, the whole analysis is time consuming. The EDS allows the immediate recording of the complete elemental spectrum, and is therefore more adequate for routine analyses.

2.3.2 Detection mode of Ba-rich particles

The EMP detection of Ba-rich particles was accomplished by one or the other of the following methods:

a) by scanning the sample at constant magnification. Every particle of high Z elements (Z > 13) was checked for dominance by Ba and S.

b) by a semi-automatic method, which consisted in scanning several fields, very slowly (during 10 min.), at a low magnification (600 or 1200 X). A 30 KV accelaration potential is applied besides the use of low lens amperages

☆ Lithium Fluoride, 345 curvature crystal

and largest electron-beam aperture. The WDS is set on the LIF_{345}-curvature crystal in order to diffract the Ba $L\alpha_{1,2}$ spectral line. Meanwhile the Ba X-ray map is photographically recorded with a polaroid camera. Comparison of this X-ray map with the normal SEM picture of the scanned field, allowed the localisation of all Ba containing particles. The complete elemental spectrum of each Ba-particle is further recorded with the energy dispersive spectrometer.

For both methods, if Ba and S were present as the only principal components (K and Sr are sometimes present in minor amounts),the particle was recorded as barium sulphate.

2.3.3 Electron microprobe analysis

A. Interpretation of the elemental spectra

Elemental spectra of the $BaSO_4$ particles are generally characterized by the presence of Al, Si, K, Ca, Fe, Cu and occasionally Sr peaks. The presence of Sr is characterized by a low energy L_α peak (1800 eV) and a high energy K_α peak (14000 eV). Since the SrL_α peak coincides with the Si $K_\alpha$peak (1740 eV) we considered that the presence of Sr was confirmed only when the SrK_α peak was detected. In the following the artefactial origin of certain of these characteristic rays in the elemental spectrum of $BaSO_4$ is discussed.

Since Al, Si, Ca, Fe and Cu were detected on nearly any particle in the samples, suspicion raised that excitation of these elements in the substrate (colloidal carbon fixing the Nuclepore membrane to the aluminium stub and the aluminium stub itself), or in nearby particles was responsible for this phenomenon. This could result from a direct excitation or a

flurescence radiation. Analysis of a blank Nuclepore membrane, mounted on an aluminium stub with colloidal carbon, revealed indeed peaks of Al, Si, Fe and Cu. Further, substraction of a background spectrum, recorded under identical conditions on a naked part of the filter, nearby the particle of interest, eliminated Fe and Cu signals, part of the originally detected Al and of the peak at 1800 ev (= Si Kα and/or Sr Lα), and in most cases Ca. The eventually present K Kα and Sr Kα peaks remained unaffected. Besides Al,Si, Fe, Cu, this background spectrum revealed the presence of Ca, an element which on the contrary was not detceted when analysing a blank Nuclepore membrane. It is thought that the detected Ca peak is due to the excitation of nearby carbonate particles. A third test consisted in the substraction of a background spectrum recorded under identical conditions on a nearby particle. Coccoliths are well suited for this purpose, since they occur in numerous amounts and are known to contain but very low traces of foreign elements (Turekian, 1965). As a result of this substraction, Fe, Cu, Al and a large part of the peak at 1800 eV (= Si Kα and/or Sr Lα) were eliminated. Again, since the Sr Kα peak remained unaffected by this operation, the net peak remaining at 1800 eV corresponds to the Sr Lα ray.

As far as $BaSO_4$ particles are concerned it is evident that the detection of Al, Fe, Cu, Ca and Si is artefactial in origin. These peaks result from the excitation of the sample substrate and/or nearby particles on the filter.

To conclude, it is evident that elemental spectra recorded with the electron microprobe (the EDS and WDS system) at single particle level in heterogenous, often heavily loaden samples, must be interpreted with care. In the case of $BaSO_4$ particles only Sr and K were observed to be genuine constituents of these particles.

The presence of Sr and K in suspended $BaSO_4$ particles is discussed further in detail in section 2.3 .

B. Attempt in quantitative microprobe analysis

Quantitative microprobe analysis of individual micron-sized particles is difficult to accomplish, though matrix corrections facilities are available. These matrix corrections include: corrections for atomic number, absorption and fluorescence effects. They were developed for thick polished samples (Ø > 15 - 20 µm and > 5 - 10 µm deep).

When single micro-particles must be analyzed, these conventional corrections cannot be applied. The following complications arise, which are not encountered for thick polished samples, (from Armstrong and Buseck, 1975):
1°) Some incident electrons may escape from the particle bottom (transmission) or particle sides (sidescatter), before they generate X-rays. The resulting decrease in X-ray intensity will vary from element to element and depends on several factors, including particle size and shape.

2°) The effect of matrix absorption on observed X-ray intensity depends on the distance X-rays must travel from point of production until they leave the specimen in the direction of the detector. For a flat polished sample the path length is a simple geometric function of the depth of X-ray production. For a particle, with an irregular shape, the X-ray path length is a far more complex function depending on particle size and shape.

3°) The amount of secondary X-ray fluorescence depends on X-ray path lengths (of both the fluorescing and the fluoresced rays) and is a complex function of particle geometry.

In their theoretical study Armstrong and Buseck (1975) adapted the particle size and particle geometry dependent terms of the correction equations originally elaborated for thick polished samples.

Today however software adapted to analysis of micro-particles is not available. The elaboration of fine grained standards, having a particle geometry and size similar to the one of the particles under study, will minimize effects of geometry and size on the intensities of the produced X-rays and is assumed to preclude the necessity of correction equations (Armstrong and Buseck, 1975).

Since we are interested in the Sr content of $BaSO_4$ particles, we elaborated $BaSO_4$ standards with varying Sr contents and with a particle size range that covers the one

of natural suspended $BaSO_4$ particles. This attempt gave no satisfactory results.

The standards were produced by precipitation. These precipitates were analyzed by X-ray (XRF) fluorescence spectrometry and with the EDS system in order to constitute a Sr-calibration curve. As a result, direct deduction of the Sr mole fraction present in any barite particle should be possible. Precipitations were obtained from 600 ml $BaCl_2$ - $SrCl_2$ solutions, to which 25 ml of 0.025 N H_2SO_4 was added, following Starke's method (Starke, 1964). Ba amounts were kept constant (0.712 g $BaCl_2.2H_2O$), while Sr amounts were varied (from 0.041 g to 0.772 g $SrCl_2.6H_2O$). The Ba, Sr solution was heated to 80°C and the H_2SO_4 was added under stirring. Precipitation was allowed to proceed for two to three hours under continuous stirring. The precipitate was recuperated by filtration on Nuclepore membranes of 0.45 µm pore size. A homogenized $Ba(OH)_2.8H_2O$ - $SrCO_3$ powder, with varying $SrCO_3$ amounts,was used as XRF standards. The precipitates contained 0.5, 4.6, 13.5 and 25.5 mol% Sr. After XRF analysis, a small fraction of the precipitate was resuspended in water and immediately filtered on Nuclepore membranes of 0.45 µm pore size. This filtrate is then prepared in the classical way for SEM-EMP analysis. The precipitates showed to be fine grained and to cover the size range of the suspended $BaSO_4$ particles in sea water.

Of each precipitate five particles, measuring between 1 and 3 µm in diameter, were analyzed and served to compute

a "mean" spectrum. From this spectrum, background counts were substracted. The integrated counts of the Sr Kα peak (14,500 KeV) were normalized to 10,000 counts for the Ba Lα peak (4,400 eV). In Figure I.3 these values are set out on the abscissa, and the corresponding XRF values on the ordinate. The large σ values (10 to 20%) for the EDS measurements show that in each precipitate the Sr/Ba ratio is highly variable from particle to particle.

A closer look at several particles of the 13.5 mol% Sr-substitution precipitate showed that the Sr respons (= Sr Kα counts normalized to 10,000 counts for the Ba Lα peak) increased with decreasing particle diameter (Figure I.4). The relation appears to be an exponential one, with Sr/Ba ratios stabilizing for diameters larger than 15 μm, a diameter largely outside the normal range observed for suspended $BaSO_4$ particles in the ocean. The Sr/Ba ratio is however extremely sensibel to particle size for diameters <5 μm. The observed 10 to 20% imprecision of the EDS measurements is therefore essentially due to particle size variability.

Quantitative microprobe analysis of micron-sized particles was abandoned, since the accuracy of the Sr content that is deduced for unknown particles would not be better than $\pm$ 40% (Figure I.3). The few data on the Sr content of barites presented in this work were obtained by application of conventional (= for thick polished samples) matrix corrections and are of semi-quantitative level.

FIGURE I.3

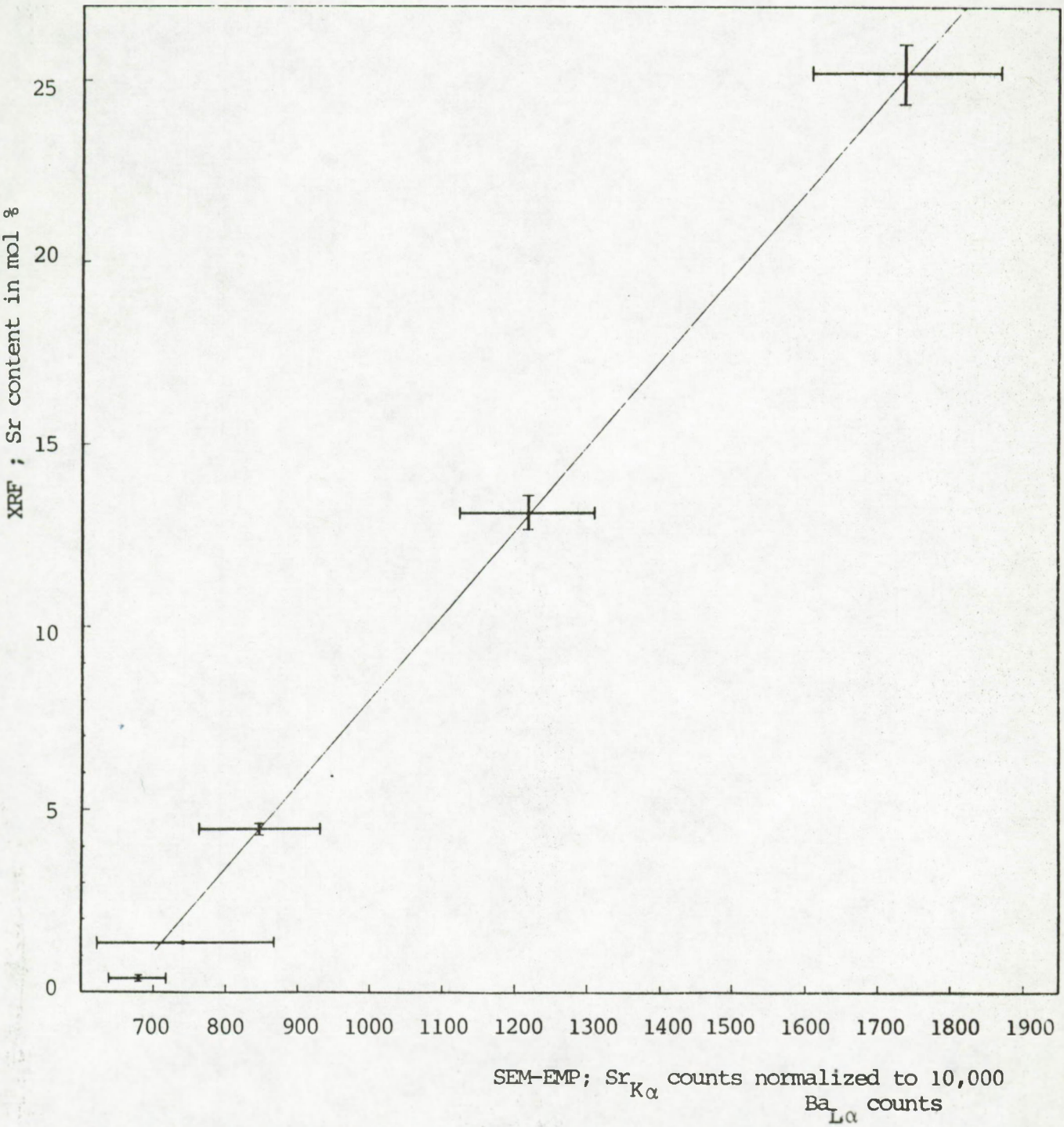

Sr- calibration curve for SEM-EMP use. Ordinate: XRF values (in mol%) for the Sr content of 5 barite precipitations with varying Sr content. Abscissa: EMP values in number of counts of Sr Kα , normalized to 10,000 Ba Lα counts. Confidence limits: $\pm$ 1σ

FIGURE I.4

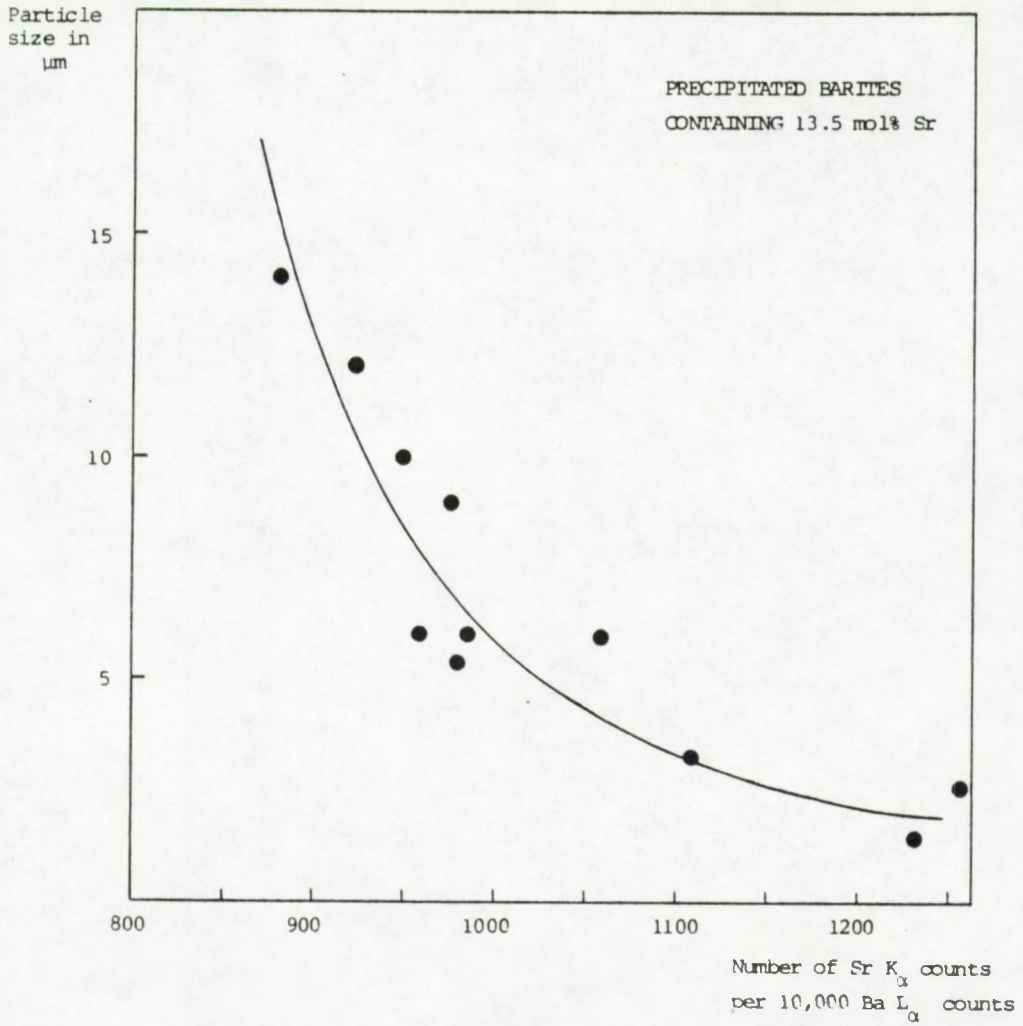

Variation of the Sr content measured by SEM-EMP ,within the same precipitate of Sr-enriched barite (13 mol% Sr), as a function of particle diameter. Curve fitted by eye.

C. Sensitivity of the spectrometer:

Insofar analysis of Sr in $BaSO_4$ particles is concerned, the sensitivity of the EDS system is better than 0.2% (by weight) since the Sr Kα ray for $BaSO_4$ particles with a 0.5 mol% substitution of $BaSO_4$ by $SrSO_4$ is still easily detected (Figure I.3). The sensitivity of the WDS lies in the range of 100 to 1000 ppm.

2.3.4 Confirmation of suspended barium sulphate particles as barite

The crystallinity of the suspended barium sulphate particles was clearly demonstrated by J.Klossa (Laboratoire R.Bernas, Orsay, France; Klossa, 1977 and pers. comm.,1979). In the following we briefly resume his method.

$BaSO_4$ particles identified by SEM-EMP (see § 2.3.1 and 2.3.2) are transfered to a high voltage electron microscope (HVEM), for high resolution photographical recording and electron diffractometry. Since the latter analysis requires the sample to be supported by a substance transparent to the electron beam it is necessary, prior to analysis, to get rid of the supporting Nuclepore membrane.The technique of sample preparation and particle location is as follows. A small piece of the membrane ($\sim$ 4 mm^2) is cut out and coated with a carbon layer of 150 Å.This coated sample is then deposited, the carbon layer down, on a transmission electron microscope grid

with numbered bars. The Nuclepore membrane is dissolved with chloroform. the particles are now retained by the carbon film, transparent to the electron beam and their coordinates are fixed. This preparation is then searched with the SEM-EMP equipment for $BaSO_4$ particles and the coordinates of these particles are recorded. The sample is then ready for analysis with the HVEM.

At first electron diffractions were obtained with a 100 KeV transmission electron microscope. Some of these analyses were performed at the ORSTOM laboratories (Bondy, France) by C.E.Lambert and Rambard, who succeeded in measuring the (2 1 0) barite reflection, corresponding to the 3.3 Å lattice spacings. However, in our case two major impediments limit the use of the 100 KeV TEM:

a) $BaSO_4$ particles have a high density and are opaque to electrons of this energy. Diffraction patterns can therefore only be obtained for the extreme edge of the particle. Therefore account has to be taken of the possibility that diffracted rays come from nearby particles as well.

b) Energy loss is very important at 100 KeV. The resulting temperature increase can degrade the particles, which may melt and recrystallize.

For these reasons a 1 MeV electron microscope, equipped with a goniometer stage, of the laboratoire d'Optique Electronique (CNRS, Toulouse, France) was used. These

PLATE 1

ELECTRON MICRO-DIFFRACTION OF A SINGLE $BaSO_4$ GRAIN

Location: GEOSECS Atlantic station 17 (74°56'N-01°07'W); 1860 m.

Dark-field micrograph, obtained with a 1 MeV transmission electron microscope, of a single $BaSO_4$ grain, previously located on the filter by SEM-EMP. Despite the penetrating power of the 1 MeV electrons, only grain margins permitted any intense reflection. One can distinguish the planes of the (212) and the $(20\bar{1})$ families, which form an angle of 85°.

From J.Klossa, Laboratoire R.Bernas, Orsay and Centre des Faibles Radioactivités, Gif-sur-Yvette.

See discussion at page 49.

PLATE I

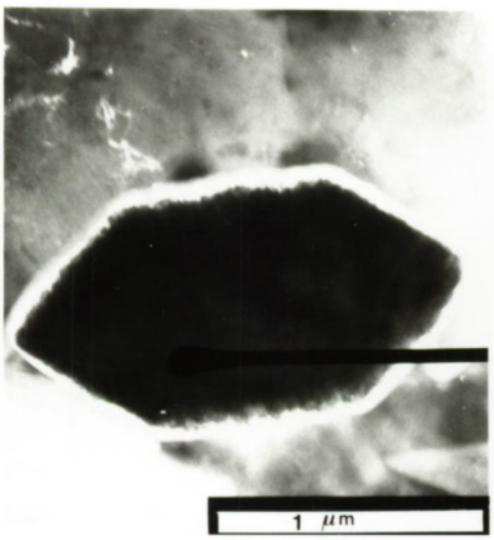

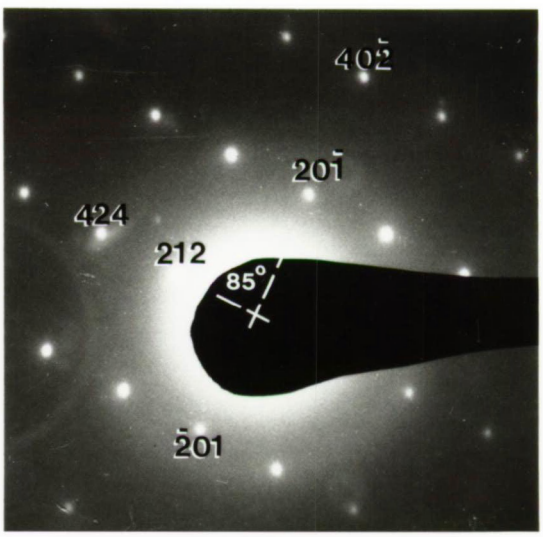

analyses were done by J.Klossa for several $BaSO_4$ particles from oceanic suspended matter. Plate 1 reproduces an easily oriented single crystal, for which it was possible to identify a large number of crystal plane families, according to the degree of rotation and inclination of the stage. The results confirm that it is a highly crystalline barite particle. The observed Ba- and S- rich particles in suspended matter therefore consist of barite crystals.

2.3.5 Method of the estimation of the Ba-mass carried by barite particles in suspended matter

In this study we have evaluated the contribution of the barite particles to the total particulate barium (Ba_p) content in suspended matter. This required the Ba-mass carried by the barite grains to be known. Particle size analysis is thus a prerequisite for the computation of particle masses. In that purpose one part (1/4) of the membrane filter was analyzed by SEM-EMP for barite particle size measurement. The remaining part of the filter was analyzed by INAA for total Ba_p. As a result both data can be compared directly.

Such a comparative study on subsamples of the same original filter requires Ba_p to be distributed homogenously on the filter surface. The presence of barite crystals in numbers that can reach several thousand per litre and the fact that in general about 10 litre of sea water were

filtered led one to suggest that this matter is distributed homogenously on a surface of about 9 cm^2 (= surface of a Nuclepore membrane of 37 mm Ø). This is confirmed experimentally. For one suspended matter sample we have analyzed the 4 quarts of the membrane separately by INAA; ATLANTIS II station 2111; 774 m:

filter part	Ba_p in ng/Kg sw	2σ %
I	43.4	22
II	48.6	24
III	46.9	23
IV	48.6	24

Arithmetic mean: 47 ng/Kg sw

A variation (1 σ) of 5.3% is observed, showing the high degree of homogeneity of the Ba load on the filter.

Particle size measurement was performed by the following procedure: In order to more easily observe the sparsely scattered grains, we reconcentrated the particles by resuspending the filtered matter, present on 1/4 (225 mm^2) of the original Nuclepore membranes, in prefiltered A.R. grade CCl_4, and refiltered on a much smaller Nuclepore membrane surface (37 mm^2). A CCl_4 medium was prefered to resuspend the filtered matter in, since this medium is supposed not to alter the composition of the filtrate, with exception of the organic matter, and since its high density favors a good resuspension of dense particles . The contact time of the filtered matter with the CCl_4 lasted only 1 to 2 min. . The operations were performed in a laminary flow hood. The

efficiency of the resuspension technique was checked and proved to be optimal, since SEM inspection of the Nuclepore filter parts treated by ultra-son showed no material left on these surfaces. Blank filters were run under identical conditions and showed that during the reconcentration operation, samples were never contaminated with Ba-rich particles.

The samples were further prepared for SEM-EMP analysis as discussed in § 2.3.1. The detection mode of Ba-rich particles is described in § 2.3.2. Detected barite particles were photographed at a constant magnification (12,000 X). The film record was projected on a scan table equipped with a coordinatograph. The final magnification on the scan table was 30,000 X and the accuracy of the size measurements was 0.003 µm. The area of each particle was obtained as follows: a maximum of points were recorded on the perimeter of the particles and these points were considered as vector-ends. vectorial calculation was performed with the help of a computer program (written by P. Kummert at the Université Libre de Bruxelles) giving the projected area and the projected area diameter of the particles. The projected area diameter is defined as the diameter of a sphere having the same projected area as the particle when viewed in direction perpendicular to a plane of stability (Allen, 1968). To calibrate the measurements, standard polystyrene spheres of 1.17 µm were photographed and measured in the same way as the barite particles.

After inserting the projected area diameters into classes of a geometric progression, which is recommended for narrowly distributed particles (Allen, 1968), a histogram of size (volume) distribution was obtained. The 0.20 µm size is the boundary of the smallest size class; particles smaller than this limit were not detected. the logarithmic progression used is: 0.2, 0.2 $\sqrt[4]{2}$, 0.283, 0.283 $\sqrt[4]{2}$, 0.336, 0.336 $\sqrt[4]{2}$, 0.475 .... µm. The mass of Ba of equivalent spheres was then calculated following the equation:

$$M = \pi/6 \cdot \rho \cdot (N_i . D_i^3) \cdot F \cdot V \qquad (1.7)$$

with M = Ba-mass carried by barite particles (g/litre sea water)
ρ = $BaSO_4$ density (4.5 g/cm^3)
N_i = particle number in size class i (number/litre sw)
D_i = projected area diameter; = class midpoint of class i (cm)
F = molar fraction of Ba in $BaSO_4$ (0.59)
V = ratio of the unit volume of sea water (1 litre) to the volume of filtered sea water, equivalent to the scanned surface of the sample

Stochastic fluctuations during the counting of barite particles were accounted for by the following formula discussed in Allen (1968):

$$\sigma(M) = M/\sqrt{N} \qquad (1.8)$$

with $\sigma(M)$ = standard deviation expressed as a % of the original weight
M = % by weight in the given size range
N = number of particles counted in the given size range

The standard deviation of the total Ba is obtained by summming the standard deviations calculated for each size range.

CHAPTER 3

IN VITRO EXPERIMENT

3.1 The culture of diatom strains in vitro and method of analysis by INAA of whole cells and siliceous fractions

The contribution of diatoms to total particulate Ba in suspended matter is one of the subjects of this study. We measured the in vitro Ba-uptake capacity of two diatom species. These were grown in natural and artificial sea water media, enriched and non-enriched in Ba. The Ba content of diatom frustules and of whole cells was measured by instrumental neutron activation analysis. Besides Ba, several other elements were analyzed: Al, V, Cu, Mn, Sr, Ca, Mg.

3.1.1 Composition of the growth media and growth conditions

Diatoms of the Rhizosolenia alata and Chaetoceros lauderi species, which both belong to genera common in the open ocean (Brongersma-Sanders, 1966), were grown in vitro at the Centre d'Etudes et de Recherches de Biologie et d'Océanographie Médicale" (CERBOM) at Nice (France).

Diatoms of the Chaetoceros genus are characterized by the formation of chain-like colonies and possess fine, long appendices (Schmidt, 1972). Diatoms of the Rhizosolenia genus are characterized by a robust, elongated body and do not possess appendices (Schmidt, 1972). These different morphological characteristics are also reflected in differences in SiO_2/organic matter ratios between both species (see later § 4.3.1 in part II).

Of each diatom species, cultures were grown in four different environments:

1° natural, coastal, aged sea water, filtered on Millipore membrane filters of 0.45 µm pore size (= type A culture)

2° artificial sea water, filtered on Millipore filters of 0.45 µm pore size (= type B culture)

3° natural aged sea water, unfiltered. (= Type C culture)

4° artificial sea water, filtered on Millipore filters of 0.45 µm pore size and enriched in Ba, up to 30 µg/l by adding $BaCl_2$ salt (= type D culture).

Of each culture type two sets were grown in 5 litre erlenmeyers. The composition of the artificial sea water is the one prescribed by Lyman and Fleming (1940); Table I.5 The nutritive substrate was elaborated, following the Provasoli formula (Haskins Laboratoria, N.Y.,1962 and Provasoli et al.1957); (composition reproduced in Table I.6). It was added to the different sea water types in a ratio of 2 ml/100 ml sea water. The cultures were grown in isothermal conditions (18°C ± 1°C) and submitted to light exposure, reconstituting the solar spectrum. The nycthermal rythm was respected. The diatom cultures were allowed to grow during five to ten days.

The diatoms were collected on Millipore filters of 8 µm pore size and were lyophilisated. Of each culture type two small preweighed aliquots (between 50 and 100 mg) were sampled. One alquot was analyzed for the Ba content of the whole cells, the other for the Ba content of the siliceous frustules only. Preliminary investigations

Table I.5: Composition of the artificial sea water used for the growth of diatoms in Vitro : Lyman and Fleming formula.

1	- Na Cl	23,477 g
2	- $Mg\ Cl_2$	4,981 -
3	- Na_2SO_4	3,917 -
4	- $CaCl_2$	1,102 -
5	- K Cl	0,664 -
6	- $Na\ HCO_3$	0,192 -
7	- K Br	0,096 -
8	- $H_3\ BO_3$	0,026 -
9	- $Sr\ Cl_2$	0,024 -
10	- Na F	0,003 -

H_2O is added in order to reach an overall weight of 1000 g .

The pH is kept between 7.9 and 8.3 .

Table I.6: Composition of the nutritive substrate used for the in vitro culture of diatoms: Provasoli formula, Haskins laboratories, New York

Solution A

	quantities
Bi-distilled H_2O	20 l
Na NO_3	70 g
Na β-glycerophosphate	10 g
Vitamine B 12 (cyanocobalamine)	2 mg
Vitamine B 1 (Thiamine)	100 mg
Vitamine H (Biotine)	1 mg
Trishydroxymethylaminomethan	100 mg

Solution B

Bi-distilled H_2O	5 l
$Fe(NH_4)_2 (SO_4)_2 - 6H_2O$	3.5 g
Titriplex III (= disodic salt of ethylene diamino-tetra acetic acid)	3.3 g

Solution C

Bi-distilled H_2O	5 l
H_3BO_3	5.7 g
$FeCl_3 - 6H_2O$	245 mg
$MnSO_4 - H_2O$	620 mg
$ZnSO_4 - 7 H_2O$	110 mg
$CoSO_4 - 7 H_2O$	24 mg
Titriplex III	5 g

These 3 solutions are mixed and kept at pH 7.8.

showed that the lyophilisated samples contained too much residual salt. This induced a too high activity and saturated the detector. Therefore the "whole cell" aliquot was first resuspended and dispersed in deionized and filtered water by ultra-son treatment. The suspension was filtered on Whatman 41 filter paper (Ø 146 mm). The filters were carefully folded to prevent loss of matter and were dried overnight at 40°C. The "siliceous frustule" aliquot was treated with 30 ml of pre-filtered, concentrated A.R. grade H_2O_2 (37 %, 110 volumes) and oxidation was allowed to proceed overnight.

The obtained suspension, of white-brown color and assumed to consist of diatom frustules only, was thereafter filtered on preweighed Nuclepore membranes of 0.45 µm pore size and was thoroughly washed with deionized, filtered water. These Nuclepore membranes were carefully folded and allowed to dry at room temperature inside a laminary flow hood. The weight differences of these samples with the "whole cell" samples are attributed to the combustion of the organic or oxidizable fraction of the cells. All samples were packed in small plastic bags and were ready for irradiation.

3.1.2 . Elemental analysis

Irradiation conditions were chosen, such as to allow measurement of Al^{28}, Cu^{66}, V^{52}, Ca^{49}, Mg, S^{37} (short period isotopes, Table I.2) and Ba^{139}, Sr^{85m}, Mn^{56} (isotopes with

longer periods; Table I.2). Two types of standards were prepared. The first consisted of a mixed solution, containing 88.24 µg Al; 10.13 µg Cu; 0.522 µg V; 102.2 µg Ca; 130.4 µg S and 98.8 µg Mg per 100 µl. The second type contained 20 µg Ba; 20 µg Sr; 0.16 µg Mn per 100 µl. In both cases 100 µl were pipetted on a Whatman 41 (Ø 50 mm) filter and allowed to dry. Thereafter filters were folded and packed in plastic envelopes. Blanks of the different filter types were analyzed. Samples with entire diatom cells were submitted to a short irradiation (1 min.) and immediately submitted to γ-spectrometry on a Ge-Li detector during 10 min. Since in this case enough material was present, all isotopes, except S, could be measured after this short irradiation. The siliceous fractions were irradiated during 3 min. A first γ-spectrometry, immediately after the irradiation, allowed to analyse for Al, Cu, V, Mg, Ca. 60 to 100 min. Later these samples were submitted to a second γ-spectrometry, to analyse for Ba, Sr, Mn. At most two samples were irradiated together, accompanied by both types of standards.

The data for Ba are discussed in § 4.3.1 in part II. The data for Al, V, Cu, Mn, Sr, Mg are given in appendix I.

PART II

OCEANIC SUSPENDED BARIUM AND BARITE

page

INTRODUCTION

In this part it is tried to give a satisfactory answer to the following questions:

- Is particulate Ba in suspended matter present mainly as a phase, distinct from the terrigenic fraction ?
- How does particulate Ba behave in the watercolumn, as compared to elements characteristic of the biogenic and terrigenic components in suspended matter ?
- What is the contribution of $BaSO_4$ as a carrier of Ba in suspended matter?
- How is suspended $BaSO_4$ introduced to the watercolumn ?

Throughout part II, the discussion will be conducted at two different levels. As concerns the quantitative analyses of Ba , the results of these will be discussed first for a selected station in the Argentine Basin (GEOSECS station 67), for which the largest number of samples was investigated. Thereafter we will extend the discussion to other stations of the World Ocean. As concerns that part of the study pertaining to suspended barite, we will discuss first the distribution and the occurrence of the different morphological types of suspended barites in the World Ocean, before considering quantitative data for the specific case of GEOSECS station 67. These data are then complemented with quantitative data for two additional stations in the North Atlantic (GEOSECS stations 3 and 5).

CHAPTER 1

THE SUSPENDED BARIUM IN THE OCEAN

1.1 THE STUDY OF A SELECTED PROFILE IN THE SOUTH-ATLANTIC OCEAN: GEOSECS STATION 67 (ARGENTINE BASIN)

GEOSECS station 67 is the station we investigated most completely. At this station INAA measurements of particulate Ba, Sr, Ca, Al, V, Mn, Cu were obtained for a total of 41 samples (the data for Sr,Mn,V,Cu,Al,Ca are reproduced in appendix II, in Table A.II.1).
Further, GEOSECS shipboard data for potential temperature, salinity, dissolved PO_4-P, NO_3-N, O_2, titration alkalinity, total CO_2, sea water density, as well as GEOSECS shore based collected data for total suspended matter were available (Tables A.III.1 to A.III.4, in appendix III).

1.1.1 The profile of particulate Ba at GEOSECS station 67

The station 67 particulate Ba (Ba_p) profile is reproduced in Table II.1 and Figure II. 6 (page 104). In this table, the fraction of total Ba_p, carried by the detritic,aluminosilicate phase is also given. It was deduced as discussed in the following. Extensive SEM-EMP and neutron activation analyses of the Al concentration in aluminosilicate particles present in the same suspended matter samples that were analyzed for Ba, confirm that Al can be used as an index of the aluminosilicate content in suspended matter (Chesselet et al.,1976; Buat-Menard and Chesselet, 1979).

TABLE II.1: Profile of particulate Ba at GEOSECS station 67 in the Argentine Basin, as measured by INAA. The data are expressed in ng/Kg sea water and in ppm of total filtered matter. Confidence levels = 2σ %. The fraction of total particulate Ba, associated with the detritic or aluminosilicate phase is also indicated; for calculation mode see text.

Depth in m	ppm	ng/Kg	2σ%	Fraction associated with aluminosilicates in %
GEOSECS station 67 (44°58'S-51°10'W); watercolumn: 5902 m				
10	126	13.3	51	23.5
42	155	19.5	54	8.5
62	166	20.8	16	7.0
105	708	45.2	15	5.5
151	1550	38.5	9	1.8
199	1969	50.5	10	2.6
251	1968	60.6	5	2.8
300	3636	91.2	24	1.2
353	2637	66.9	4	1.9
405	2379	49.2	12	2.2
445	2744	50.5	11	1.5
445	2431	56.4	3	2.2
658	2358	50.5	7	3.7
760	3797	40.8	21	2.7
857	2381	54.8	7	4.2
953	2992	42.1	10	2.7
1053	2579	50.0	6	2.0
1127	3252	29.6	11	4.4
1316	3857	40.9	4	3.0
1438	1925	38.4	14	4.3
1499	3472	48.2	5	3.8
1590	2408	32.2	14	3.7
1741	2907	39.7	6	1.6
1959	4555	36.5	11	3.3
2193	3067	37.7	4	5.3
2392	2144	23.2	17	4.7
2574	2352	25.6	5	5.9
2758	1534	27.8	19	4.1
1982	3004	28.2	5	4.8
3444	2398	15.7	12	5.9
3601	1024	19.2	9	8.9

TABLE II.1: Particulate Ba at GEOSECS station 67, continued.

Depth in m	ppm	ng/Kg	2σ%	Fraction associated with aluminosilicates in %
GEOSECS station 67				
3841	318	22.6	8	7.4
4035	2390	19.2	8	8.0
4221	2190	31.3	21	5.9
4424	1750	19.4	9	11.3
4633	4281	26.0	28	5.4
4839	2004	20.8	16	15.6
5051	1497	19.6	31	18.0
5304	1920	33.0	13	22.6
5526	759	17.4	43	35.5
5599	622	29.6	20	67.4
5634	1503	98.3	24	23.4
5804	1097	170.0	28	64.1

These analyses confirm estimations of Arrhenius (1963) that particulate Al represents 7 to 9% of the inorganic component of total suspended matter (TSM). This quantity is equal to the Al content of shales: 8% by weight (Turekian and Wedepohl, 1961). In short, one assumes the suspended detritic matter to have the composition of shales. The fraction of total particulate barium associated with detritic matter is then:

$$\left[\frac{Ba_{shales}}{Al_{shales}} \cdot Al_{sample}\right] / Ba_{sample},$$

with Ba_{shales} = 600 ppm and Al_{shales} = 80,000 ppm (Turekian and Wedepohl, 1961)

The first important conclusion one must draw from the Ba profile in Table II.1, is that the total particulate Ba amount is largely in excess over the fraction that is associated with aluminosilicates, confirming the earlier findings of Darcourt (1973). In bottom waters this excess is reduced. This is discussed below.

A Ba_p maximum of 94 ng/Kg sw occurs at 300 m in surface water. In deeper water the Ba_p concentration decreases to 20 ng/Kg sw while in approach of the sea floor the Ba concentration increases again to reach a peak value of 170 ng/Kg sw at 5804 m. This increase is related with a sharp increase in the content of particulate Al (Table A.II.1 in appendix II) and in total suspended matter (from

10 µg/Kg sw at 5000 m to 150 µg/Kg sw at 5804 m (Table A.III.4 in appendix III). This indicates that these bottom samples were taken in the nepheloid layer, which is well developed in the Argentine Basin (Ewing and Eittreim, 1977). From Table II.1 it appears that this sharp increase in Ba_p is only in part (for 64%) due to the presence of alumino-silicates. The remaining non-terrigenic fraction (36%) is still high in terms of absolute concentration (61 ng/Kg sw), compared to values for intermediate and deep water (20 ng/Kg). This can be explained by the fact that sediment resuspension introduces also a non-terigenic Ba phase to bottom water. This phase is likely to consist of authigenic, sedimentary barite, which was observed by Church (1970) to represent the main Ba phase in the carbonate-rich sediments of the East Pacific Rise.

For the watercolumn extending above the bottom waters at station 67, it is clear that the distribution of Ba_p is not controlled by the input of terrigenic matter. How does particulate Ba behave then, when compared with elements of the particulate phase which are known to be controlled biologically ?

1.1.2 Comparison of the Ba_p profile with those of Sr_p and Ca_p, as biologically controlled elements

The profiles of particulate Sr and Ca are given in appendix II, Table A.II.1 . In Figure II.1 Ca_p

FIGURE II.1

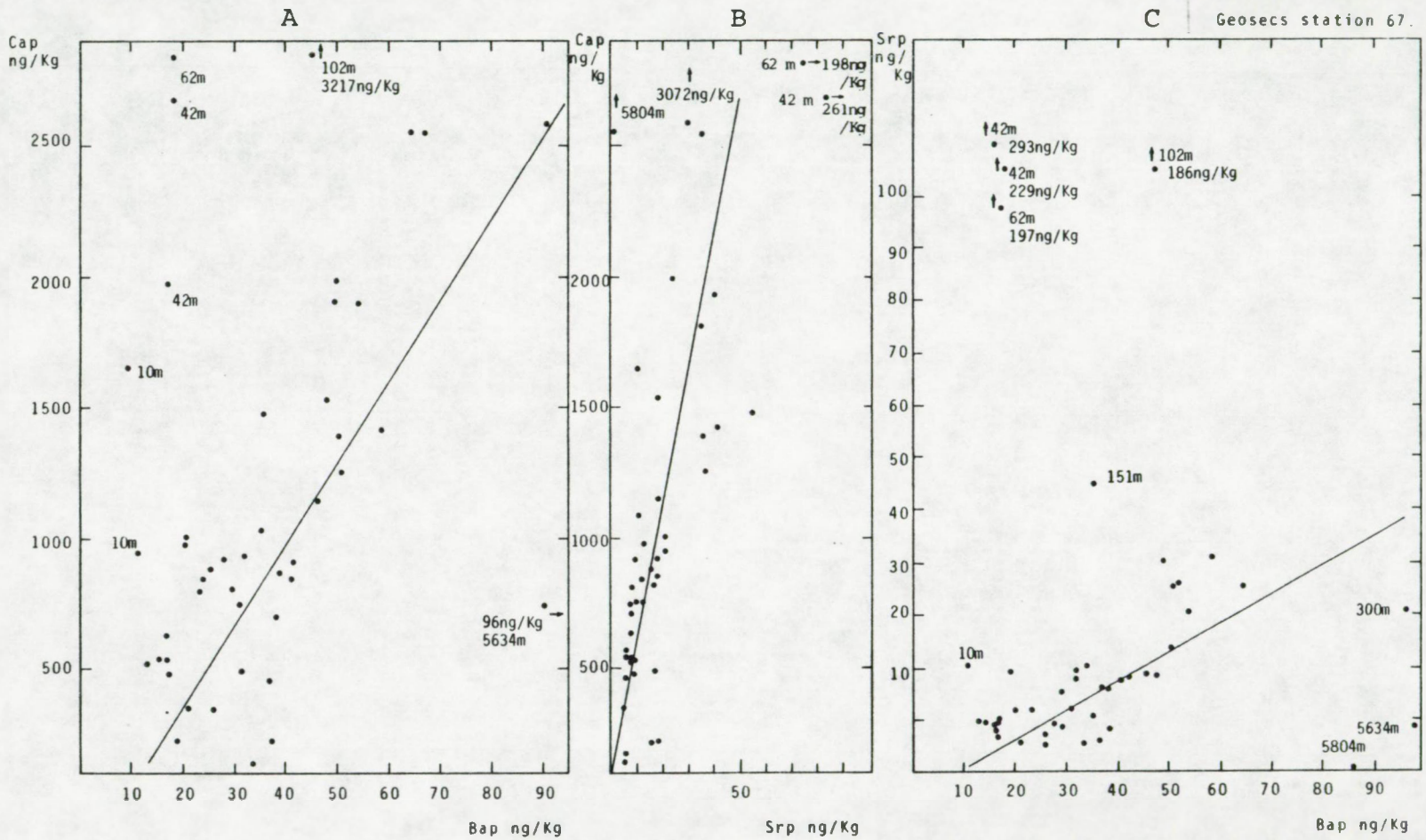

GEOSECS station 67. Covariation of, A: Ca_p and Ba_p; B: Ca_p and Sr_p; C: Sr_p and Ba_p. Labelled dots were not taken into account when computing the regression lines.

is plotted versus Ba_p; Sr_p versus Ca_p and Ba_p versus Sr_p. It appears from this figure that Ba, Sr and Ca are positively correlated,when omitting the samples taken in the first 200 m of the watercolumn and in bottom water (= below 5000 m), which are regions where the effect of source proximity (respectively biological activity and resuspension of sediments) is sensed. For the depth range between 200 and 5000 m (36 samples), the following Bravais-Pearson correlation coefficients and regression lines are calcuated:

$$r_{Ba,Sr} = 0.58;\ Y_{Sr} = 0.53X_{Ba} - 4.4$$

$$r_{Ba,Ca} = 0.67;\ Y_{Ca} = 31.2X_{Ba} - 269.5$$

$$r_{Sr,Ca} = 0.76;\ Y_{Ca} = 59.4X_{Sr} - 7.5$$

All correlations are significant at the 99% confidence level. Thus for the main part of the watercolumn Ba_p, Sr_p and Ca_p behave similarly, reflecting the existence of similar processes governing their vertical distribution. In surface and bottom waters each element appears to have a specific behaviour.

1.1.3 The possible carrier phases of Ca_p, Sr_p and Ba_p

The importance of $CaCO_3$ producing Coccolithophorids and $SrSO_4$ producing Acantharia as a source of suspended Ca_p and Sr_p is well documented (Aubey, 1976; Honjo, 1976; Botazzi and schreiber, 1971; Bishop et al.,1977;1979; Brass and Turekian, 1974). Since the Ba_p maximum occurs in, or close

to the euphotic zone were the Ca_p and Sr_p maxima occur (Table II.1,and Table A.II.1, in appendix II), the formation of Ba_p may also be related with biological activity. However,the occurrence of the Ba_p, Sr_p and Ca_p maxima at different depths in the surface waters, emphasizes the specificity of biological activity leading to towards the production of particulate Ba, Sr and Ca, and this is responsible for the lack of correlation between these three phases in the first 200 m of the watercolumn.

The Ca_p fraction is shown by Aubey (1976), who studied the Ca_p profile at GEOSECS station 67, to be composed in the mean for 60% of a hydrosoluble fraction that is eliminated after a short rinse of the samples with deionized, distilled water at pH 5.5. It is shown that this hydrosoluble fraction is composed of gypsum (see discussion later in section 2.1 of part II). Two possible origins are proposed: either these particles were precipitated during dessication of sea water droplets on the membrane filters and were not eliminated due to insufficient rinsing on shipboard, or they are genuine structures, present in sea water before the filtration operation. The presence of an organic coating could explain the fact that they were not eliminated during the shipboard rinsing of the filters. Several months of storage of the filters might have resulted in the oxidation of this organic coating (trough bacterial activity, Chesselet, pers. comm.). The fraction of total Ca_p that is carried

by suspended aluminosilicates is computed by applying the already discussed Al-index method:

$$\left[\frac{Ca_{shale}}{Al_{shale}} \cdot Al_{sample}\right] / Ca_{sample}$$

with Ca_{shale} = 22,000 ppm and Al_{shale} = 80,000 ppm (Turekian and Wedepohl, 1961)

The detritic Ca fraction is given in Table A.II.1 (appendix II). With the exception of the nepheloid layer where the Ca_p associated with aluminosilicates rises to 100% of the total amount present, the detritic Ca fraction is mostly less than 10%. The fact that the resuspended sediments in bottom water are $CaCO_3$ - free, is consistent with observations of Biscaye and Kolla (1976) of low $CaCO_3$ (< 10%) content in the sediments of the Argentine Basin. The fraction of total Ca_p that is neither associated with gypsum nor with aluminosilicates, consists essentially of coccoliths, of which 80% are Coccolithus huxleyi occurring either as discrete individuals or packed in small aggregates thought to be fecal pellets (Aubey, 1976).

Sr in suspended matter is essentially distributed over three different phases: celestite, organics and carbonate (Bishop et al.,1977, 1979). Some data exist on the relative importance of each of them. Bishop et al. (1977) observed, for the Equatorial Atlantic surface water, that 17% of total Sr_p in the 1 to 53 μm size range of the

particulate matter is bound to ion exchangeable positions on the organic matter. The importance of celestite as a carrier of Sr_p was emphasized by Brass and Turekian (1974), who showed that if Sr were introduced in deep water only by dissolution of carbonate tests, the concentration of Sr in the calcium carbonate would be 20,000 ppm. This is an order of magnitude higher than the Sr concentration measured in carbonate tests. Indeed, from measurements of Sr in coccolithal oozes (Thompson and Bowen, 1960; Turekian, 1964), pelagic foraminifera (Emiliani,1955) and marine molluscan shells (Turekian and Armstrong, 1960) it is deduced that these $CaCO_3$ skeletons contain an average of only 1500 ppm of Sr. We calculated the fraction of total Sr_p, carried by $CaCO_3$ tests, by considering that about 40% of the total Ca_p we measured is in the carbonate form (see discussion above) and by taking 1500 ppm as the Sr content of $CaCO_3$ skeletons. This $CaCO_3$- associated Sr fraction is given in Table A.II.1 in appendix II. It appears from this table that $CaCO_3$, with a maximum of 10%, is a minor carrier of Sr. The fraction of total Sr_p associated with detritic matter is calculated by applying the Al-index method:

$$\left[\frac{Sr_{shale}}{Al_{shale}} \cdot Al_{sample} \right] / Sr_{sample}$$

with $Sr_{sale} = 300$ ppm and $Al_{shale} = 80{,}000$ ppm
(Turekian and Wedepohl, 1961)

It is seen from Table A.II.1 (appendix II) that outside the nepheloid layer, aluminosilicates account generally for less than 10% of the total Sr_p. In the nepheloid layer this fraction rises up to 100% of the total Sr amount. Above bottom waters, the combined $CaCO_3$ and aluminosilicate phases contribute for 20% of total Sr_p . When adding this amount to the Sr fraction, associated with organic matter (some 17%) it is seen that about 60% of the total Sr_p amount is carried by another phase, which must be supported by celestite. However, one can not exclude the possibility that part of these 60% are incorporated in gypsum, which represents the main fraction of total Ca_p (see above).

For Sr and Ca it is probable that they occur essentially as distinct particulate phases in suspension.

Ba in suspended matter is probably present in different particulate phases, with $BaSO_4$ being one of these. $BaSO_4$ occurs as well crystallized barite particles, as shown in § 2.3.4 in part I. In § 1.1.1 of this part, we have evaluated the contribution of suspended aluminosilicates to total Ba_p. This detritic matter was shown to represent only a minor carrier of Ba. Other carriers of Ba can be, the siliceous and calcareous skeletons, and the particulate organic matter. These particulates are known to contain only trace amonuts of Ba (Martin and Knauer, 1973). However,since they compose a large fraction of total sus-

pended matter, their contribution to total Ba_p can be important. This matter is discussed later in chapter IV of this part.

The following approach will enable to select the most important one of the possible Ba-carrier candidates which were aligned above. This approach will further enable to identify the main processes which govern the distribution of particulate Ba, Sr and Ca in the water-column.

1.1.4 Interpretation of the GEOSECS station 67 multi-variable system by Factor Analysis

The successful application of Factor Analysis to the field of geochemistry has been demonstrated for instance by Spencer et al. (1968) and Herbosch (1974 a,b). This method provides a way to uncover, through the analysis of the experimental data, the natural fundamental variables (= factors), which govern the behaviour of the parameters under study. The method performs a condensation of a multi-variable system into a system with a reduced number of variables (= factors),

without loss of information and makes possible an interpretation of these factors in terms of geochemical processes. Mathematically factor analysis is an attempt to fit the following a priori linear model (Harman, 1967) :

$$z_j = a_{j1} \cdot f_1 + a_{j2} + \ldots\ldots a_{jm} \cdot f_m + a_j \cdot v_j$$

where z_j is the reduced variable j; $f_1 \rightarrow f_m$ are a series of factors common to several variables; v is a specific factor, proper to each variable; $a_{j1} \rightarrow a_{jm}$ are factor coefficients called factor loadings, expressing the degree to which the value z_j is dependent from each factor (common and specific). All factors are mutually independent (= orthogonal factors). In this model it is assumed that each initial variable is linearly dependent of a series of fundamental, hypothetical variables called factors, in which common factors (proper to several variables) and specific factors (proper to each variable) are distinguished. It is further possible to compute the reduced values (= factor scores) of these fundamental variables or factors. By plotting these factor scores in a factor space it is possible to display possible similarities between samples.

The basic data on which factor analysis is build up, is the correlation matrix in which all variables are considered. The successive steps performed to obtain the factor matrix (VARIMAX factor matrix) are given in appendix IV. In appendix IV we have also reproduced the computer prints of the results of the intermediary steps. The orthogonal solution

(VARIMAX matrix) explains successfuly the nature of the factors under study.

A. Analysis of the complete station 67 profile

We have applied factor analysis to all elements analyzed by INAA; these are: particulate Ba,Sr,Ca,Al,V, Mn and Cu. With exception of the Ba profile which is reproduced in Table II.1, all other profiles are given in Table A.II.1 (appendix II). Also considered in this approach are several parameters measured either on shipboard or on shore during the GEOSECS campaign: dissolved sil., PO_4-P, NO_3-N and O_2; carbonate alkalinity; total suspended matter concentration; salinity and potential temperature (see Tables A.III.1 to A.III.4 in appendix III).

In total 15 variables and 41 samples were considered. All data were Log - transformed. The factor matrix is reproduced in Table II.2. In this matrix 4 orthogonal factors called common factors represent 88.7 % of the variance of the initial data (= variance of 15 variables in 41 samples) and account for the whole of the correlations of the 15 variables analyzed at station 67. In Table II.2 are also reproduced the significant factor loadings, the contribution of the factors to the total variance and the communalities or common variances, which represent that part of the variance that accounts for the intercorrelations of the variables. Very high communalities indicate that the distribution of the

corresponding variables is not influenced by important casual variation. Figure II.2 represents the factor diagram corresponding to Table II.2. It is more explicit than the bare numbers and will serve as the basis for the interpretation of the factors. The factors are reproduced in a rectangle with the abscissa representing the respective contributions to the variance in common factors (this is the importance of each factor) and with the ordinate representing the weight (loading) of each variable in each factor. As a result co-variant groups are clearly emphasized. The four selected factors were identified as follows:

factor 1: Represents the fast dissolution of biogenic inorganic components ($CaCO_3$ and/or $CaSO_4.2H_2O$; $SrSO_4$) and the regenaration of nutrients, through the oxidation of particulate organics.

factor 2: Represents the input of detritic, continental matter in the watercolumn, as well as the resuspension of fine bottom sediments. This factor is explained in appendix IV.

factor 3: Represents the dissolution and advective transport of a slowly dissolving Ca ($CaCO_3$?) and Ba ($BaSO_4$?) phase.

factor 4: Is a one-element factor for Cu. It is discussed in appendix IV.

Factors 1 and 3 are discussed now in more detail:

Table II.2 : Factor diagram of the complete GEOSECS station 67 profile

variable	factors				communalities
	1	2	3	4	h^2
Ba		-.37	.81		.801
Sr	.84				.821
Ca	.65		.56		.756
Al	-.25	-.93			.950
V		-.90			.848
Cu		-.28		-.93	.966
TSM	.49	-.71			.789
Mn		-.95			.920
Calk	-.77		-.56		.973
sal			-.90		.863
Tpot	.72	.49	.35		.917
sil	-.93		-.28		.980
PO_4	-.98				.976
$-NO_3$	-.98				.981
O_2	.77		.30		.764
Contribution of the factors to the total variance					Σh^2
%	40.1	24.7	16.6	7.3	13.305
cumul. %	40.1	64.8	81.4	88.7	

* factor loading $< |0.25|$ have been omitted, since they are not significant according to criteria of HARMAN (1967).

factor 1: (40.1% of the total variance) is statistically the most important. It is a bipolar factor with high positive loadings for Sr_p, Ca_p, Tpot; a significant loading for total suspended matter (TSM); high negative loadings for dissolved PO_4, NO_3, sil., and carbonate alkalinity (Calk). The opposition of elements of the particulate phase (Sr_p, Ca_p, TSM) to sil. an element of the dissolved phase, resulting from the dissolution of opal (diatom tests) and to Calk, a variable that regulates the dissolution of the $CaCO_3$ phase, points towards a dissolution process. The Sr_p phase consists probably of Sr-enriched organics, while the Ca_p phase can be either $CaCO_3$ or $CaSO_4.2H_2O$, or both. A definitve identification of this Ca_p phase will be possible when having discussed factor 3. Further, the opposition of O_2 to PO_4 and NO_3 is interpreted as reflecting the oxidation and mineralization of the organic matter in sea water. The significant loading for TSM points towards the fact that all these biogenic components represent an important fraction of the total suspended particulate matter. We propose factor 1 to represent the dissolution of gypsum, calcium carbonate and celestite particles and the regenaration of nutrients trough the oxidation of particulate organics. The fact that the same factor reflects a degradation process, affecting both inorganic and organic particulates, suggests that the former particulates consist of fast dissolving components.

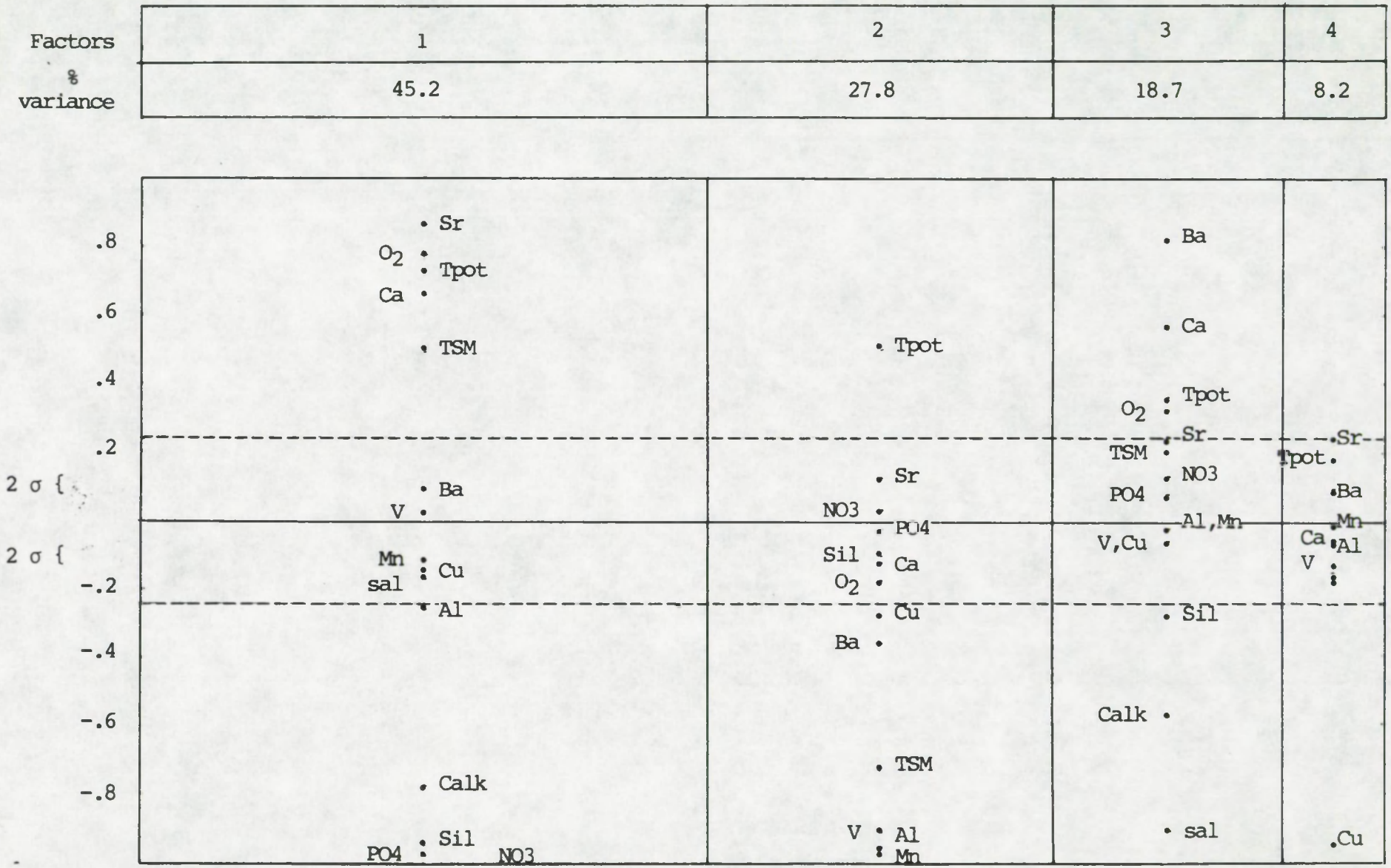

Factor loadings < | 0.25 | (= 2 σ) are not significant according to criteria of Harman (1967)

Figure II.2: Factor diagram of the complete profile of GEOSECS station 67

Factor 3 (16.6 % of the total variance), a bipolar factor, has positive loadings for Ba_p, Ca_p, Tpot, O_2 and negative loadings for sal, Calk and sil. The presence again of a high factor loading for Ca is quite surprising.

Since the square of a factor loading represents the fraction of the variance of a variable, that is accounted for by that common factor, it is easily deduced that for Ca_p:-

- factor 1 accounts for 42 % (= 0.65^2) of its total variance, or as compared to its communalities, for 55 % (0.42/0.76; see Table II.2) of its intercorrelations.
- factor 3 accounts for 31 % (= 0.56^2) of its total variance, or as compared to its communalities, for 41 % of its intercorrelations.

It is evident that the distribution of the particulate Ca is governed by two fundamental and independent processes. (we remind here that an orthogonal solution was imposed). The first of these fundamental processes (= factor 1) was identified as the dissolution of the $CaCO_3$ or $CaSO_4.2H_2O$ phases. A second Ca_p phase appears to exist with a similar distribution as Ba_p, but quantitatively less important than the Ca_p phase whose distribution is governed by factor 1. The observation by Aubey (1976) that the major part (60%) of the Ca_p amount detected at station 67, is carried by gypsum (see also § 1.1.3 and later, section 2.1 in this part) explains the dichotomic behaviour of Ca_p.

The high loading for Calk and the significant loading for dissolved sil. in factor 3, opposed to high loadings for Ca_p and Ba_p is assumed, such as for factor 1, to reflect a dissolution process. This indicates that Calk can be regarded as a "general" indicator of dissolution. In factor 3 the opposition of Ca_p, Ba_p to salinity can be interpreted as reflecting a relationship between the distribution of these particulates and hydrology. The Tpot-salinity diagram in appendix V shows that a pronounced stratification of the watercolumn exists at GEOSECS station 67. We can therefore assume that influences of advective transport mechanisms are observed here. This is analyzed more extensively below, when discussing the results of factor analysis as applied to the reduced station 67 profile. Since effects of advective transport are visible, the dissolution of the Ca_p and Ba_p phases must be slow. Parallel to this, evidence exists that the Ca_p phase governed by factor 1 is in fact a fast dissolving one: Indeed, since Ca_p and Sr_p are opposed to dissolved PO_4 and NO_3, they are likely to be involved in a fast regenarative cycle, similar to the one of phosphate and nitrate. This fast dissolving Ca_p phase in factor 1 is then more likely to consist of gypsum, while the slowly dissolving Ca_p phase in factor 3 would consist of $CaCO_3$, shown by Aubey (1976) to be carried essentially by coccoliths. The dependency of the vertical distributtion of $CaCO_3$ on advective transport was also noticed by Aubey (op.cit.). In the case of GEOSECS station 67 Aubey obser-

ved a very pronounced decrease in number of coccoliths at 1959 m (500 individuals/litre) while above and below this depth coccoliths were more abundant up to 3 orders of magnitude (10^4 individuals/litre). Aubey shows that this $CaCO_3$ anomaly is closely related with the presence of AAIW* (Antarctic Intermediate Water) in which the saturation degree, expressed as $[CO_3^{2-}]_{measured}/[CO_3^{2-}]_{calculated}$ is close to unity, the saturation limit, while waters above and below are oversaturated with respect to $CaCO_3$.

To resume, we propose factor 3 to represent the slow dissolution and the advective transport of calcium carbonate and of the particulate Ba phase. The significant loadings for Ca_p and diss. sil., besides Ba_p, suggest an association of Ba with calcareous and siliceous particles, which both are slowly dissolving phases as compared to celestite and gypsum. However, this apparent covariation of Ba_p with Ca_p and silica can be fortuitous. It can result merely from the fact that these 3 particulates are to a large degree affected in a similarly way by dissolution and advection. Later, in chapter 4 of this part, the contribution of calcareous and siliceous debris to the total Ba_p content of suspended matter is evaluated. It appears that for intermediate and deep waters, such debris account only for a maximum of 8% of total Ba_p, while this can attain 50% in surface waters. Barite thus emerges as the best candidate as main carrier of Ba_p.

---

* The hydrological situation of station 67 is given in appendix V.

The factor scores which are the values of the fundamental variables (the factors) for each sample, were set out in the factor space composed of factors 1 and 3. This factor space is reproduced in Figure II.3.A. It appears that the samples form clusters corresponding to the watermasses identified in the Tpot-salinity diagram (appendix V). From Figure II.3.A we see that:

- Down to 251 m no clustering occurs.
- Four samples (300 to 445 m) cluster together, representing the thermocline and sub-thermocline waters.
- Four samples (857 to 1053 m) which compose the core of the AAIW, are separated from the thermocline and sub-thermocline waters by a sample at 658 m with an intermediate score.
- Five samples (1127 to 1590 m) located in between the AAIW and the NADW core (see Figure A.V.1 in appendix V), group together. They coincide with the upper mass of Circumpolar Water (CPWu). Two samples (1741 and 1959m) identify nearly entirely with AABW and more specifically with the lower mass of CPW (CPWl).
- Three samples (2392 to 2574 m) appear as an isolated group with no affinity at all with the waters above them and but slightly related with the AABW group. They correspond to the NADW core, limited to a narrow depth interval at these latitudes.
- Twelve samples (3051 to 5304 m) form the AABW group, which consists of Weddell Sea Deep Water (WSDW) and CPWl masses.
- The 5634 m sample behaves like the CPWu core samples.

FIGURE II.3: A. Samples of the complete station 67 profile, set out in the factor space composed of F I and F III.
B. Idem for the reduced station 67 profile

Numbers = sample depths; letters = symbols for watermasses, as discussed in the text and appendix V.

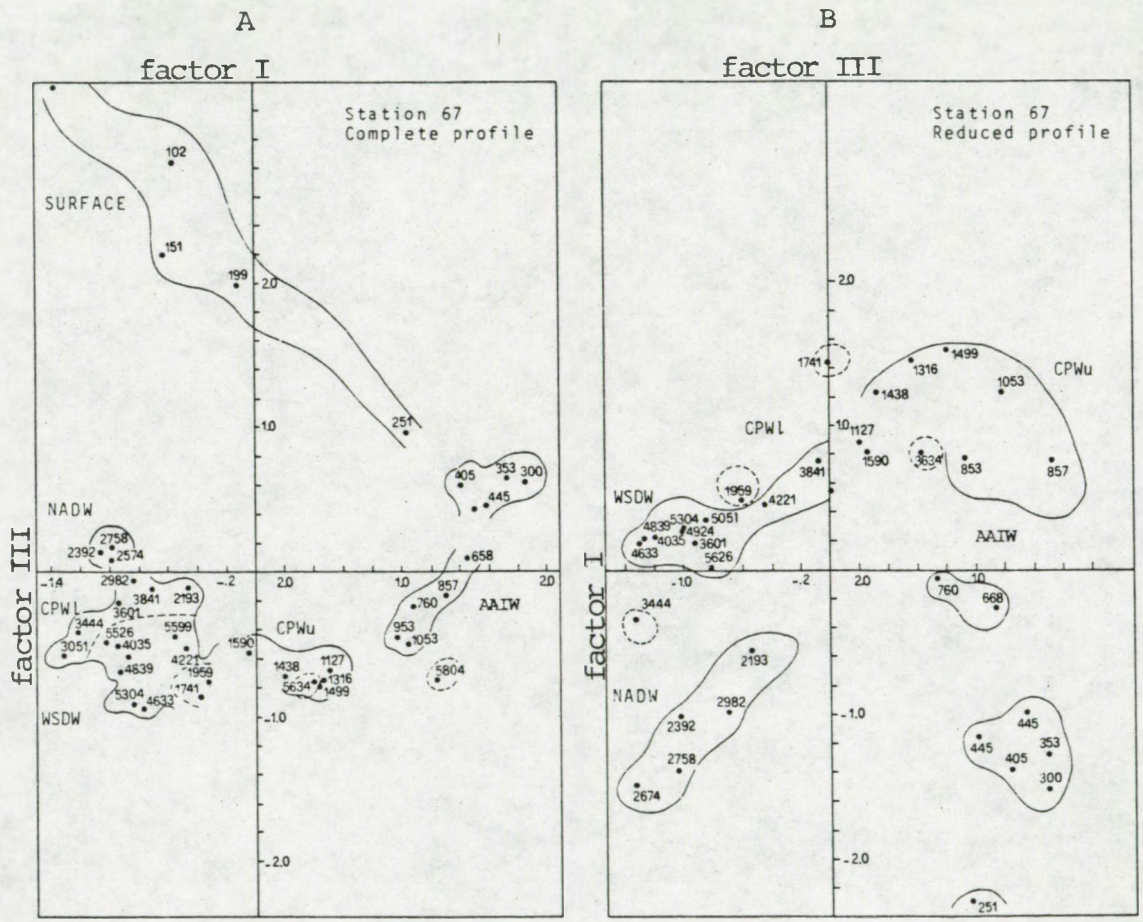

- The bottom-most sample (5804 m) seems unrelated with the other samples.

From these observations it is clear that the elements with high loadings on factors 1 and 3, all appear to behave partly as conservative elements in the sense that they remain associated up to an important degree with their original watermasses. Further, the transition between NADW and AAIW above it is shown to be very sharp, pointing towards small vertical exchanges. The samples in CPW1, WSDW and some of the CPWu masses have similar characteristics, reflecting a similar origin .

B. Analysis of the reduced station 67 profile

The surface most waters are affected by input effects, due to organic productivity, eolian and river input while the bottom waters are affected by sediment resuspension. The elimination of these samples from the profile is therefore likely to allow an easier interpretation of the processes that govern the distribution of the different variables on from the moment they are introduced into the watercolumn. In other words, in this approach the "noise", due to complex processes in the surface-most and bottom-most regions should be eliminated.

All samples above 251 and below 5304 m were eliminated for this second analysis.

The factor matrix is presented in Table II.3 and Figure II.4.

Table II.3: Factor diagram of the reduced GEOSECS station 67 profile.

variable	factors				communalities
	1	2	3	4	h^2
Ba	.85				.780
Sr	.82		-.29		.758
Ca	.71		-.46		.785
Al		-.90			.910
V		-.89			.809
Cu				.92	.935
TSM	.49	-.53		.50	.778
Mn		-.95			.923
Calk	-.78		.54		.960
sal	-.89				.828
Tpot	.61	.63	-.37		.923
sil	-.75		.60		.978
PO_4			.93		.963
NO_3	-.25		.94		.968
O_2	.40	-.29	-.75		.812
Contribution of the factors to the total variance					Σh^2
%	32.2	23.7	23.2	8.4	13.111
cumul. %	32.2	55.9	79.1	87.5	

* factor loadings $<|0.25|$ have been omitted, since they are not significant, according to criteria of HARMAN (1967).

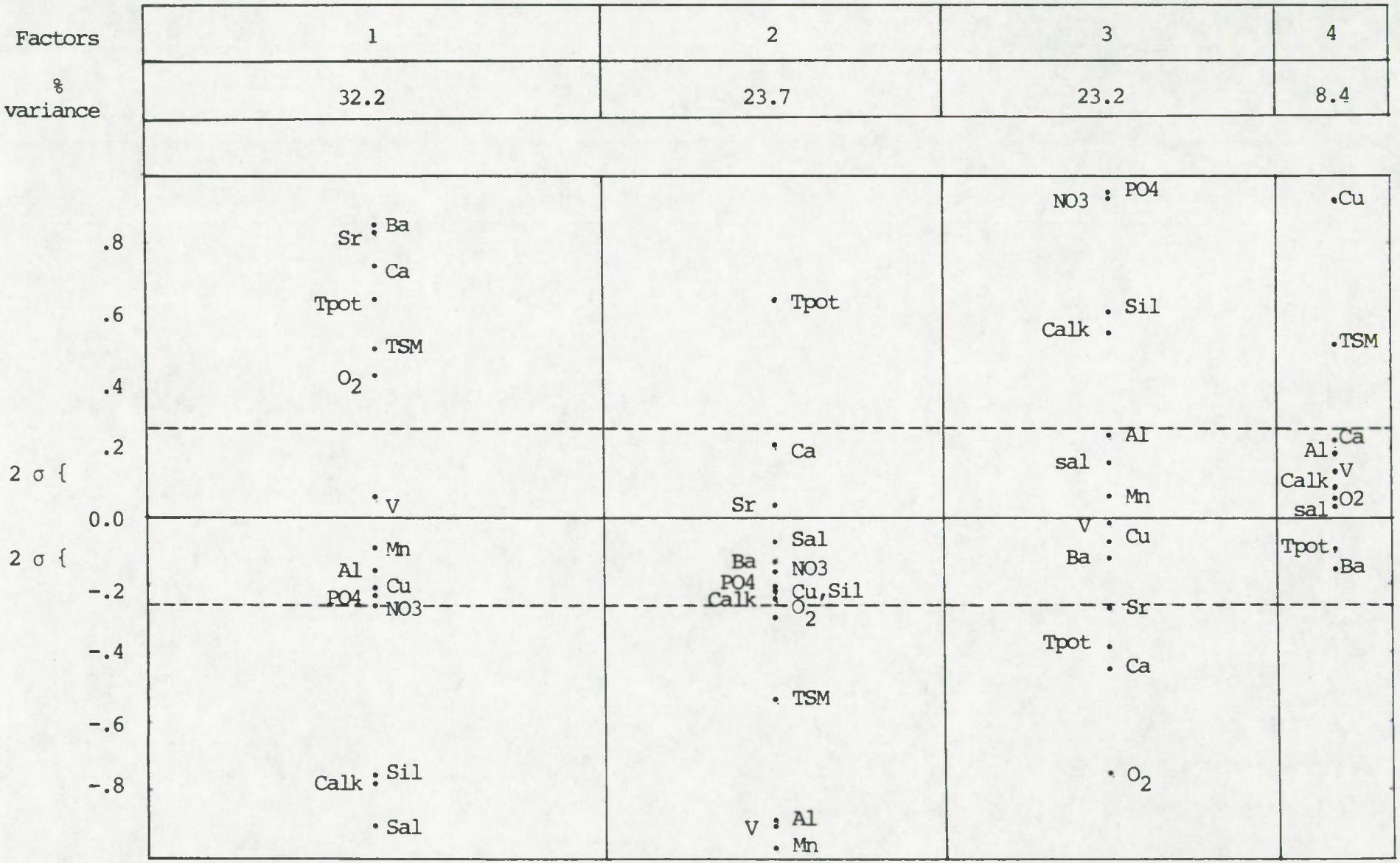

Factor loadings < |0.25| (= 2 σ) are not significant, according to criteria of Harman (1967)

Figure II.4: Factor diagram of the reduced profile of GEOSECS station 67

Again, four factors are selected, representing a nearly identical part (87.5 % compared to 88.7 % observed previously) of the total variance. However it appears that an inversion has occured between the previous factors 1 and 3. Further, the contribution to the total variance of the factor identified earlier as the dissolution and oxidation of the biogenic particulate phase composed of inorganic and organic fractions, has decreased. The interpretations of the factors obtained from this second analysis are globally similar to those proposed previously:

factor 1: Represents the dissolution and the advective transport of particulate Sr, Ca and Ba phases. These are resp. identified as slowly dissolving celestite and calcium carbonate, and barite.

factor 2: Remains unchanged (see above point A and appendix IV).

factor 3: Represents the fast dissolution of Acantharia debris and gypsum, as well as the regenaration of nutrients through oxidation of particulate organics.

factor 4: Remains unchanged (see appendix IV).

Factor 1 (32.2 % of the total variance) has high positive loadings for Ba, Sr and Ca, opposed to high negative loadings for sal., Calk. and diss. sil. . Sr has joined Ba and Ca and behaves dichotomically such as Ca does; indeed, Ca and Sr have also a significant loading on factor 3 (see below). The opposition in factor 1 of elements of the dissolved phase to elements of the particulate phase reflect a dissolution process. Further the high loading for salinity reflects the

influence of advective transport. This is illustrated by Figure II.5.A,B,C in which salinity is set out against total Ba_p, Sr_p and Ca_p. It appears from this figure that in all three cases (but especially for Ba_p),samples taken in the NADW and the AABW cluster together. In all 3 cases NADW and AABW can be distinguished. It thus appears that up to some degree the particulate Ba, Sr and Ca phases act as conservative elements, whose distributions are in part governed by advective transport mechanisms. Since effects of advective transport are clearly sensed , the dissolution of these three particulate phases must be slow. This puts restrictions on the possible composition of the Ca_p and Sr_p phases whose distribution is governed by factor 1. As discussed above, this Ca_p phase is probably present as carbonate, carried mainly by coccoliths. The Sr_p phase must be more resistant to dissolution than the Sr_p phase in factor 3. It can be assumed to consist of discrete $SrSO_4$ particles that we have observed to occur at much greater depths than the $SrSO_4$ debris of Acantharia, whose presence appears to be restricted to the first 500 m (see discussion in section 2.3 of part II). These discrete $SrSO_4$ particles have no biogenic habit and contain traces of Ca, Ba and K. These impurities can make them more resistant to dissolution. For Ba_p we propose again barite as the main carrier.

Figure II.5.A

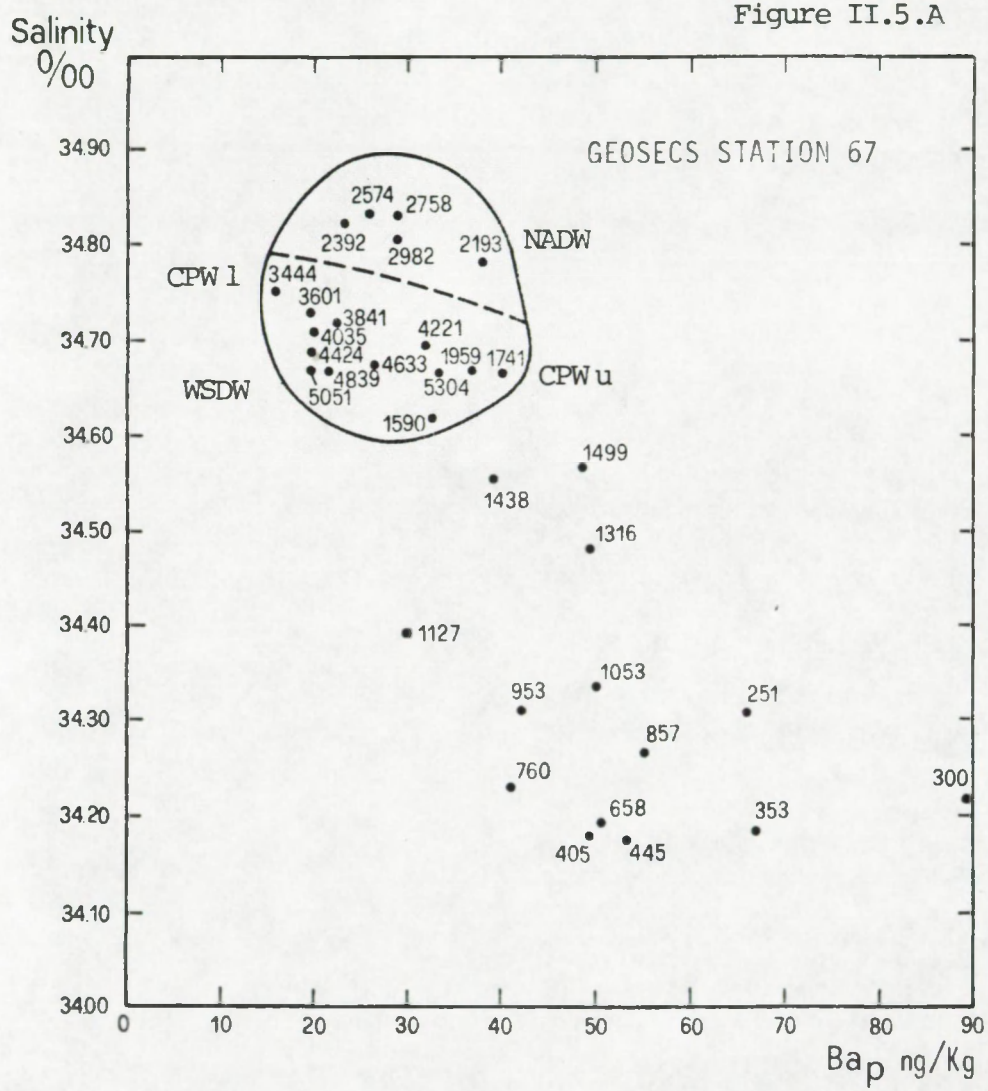

Figure II.5.B

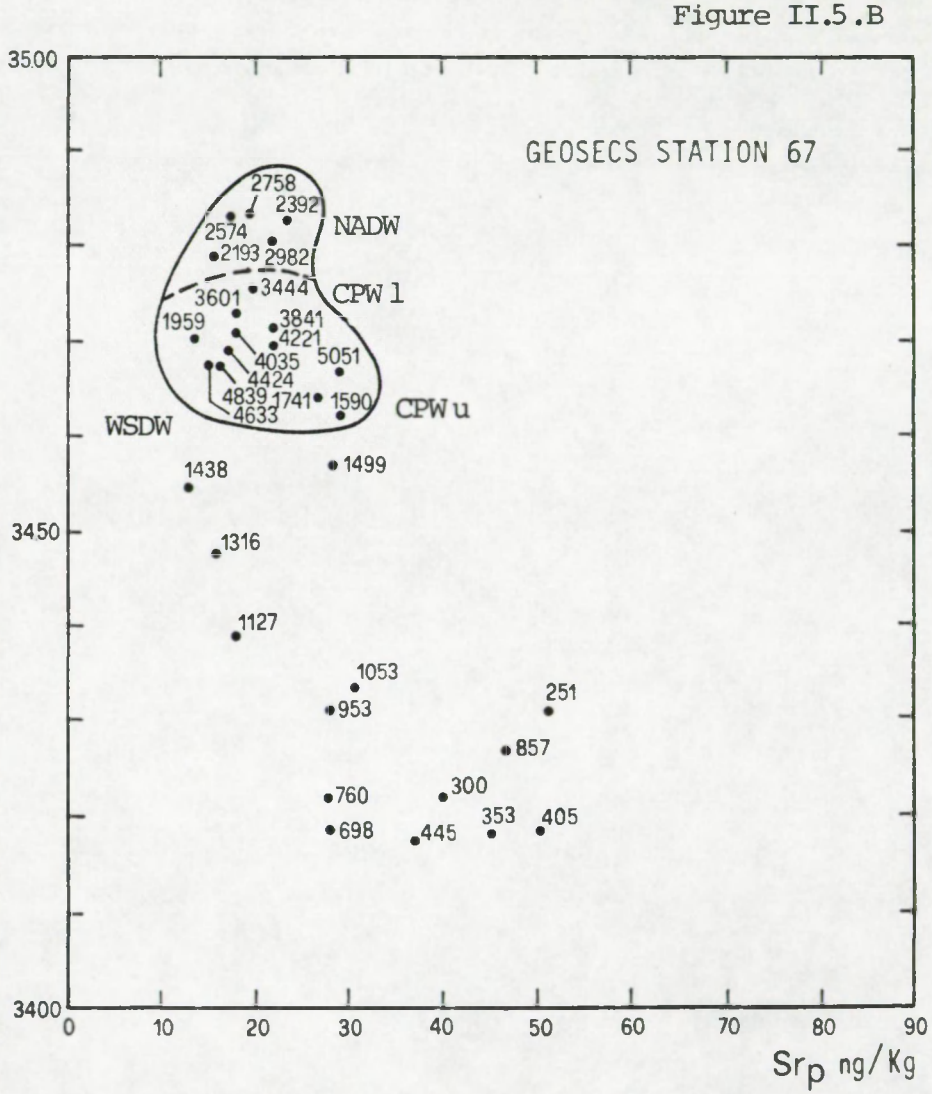

GEOSECS station 67: identification of deep-sea watermasses on the basis of their salinities and loads of particulate Ba and Sr.

Figure II.5.C

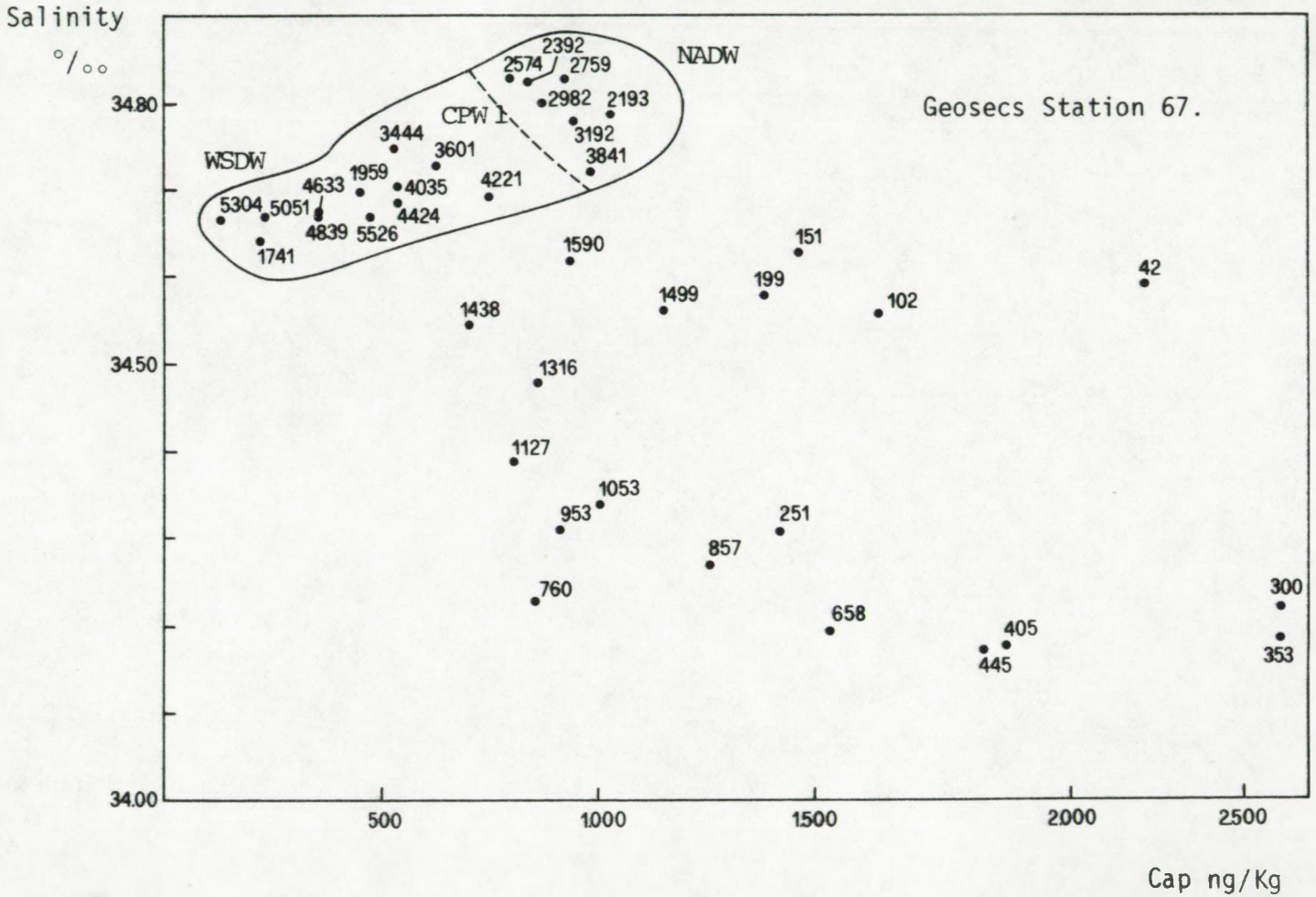

GEOSECS station 67: identification of deep-sea watermasses on the basis of their salinities and load of particulate Ca.

Factor 3: (23.2% of the total variance), shows Ca_p, Sr_p and O_2 to be opposed to dissolved PO_4, NO_3, sil. and Calk. The loading for Sr_p although significant, is much smaller than previously observed (see point A above). The same holds, but to a lesser degree, for Ca_p. Again we believe this factor to represent the dissolution process of fast dissolving Sr_p (Acantharia debris and Sr associated with particulate organics) and Ca_p (gypsum) phases, as well as the regenaration of nutrients through oxidation of particulate organics. As a result of the elimination of the surface-most samples, the contribution of this fraction to the total variance is lessened.

The distribution of the factor scores in the factor 1 - factor 3 factor space is reproduced in Fig.II.3,B . It is evident that the same clusters of samples are formed, as observed during the previous approach. The distinction between samples of the NADW and the Antarctic waters is however more pronounced now.

Conclusions: The susceptibility of part of the Ca_p and Sr_p phases to be influenced by advective transport mechanisms, suggests the existence for Ca_p and Sr_p of two disitnct phases: a slowly dissolving one and a fast dissolving one with a behaviour similar to the one of the organic fraction. For Sr_p the dissolution resistant phase is thought to consist of discrete $SrSO_4$ particles containing minor amounts of foreign elements, such as Ca, Ba and K. The Acantharia debris, together with Sr-enriched organics, are thought to compose the fast dissolving Sr_p phase. For Ca_p, indications exist that the slowly dissolving phase consists of $CaCO_3$, carried by coccoliths, while the fast dissolving Ca_p phase consists of gypsum.

Uncertainty exists concerning the genuinity of gypsum, although factor analysis speaks against the artefact hypothesis. The overall Ca_p profile shows production in the surface waters and dissolution at depth and is typical for biologically controlled materials. On the other hand, the gypsum profile would look genuine if during the sampling gypsum formation is related with the presence of organic matter. This would explain the opposition in factor 1 (see analysis of the complete profile in point A) of gypsum to dissolved PO_4, NO_3 which are elements that reflect the decomposition of organic matter. The observation of Aubey (1976) that re-filtration of sea water (on membranes of 0.45 μm pore size) that was pre-filtered resulted in the formation of gypsum crystals on the filter, emphasizes still

further the artefactial origin of this particulate Ca phase. At present, data exist also for GEOSECS stations 76 and 58, showing again that some 55% of the total Ca_p amount is hydrosoluble gypsum (Auger, CFR-CNRS, pers.comm.,1978).

The study of the GEOSECS station 67 profile has shown the presence in suspended matter of an excess Ba that is not controlled by the input of terrigenic matter to the watercolumn. This Ba seems to consist of a slowly dissolving phase whose distribution is controlled by the combined effect of a dissolution process and of advective movement with the main watermasses in presence. There exists evidence that this slowly dissolving phase is the least soluble Ba salt in sea water, barite.

The "excess" Ba is an ubiquitous component of oceanic suspended matter, as shown in the following section.

1.2 THE PROFILES OF TOTAL PARTICULATE BARIUM AT OTHER STATIONS IN THE ATLANTIC AND PACIFIC OCEANS

1.2.1 Tables and figures

Besides the station 67 profile, several other profiles were investigated for total particulate Ba by INAA: GEOSECS Atlantic stations 82, 58, 115, 120, 31, 37, 3, 5, 17; GEOSECS Pacific stations 282,269, 310, 257; HARMATAN (1971) station 15; MIDLANTE (1974) stations 9, 50, Madcap; TRANSAT (1975) stations 17, 37, Table II.4 reproduces the Ba_p profiles for all these stations. These profiles are also reproduced in Figure II.6, excepted those of GEOSECS stations 37, 115, 120, 17; HARMATAN station 15; MIDLANTE station 9 and TRANSAT station 37, for which only a few samples were analyzed.

1.2.2 Discussion of the data

Such as we have observed previously for GEOSECS station 67 (§ 1.1.1) the first 300 m of the watercolumn are characterized by the presence of a Ba_p maximum. In this region, peak values of: 49 ng/Kg sw (GEOS. st. 82; 200 m); 23 ng/Kg sw (GEOS. st. 58; 197 m); 36 ng/Kg sw (GEOS. st 31; 252 m);45 ng/Kg sw (GEOS. st 3; 28 m) are observed (Table II.4). In deeper waters concentrations decrease to less than 10 ng/Kg sw (GEOS. st 31; MIDL.1974, st Madcap) and to 20 ng/Kg sw (other stations). The occurrence of the Ba_p maximum in surface water is discussed further in chapter V of this part.

The 4 profiles of the Pacific Ocean show concentrations of Ba_p in the same range as observed in the Atlantic. An important increase of Ba_p is observed close to the bottom at GEOSECS station 282 in the Antarctic: from 21 ng/Kg sw at 4134 m to 75 ng/Kg sw at 5187 m. This is again related with the presence of a nepheloid layer, as demonstrated by the sharp increase in total Al_p at this depth: from 207 ng/Kg sw at 4134 m to 2264 ng/kg sw at 5187 m (see Table A.II.2; appendix II). At 5187 m the Ba fraction carried by aluminosilicates is 22% of the total Ba_p amount. This leaves some 59 ng Ba/Kg to be carried by other phases, what is larger than observed in intermediate and deep water. The most likely carrier of this excess Ba in bottom water is resuspended sedimentary barite (see also § 2.1.1, above), which is known to represent the main part of sedimentary Ba (Church, 1970).

As a general rule it can be said that the fraction of Ba associated with aluminosilicates increases close to the sea floor, but the <u>total</u> Ba_p amount increases only in those regions which are characterized by the presence of a nepheloid layer.

Table II.4: Profiles of particulate barium in the Atlantic and Pacific Oceans, as measured by INAA. The data are expressed in ng/Kg sea water and in ppm of total filtered matter. Confidence levels = 2 σ %. The fraction of Ba_p total, associated with the detritic or aluminosilicate phase is also indicated; for calculation mode see text.

A. GEOSECS Atlantic Ocean cruises

Depth in m	ppm	ng/Kg	2σ %	Fraction associated with aluminosilicates in %
GEOSECS station 82 (56°15'S-24°55'W); watercolumn: 7873 m				
1	100	8.2	11	5.8
47	495	43.6	5	1.5
97	630	35.4	19	1.7
200	1480	49.1	4	2.8
287	1046	36.6	7	2.0
372	1070	35.5	7	2.5
582	1030	19.5	11	4.7
832	1300	30.5	5	3.3
1180	2145	19.5	22	2.8
1577	1185	11.7	8	4.3
1786	1270	30.3	15	--- ♦
2186	2654	24.5	8	3.9
2386	2140	24.1	8	5.1
2583	1400	22.1	6	7.0
2789	140	2.8	30	49.7
3390	597	13.7	8	8.3
3592	1790	19.7	7	6.3
3783	3645	24.4	9	4.7
4296	427	11.3	10	14.2
4598	973	11.3	10	13.5
4901	813	20.8	11	8.9
5202	550	12.2	13	12.3
5502	724	12.1	30	17.3
5797	610	9.9	47	18.7
6100	6100	19.9	10	--- ♦
6502	1055	20.0	25	14.8

Table II.4: Particulate Ba, continued.

Depth in m	ppm	ng/Kg sw	2σ %	Fraction associated with aluminosilicates in %
GEOSECS station 58 (27°02'S-37°00'W); watercolumn:4588 m				
197	2460	23.4	22	3.6
278	1880	16.3	23	3.8
1786	1780	11.0	50	7.0
2085	762	9.6	50	10.6
3097	<1000	<5.0		>20.0
4422	480	11.3	60	64.8
GEOSECS station 37 (12°01'N-51°00'W); watercolumn: 5064 m				
349	1800	27.3	14	13.3
1940	1600	19.5	16	♦
GEOSECS station 31 (27°00'N-53°31'W); watercolumn: 5979 m				
1	<250	<10	3	>52.6
60	< 85	< 3		>11.3
152	<200	< 6		> 6.7
252	2464	36	48	1.5
403	<730	< 9		> 3.0
603	822	7	40	6.9
799	902	8	9	4.7
901	<1170	<10		> 7.5
1003	<720	< 6		> 9.6
1103	530	4	25	12.6
1900	<480	< 6		>13.1
2300	680	8	37	7.6
2700	<461	< 7		>15.5
3500	797	7	46	5.9
3700	234	3	30	14.5
4100	1140	4	29	2.6
4701	<2390	< 8		>14.0
5500	220	3	100	68.2

Table II.4 : Particulate Ba, continued.

Depth in m	ppm	ng/Kg	2σ%	Fraction associated with aluminosilicates in %
GEOSECS station 115 (28°04'N - 25°54'W); watercolumn:				
1145	481	14.1	12	4.7
1393	434	6.7	12	9.5
3732	< 75	< 0.8		66.0
GEOSECS station 3 (51°01'N - 43°01'W); watercolumn: 4283 m				
28	260	45.5	10	4.4
105	1390	27.8	9	7.6
274	3250	36.4	22	4.7
377	1450	36.9	9	2.4
464	1390	22.1	17	15.4
575	1210	20.8	26	12.5
813	6560	44.2	28	4.5
1083	1150	16.9	10	13.0
1376	710	14.9	7	10.1
1575	2230	46.3	10	8.4
1875	2730	35.1	70	6.0
2039	1000	16.9	10	17.8
2356	2730	35.7	32	6.4
2479	1260	18.6	14	12.9
2696	470	5.4	19	46.3
2989	880	33.6	19	11.3
3267	2080	29.5	37	8.5
3368	870	10.4	11	28.8
3630	430	10.1	12	39.6
4049	400	12.0	13	100.
GEOSECS station 17 (74°56'N - 01°07'W); watercolumn: 3740 m				
992	490	70.	16	♦
3005	660	76.	12	
3439	600	64.	13	

Table II.4: Particulate Ba, continued.

Depth in m	ppm	ng/kg	2σ%	Fraction associated with aluminosilicates in %
B. GEOSECS Pacific Ocean cruises				
GEOSECS station 282 (57°35'S - 169°36'E); watercolumn: 5502 m				
2131	2377	39.4	18	2.9
3034	1768	24.1	29	4.7
4358	1117	49.0	34	3.5
4134	1764	20.7	38	7.3
5187	1805	75.5	22	21.7
GEOSECS station 310 (26°55'S - 157°11'W); watercolumn: 5454 m				
1557	2728	30.6	29	2.0
2734	1040	9.7	60	6.3
3049	1136	12.8	50	3.5
3227	1081	11.5	50	20.6
3310	1978	26.9	27	1.6
3748	2267	23.7	31	2.8
4489	< 1750	< 2.7		> 29.2
4789	1363	14.7	50	6.2
GEOSECS station 269 (23°59'S - 174°26'W); watercolumn: 6371 m				
1253	692	10.5	60	2.4
2897	< 432	< 4.2		> 11.2
3342	668	9.2	55	6.0
3962	325	5.4	60	6.5
5172	241	9.3	47	51.6
6193	1351	9.2	57	35.7
6348	762	7.9	79	51.9

Table II.4: Particulate Ba, continued.

Depth in m	ppm	ng/Kg	2σ%	Fraction associated with aluminosilicates in %
GEOSECS station 257 (10°10'S - 170°00'W); watercolumn: 5177 m				
1263	1801	24.9	50	3.4
2464	2000	13.3	51	2.2
2813	1490	20.8	49	1.9
3737	1685	15.8	50	8.6
4234	240	7.8		11.0
4334	1340	12.8	50	6.7
4480	729	12.1	49	10.5
4829	666	10.7	50	10.7
5125	3569	7.5	41	26.5
5158	968	17.2	48	6.7
HARMATAN station 15 (00°00' - 05°30'W)*				
1000	1800	46.8	44	3.5
2000	2400	36.7	17	14.5
3000	1200	25.0	17	44.
4000	290	15.6	17	14.5
MIDLANTE station 9 (24°03'N - 28°56'W); watercolumn: 5400 m				
910	680	16.	17	♦
1856	750	18.	25	
2265	1070	11.	25	
MIDLANTE station Madcap (28°40'N - 25°25'W); watercolumn: 5200 m				
1075	1310	17.	20	4.7
1110	680	14.	3	6.2
1250	1800	24.	25	6.4
1350	430	7.6	4	4.9
1480	1660	14.	21	5.8

Table II.4: Particulate Ba, continued.

Depth in m	ppm	ng/Kg	2σ%	Fraction associated with aluminosilicates in %
MIDLANTE station Madcap (28°40'N - 25°25'W) (continued)				
1895	1460	22.	20	3.1
1905	660	12.	18	5.1
2070	2940	13.	20	4.7
2680	500	6.7	30	4.5
3460	530	6.7	12	4.4
4170	510	7.7	35	7.7
4350	1390	9.1	60	6.2
4455	370	5.6	45	7.5
4895	420	10.	20	6.7
4905	1730	16.	20	5.8
5043	1030	5.5	40	12.2
MIDLANTE station 50 (34°43'N - 29°34'W); watercolumn: 3520 m				
985	880	19.	20	♦
1835	920	18.	25	
2675	780	10.	25	
3370	1300	26.	17	
3510	730	14.	18	
TRANSAT station 37 (14°48'N - 74°12'W)				
1010	560	11.	50	♦
TRANSAT station 17 (34°06'N - 61°17'W); watercolumn: 4700 m				
5	110	1.4	90	23.8
300	1150	16.	28	3.2
600	1290	21.	25	2.9
990	1550	14.	25	5.1
1190	2070	22.	20	5.3

Table II.4: Particulate Ba, continued

Depth in m	ppm	ng/Kg	2σ%	Fraction associated with aluminosilicates in %
TRANSAT station 17 (continued)				
1750	580	22.	25	11.5
2250	1010	8.6	30	8.6
2260	1350	19.	45	9.1
3250	1930	7.9	70	7.0
3680	720	18.	40	55.0
4380	860	5.6	60	18.3
TRANSAT surface sea water (0.5 m)				
29°41'N-65°18'W	28	1.3	85	♦
25°12'N-67°15'W	260	6.3	80	
20°39'N-65°49'W	69	1.3	90	
14°48'N-74°12'W	395	11.0	65	

♦ No data for particulate Al

☆ Data from Darcourt (1973)

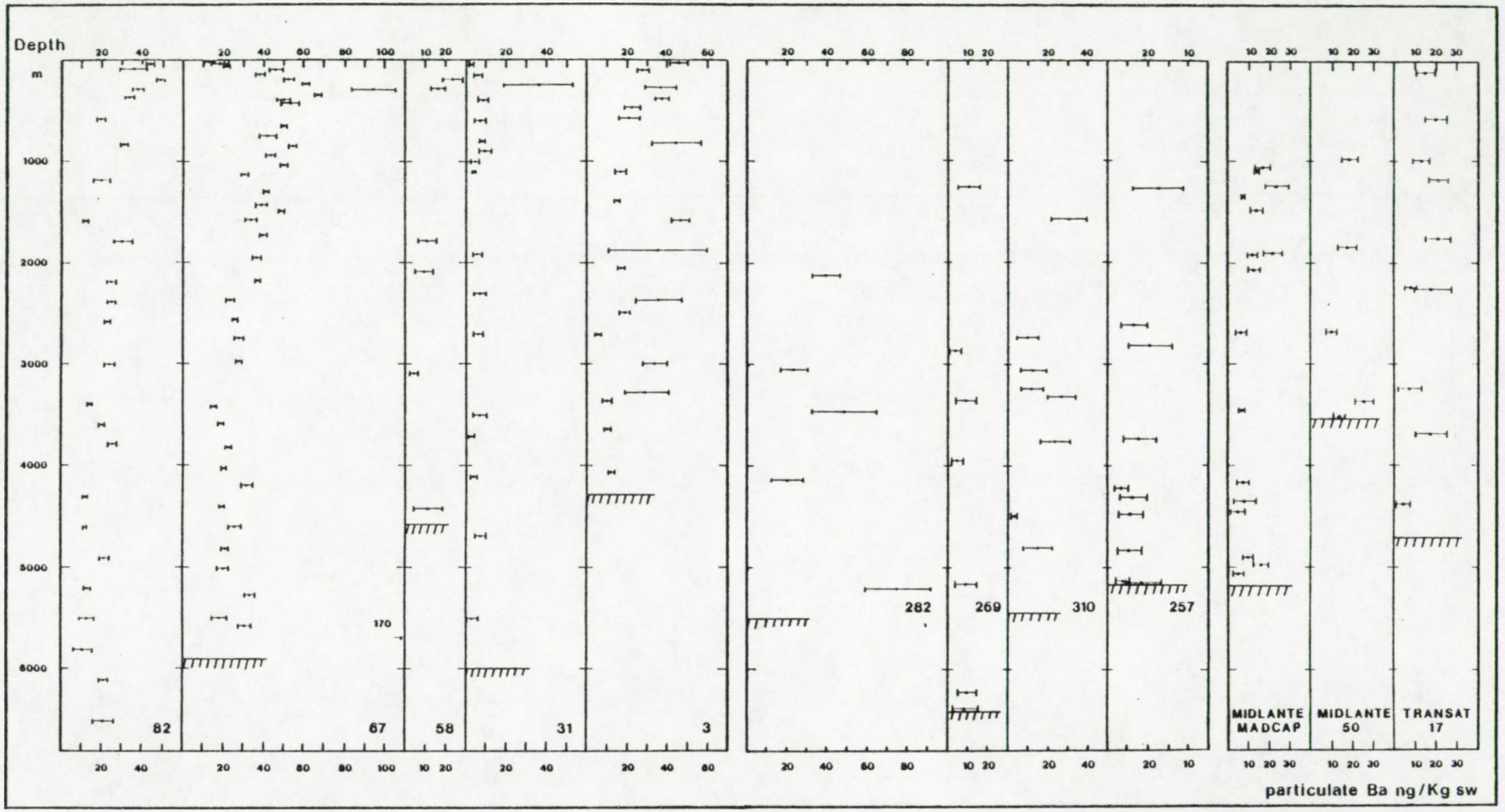

FIGURE II.6

Profiles of particulate Ba measured by INAA. GEOSECS Atlantic stations 82, 67, 58, 31, 3; GEOSECS Pacific stations 282, 269, 310, 257; MIDLANTE Atlantic stations Madcap, 50; TRANSAT Atlantic station 17. For geographical location see Table I.1 in part I. The depths of the watercolumns are idicated by a hatched line; at station 82 this depth is 7873 m.

Discussion of chapter 1:

Particulate Ba is an ubiquitous component of suspended matter and occurs largely in excess over the quantities which are associated with suspended aluminosilicates.

The particulate Ba profiles exhibit a typical maximum in subsurface water (thermocline region). At greater depths concentrations decrease, reflecting a dissolution process. In bottom waters the aluminosilicate-bound Ba fraction always increases and can attain 100% of the total Ba amount measured in these waters. In those regions characterized by the presence of a nepheloid layer in bottom water, the total amount of Ba increases sharply towards the sea floor. Although the fraction of total Ba_p associated with aluminosilicates increases also in such waters, the excess Ba can be several times larger than what is observed for intermediate and deep water. This points towards the introduction to the water-column of an additional non-terrigenic Ba_p phase from the sediments. This additional phase consists most likely of sedimentary barite crystals, known to represent the major fraction of sedimentary Ba.

A close relationship exists between particulate Ba,Sr and Ca, in intermediate and deep water. Instead of pointing towards their partial occurrence inside a common particulate phase, what is not confirmed by other observations, this rather reflects the existence of a common process which

governs the distribution of these particulates in the intermediate and deep waters.

Particulate Ca and Sr have a dichotomic behaviour. They are both composed of a dissolution-resistive and a dissolution-sensitive phase. The distribution of the resistive phases of Ca and Sr, together with particulate Ba, is controlled by a double process: dissolution and advective transport. For Ca_p and Sr_p the dissolution-resistive phases are thought to consist respectively of $CaCO_3$ (coccoliths) and a $SrSO_4$, which as a result of the presence of minor amounts of Ba Ca and K , has become less soluble than the pure celestite. The sensitive Ca and Sr phases consist probably of gypsum and Acantharia debris (celestite)plus Sr-enriched organics. The origin of gypsum is doubtful. Evidence exists for its artefactial production during sea water dessication on the filters.

The fact that the excess Ba (= non-terrigenic Ba) in suspended matter appears to consist of a slowly dissolving phase is in concordance with its observed occurrence as the least soluble Ba salt in sea water: <u>barite.</u>

This suspended barite must now be investigated more thorouhgly. From the quantitative, but "blind", method of analysis for total Ba we have performed until now, we will pass on to a more selective method of analysis, which allows the study of specific Ba-components diluted within the total mass of suspended matter. The following chapter concerns the study of <u>Ba as barite</u> in suspended matter.

CHAPTER 2

THE SUSPENDED BARITE IN THE OCEAN

2.1 GEOGRAPHICAL DISTRIBUTION OF SUSPENDED BARITE IN SEA WATER

When analyzing suspended matter with the SEM-EMP equipment, it appears that the Ba is nearly exclusively detected in discrete micron-sized particles. In such particles Ba and S represent the major constituents , what suggests that they consist of $BaSO_4$. These $BaSO_4$ particles were identified as well crystallized particles of barite (see § 2.3.4 in part I).

Barite crystals were detected in suspended matter collected in the North-Atlantic, Equatorial-Atlantic, South-Atlantic, Antarctic and Central-Pacific Oceans and in the Mediterranean Sea. Every investigated sample contained barite crystals. The studied stations, and depth intervals are listed in Table II.5. Recently barite was observed in suspended matter samples from the South-East Indian Ocean (CFR data, C.E.Lambert , pers. comm.,1979)

Suspended barite thus appears as an ubiquitous component of oceanic suspended matter.

Before starting the study of these barite particles it is necessary to ascertain that they are a genuine component of the marine environment.

Table II.5 : Distribution of suspended barite in the World Ocean

Stations	Position	Investigated depth range in m		Barite presence
Atlantic Ocean				
GEOSECS station 5	56°54'N-42°47'W	363	2464	positive
3	51°01'N-43°01'W	28	3660	"
27	42°00'N-41°59'W	1441	4858	"
58	27°02'S-37°00'W	200		"
67	44°58'S-51°10'W	10	5804	"
91	49°36'S-11°37'E	486	3074	"
82	56°15'S-24°55'W	1	5202	"
ATLANTIS II station				
2111	33°41'N-57°38'W	2195		"
715	52°56'N-36°13'W	2000		"
HARMATAN station 6	04°30'N-19°35'W	2000	3000	"
15	00°00' -05°30'W	1000	4000	"
Pacific Ocean				
GEOSECS station 257	10°10'S-170°00'W	1263	5182	"
263	16°36'S-167°05'W	676		"
269	24°00'S-174°26'W	2597		"
310	26°55'S-157°11'W	2338		"
Mediterranean Sea				
In front of Calvi (Corsica)		45	1500	"

2.2 BARITE AS A GENUINE COMPONENT OF OCEANIC SUSPENDED MATTER

The contamination by Ba-rich particles during the sampling (= contamination with exogenic particles) and the possibility of $BaSO_4$ precipitation due to physical and chemical processes inherent to the sampling procedure (= contamination with endogenic particles) have been considered and rejected as significant problems. This is based on the following arguments:

a) exogenic origin

i) On shipboard GEOSECS blanks were run under the same technical conditions as the samples. They never showed any sample contaminated by Ba rich particles.

ii) Barite particles were observed in all samples collected since 1972 during various expeditions by different research vessels. All these samples contain the same morphological types of barite particles. This is incompatible with occcurrences of accidental contaminations. Furthermore, the use of different equipment for sample collection and handling during GEOSECS, ATLANTIS II, HARMATAN, MIDLANTE and TRANSAT expeditions makes a systematic contamination of the samples unlikely.

iii) On several occasions we observed barite crystals inside low density pellet-like particles, probably of organic composition (Plate 11). Barite particles were also found in large size aggregates containing different species of diatoms and coccoliths. These pellets and aggregates are thought to represent fractions of the fecal material described by Bishop et al. (1977). The barite particles were either scavenged by zooplankton and excreted together with the fecal material, or were formed inside such pellets. An exogenic origin can be excluded in both cases.

b) endogenic origin

Several processes can induce a precipitation of barium sulphate during sample recovery:

i) Deep-sea water samples are enriched in dissolved Ba and may approach and eventually reach saturation, when hauled to the surface, since the effects of decompression and temperature transition decrease the Ba saturation level by a factor two (Church and Wolgemuth, 1972) However, according to Church and Wolgemuth such a precipitation process, especially in heterogenous systems with a large sulphate excess, should take days. Even for the deep-sea samples, recovery is only a matter of hours. Since deep-sea water Ba concentrations are in fact much lower than the sediment pore waters discussed by Church and Wolgemuth (1972), we conclude that barite

precipitation does not take place during sample recovery. In fact, barite particles were observed in two samples of suspended matter which were filtered in situ, at depths of 2000 m (ATLANTIS II station 2111) and 2195 m (ATLANTIS II station 715) with an especially designed titanium bottle of the Woods Hole Oceanographic Institution. This technique effectively precludes barite precipitation during sampling.

ii) The study of Aubey (1976) on particulate calcium carbonate in sea water has shown that dessication of microdrops of sea water, which probably remain on the surface of the Nuclepore membrane after filtration of sea water, must be considered as a process possibly leading to contamination with endogenic particles such as gypsum, and this despite the rinsing of the filters on board the ship. It is shown below that if such processes would indeed lead to the production of barite, they would account for an extremely small fraction of the particulate Ba we measured. SEM-EMP analyses of GEOSECS samples revealed the presence of gypsum particles. Aubey observed that gypsum particles were formed when prefiltered (through 0.45 µm membranes) sea water was refiltered on 0.45 µm Nuclepore membranes. By rinsing these filters, prepared in the laboratory, and several GEOSECS filters of stations 67* , 76 and 58, in deionized water at pH 5.5, Aubey observed that:

* For station 67 Aubey measured the dissolvable Ca fraction of some samples, by analyzing a previously rinsed quart of a membrane by atomic absorption. These data were compared with our INAA data on total particulate Ca, which in these specific cases were obtained by analyzing only 1/2 of a membrane.

1°) The gypsum on the Nuclepore membranes prepared in the laboratory had dissolved.

2°) A mean of 55 % of the total particulate Ca of the GEOSECS filters had dissolved .

3°) Gypsum particles were no longer observed on rinsed GEOSECS samples.

Aubey concluded that the dissolved Ca fraction of the GEOSECS filters was originally present as gypsum. It ensues that the shipboard rinsing was inefficient. We have already discussed, in § 2.2.1 of this part, the possibility that particles were initially protected by an organic coating.
Decomposition of this coating (trough bacterial activity?) might explain the elimination of these particles during a later rinsing.

It was checked that refiltration of filtered sea water did not result in the formation of barite (O. Aubey, P. Buat-Menard, pers. comm.). It is nevertheless necessary to verify to what extent such a dessication process, when occurring on board the ship, would contribute to the total particulate Ba concentration. This problem can be settled by the following calculation:
For the suspended matter samples of GEOSECS station 67, analyzed by Aubey, a mean hydrosoluble Ca fraction (= 60 % of total particulate Ca) of 4.9 µg is measured for a total Nuclepore membrane through which in the mean 8.4 Kg sea water were filtered (GEOSECS shipboard data). Since sea water contains 400 mg of dissolved Ca per litre, it appears that these 4.9 µg of

hydrosoluble particulate Ca can have originated from the complete precipitation of the dissolved Ca content of 12 µl sea water. We assume this value to represent the upper limit of the sea water volume that can have dessicated on the Nuclepore membrane. Considering a mean dissolved Ba concentration of 10 µg/Kg sea water in the Atlantic (Chan et al.,1977), the hypothetical precipitation of all dissolved Ba from these 12 µl sea water would produce 1.2×10^{-4} µg of particulate Ba on the entire filter membrane. This is 1700 times less than the mean total Ba_p we actually measured by INAA for these same samples, and which is shown to be balanced for 90 % by barite (see section 4.2 in this part).

We conclude from the set of arguments presented above that the barite particles we observe are a genuine component of the natural marine environment.

2.3 THE MORPHOLOGICAL TYPES OF SUSPENDED BARITE PARTICLES

The analysis of over a thousand barite particles from various regions in the World Ocean (see Table II.5) has enabled us to recognize essentially four morphological types of barite particles. In decreasing order of frequencies we observe:

1) ellipsoidal and spherical particles
2) particles with a distinct crystalline habit (automorphic, euhedral particles)
3) irregularly shaped particles, that were apparently affected by dissolution
4) aggregates exclusively composed of sub-micron sized euhedral and ahedral particles

In the following, these different morphological types will be discussed in detail, with references to SEM recordings.

1) Ellipsoidal and spherical particles (Plate 2).

The particle surfaces and contours are generally smooth, without sharp edges. Sometimes surfaces may show clear patterns of a dissolution process. The occurrence of dissolution traces on the particles is not surprising, since the surrounding sea water is undersaturated with respect to barium sulphate (Church 1970; Church and Wolgemuth 1972; see further Section 5.1 in this part).

It is thought that these rounded particles originally had a crystalline habit. In some cases (Plate 2, n° 6,8) the

particle shape is definitly a transient one between the original polygonal, euhedral and the rounded, ellipsoidal shape.

2) Automorphic particles (Plate 3).

The original crystalline habit is generally slightly altered, but remains easily recognizable. Polygonal particles, including rhombic prisms, elongated prisms, octogones and twins are found. Twins were observed only occasionally (Plate 4); GEOSECS station 27 in the North Atlantic is however rich in it, especially at 2231 m. Although they do not exhibit the clear euhedral shapes found elsewhere, due to important corrosion, the twins are evident (Plate 4, n° 1,4). These crystals are covered with small cavities, due to corrosion, but also with small spherical outgrowings, typical for growth sites (prof. J. Jedwab pers. comm.). This indicates that dissolution and crystallization processes have taken place at different stages of the life cycle of these particles.

The single crystals as well show corrosion traces, such as ripple marks (Plate 3, n° 2) and layer by layer alterations (Plate 3, n° 5). It is further not uncommon to observe, at the same depths, intact, euhedral particles with smooth, unaffected surfaces and slightly corroded ones. This may point towards a preferential dissolution of some of the particles, or may simply result from differences in contact times with the undersaturated ambient sea water, due to differences in settling velocities.

3) Dissolution altered particles; irregularly shaped particles (Plate 5).

A common morphological feature can not be found among such particles. Instead of this, a whole variety of shapes is observed. This probably results from the quite different ways dissolution affects these particles. Dissolution can affect the whole particle surface at a time and, as result, particles acquire a smooth, rounded aspect (Plate 5, n° 1, 2, 3), as discussed above (Plate 2). Step-like, or layer by layer alterations and hollowing of the particles are also observed (Plate 5, n° 8,9). The latter process can result in a piercing of the particles (Plate 5, n° 4,5,6 and 10, 11, 12). Dissolution can also proceed at the extremities of ellipsoidal particles, generally with a step-like proceeding alteration (Plate 5, n° 7).

4) Aggregates of barites with and without clear crystalline habits (Plate 6).

Aggregates of euhedral barites are rather small (at most a few micron) and can contain numerous small prisms (Plate 6, n° 1,3,4,5,). In some cases they consist of an irregular shaped, rather amorphous matrix in which subunits are not easily distinguished (Plate 6 n° 2). High Ba and S concentrations are found throughout the matrix. Such matrices may represent barite crystallization sites. As such they can be compared with the sulphate-rich, organic microenvironment in which Chow and Goldberg (1960) assumed barite precipitation to occur. This assumption gains further support from the

observations of J.Klossa (pers. comm.) who showed, by using a HVEM, that barite could occur as grapes of small prisms inside electron transparent pellet-like particles. It is possible that the crystal aggregates we observe, were originally packed as well in organic pellets. This organic envelop can have been largely destroyed during the resuspension of our samples by ultrason treatment in a CCl_4 medium (see § 2.3.5 in part I). Aggregates with ahedral subunits are also observed but they are much scarcer (Plate 6, n° 8,9). The egg- shape of the subunits is characteristic here. In some cases the individual particles appear to be held together by a thin membrane, probably of organic composition (Plate 6, n° 8,9). Instead of being the result of a crystallisation in an organic microenvironment, the latter type of aggregate may rather result from a mechanical concentration. Passage through the intestinal tract of some zooplanktonic organism and excretion as an organic matter coated pellet, might be such a mechanism.

It is thought that these four morphological types represent different phases in the cycle of formation and decay of barite particles in suspension. The observed aggregates, from the rather amorphous matrix to the aggregate containing well crystallized small prisms, must be regarded as consecutive phases in the growth process of particles. Through recrystallization inside the micro-environment, or eventually through direct precipitation, larger single crystals may be formed. These precipitation and growth

processes probably continue till the organic matrix or organic coating decomposes and liberates the individual polygonal particles. This process can explain the presence, mentioned previously, of non-corroded crystals at great depths, in the same environment in which dissolution altered particles occur. Once the protective organic membrane decomposed, these particles are affected by dissolution, since the whole watercolumn is undersaturated with respect to $BaSO_4$ (Church,1970; Church and Wolgemuth, 1972), and will form the continuous dissolution series we observe.

For several samples of suspended matter, listed in Table II.6, a sufficiently large part of the membrane filters (1/4 of the filter) was utilized for a quantitative assessement of the numbers and masses of barite particles per unit volume of sea water with the SEM-EMP. The samples were chosen at random along the selected profile in the Argentine Basin (GEOSECS station 67) and along two profiles in the North American Basin (GEOSECS station 3 and 5). Samples close to the surface and close to the sea floor could not be analyzed quantitatively since they carried a too thick filtration cake, masking an important fraction of the particles of interest. These profiles intersect hydrological situations which are typical for the southern and nothernmost part of the West-Atlantic Basin. The hydrological situation in the Argentine Basin and the North American Basin are discussed in appendix V.

PLATE 2

ELLIPSOIDAL AND SPHERICAL BARITE PARTICLES

1. GEOSECS Atlantic station 67 (44°58'S-51°10'W); 2193 m
2. GEOSECS Atlantic station 67 (" "); 1499 m
3. GEOSECS Atlantic station 67 (" "); 4424 m
4. GEOSECS Pacific station 310 (26°55'S-157°11'W);2338 m
5. GEOSECS Atlantic station 67 (44°58'S-51°10'W); 3841 m
6. GEOSECS Atlantic station 82 (56°15'S-57°38'W); 2583 m
7. ATLANTIS II Atlantic station 715 (52°56'N-36°13'W); 2000 m (in-situ filtration)
8. GEOSECS Atlantic station 82 (56°15'S-57°38'W); 4598 m
9. GEOSECS Atlantic station 3 (51°01'N-43°01'W); 3276 m

See discussion at page 114.

PLATE 2

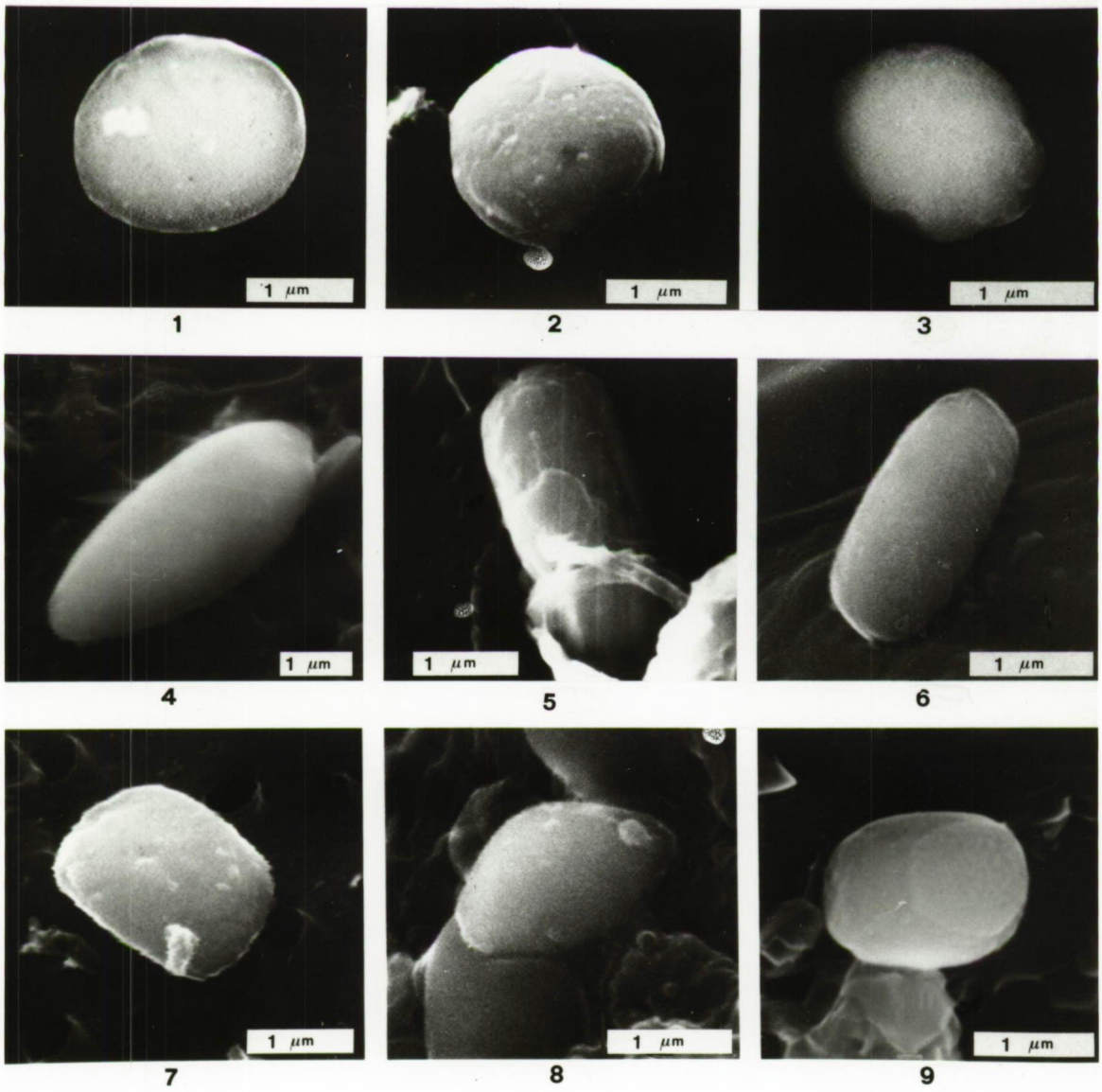

1 2 3

4 5 6

7 8 9

PLATE 3

AUTOMORPHIC BARITE PARTICLES

1. GEOSECS Atlantic station 67 (44°58'S-51°10'W); 2193 m
2. GEOSECS Atlantic station 67 (" "); 2982 m
3. GEOSECS Atlantic station 82 (56°15'S-57°38'W); 1577 m
4. GEOSECS Atlantic station 67 (44°58'S-51°10'W); 658 m
5. GEOSECS Atlantic station 67 (" "); 2982 m
6. GEOSECS Atlantic station 67 (" "); 4424 m
7. GEOSECS Atlantic station 67 (" "); 2982 m
8. GEOSECS Atlantic station 67 (" "); 2982 m
9. GEOSECS Atlantic station 67 (" "); 2982 m
10. GEOSECS Atlantic station 67 (" "); 4424 m
11. GEOSECS Atlantic station 3 (56°15'S-57°38'W); 2696 m
12. GEOSECS ATlantic station 67 (44°58'S-51°10'W); 5599 m

See discussion at page 115.

PLATE 4

BARITE TWINS

1. GEOSECS station 27 (42°00'N-41°59'W); 2231 m
2. GEOSECS station 3 (51°01'N-43°01'W); 3630 m
3. GEOSECS station 27 (42°OO'N-41°59'W); 2231 m
4. GEOSECS station 27 (" "); 2231 m

See discussion at page 115.

PLATE 4

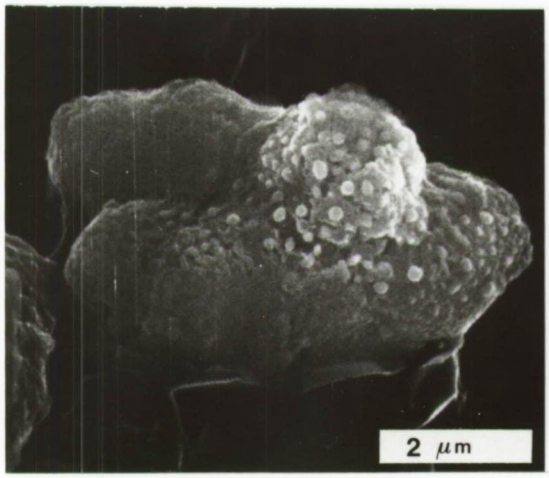

1

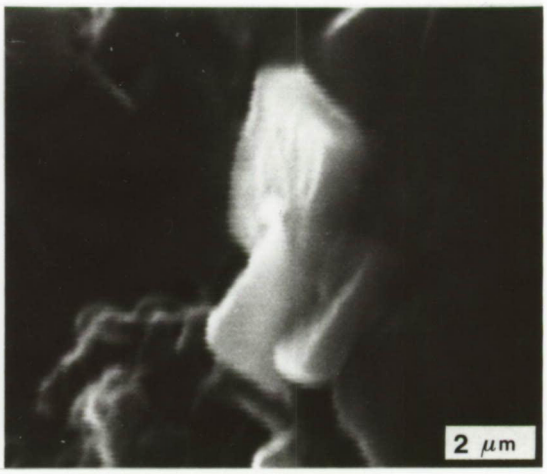

2

3

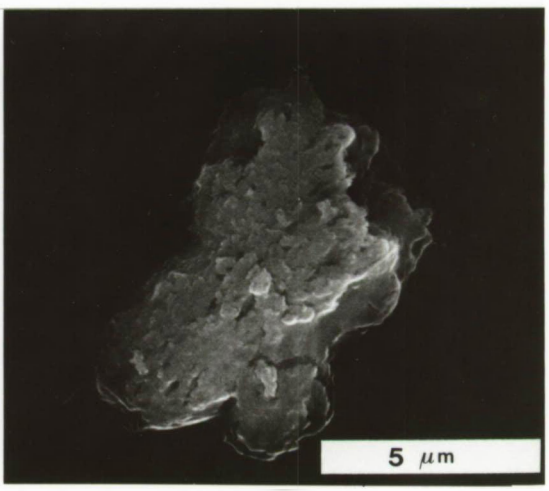

4

PLATE 5

DISSOLUTION ALTERED AND IRREGULARLY SHAPED BARITE PARTICLES

All examples shown were collected at GEOSECS Atlantic station 67 (44°58'S-51°10'W)

1. 2982 m
2. 2193 m
3. 2982 m
4. 2193 m
5. 2193 m
6. 4424 m
7. 2982 m
8. 2982 m
9. 2193 m
10. 2982 m
11. 5599 m
12. 4424 m

See discussion at page 116.

PLATE 5

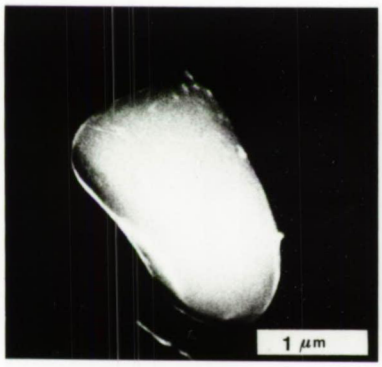

1

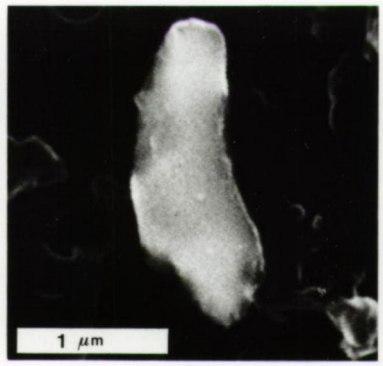

2

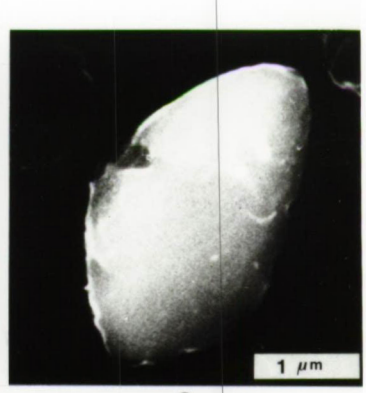

3

4

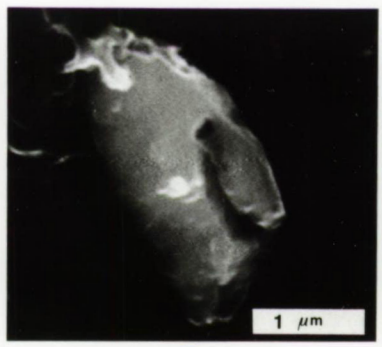

5

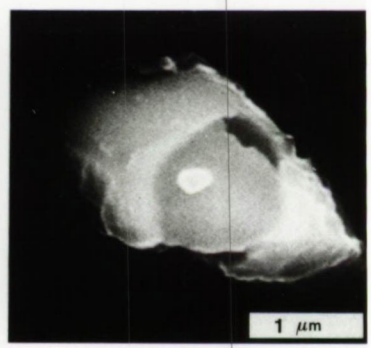

6

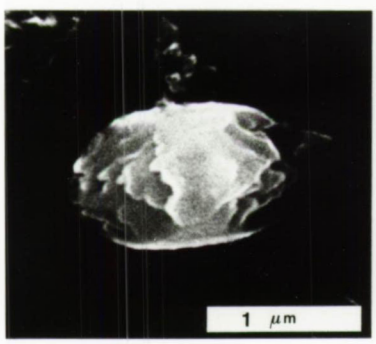

7

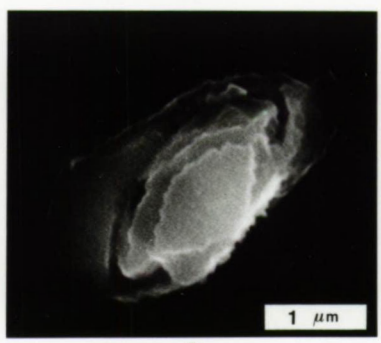

8

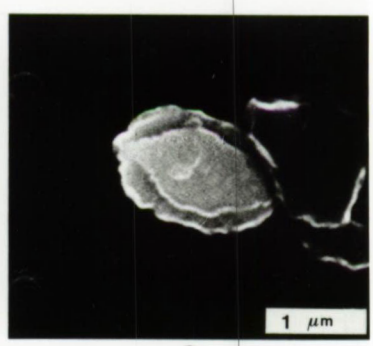

9

10

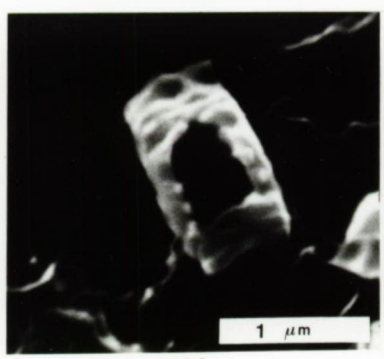

11

12

PLATE 6

AGGREGATES OF BARITES WITH AND WITHOUT A CLEAR CRYSTALLINE HABIT

1. GEOSECS Atlantic station 67 (44°58'S-51°10'W); 62 m
2. GEOSECS Atlantic station 3 (51°01'N-43°01'W); 1083 m
3. GEOSECS Atlantic station 3 (" "); 1083 m
4. GEOSECS Atlantic station 67 (44°58'S-51°10'W); 4424 m
5. GEOSECS Atlantic station 67 (" "); 658 m
6. HARMATAN Atlantic station 6 (04°30'N-19°35'W); 3000 m
7. GEOSECS Pacific station 263 (16°36'S-167°05'W); 676 m
8. GEOSECS Atlantic station 3 (51°01'N-43°01'W); 1875 m
9. GEOSECS Atlantic station 91 (49°36'S-11°37'W); 486 m

See discussion at page 116.

PLATE 3

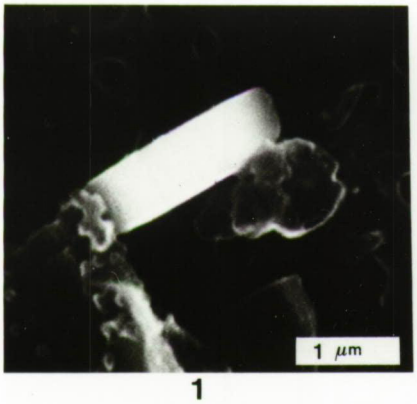

1

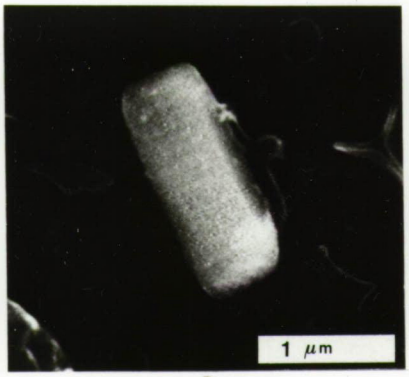

2

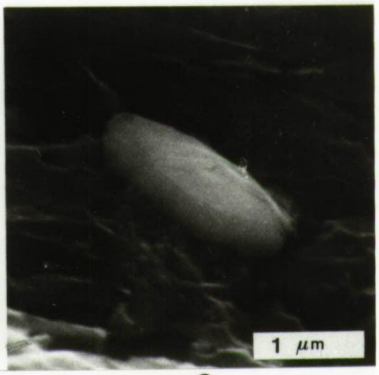

3

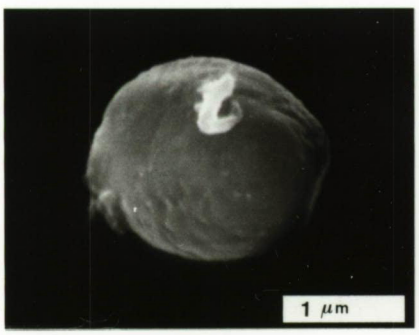

4

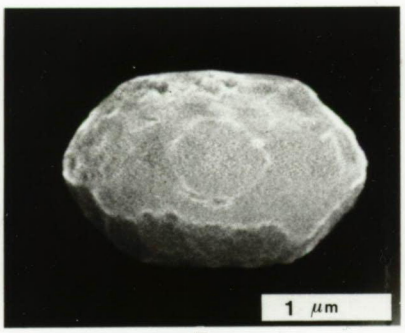

5

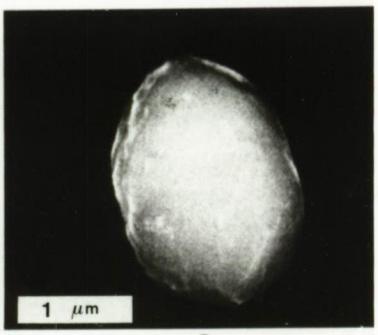

6

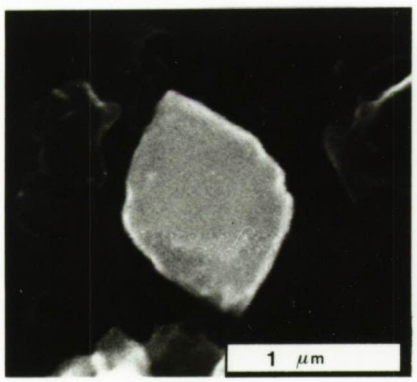

7

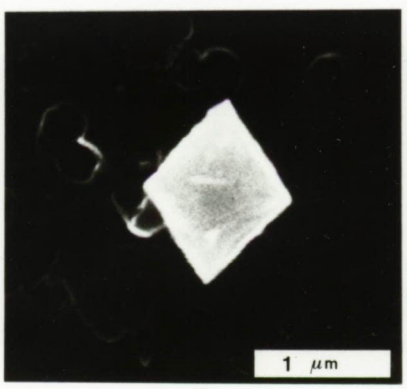

8

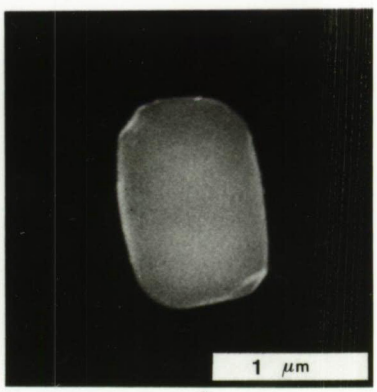

9

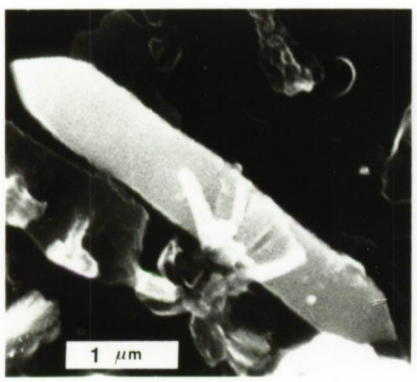

10

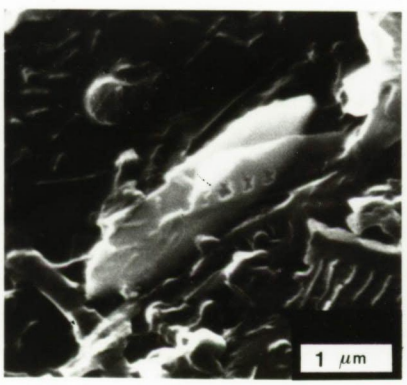

11

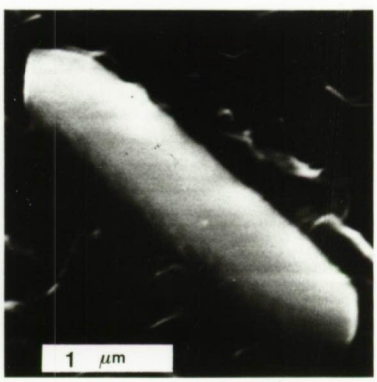

12

PLATE 4

BARITE TWINS

1. GEOSECS station 27 (42°00'N-41°59'W); 2231 m
2. GEOSECS station 3 (51°01'N-43°01'W); 3630 m
3. GEOSECS station 27 (42°OO'N-41°59'W); 2231 m
4. GEOSECS station 27 (" "); 2231 m

See discussion at page 115.

PLATE 4

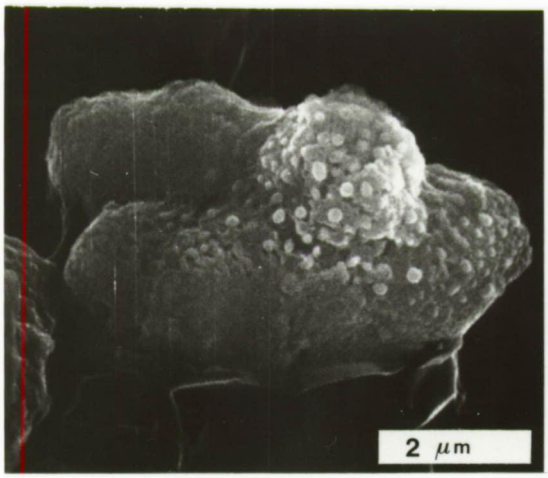

1

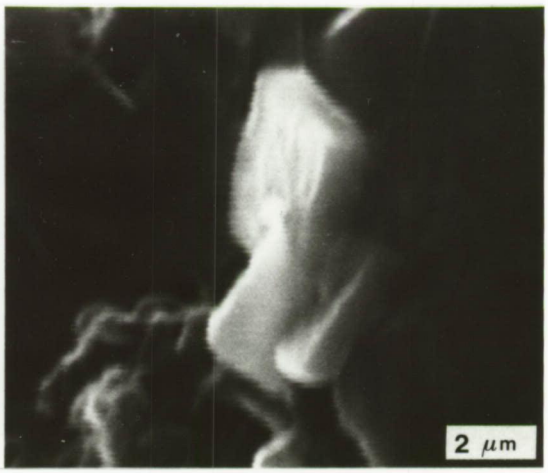

2

3

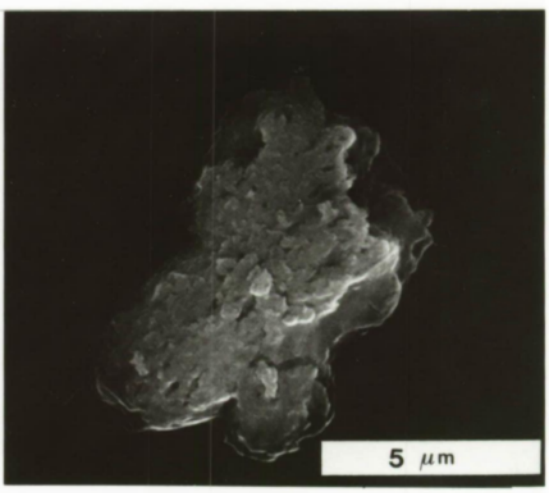

4

PLATE 5

DISSOLUTION ALTERED AND IRREGULARLY SHAPED BARITE PARTICLES

All examples shown were collected at GEOSECS Atlantic station 67 (44°58'S-51°10'W)

1. 2982 m
2. 2193 m
3. 2982 m
4. 2193 m
5. 2193 m
6. 4424 m
7. 2982 m
8. 2982 m
9. 2193 m
10. 2982 m
11. 5599 m
12. 4424 m

See discussion at page 116.

PLATE 5

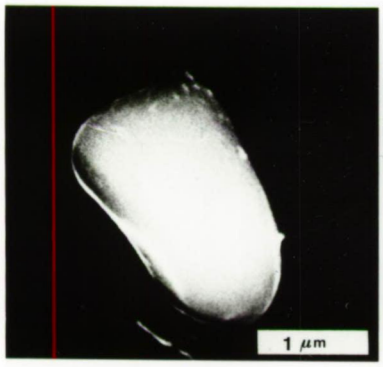

1

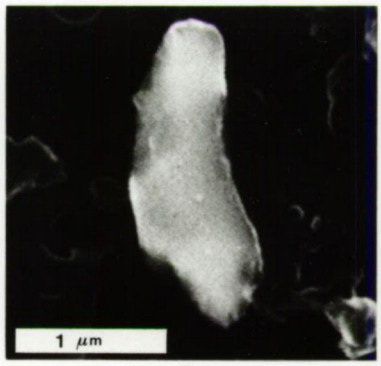

2

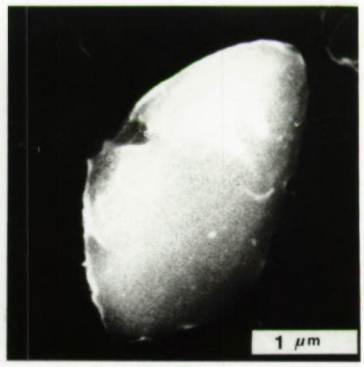

3

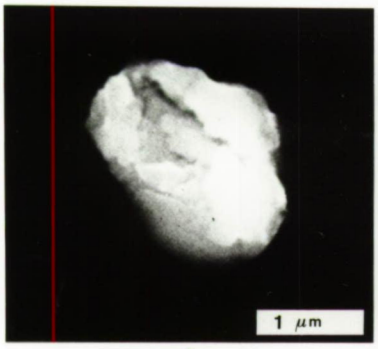

4

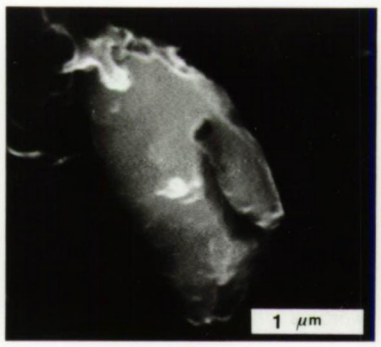

5

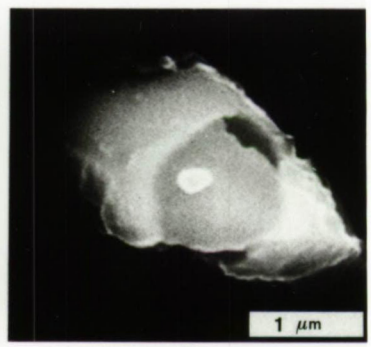

6

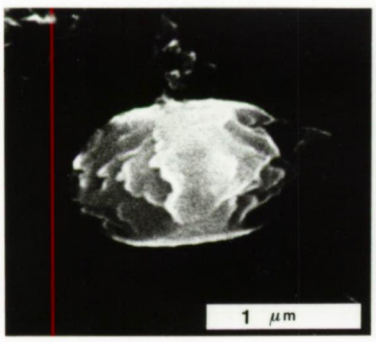

7

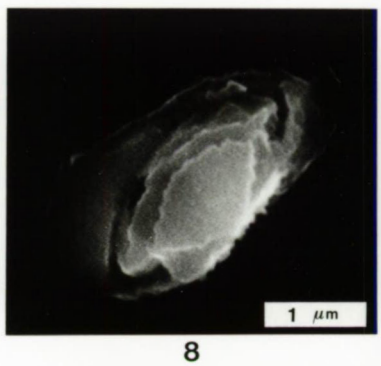

8

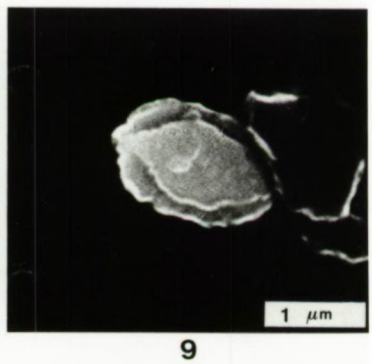

9

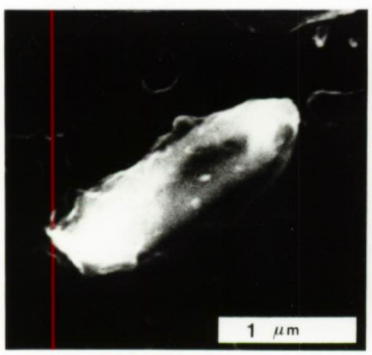

10

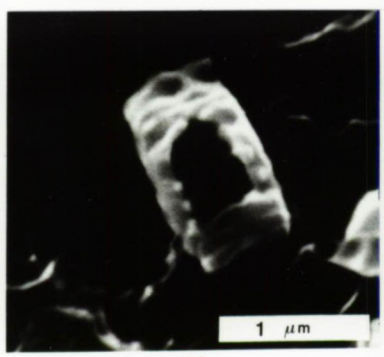

11

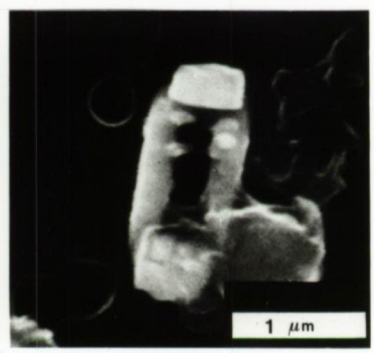

12

PLATE 6

AGGREGATES OF BARITES WITH AND WITHOUT A CLEAR CRYSTALLINE HABIT

1. GEOSECS Atlantic station 67 (44°58'S-51°10'W); 62 m
2. GEOSECS Atlantic station 3 (51°01'N-43°01'W); 1083 m
3. GEOSECS Atlantic station 3 (" "); 1083 m
4. GEOSECS Atlantic station 67 (44°58'S-51°10'W); 4424 m
5. GEOSECS Atlantic station 67 (" "); 658 m
6. HARMATAN Atlantic station 6 (04°30'N-19°35'W); 3000 m
7. GEOSECS Pacific station 263 (16°36'S-167°05'W); 676 m
8. GEOSECS Atlantic station 3 (51°01'N-43°01'W); 1875 m
9. GEOSECS Atlantic station 91 (49°36'S-11°37'W); 486 m

See discussion at page 116.

PLATE 6

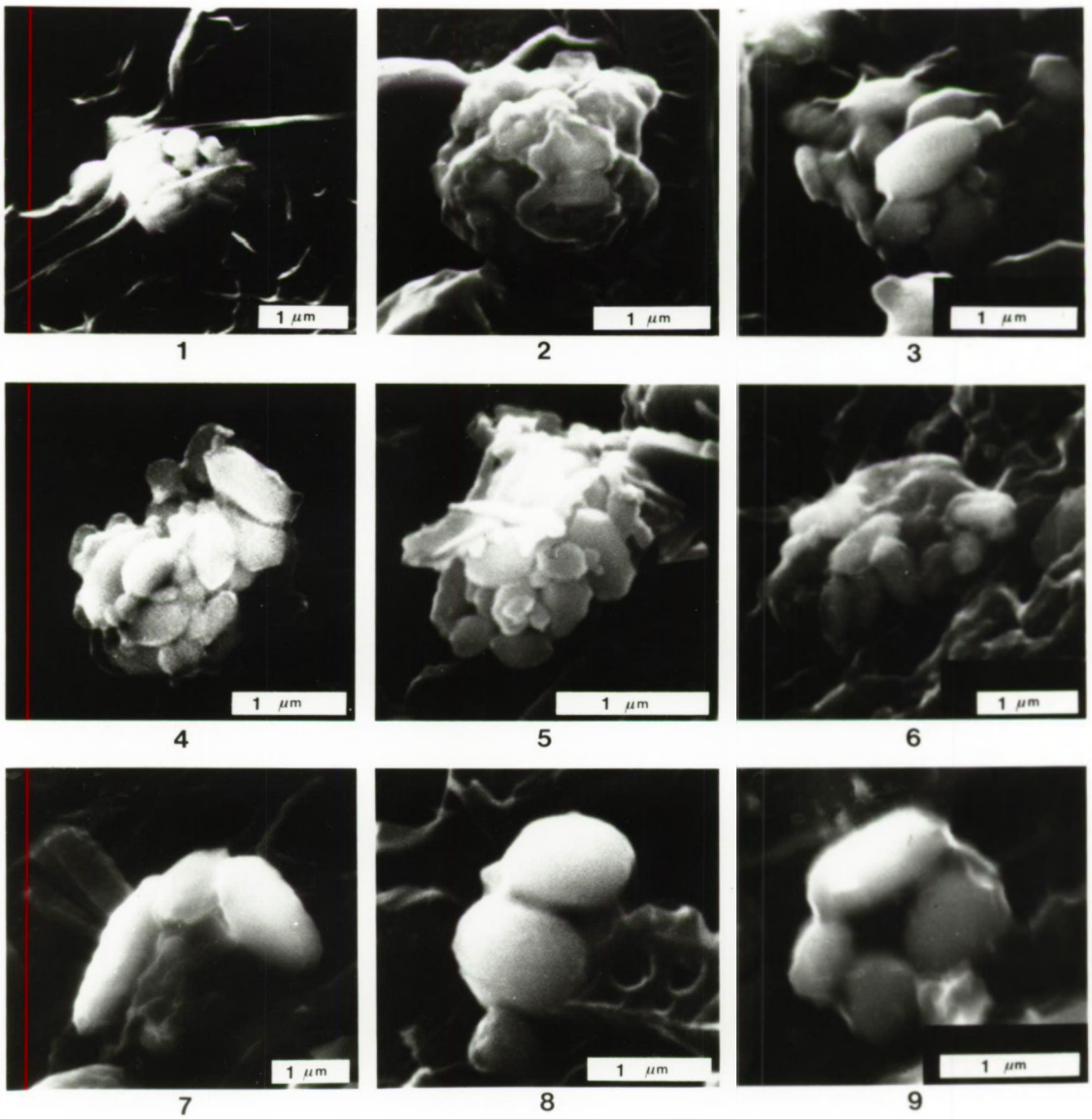

1 2 3

4 5 6

7 8 9

2.3.1 The study of the barite particle morphology at GEOSECS station 67 in the Argentine Basin

Samples towards the surface (353 m, 658 m, 1053 m) have the highest number of barite particles per Kg sea water and are characterized by a more important contribution of euhedral barites (= combined fractions of discrete euhedral barites and aggregates of euhedral barites; = columns C + D in Table II.6), compared to samples from intermediate waters. The samples taken between 1499 and 3601 m, a depth interval which includes the NADW[☆] (North Atlantic Deep Water) core and the mixing zones of CPWu[☆] (upper part of the Circumpolar Water) with NADW and AABW[☆] (Antarctic Bottom Water), have the largest fraction of dissolution affected barites (= columns A+B in Table II.6). Both deep water samples are again characterized by a more important fraction of euhedral barites (Table II.6), compared to the samples of the intermediary waters. Hypothesis testing shows that the mean fraction of euhedral barites (columns C+D in Table II.6) of the samples in the 1499 to 3601 m depth interval is significantly different at the 95% confidence level, from the mean fraction of euhedral barites sampled in AABW, CPWu, AAIW[☆] (Antarctic Intermediate Water) and subthermocline water (= samples at 5304 m; 4424 m; 1053 m; 658 m; 353 m). The AABW and CPWu, AAIW masses, which are younger, here in the Argentine Basin, than the NADW mass (Stuiver, 1976) have apparently younger barite particle populations. These observations suggest that:

☆ The hydrological situation at GEOSECS station 67 is explained in appendix V.

Table II.6: Relative contribution of the different morphological types to the total barite number

Depth in m	Number of barites per litre sw	σ	A Rounded partic. %	B Irregul. partic. %	dissol. affected partic. A+B %	C Automorph. partic. %	D Aggreg. %	euhedral particles C+D %
GEOSECS station 67								
151	10600	1550	52.1	33.4	85.5	10.4	4.2	14.6
353	20400	1960	46.3	22.2	68.5	23.1	8.3	31.4
653	16850	1670	52.0	6.9	58.9	35.3	5.9	41.2
1053	17820	1760	49.0	14.7	63.7	30.4	5.8	36.2
1499	12240	1280	53.2	30.4	83.6	14.1	2.2	16.3
2193	5440	670	69.3	12.3	81.6	15.4	3.1	18.5
2574	7160	970	48.1	25.9	74.0	24.1	2.0	26.1
2982	4180	600	63.2	10.2	73.4	22.4	4.1	26.5
3601	5660	1030	40.0	33.3	73.3	23.3	3.3	26.6
4424	3440	490	46.9	14.3	61.2	24.5	14.3	38.8
5304	8820	1260	47.0	14.2	61.2	30.6	8.1	38.7
GEOSECS station 3								
105	5830	580	40.2	35.3	75.5	19.6	5.0	24.6
813	3900	390	50.0	39.0	89.0	9.0	2.0	11.0
1083	4480	630	64.7	21.6	86.3	7.8	5.9	13.7
1875	25000	2550	37.5	31.2	68.7	31.2	0.0	31.2
2479	3930	410	45.6	42.4	88.0	10.9	1.1	12.0
2696	1970	300	50.0	27.3	77.3	22.7	0.0	22.7
2982	24850	2740	21.9	43.9	65.8	19.5	14.6	34.1
3267	2920	470	41.0	38.5	79.5	17.9	2.6	10.5
GEOSECS station 5								
363	16040	1830	74.6	9.8	84.4	12.7	2.8	15.5
760	46990	5070	64.4	6.7	71.1	27.8	1.1	28.9
2464	21160	2960	74.6	12.7	87.3	12.7	0.0	12.7

$\sigma = 1 / \sqrt{N}$, with N = number of effectively counted barite particles (Allen, 1968).

- the distribution of fine particulates in suspension in sea water is not only governed by gravitational force , but is probably determined to a large extent by advective transport mechanisms. This is fully in accord with the conclusions we drew from the results of factor analysis of the station 67 multi-variable system (see § 2.2.2 in this part).
- Barite particles dissolve in the watercolumn, since in older watermasses their populations are characterized by a larger contribution of the dissolution affected particles, as compared to younger watermasses.

However, the shifts between the different morphological classes when passing from an AAIW to a NADW regime are small. This is probably due to the fact that the eventual loss of particles resulting from the dissolution process is partly compensated for, by incoming particles from the surface waters. Indeed, the barite aggregates may settle out of the surface waters and sink to different depths according to their masses and to the resistivity of the organic membranes by which they are surrounded (see section 2.2 in this part). The different depths may be fed with such sinking and disintegrating aggregates, explaining the smallness of the shifts between morphological types along the vertical profile.

2.3.2 The study of the barite particle morphology at GEOSECS stations 3 and 5 in the North American Basin

Station 3: (Table II.6) Samples enriched in euhedral barites do occur at this station as well. However, in contrast to the situation at station 67, these are isolated cases occurring in intermediate and deep water (1875 m and 2982 m). both these samples are characterized by a very high number of barite particles (respectively 23,490 and 24,850 per litre), compared to <6000/litre for the other samples. They were sampled in a depth region considered as the formation site of NADW (see appendix V).

Station 5: (Table II.6) The sample at 760 m is enriched in euhedral barites.

However, such as for station 67 (see above), it are again the dissolution-affected barite particles which dominate the barite population at these two stations, since they represent from 75.5% to 89.0% of the total number (see Table II.6).

In section 4.3 of this part, the discussion concerning the relationship between the distribution of suspended barite and hydrology is continued.

2.4 THE ELEMENTAL COMPOSITION OF SUSPENDED BARITE PARTICLES

Only Sr and K were identified as genuine minor constituents of the barite particles (see § 2.3.3.A in part I). The analysis of artificial barites enriched in Sr, has shown (see § 2.3.3.B in part I) that Sr contents as low as 0.5 mol% (= 0.2% by weight) could still be detected by SEM-EMP. The detection limit for Sr is thus situated below the 2000 ppm level. For K we have no quantitative data, but since the K Kα peak rises but poorly above the background spectrum, the K content must be close to the estimated detection limit of 1000 ppm. For sedimentary barite Church (1970) reports a K concentration range of 100 to 1000 ppm. Church observed the Ca concentration to range also between 100 and 1000 ppm. Since Ca was not detected in suspended barite, at least not as a genuine component (see discussion in § 2.3.3.A in part I), its concentration must certainly not exceed the range reported by Church, for sedimentary barite. More detailed information was obtained for Sr.

A north and a south Atlantic profile (GEOSECS stations 67 and 3) were submitted to a systematic analysis of the Sr content of suspended barite. The analysis of about 200 barite particles measuring between 0.4 and 5 μm showed 13 % of them to contain detectable amounts of Sr, estimated at ≤ 5 mol %. At station 3, Sr-containing barite appears to be restricted to the upper part of the watercolumn (= first 1000 m). At great depth (> 3000 m) no Sr was detected in the barite

particles. The situation at station 67 is different. Here the fraction of barites with minor amounts of Sr is relatively small (0 to 8%) in surface water (above 200 m),but is large (∿ 40%) between 1500 and 3000 m. This apparent enrichment at depth can be explained by the fact that these deep samples are relatively poor in small barites (< 1 µm) which have mostly dissolved (see later section 4.3 in this part) and which were not observed to contain Sr. At station 67 no evolution of the Sr content with depth is apparent and the Sr concentrations in deep water are of the same magnitude (< 5 mol%) as observed in shallower water.

The presence of Sr appears to be dependent on particle size ,since small barites (< 1 µm), which in most cases are highly corroded, were observed to be Sr-free. This can be interpreted as the result of a preferential dissolution of the $SrSO_4$ fraction in the solid solution, what is in accord with recent observations of Church (1979) (see also later § 5.1.2 in this part), that solid solutions with $BaSO_4$ tend to be less stable in sea water. Church assumes that, as a result of this undersaturation, the composition of the solid solution will evolve to the one of the most stable phase in sea water (i.e. pure barite), by purifying itself from the substituting elements.

P.Buat-Menard and C.Jehanno (CFR - CNRS, Gif-sur-Yvette) showed that for the sub-tropical GEOSECS station 58 Sr containing barites are confined to the surface waters.

FIGURE II.7

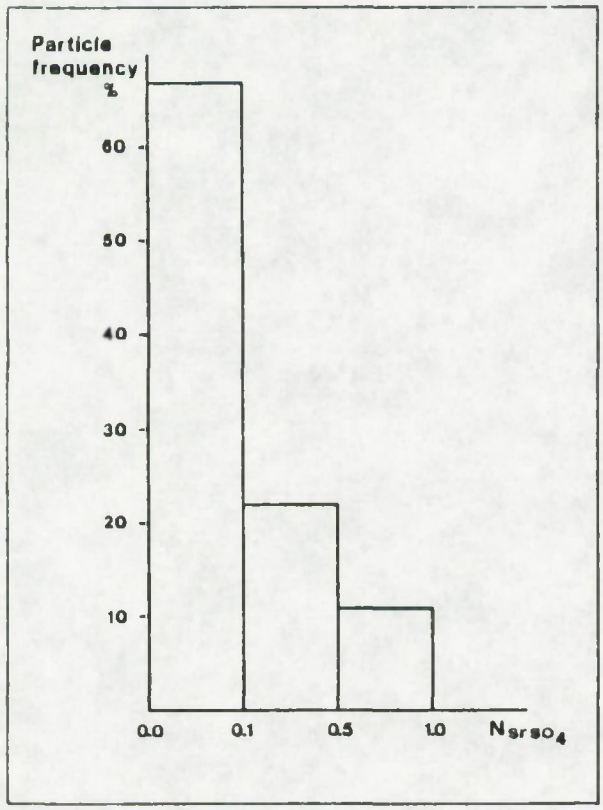

GEOSECS station 58; 200 m.
Frequency histogram of $(Ba,Sr)SO_4$ and $(Sr,Ba)SO_4$ particles in function of their $SrSO_4$ molar fraction (N_{SrSO_4}) ; $N_{BaSO_4} + N_{SrSO_4} = 1$.

At this station, a semi-quantitative analysis (see § 2.3.3.B in part I) of a 100 Ba-, Sr- and S-rich particles, collected at 200 m, revealed that 67% of the particles had Sr/Ba molar ratios ≤ 0.11; 22% had molar ratios between 0.11 and 1 and 11% had molar ratios > 1; see Figure II.7 (P.Buat-Menard and C.Jehanno, pers. comm.,1977).

Celestite particles occur as biogenic debris (Acantharia debris; Plate 7, n° 2,3) and as discrete particles with no obvious biogenic morphology, resembling barite particles (Plate 7, n° 5,6,7). Besides morphological differences we observe differences in chemical composition. In Acantharia we did not detect any Ba, while the barite-like celestites in most cases contain minor amounts of Ba. Both celestite phases can contain minor amounts of K and Ca. The presence of particles definitely recognizable as biogenic structures (Acantharia debris) is restricted to the surface waters (the first 500 m). This is in agreement with the observation of Bishop et al.(1977, 1979; Equatorial Atlantic and Cape Basin), that 50 to 75% of the Sr fraction associated with the Acantharia is dissolved in the upper 400 m of the watercolumn. The barite-like celestite particles are observed down to much greater depths (1499 m at station 67 and 3700 m at station 3). These strontium sulphate phases are thought to be more stable in sea water than the Acantharia debris due to the fact that they are solid solutions of $SrSO_4$ with $BaSO_4$. Such particles might consitute the major

part of the detected Sr_p amount below 500 m (see § 2.2.3 point B, in this part). In the surface waters (= above 500 m) we further observed amorphous, aggregate-like particles, essentially rich in Sr and S and containing minor amounts of K and Ca. We may be in the presence of organic phases enriched in sulphate and strontium (Plate 7, n°4), (see § 2.2.2 in this part).

Quite a broad spectrum of solid solutions of $BaSO_4$ with $SrSO_4$ exists in suspension in sea water. This substitution series extends from the Ba-free celestite phase ($SrSO_4$ Acantharia debris), over celestites with Ba and barites with Sr traces, to the Sr-free barite phase (Plate 7, Figures II.7 and II.8).

FIGURE II.8

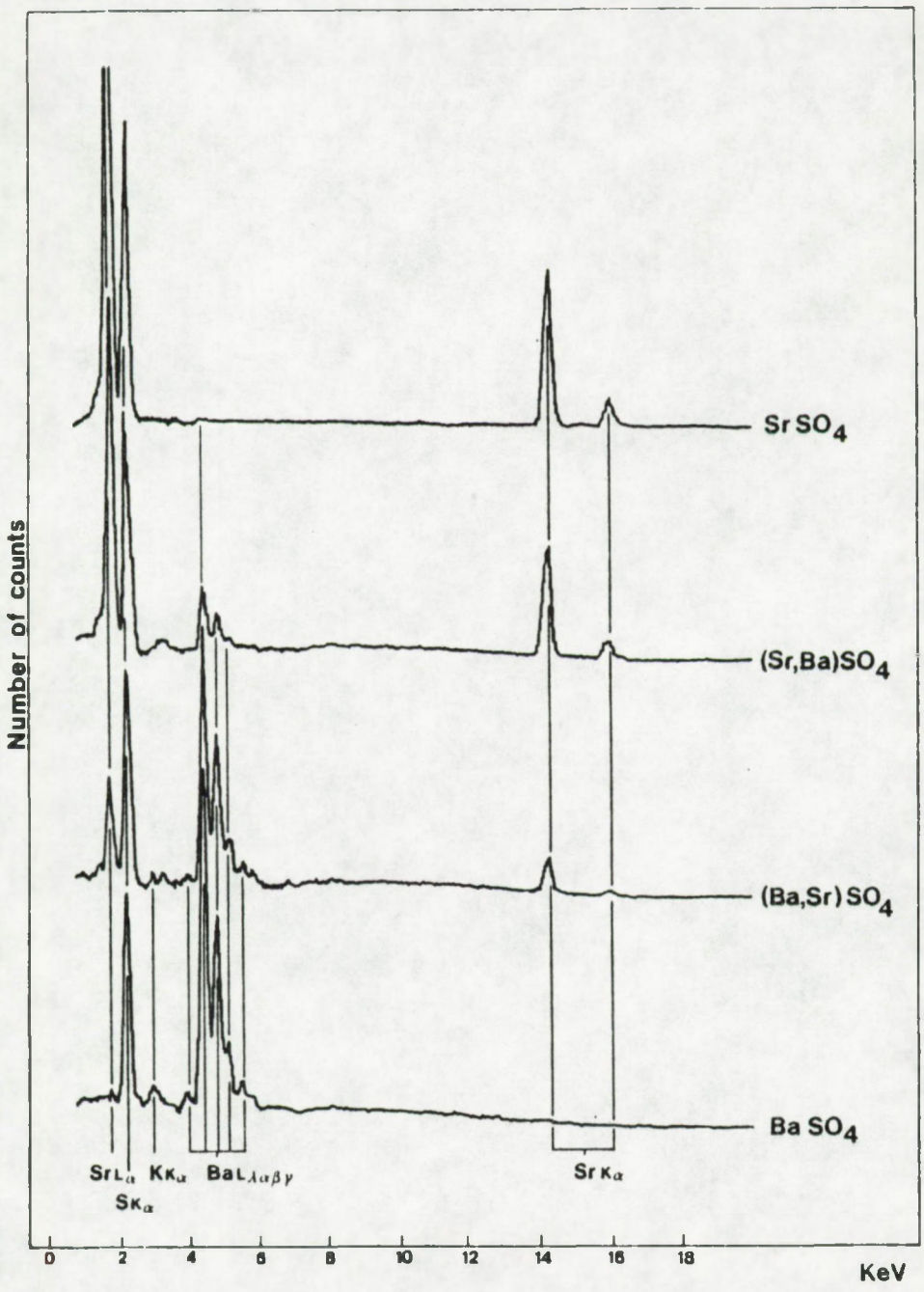

Energy dispersive spectra of barite, celestite and intermediate solid solutions, as observed in oceanic suspended matter. Vertical scales are arithmetic, but are normalized to the S Kα peak, which represents 58,000 counts. Horizontal scale: energies of the X-rays in KeV.

PLATE 7

CELESTITE PARTICLES

A. Particles with a distinct biogenic morphology:

1. GEOSECS Atlantic station 115 (28°04'N-25°54'W);
   a. SEM picture of Acantharia skeleton
   b. EMP picture of Sr
2. GEOSECS Atlantic station 67 (44°58'S-51°10'W); 151 m
   Skeleton debris
3. GEOSECS Atlantic station 67 (" ");
   Spicule debris
4. GEOSECS Atlantic station 67 (" "); 62 m
   Organic particle enriched in S and Sr

B. Particles with a morphology similar to the one of suspended barite

5. GEOSECS Atlantic station 67 (" "); 1499 m
   Euhedral, slightly corroded particle. The elemental spectrum is given in Figure II.8, "$SrSO_4$". No Ba detected.
6. GEOSECS Atlantic station 67 (" "); 600 m
   Rounded particle. The elemental spectrum is given in Figure II.8, "$SrSO_4$". No Ba detected.
7. GEOSECS Atlantic station 67 (" "); 151 m
   Rounded, ellipsoidal particle; contains minor amounts of Ba. The elemental spectrum is given in Figure II.8, "$(Sr,Ba)SO_4$". Corrosion traces are evident.

See discussion at page 126.

PLATE 7

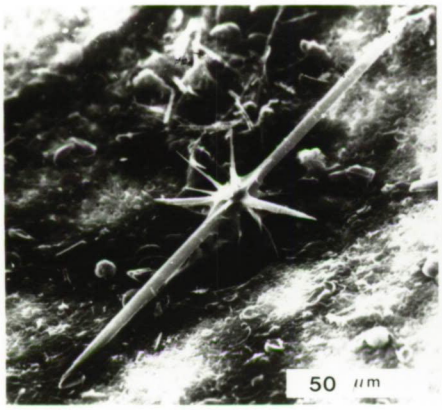

1a

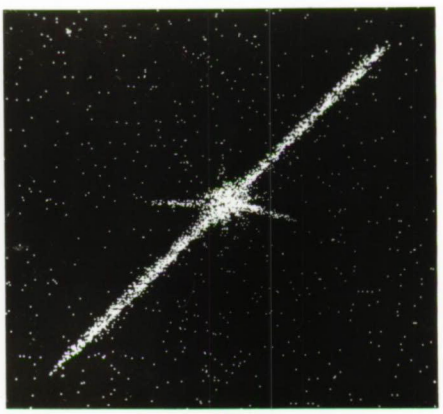

1b

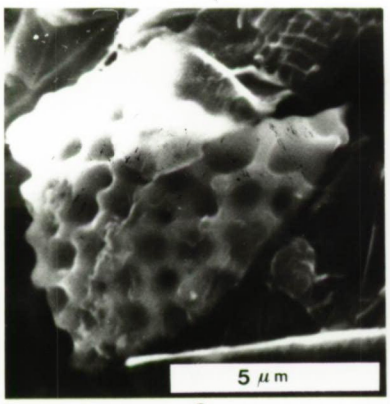

2

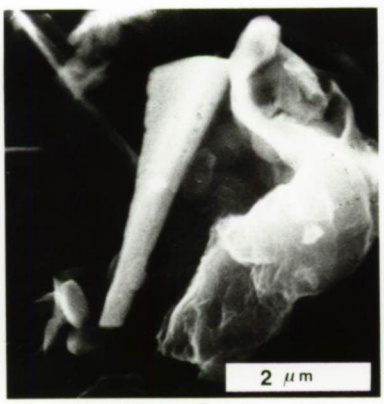

3

4

5

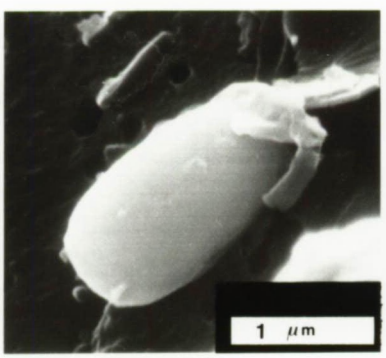

6

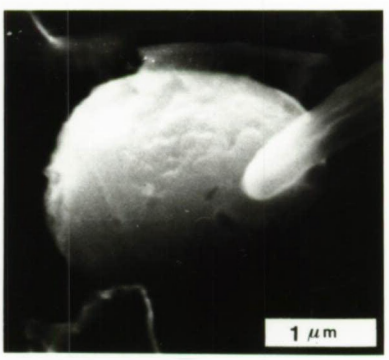

7

2.5 ANTHROPOGENIC BARIUM SULPHATE PRODUCTION

$BaSO_4$ is a salt produced in relatively large quantities. It is used in the manufacturing of a whole series of materials, and in oil-well drilling at sea.

The following informations were taken from a technical report by Miner, to the National Air Pollution Control Administration (Miner, 1969). These data concern only the U.S.A.
Production of barite and its industrial use:
About 90 % of the mined quantity of barite is used in oil-well drilling, in a ground and crushed state. Ground barite is also used as a filler in paper, rubber, cloth, linoleum, oil-cloth and in the manufacturing of glass, ceramic glazes and enamels. Mined barite is further used in the production of barium chemicals and lithopone. The latter consists of about 70 % $BaSO_4$ and 30 % $ZnSO_4$ and is used in the manufacturing of white pigment. Further, chemically precipitated (from BaS and Na_2SO_4), $BaSO_4$ (= Blanc-fixe) is used in the manufacture of coloring compounds and high-grade paint pigments. The total produced barite quantity remained more or less constant in the U.S., in the period extending from 1957 to 1966. The utilisation of ground, crushed barite in the U.S. in 1966, is distributed as follows over the different industrial branches:

oil-well drilling:	1,022,106	short tons*	85 %
glass	73,660	" "	6
paint	69,805	" "	6
rubber	38,805	" "	3
undistributed	4,605	" "	
	1,208,515		100 %

In 1975, 1,4 million metric tons of barite were used by the U.S. alone, as a drilling mixture for off-shore oil and gas exploration (Chow, 1976).

A barium-base organo-metallic compound is used as an additive in diesel fuel to reduce smoke emissions. Chemical analysis of the solids emitted by these engines revealed the presence of $BaSO_4$ and $BaCO_3$ (Miner, 1969). Measurements of environmental air samples in some major U.S. cities showed the presence of Ba. No quantitative data were available at the time of reporting by Miner. However, no Ba in excess over the quantity that is associated with aluminosilicates (= 600 ppm; Turekian and Wedepohl, 1961; Turekian, 1968) was ever detected in atmospheric samples collected above the marine environment (Buat-Menard and Chesselet, 1979 ; Chester and Stoner, 1973), and barite was never observed in samples of marine aerosols (Chesselet pers. comm.).

Chow (1976) anticipates the anthropogenic origin of dissolved Ba in sea water of drilling regions. The eventual dissolution of such anthropogenic barite is thought to increase the dissolved Ba concentrations in such regions.

---

* one metric ton = 0.907 x one short ton.

From our data on particulate Ba we derive a mean Ba_p concentration of 20 ng/Kg sea water (geometric mean obtained by considering all analyzed samples). Assuming this mean value to be valid for the World Ocean, the total Ba_p quantity in the oceans is:

$$1.1\times10^{21} \text{ litres} \times 20\times10^{-9} \text{ gr of } Ba_p = 2.2\times10^{13} \text{ gr Ba}$$
$$= 2.2\times10^{7} \text{ metric tons Ba}$$

If all Ba_p is in the barite form, this quantity represents some 4×10^7 metric tons of barite in suspension in the oceans, which is only 30 times more than the annual barite utilization in U.S. drilling operations.

Although anthropogenic Ba_p input in the oceans appears to be important, its utilisation is very local, restricted to accessible depths on the continental shelf and only a fraction of the utilized barite should contaminate surrounding sea water. It is further difficult to imagine a fast enough transport mode able to distribute this barite throughout the World Ocean. Theoretically the study of the elemental and isotopical composition of barites recovered from drilling sites and barites recovered from the open ocean should allow to distinguish between both. Since the former are from continental origin and the latter are formed by biological activity in the sea (see chapter 4 in this part), their Th and U content, their Sr^{87}/Sr^{86} ratio, as well as their δS^{34} will differ. Indeed, Church (1970) and Goldberg et al. (1969) showed sedimentary marine barite to be enriched in Th and U compared to continental barite. Further it was shown that the Sr^{87}/Sr^{86}

ratio and the δS^{34} values of marine sedimentary barite are generally similar to the one of sea water (Goldberg et al., 1969), while continental barite has generally a slightly higher Sr^{87}/Sr^{86} ratio and can have δS^{34} values up to 4 times higher (Goldberg et al., 1969). However, Church (1970) observed that the δS^{34} of continental barite is highly variable and his range of values includes those observed for sedimentary barite. Further, morphological differences can exist between both types of barite. To solve this kind of problem the combined punctual analysis method, proposed by Klossa (1976) can be considered. This method was devised to analyse a single microparticle with different equipment, which may consist of:

1) the high voltage electron microscope (HVEM), to analyze the habit, state of aggregation and crystallinity of the particles (see § 2.3.4 in part I)
2) the SEM-EMP equipment, to analyze particle morphology and elemental composition
3) the ionic micro-analyzer to analyze the isotopic composition of the particles

Further research on this matter is badly needed, but lays outside the scope of the present study.

CHAPTER 3

SUSPENDED PARTICLES CONTAINING BARIUM AS A MINOR COMPONENT

Generally speaking this "alternative" Ba phase is represented by relatively large particles, measuring from 3 µm to 20 µm for their largest diameter. Their morphology unmistakeably distinguishes them from what we call "classical" barite structures. In most cases they have very irregular contours and rough surfaces. Ba is either dispersed homogenously over the particle or is especially concentrated in some loci. In some of the latter cases we probably face aggregates enclosing barite particles.

3.1 ELEMENTAL COMPOSITION

On the basis of their elemental composition, two families of non-barite Ba-containing particles are distinguished:

1°) Particles with Fe as main component (Plate 8; Figure II.9.a). Si, Ca, Cl, S, Mg and Al can be present. Ba is either distributed uniformly over the particle (Plate 8 n° 3 a,b) or is concentrated in some loci (Plate 8 n° 1 a,b; 2 a,b). It was shown that discrete iron-rich particles in suspended patter are mainly present as goethite (Lambert, 1979). Adsorption of barium sulphate from solution, or scavenging of foreign particles such as suspended barites could explain the presence of barium and sulphur in these

FIGURE II.9.b

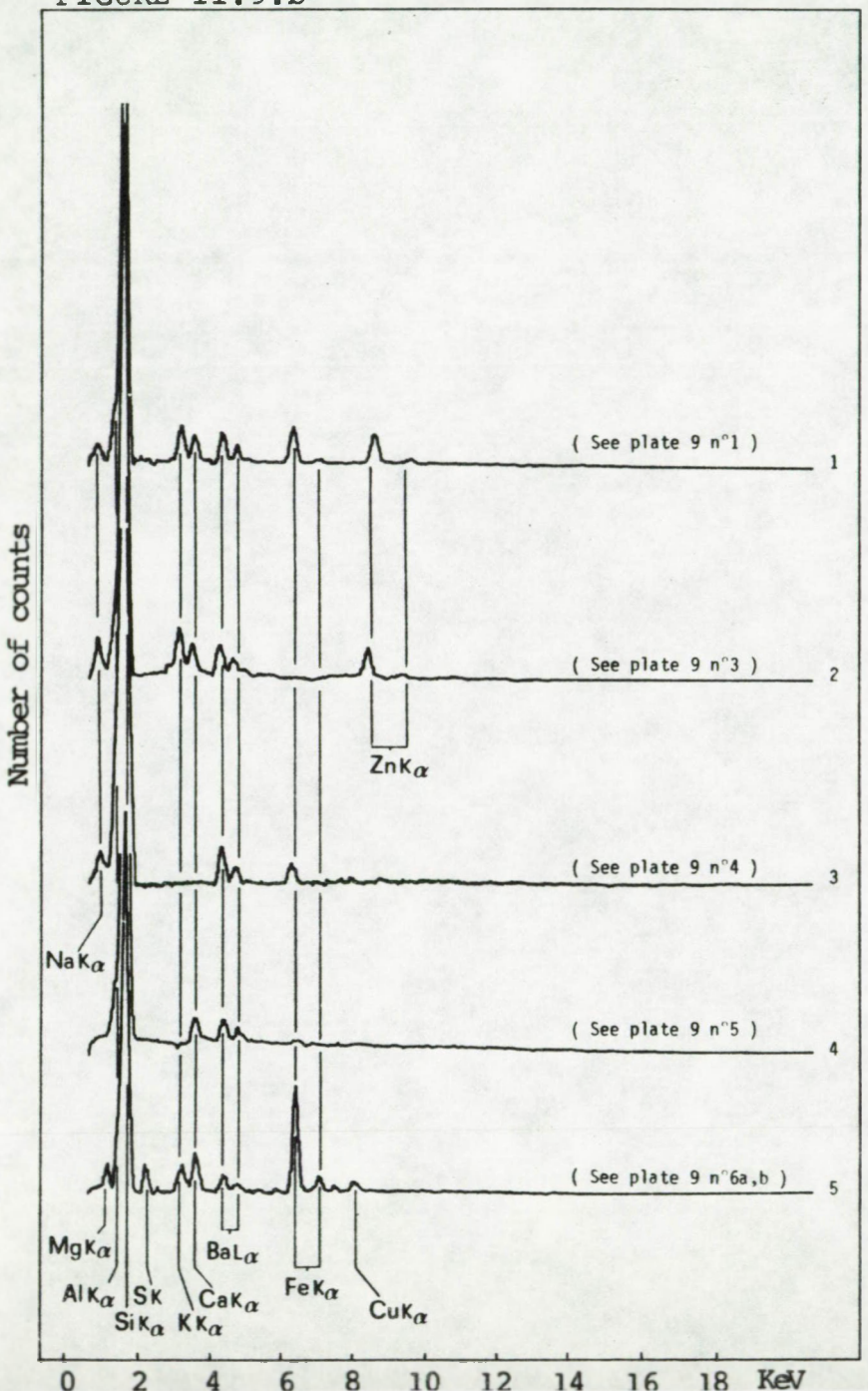

FIGURE II.9.a

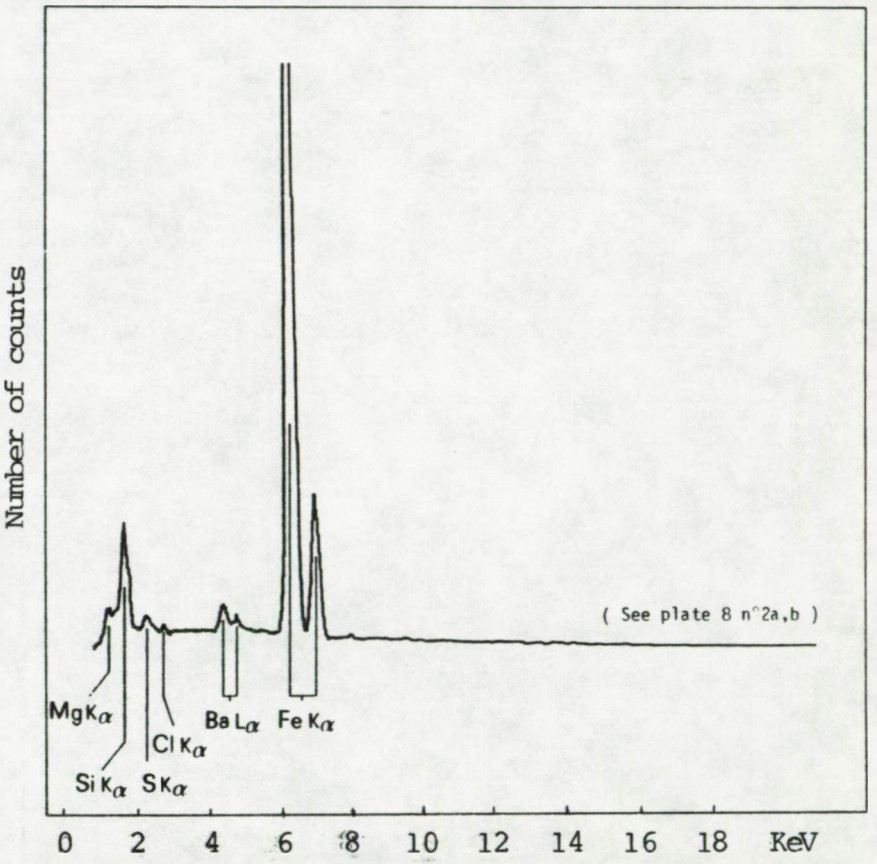

Energy dispersive spectra of particles containing Ba as a minor component. a: particles with Fe as major component. b: particles with Al and Si as major components. Vertical scales are arithmetic, but are normalized to the Ba Lα peak which represents 10,000 counts. Horizontal scales: energies of the X-rays in KeV.

particles.

2°) Particles with Al and Si as main components (Plate 9; Figure II.9.b). Fe, Ca, Na, K, Zn and S can be present. Three categories can be distinguished:

a) particles with a harmotome-, or Ba-feldspar-like composition (Plate 9, n°4):

- spectrum n°3 in Figure II.9.b shows only the presence of Na besides Al, Si ,Ba and Fe. Harmotome as a zeolite reported to occur in the marine environment (i.e. the sediments; Arrhenius, 1963; Cronan, 1974), is the most likely candidate. Deer et al. (1975) give the following composition for a continental harmotome:

  Harmotome: 45.51% SiO_2; 16.50% Al_2O_3; 0.27% MgO; 0.12% CaO; 19.89% BaO; 1.18% Na_2O; 1.77% K_2O; no Fe

  Although less evident, the presence in the marine environment, of Ba-feldspars is not impossible, when considering continental and/or submarine weathering processes. In this case, spectrum n°3 in Figure II.9.b could be the one of banalsite or barium-plagioclase, for which Deer et al. (1975) give the following compositions:

  Banalsite: 34.7% SiO_2; 31.2% Al_2O_3; 0.03% MnO; 1.00% MgO; 21.99% BaO; 0.81% CaO; 8.43% Na_2O; 0.66% K_2O; n oe Fe

  Barium-plagioclase: 55.1% SiO_2; 23.2% Al_2O_3; 0.45% Fe_2O_3; 0.56% MgO; 7.3% BaO; 1.83% CaO; 7.45% Na_2O; 0.83% K_2O; 0.45% Fe_2O_3.

  The presence of Fe in spectrum n°3, favors the Ba-plagioclase composition

- spectrum n°4 in Figure II.9.b shows no Na, but only Ca besides Si, Al and Ba. We assume the particle (Plate

9 n°5) to consist of the barium-feldspar calciocelsian, for which Deer et al. (op. cit.) give the following composition:

Calciocelsian: 42.0% SiO_2; 25.8% Al_2O_3; 25.8% BaO; 4.0% CaO; 0.3% Na_2O; 1.4% K_2O

b) aggregate-like particles containing biogenic debris:

- spectrum n°5 in Figure II.9.b shows the presence Mg, S, K, Ca, Cu besides Si, Al and Ba. The aggregate-like habit, the presence of diatom debris and of sulphur, suggests that the particle has gone through a biological transformation. A likely process can have been: uptake of detritic continental matter by zooplankton and excretion, together with biogenic components, as fecal material. The result is an aggregate-like structure with both, a detritic (high Si and Al content) and a biogenic (sulphur presence and diatom debris) component . This would further explain the presence of barite crystals on this particle, which could have formed inside this fecal material, according to Chow and Goldberg's model (1960).

c) pipe-like particles:

- spectra n°1 and 2 in Figure II.9.B show these particles to contain Na, K, Ca, Fe and Zn besides Si, Al and Ba. Such particles (Plate 9, n°1 to 3) were observed mainly in the Pacific Ocean. Identification was not possible

3.2 DISTRIBUTION IN THE OCEAN

As concerns the Atlantic Ocean these non-barite Ba containing particles are observed throughout the watercolumn, at stations extending from the Norwegian Sea to the Antarctic Ocean (GEOSECS stations 5, 3, 67, 82), including the equatorial region (HARMATAN stations 6, 15). The large discrete particles are probably of continental origin. The fact that samples were collected in the open ocean; favors the possibility of an eolian transport,shown by Buat-Menard (1979) to be the main process by which aluminosilicate material is brought to the open ocean surface water. Aggregates on the contrary can be the product of an in-situ process affecting detritic, biogenic and possibly authigenic particles. As a result of their important dimensions such particles must transit quite rapidly through the water-column to enter the sediments. Therefore, they are unlikely to feed the deeper waters in dissolved elements through ion-exchange or solubilisation processes. The question concerning the contribution of the detritic, continental matter to the total particulate Ba content in suspended is discussed further in section 4.4 of this part.

PLATE 8

IRON RICH PARTICLES CONTAINING BARIUM AS A MINOR CONSTITUENT

a. SEM picture; b. EMP picture of Ba

1. GEOSECS Atlantic station 5 (56°54'N-42°47'W); 363 m
   Barium is dispersed over the particle and is slightly concentrated in two loci. For elemental spectrum, see Figure II.9.a
2. GEOSECS Atlantic station 5 (56°54'N-42°47'W); 2464 m
   Barium is especially concentrated in two loci. For elemental spectrum see Figure II.9.a.
3. HARMATAN Atlantic station 15 (00°00' -05°30'W); 1000 m
   Ba is dispersed over the particle and is concentrated in several loci. For elemental spectrum see Figure II.9.a.

See discussion at page 133.

PLATE 8

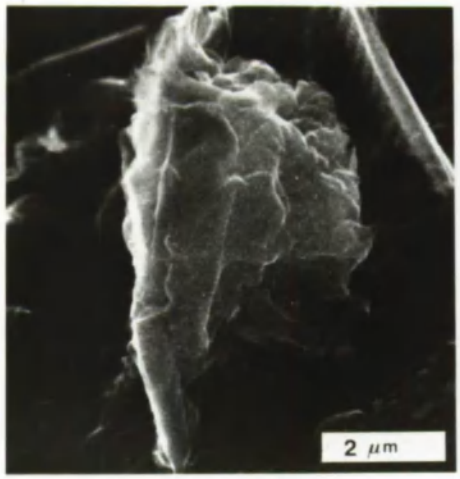

1a

1b

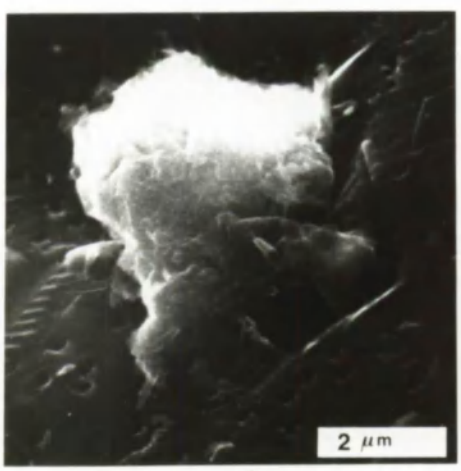

2a

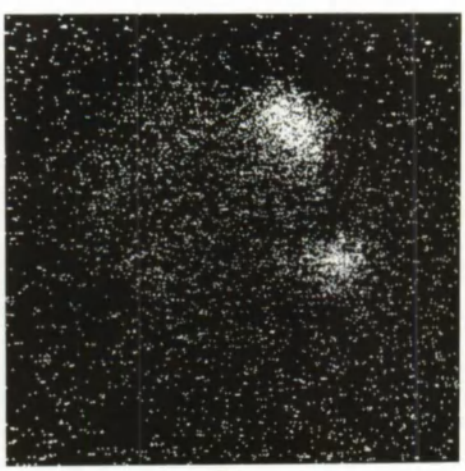

2b

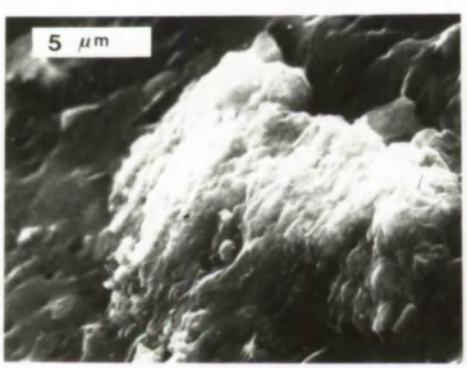

3a

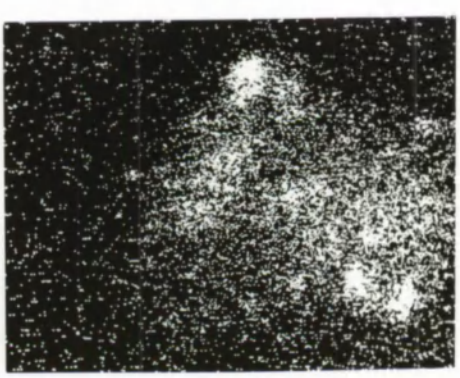

3b

PLATE 9

ALUMINIUM AND SILICON RICH PARTICLES CONTAINING BARIUM AS A MINOR CONSTITUENT

1. GEOSECS Atlantic station 67 (44°58'S-51°10'W); 3601 m
   Pipe-like particles containing Ba, K, Ca, Fe, Zn and Na as minor constituents besides Si, Al as major constituents The elemental spectrum is given in Figure II.9.b, n°1.
2. GEOSECS Pacific station 257 (10°10'S-170°00'W); 3737 m
   Pipe-like particle. Composition similar as 1 above.
3. GEOSECS Pacific station 257 (10°10'S-170°00'W); 3737 m
   Pipe-like particle. For composition see Figure II.9.b, n°2. No Fe detected.
4. GEOSECS Atlantic station 5 (56°54'N-42°47'W); 363 m
   Particle containing Ba, Na and Fe as minor constituents besides Al and Si as major constituents. The elemental spectrum is given in Figure II.9.b, n°3.
5. GEOSECS Atlantic station 3 (51°01'N-43°01'W); 2696 m
   Particle containing Ba, Ca as minor constituents, besides Al and Si as major constituents. The elemental spectrum is given in Figure II.9.b, n°4
6. GEOSECS Atlantic station 67 (44°58'S-51°10'W); 2193 m
   a. aggregate with Al and Si as major constituents and containing Ba, S, Ca, Fe, Mg and Cu as minor constituents. The elemental spectrum is given in Figure II.9.b n°4. Ba is concentrated in specific loci (=barite particles ?). The particle carries also biogenic debris what suggest that it has undergone a biological transformation (= ingestion and excretion)
   b. EMP picture of Ba.

See discussion at page 135.

PLATE 9

1

2

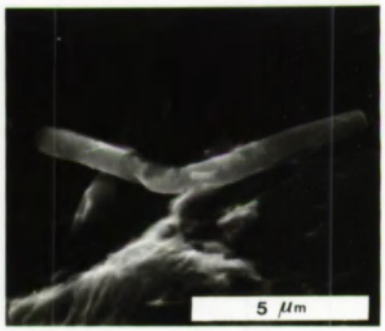

3

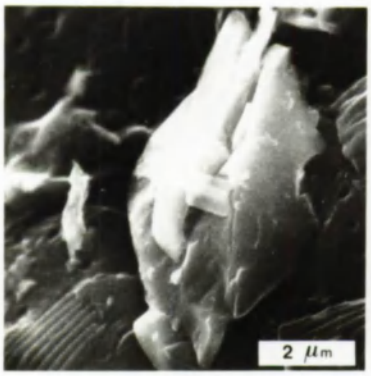

4

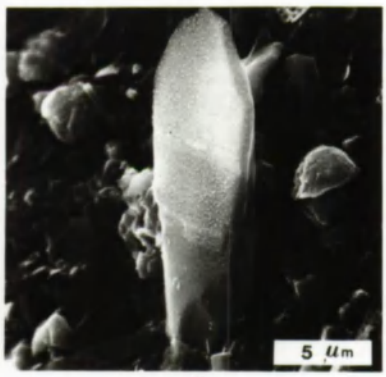

5

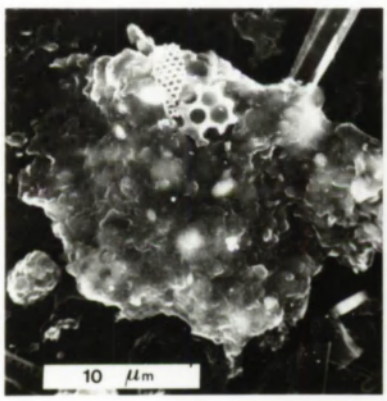

6a

6b

CHAPTER 4

BARITE AS THE MAIN BARIUM CARRIER IN OCEANIC SUSPENDED MATTER

4.1. SIZE AND MASS DISTRIBUTIONS OF SUSPENDED BARITE PARTICLES AT GEOSECS STATIONS 67, 3 AND 5

4.1.1. Tables and Figures

For the three selected profiles in the Argentine Basin (GEOSECS station 67) and the North American Basin (GEOSECS stations 3 and 5) (section 2.3; part II) barite particles size distributions were computed.

The barite particles sizes were deduced as described in § 2.3.5 part I . The size distributions are given in Figure II.10.A,B,C We remind that the diameters were classified in a geometric progression. The modes of the size distributions, and the numbers of barites are plotted against depth in Figure II.11 From Figure II.10 it appears that the size distributions are of the log-normal type. This was verified by plotting the cumulated frequences against particles diameter on gausso-logarithmic graphs. Some of these plots are shown in Figure II.12. This type of distribution is not unusual and has been observed by SEM-EMP for other categories of suspended particles, including aluminosilicates (Lambert, 1979) and

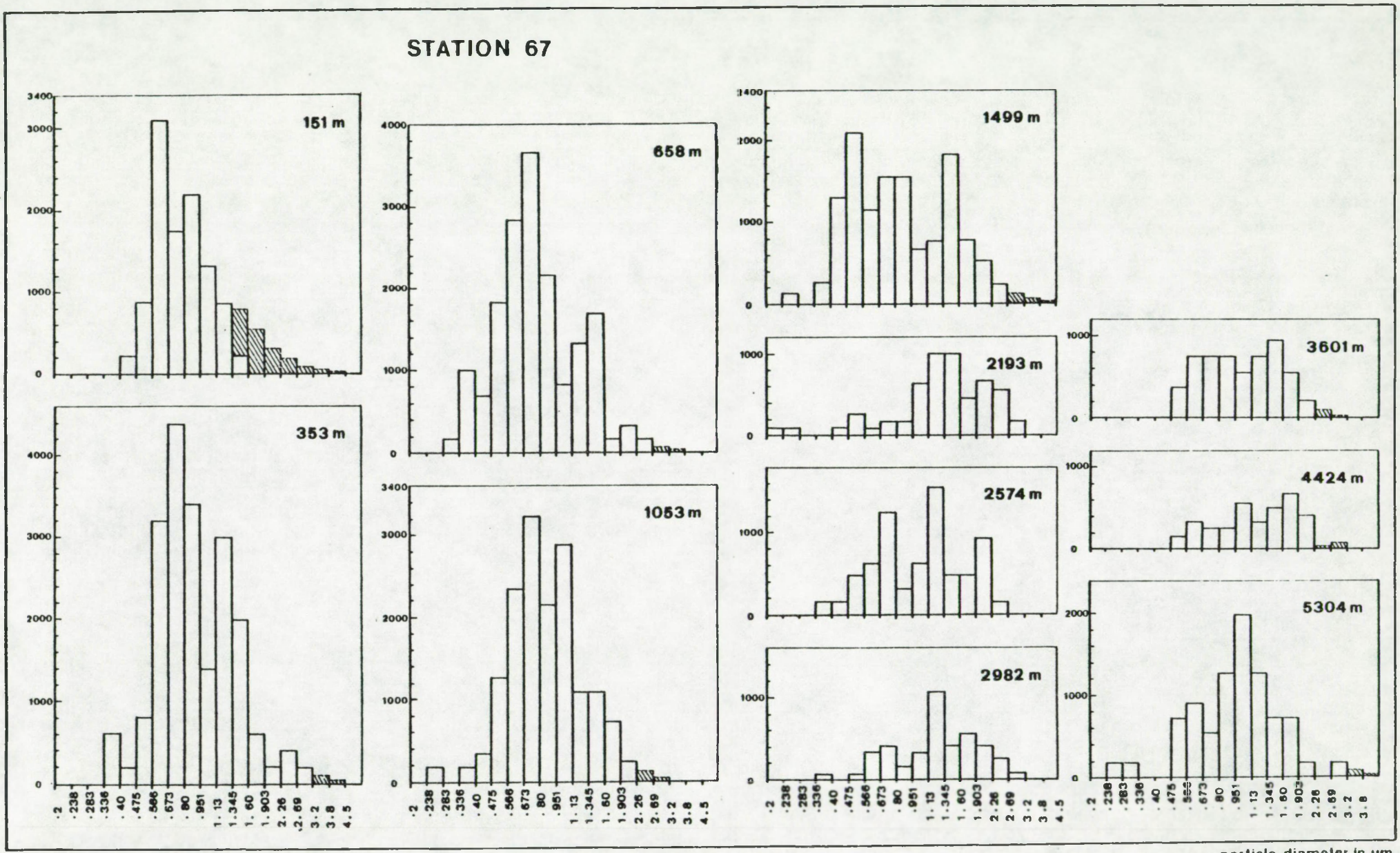

FIGURE II.10.A

See page 140 for figure caption

FIGURE II.10.B

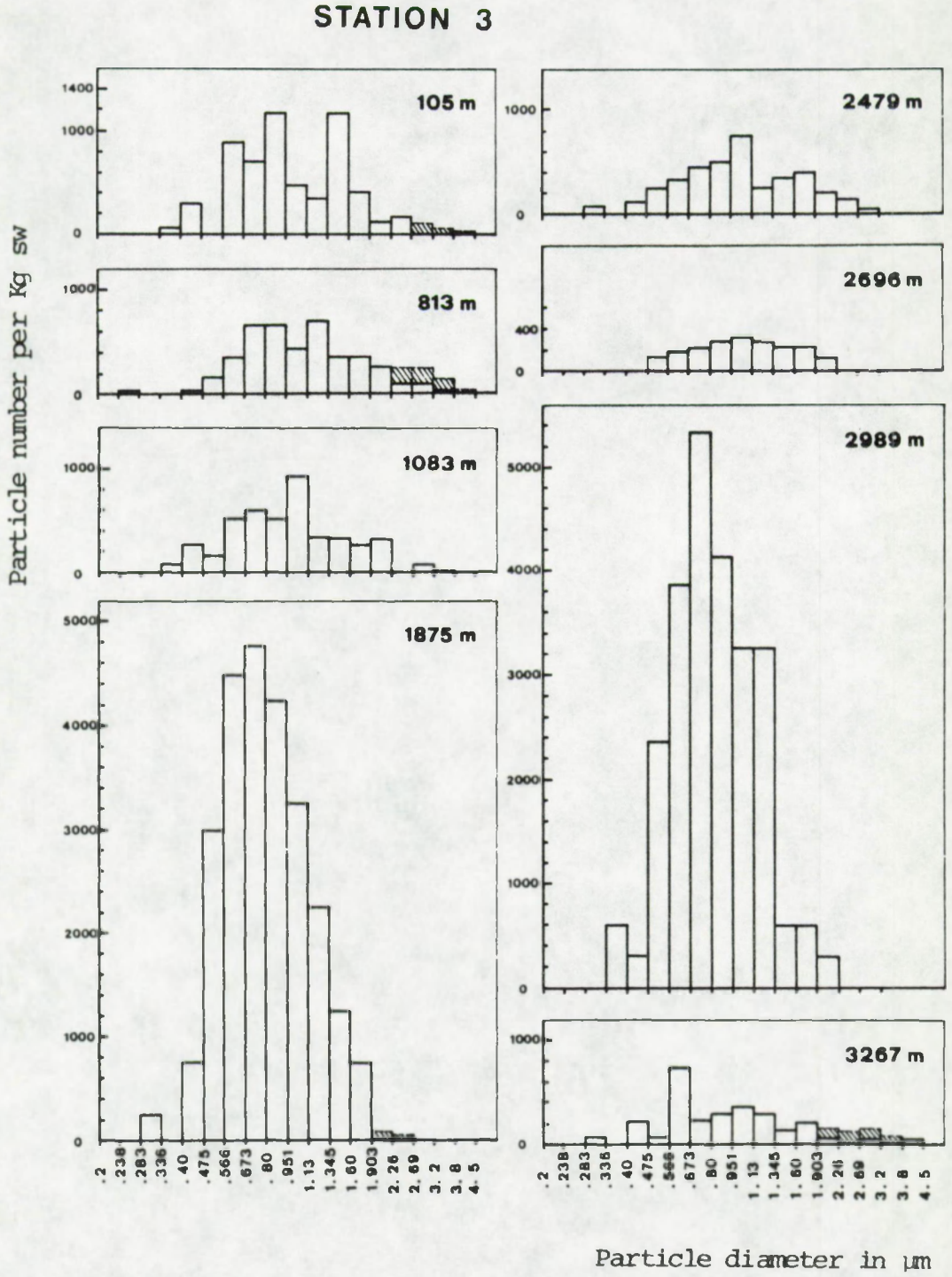

Number frequency versus size histograms for barite particles from various depths at GEOSECS stations 67 (II.10.A), 3 (II.10.B), 5 (II.10.C). For the abscissa sizes are classed in a logarithmic progression (see § 2.3.5 in part I). Particles smaller than 0.2 µm were not detected. Hatched areas on the right side of the histograms represent non-recorded particles, whose presence is required in order for barite to account for the total Ba_p mass. The frequencies under the hatched areas were deduced from the cumulative Ba mass distributions in FIG. II.13.

FIGURE II.10.C

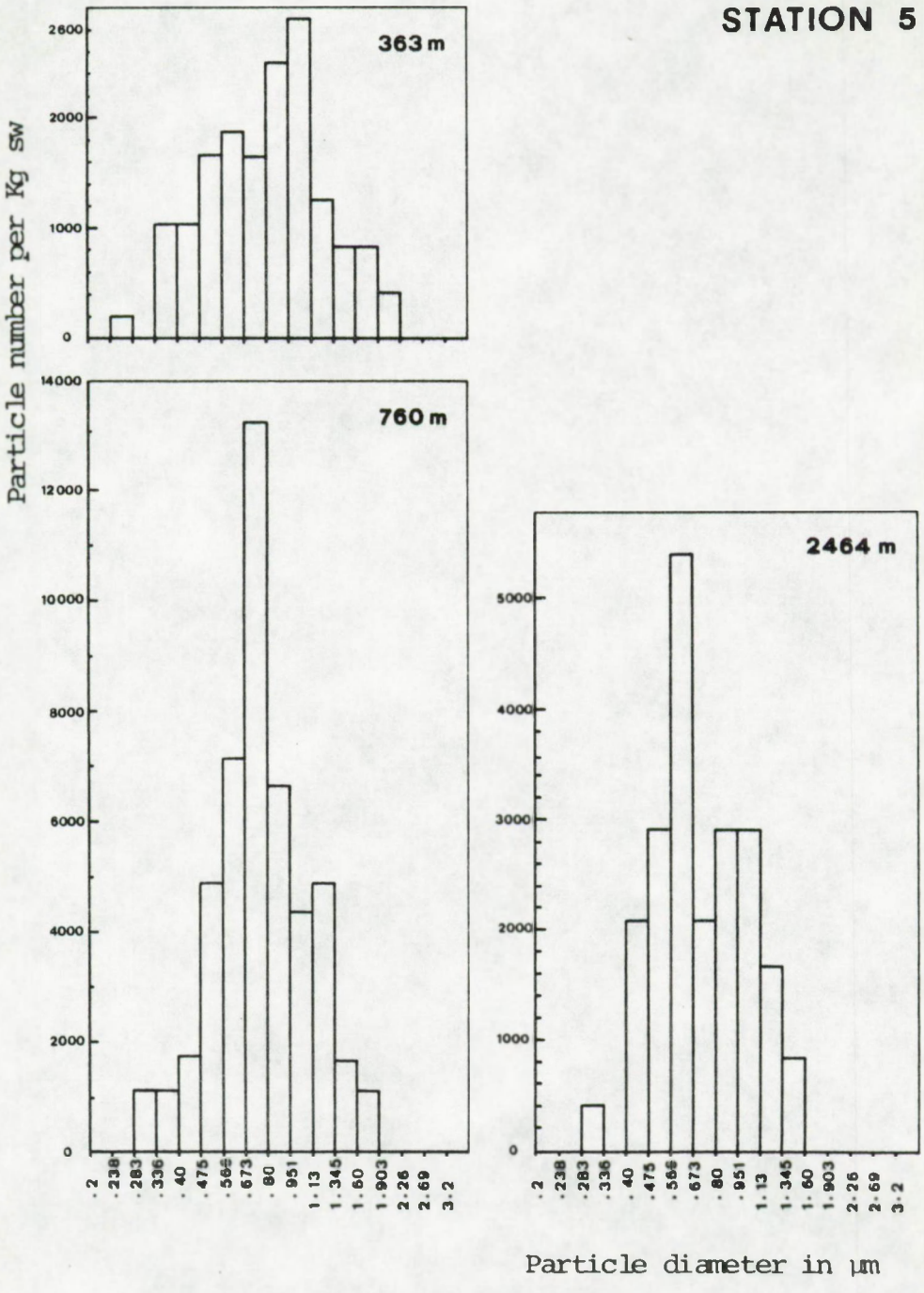

See page 140 for figure captions.

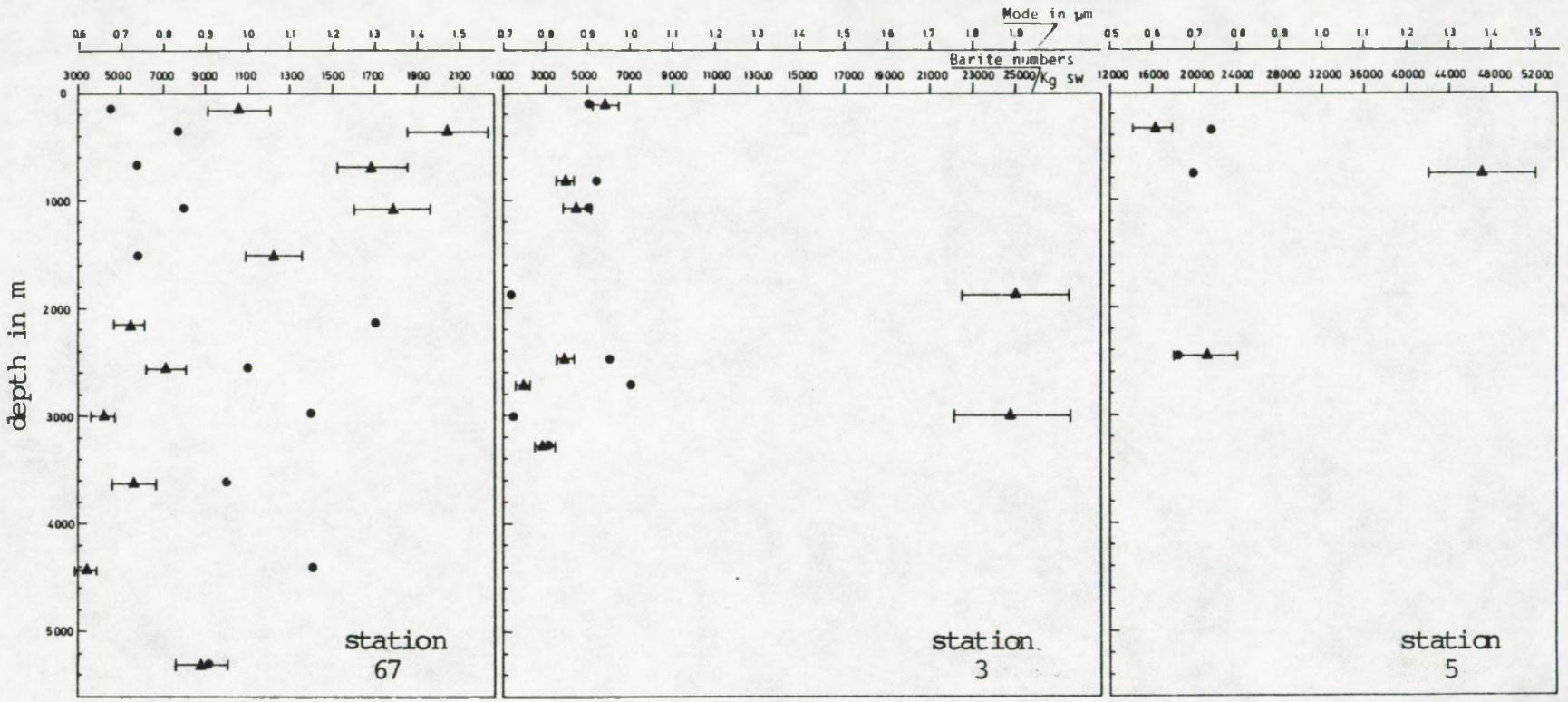

FIGURE II.11

GEOSECS stations 67, 3 and 5. Vertical distributions of the mode values for the size distributions given in FIG. II.10.A,B,C, and of the numbers of barite particles per Kg sea water

FIGURE II.12

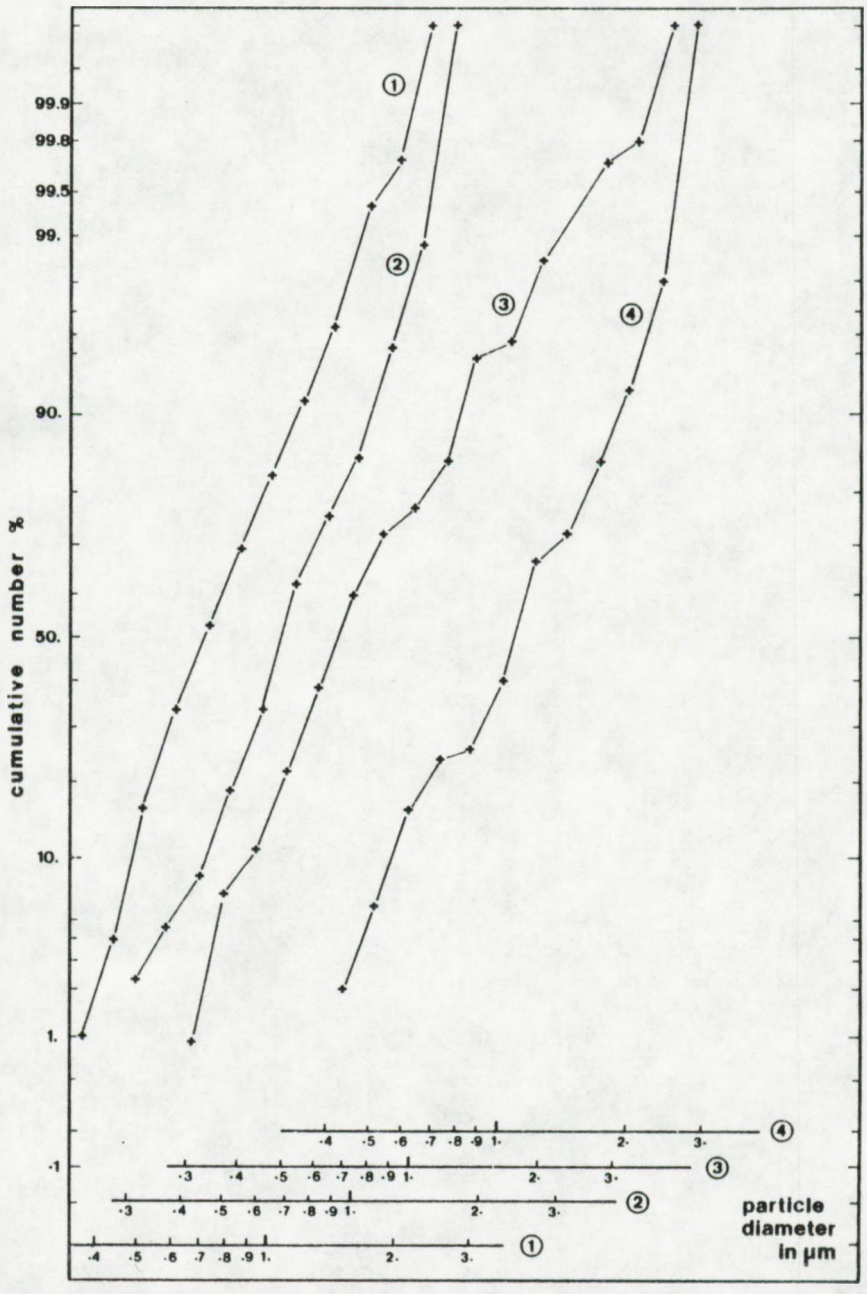

Cumulative number versus particle diameter for barite particles from samples at 658 m, 2982 m, GEOSECS station 67 (n° 3,4); at 1875 m, GEOSECS station 3 (n°1); at 760 m, GEOSECS station 5 (n°2). Ordinate: gaussian scale; abscissa: logarithmic scale. The fact that the cumulative size distributions fit well to straight lines, indicates that the log-normal distribution is approached.

calcareous and siliceous debris (Lambert et al., 1979; Aubey, 1976). These barite size distributions enabled us to compute the mass of Ba carried by suspended barite, by solving eq. (1.7 ; Chapter 2, part I).

In this computation the influence of barite occurring as solid solutions with $SrSO_4$ was not considered since:

a) the solid solutions with an important $SrSO_4$ contribution occur mainly in surface waters (first 200 m), while the samples we analyzed for barite content were essentially taken in deeper water (= below 200 m)
b) the solid solutions occuring below surface waters are generally characterized by a small ($\leq$ 5 mol %) $SrSO_4$ content.

In Figure II.13 the cumulated Ba masses carried by the suspended barite particles are plotted against particle diameter in gausso-logarithmic graphs. These cumulated Ba masses are expressed as fractions of the total Ba_p quantity measured for the same samples by INAA:

$$F(D) = W/W_t = 1/W_t \cdot \int_{D_o}^{D} f(D) \cdot dD$$

with $F(D)$ = cumulative distribution of the Ba mass in function of barite particle size
D_o = observed lower limit of particle size
W = Ba mass of the barite particles
W_t = total Ba mass, measured by INAA
$f(D)$ = distribution of the Ba mass in function of particle size.

FIGURE II.13

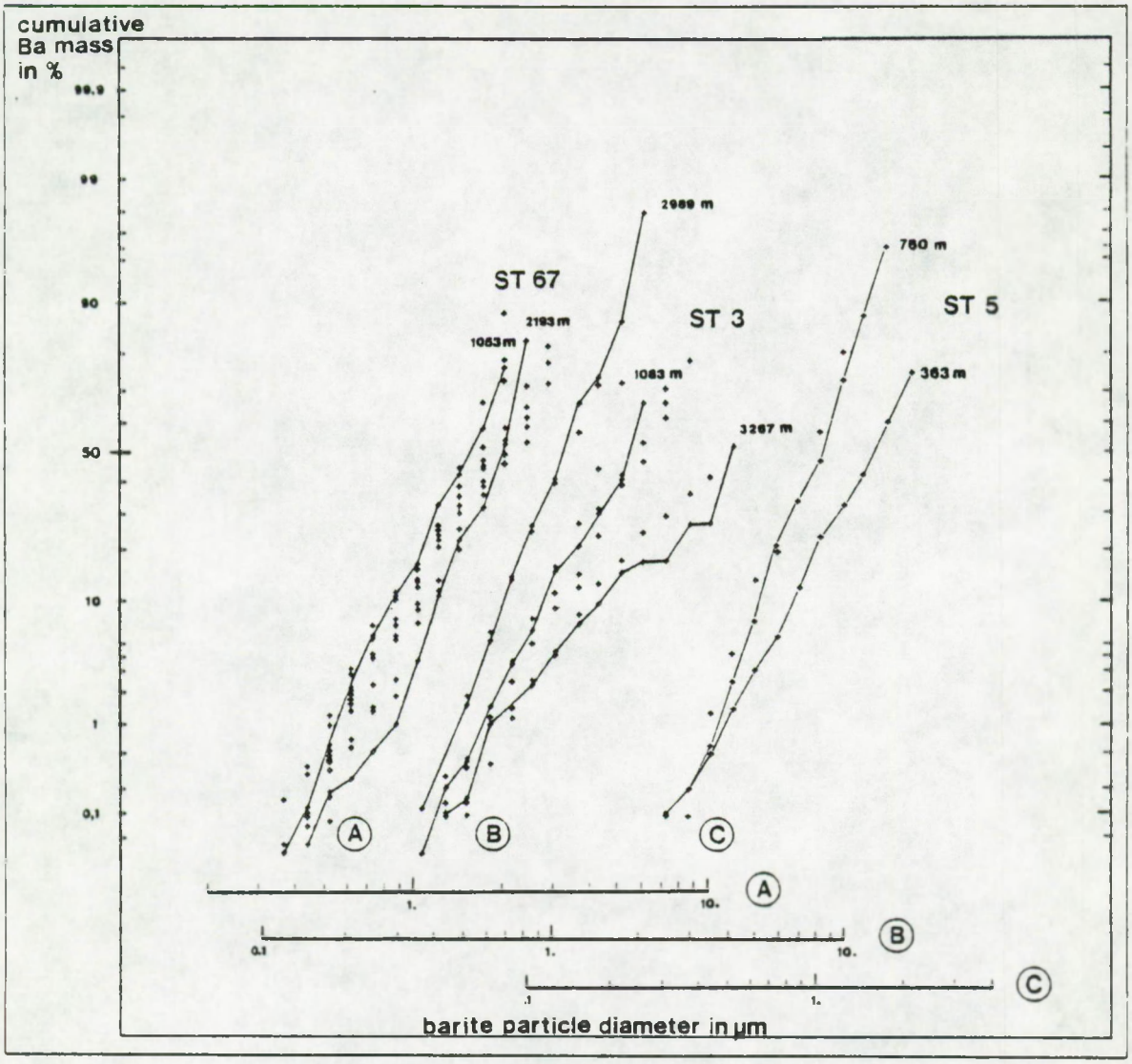

Profiles of cumulative Ba-mass distributions. Ordinate (gaussian scale): cumulative Ba mass in %, calculated with respect to the total Ba_p amount measured by INAA. Abscissa (logarithmic scale): barite particle diameter in µm. Crosses refer to measured values of cumulated Ba mass in %.
A: GEOSECS station 67; depth interval 151 to 5304 m; only the distributions at 1053 and 2193 m are displayed as a solid line. B: GEOSECS station 3; depth interval 105 to 3267 m; only the distributions at 1083 , 2989 and 3267 m are displayed as solid lines; C: GEOSECS station 5; depth interval 363 to 2464 m; only the distributions at 363 and 760 m are displayed as a solid line.

From Figure II.13 it appears that the mass distributions fit well the log-normal distribution, as shown already for the barite size distributions (Figure II.12). The mass distribution function can thus be approximated by:

$$f(D) = \frac{1}{(b\sqrt{2\pi}).D} \exp\{-1/2[(\frac{\ln D - a}{b})^2]\}$$

with a and b representing numbers such that:

$\ln D = a + b \cdot u$, with $u = (\frac{\ln D - a}{b})$, which is the reduced value of $\ln D$; D = particle diameter.

The characteristic parameters of this distribution are:

- the mode: $e^{(a-b)^2}$
- the mean: $e^{(a+b^2/2)}$
- the median: e^a
- the standard deviation: $= e^{(a+b)^2} \cdot \sqrt{1 - e^{-b^2}}$

The parameters can be deduced eaily from the gausso-logarithmic graphs (Figure II.13), since:

$a = \ln D$ for $F(D) = 50$ th percentile

$b = \ln(D/D')$ for $F(D) = 50$ th and $F(D') = 16$ th percentile.

The central tendency parameters and the standard deviation of the mass distributions are presented in Table II.7 .

It appears from Figure II.13, that in most cases, suspended barite is the main carrier of Ba. This matter is discussed more extensively below in section 4.2 .

Table II.7: Central tendency parameters and standard deviation values of the Ba-mass distributions in function of barite particle size.

Depth in m	a	b	median µm	mode µm	mean µm	standard deviation µm
GEOSECS station 67						
151	0.55	0.56	1.7	1.0	2.0	1.2
353	0.64	0.58	1.9	1.0	2.2	1.4
658	0.65	0.60	1.9	1.0	2.3	1.5
1053	0.42	0.46	1.5	1.0	1.7	0.8
1499	0.69	0.57	2.0	1.0	2.3	1.4
2193	0.72	0.41	2.0	1.1	2.2	1.0
2574	0.57	0.47	1.8	1.0	2.0	1.0
2982	0.68	0.41	2.0	1.1	2.1	0.9
3601	0.42	0.42	1.5	1.0	1.7	0.7
4424	0.63	0.41	1.9	1.0	2.0	0.9
5304	0.54	0.46	1.7	1.0	1.9	0.9
GEOSECS station 3						
105	0.72	0.52	2.1	1.0	2.3	1.3
813	1.12	0.64	3.0	1.3	3.8	2.7
1083	0.60	0.48	1.8	1.0	2.0	1.0
1875	0.16	0.40	1.2	1.1	1.3	0.5
2479	0.68	0.48	2.0	1.0	2.2	1.1
2696	0.45	0.43	1.6	1.0	1.7	0.8
2989	0.12	0.38	1.1	1.1	1.2	0.5
3267	1.32	0.74	3.7	1.4	4.9	4.2
GEOSECS station 5						
363	0.42	0.50	1.5	1.0	1.7	0.9
760	-0.01	0.33	1.0	1.1	1.0	0.4
2464	0.03	0.39	1.0	1.1	1.1	0.5

median = e^{a}; mode = $e^{(a-b)^2}$; mean = $e^{(a+b^2/2)}$; st.dev.= $e^{(a+b^2)}\sqrt{1 - e^{-b^2}}$

with a = lnD for D= particle diameter corresponding to the 50 th percentile of the cumulated mass; b = ln(D/D') for D and D' resp. = particle diameter for the 50th and 16th percentiles of the cumulated mass.

4.1.2 Interpretation of the vertical profiles of the barite size and mass distributions

i) Station 67:

The numbers of barite particles per Kg sea water decrease from 20400 at 353m to 12240 at 1499 m (Figure II.11). Below 1499m, when entering the high salinity NADW* layer, barite numbers decrease further to 5440 per Kg sw at 2193m. This decrease is due to a scantiness of the small-sized (< 1µm) barites (Fig. II.10.A), which can have largely dissolved. This shifts the modes of the size distributions towards the larger diameters (Fig. II.11). The assumption that effects of a dissolution process are seen here, is concordant with the results of our morphological analyses, showing an increase, at this depth,of the fraction of barites altered by dissolution (see § 2.2.1 in this part). The decrease of barite numbers below 1499m results further in a narrowing of the Ba-mass distributions. Indeed, in Table II.7 the standard deviations are seen to be > 1 at 1499m and at shallower depths (except for the sample at 1053m), while they are ⩽ 1 below 1499 m. Central tendency parameters of the mass-distribtions, on the contrary, remain quite constant all along the profile (Table II.7). Since the relative scantiness of small-sized barites has not led to an increase of the central tendency parameters, the number of large-sized barites must decrease as well with depth. Barite numbers attain a minimum of 3440 per Kg sw at 4424m in the AABW*. The relative increase, here at 4424m, of the fraction of euhedral barites (essentially due to the relative increase of aggregates of barite prisms (Table II.6)) compared to waters of the NADW core above, was inter-

* the hydrological situation of station 67 is discused in appendix V.

preted as reflecting advective transport of particles (see § 2.2.1, in this part). This shows that dissolution is not the only process which controls the barite particle numbers and sizes at depth, what is concordant with our Factor Analysis data (§1.1.4).

At 5304m, in bottom water, barite numbers increase again. We have seen in § 1.1.1 (in this part) that the increase of the absolute amount of "excess" Ba_p (= non-terrigenic Ba_p fraction) in bottom waters could result from the resuspension of sedimentary barite. The influence of this resuspension might be sensed up to 5304m, explaining the increase of barite numbers we observe at this depth.

On the basis of the barite size and mass distribution shapes, samples above 1500 m are distinct from those below this depth. This depth coincides with the boundary between AABW + NADW and AAIW + surface water (see appendix V). However, distinctions between individual water types, such as were made in § 1.1.4 (in part II) with the results of factor analysis, can not be made here.

At station 67 a direct proportionality exists between the total Ba mass and the number of barites (Figure II.14.a).

ii) Station 3:

Two groups of size distributions are distinguished:

1) size distributions with the mode at ~ 1 µm; the particle frequencies are low; total barite numbers do not exceed 6000/Kg SW (samples at 105 m; 813 m; 1083 m; 2499 m; 3267 m; Figure II.11). Central tendency parameters and standard deviations of the Ba-mass distributions are relatively high (Table II.7).

Figure II.14.a

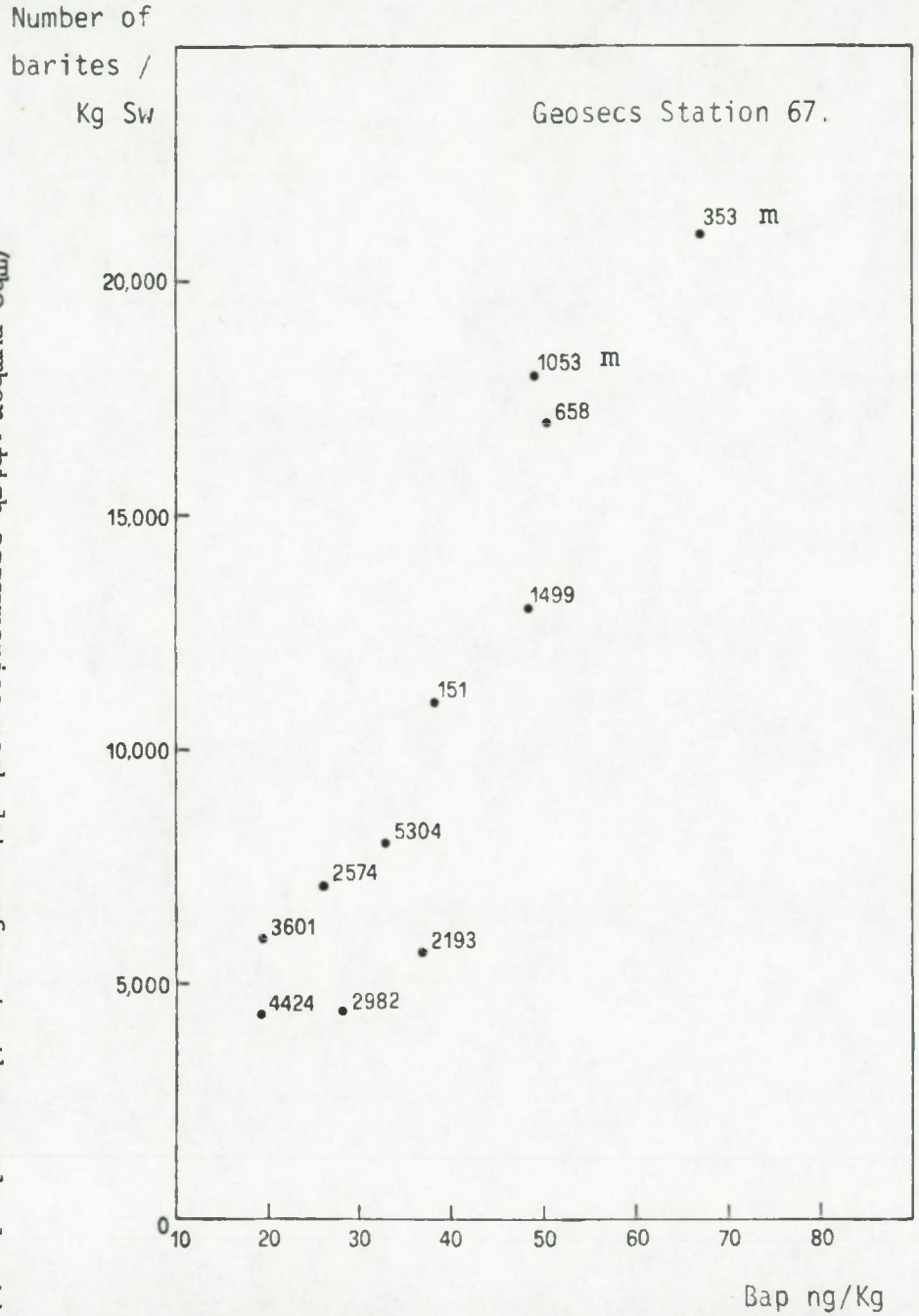

(The number which accompanies each dot, refers to the sample depth)

a: GEOSECS station 67; covariation between -umbers of barite particles and total Ba_p

Figure II.14.b

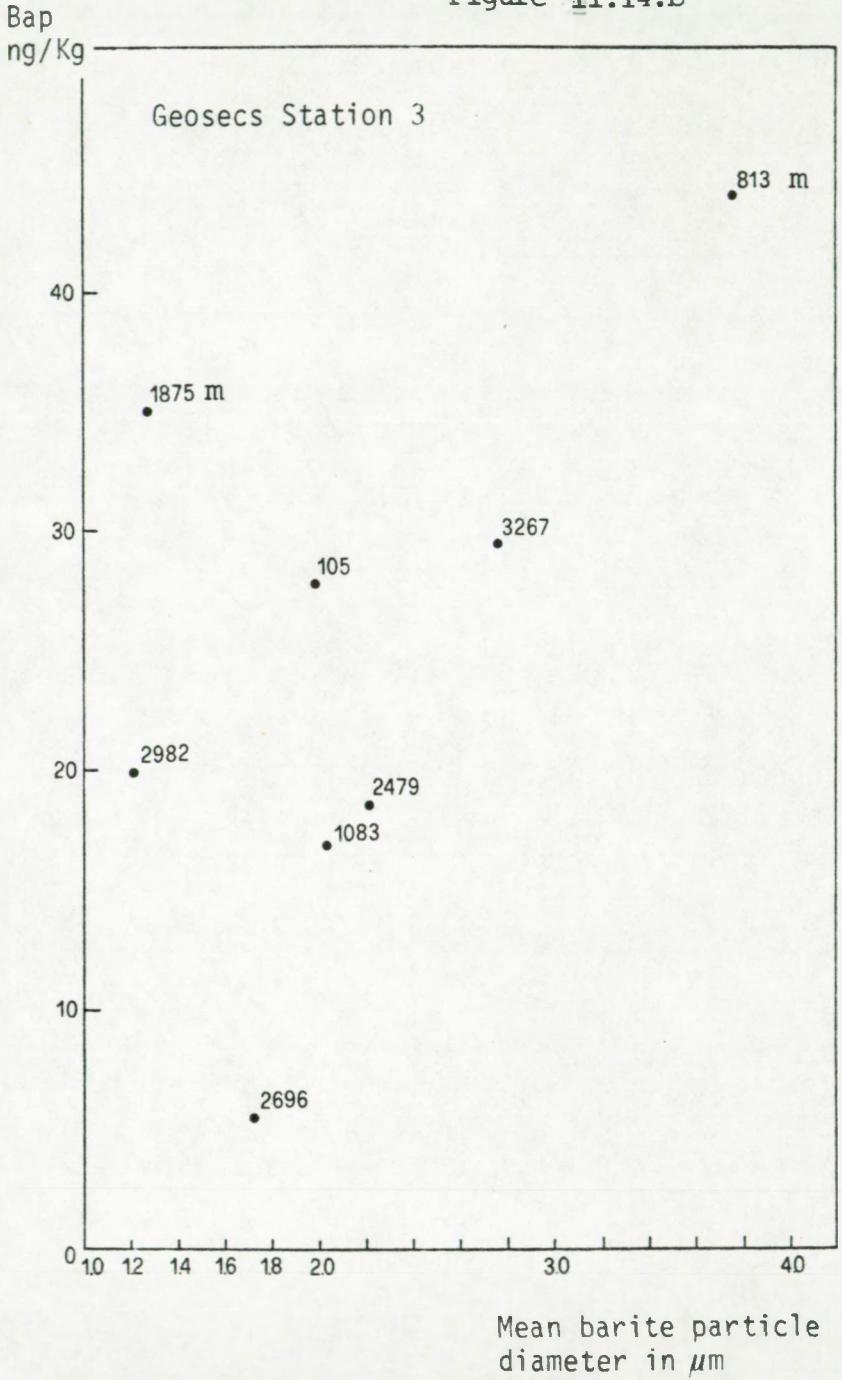

b: GEOSECS station 3; covariation between total Ba_p and mean barite particle diameter

FIGURE II.14

2) size distributions with the mode at ~ 0.7 μm; particle frequencies are high; total barite numbers exceed 20,000/ Kg (samples at 1875 m ; 2989 m; Figure II.11). Central tendency parameters and standard deviations are small compared to those of point 1 (Table II.7).

The 2696 m sample does not fit into this classification, since it has both, a low particle number (Figure II.11) and low values for central tendency parameters and standard deviation (Table II. 7). As a result, this sample has the lowest Ba_p content along the profile (Table II.4 , chapter II).

At station 3, in 5 cases over 8, central tendency parameters (i.e. particle size) rather than particle number are positively related with the Ba_p concentration (Figure II.14.b).

Surface water is not enriched in barites, compared to deep water, such as observed at station 67. No continuous evolution of barite numbers with depth exists. For two isolated cases (1875 m and 2696 m) barite numbers increase sharply. We have no clear explanation for this situation, which could be tentatively explained by the complex hydrology of this station (Spencer pers. comm.), (see appendix V).

iii) Station 5:

This station is characterized by the same complex hydrological conditions as observed at station 3 (see appendix V). Again important variations in barite particle frequency occur with depth (Figure II.11). The shift of the size

distribution modes at 760 m and 2464 m to smaller diameters points toward a relative enrichment in small barites (Figure II.11). This is also reflected in smaller median and mean values of the corresponding Ba-mass distributions (Table II.7). Further standard deviations of the mass distributions at 760 m and 2464 m are smaller than at 363 m. The barite number at 760 m is the highest observed for all three profiles.

The hydrological situation in the North American Basin (appendix V) reveals a complex interaction of Labrador-, Greenland-, Norwegian-Sea and Antarctic Intermediate (AAIW) waters. The young ages of these watermasses (with exception of AAIW), which are close to their source regions, the complexity of their flow pattern and the temporal variability in the overflow of Greenland and Norwegian Sea waters (Dietrich et al., 1972; Chan et al., 1977), may be responsible for the observed lack of continuity, with depth, in the size distribution profiles at stations 3 and 5.

4.2. BARITE AS THE MAIN CARRIER OF BARIUM IN OCEANIC SUSPENDED MATTER

The Ba masses carried by suspended barite, as calculated by eq. (1.7, chapter 2, part I), are given in Table II.8 (column B) and are compared with the total Ba_p measured by INAA on the same filters (column C), expressed as a percentage (column D). As concerns GEOSECS station 5, our barite-barium data are compared with INAA data for total Ba_p measured by P. Brewer for this station (GEOSECS shore-based data). However, since Brewer's data concern other samples in the profile than those we analyzed by SEM-EMP, we deduced the values of total Ba_p by intrapolation of his data.

The conclusion that barite is the principal carrier of barium in these samples is inescapable, considering the nature and limitations of the method. In 15 cases out of 23, calculated barite contributions account for over 70% of the total Ba_p and for several samples the values are virtually 100%. There are only a couple of cases where the percentage drops below 50%.

Part of the Ba that is nor accounted for by detected barites is certainly carried by phases other than barite (see below). We believe that large barite grains (> 3 μm), which are very scarce and thus statistically missed during counting procedures, but which have large mass, can account partly for the apparently low percentages in Table II.8 .

Table II.8: Comparison between the amount of particulate barium carried by barite particles, measured by SEM-EMP, and the total particulate barium measured by INAA.

	A		B		C		D
Depth	Number of barites		Particulate Ba in barites		Total Ba_p (INAA data)		Fraction of total Ba_p carried by barite
m	N/Kg sw	σ♦	ng/Kg sw	σ%■	ng/Kg sw	2σ%▲	%
GEOSECS station 67							
151	10600	1550	10	45	38.5	9	25
353	20400	1960	48	54	66.9	4	72
658	16580	1670	27	50	50.5	7	53
1053	17820	1760	38	37	50.0	6	76
1499	12240	1280	31	44	48.2	5	64
2193	5440	670	37	44	37.7	4	100
2574	7160	970	27	51	25.6	5	100
2982	4180	600	23	78	28.2	5	82
3601	5660	1030	15	59	19.2	9	79
4424	3440	490	15	41	19.4	9	75
5304	8820	1260	25	67	33.0	13	76
GEOSECS station 3							
105	5830	580	17	39	27.8	9	61
813	3900	390	18	53	44.2	28	41
1083	4480	630	14	59	16.9	17	83
1875	25000	2550	31	36	35.1	70	88
2479	3930	410	15	48	18.6	14	81
2696	1970	300	5	47	5.4	19	93
2989	24850	2740	33	54	33.6	17	98
3267	2920	470	15	87	29.5	19	51
GEOSECS station 5 ♦							
363	16040	1830	27	47	36		75
760	46990	5070	48	40	50		96
2464	21160	2960	19	46	9		

♦ Total Ba_p data for the samples we analyzed for barite content by SEM-EMP were not available; we deduced total Ba_p values by interpolation of the data of P. Brewer (GEOSECS shore-based data), for depths immediately above and below depths investigated by SEM-EMP.

♦ $\sigma = 1/\sqrt{N}$, with N = number of effectively counted barites

■ $\sigma = \Sigma \sigma_i$; $\sigma_i = M_i/\sqrt{n_i}$, with M_i = % by weight in a given size range; n_i = number particles counted in this size range

▲ σ is determined by the counting statistics in the 166 KeV photo-peak region.

In Figure II.10 we show the projected shape of the tails of the histograms, if the cumulative curves of Ba-mass versus barite particle diameter in Figure II .13 are extrapolated to 100%. These tails represent the number of large barite grains which would be required to completely account for the INAA Ba_p values, if the other sources of particulate Ba are ignored.

The percentage Ba_p as barite figures are subject to error due to the limitations of the counting, volume estimate and mass extrapolation procedures. There are other carriers of barium in oceanic suspended matter. As discussed below in section 4.3 , these may account for as little as 8.5% of the total Ba_p in intermadiate and deep water and as much as 50% when considering the contributions within the surface waters (first 150 m). Within the great bulk of the oceanic watercolumn, however, it is barite which is the dominant carrier of Ba_p.

4.3. THE CONTRIBUTION OF NON-BARITE, BIOGENIC AND TERRIGENIC Ba-CARRIERS TO THE TOTAL Ba LOAD IN SEA WATER

Silica and carbonate skeletons, particulate organic matter and aluminosilicates represent the main fraction of total suspended matter (TSM) in sea water (Krishnaswami et al., 1977). It is known that these phases contain various amounts of Ba. We will estimate their upper limit contribution to the concentration of total Ba_p throughout the watercolumn.

As concerns the vertical and horizontal distribution of TSM, observed during the Atlantic GEOSECS expeditions (Brewer et al., 1976), different compartments can be distinguished in the ocean:

1) surface water ; first 150 m: North of 45°N and south of 45°S TSM attains a maximum of 200 µg/Kg sw. In between these latitudes TSM attains a maximum of 50 µg/Kg sw. These concentrations are mainly defined by the intensity of organic productivity (Brewer et al., 1976).
2) Intermediate and deep water: over large regions of the Atlantic, TSM concentrations remain below 12 µg/Kg and between 12 to 20 µg/Kg. In the North Atlantic concentrations can be higher, with values reaching 50 µg/Kg sw. We will consider a maximum value of 25 µg/Kg sw.
3) Bottom water: water layer of a few hundred meters thick above the sediments. TSM values vary between 12 and 100 µg/Kg sw.

The mean concentrations (geometric means) of total Ba_p in these 3 regions of the watercolumn are given in Table II.9 . These mean concentrations are based upon our Ba_p data, presented in Tables II.I and II.4 and in Figure II.6 which are discussed in chapter 1 of this part. A distinction was made between stations in the high productivity zones (north of 45°N and south of 45°S) with high Ba_p concentrations and stations in between these latitudes, with low Ba_p concentrations. Since the TSM content in surface water is determined essentially by the rate of organic productivity (Brewer et al. 1976), the similarity between the TSM and the Ba_p distribution in surface water suggests the existence of a relationship between the Ba_p content and productivity; this possible relationship is discussed further in section 5.2 of part II.

We measured the particulate Ca and Al content in suspension at several stations in the Atlantic and Pacific Oceans; these data are given in appendix II. We further measured the in-vitro uptake of Ba by two common diatom species. These data, together with literature data on the Ba content of biogenic $CaCO_3$, aluminosilicate and particulate organic matter (POM), enabled us to estimate the importance of SiO_2 and $CaCO_3$ skeletal material, and of particulate organic matter, as barium-carriers.

Table II.9: Mean suspended barium concentration (geometric means) in surface water, in intermediate and deep water and in bottom water.

Region in the watercolumn	stations at high latitudes: north of 45°N and south of 45°S			stations between 45°N and 45°S		
	stations	number of investigated samples	Ba_p in ng/Kg sw	stations	number of investigated samples	Ba_p in ng/Kg sw
Surface water	GEOS. St. 82,67, 3	14	27	GEOS.St. 58,31	5	11
Intermediate and deep water	GEOS. St. 82,67, 3,282	72	27	GEOS. St. 58,31, 310,269,257; MIDL. St. 50, Madcap; TRANS. St. 17	62	10

Region in the watercolumn	stations	number of investigated samples	Ba_p in ng/Kg sw
Bottom water ♦	GEOS. St. 82,67, 58,31,3,310,269, 257,282; MIDL. St. 50, Madcap; TRANS. St. 17	28	14

♦ For the bottom waters no systematic variation of the Ba_p content with latitude is observed.

4.3.1. The contribution of Ba associated with diatom skeletons

i) Experimental data

Results:

Several authors have put forward the role of diatoms in the transport of Ba in the watercolumn (Li et al., 1973; Ku et al., 1970; Bacon and Edmond, 1972; Edmond, 1970; see introduction). However, very few experimental data exist on the uptake of Ba by diatoms. Diatoms of the Rhizosolenia and Chaetoceros genera, common in the open ocean were observed to be important accumulators of Ba (Vinogradova and Kovals'kiy, 1962; Brongersma-Sanders, 1966 and Li et al., 1973). We have checked this Ba-uptake for the Rhizosolenia alata and the Chaetoceros lauderi species. These diatom species were obtained from the Centre d'Etudes et de Recherche de Biologie et d'Océanographie Médicale (CERBOM; Nice, France). Pure strains were grown in controlled media composed of natural Mediterranean sea water and artificial sea water (for technical details see section 3.1 in part I). The natural sea water media were not enriched in dissolved Ba; they were assumed to contain about 10 µg/Kg of Ba (which is the value measured by Bernat et al., 1972 for Mediterranean surface sea water). One of the artificial media was enriched in dissolved Ba up to 30 µg/Kg The culture growth was allowed to proceed during 5 to 10 days. Whole cells and silica skeletons obtained after oxidation of the organic matter with H_2O_2, were analyzed separately by INAA. The siliceous fraction represents 26 % of the whole dry weight for Chaetoceros lauderi and 50 % for Rhizosolenia alata (Table II.10).

Table II.10 : % of weight loss after oxidation of the organic fraction with H_2O_2

Culture type	Rhizosolenia alata	Chaetoceros lauderi
A	55	51☆
B	13☆ mean of A,C,D:	72 mean of B,C,D:
C	49 50 % ± 5 %	76 74.3 % ± 2 %
D	45	75

☆ values are doubtful; they result from a bad dispersion of the lyophilisated diatom pellets in the H_2O_2 medium (see section 1.4)

A = natural, filtered sea water; B = artificial, filtered sea water; C = natural, aged ,unfiltered sea water; D = artificial sea water enriched in Ba, up to 30 µg/Kg.

The Ba content of the whole cells and the silica fractions of both diatom species are given in Table II .11 . Both values are expressed in ppm of whole dry matter. The data for Sr, Ca, Mn, Cu, V, Mg, Al, which were measured simultaneously, are given in appendix I.

Our data show the Ba-uptake capacity to be species dependent: while for Chaetoceros l. the Ba uptake did not exceed the INAA detection limit (estimated here at 1 ppm), Ba was accumulated in Rhizosolenia a. This accumulation is a positive function of the Ba concentration in the growth medium. Diatoms grown in media that were not enriched in dissolved Ba (Ba_s) (of these, the natural sea water media are assumed to contain about

10 µg Ba_s/Kg sw; see above) accumulated Ba up to 68 ppm of their whole dry weight. Diatoms grown in the medium enriched in Ba_s (Ba_s = 30 µg/Kg sw) accumulated Ba up to 200 ppm of their whole dry weight.

Table II.11: Ba content of whole cells and siliceous fractions of the diatoms Rhizosolenia alata and Chaetoceros lauderi; all concentrations in ppm of whole dry matter

Culture type	Whole cells Ba in ppm	Whole cells 2 σ %	Siliceous fraction Ba in ppm	Siliceous fraction 2 σ %
Rhizosolenia alata				
A	N.A.		75	21
B	12▲	>100	69	45
C	68	68	40	49
D	195	35	196	13
Chaetoceros lauderi				
A	< 1☆		< 1☆	
B	< 1		< 1	
C	< 1		< 1	
D	< 1		< 1	

N.A. = not analyzed
☆ Ba content below INAA detection limit (~ 1 ppm for these analyses).
▲ erroneous value, due to a too large dead time during γ-spectrometry.
A = natural, filtered sea water; B = artificial, filtered sea water; C = natural, aged and unfiltered sea water; D = artificial sea water enriched in Ba_p up to 30 µg/KG.

For the siliceous fraction of Rhizosolenia a. grown in media that were not enriched in Ba, a mean Ba concentration of 61 ± 20 ppm of the whole dry cell weight is found. It appears further that Ba is almost entirely associated with this siliceous fraction; this is especially true for the values of culture type D. Although the analyzed aliquot of type B diatoms is characterized by an inefficient elimination of the organic fraction (Table II.10), the "siliceous fraction" Ba value (Table II.11) is in agreement with those observed for types A and C. This confirms in fact the association of Ba with the siliceous fraction. Since type B diatoms were grown in artificial sea water that was not enriched in Ba, the Ba accumulated by these diatoms was probably introduced in the medium as impurities present in some of the constituents used ($SrCl_2$; $MgCl_2$, $FeCl_3$, $MnSO_4$, $ZnSO_4$, $CaSO_4$,..., see Tables I.5 and I.6 in part I).

Comments:

On a whole dry matter basis our values are 10 to 100 times smaller than those of Vinogradova and Kovals'kiy (1962) concerning two other species of the Rhizosolenia and the Chaetoceros genera in the Black Sea. For ashed samples of Chaetoceros curvisetus and Rhizosolenia calcar avis, these authors obtained Ba values of resp. 4000 and 20 000 to 30 000 ppm (the ash is considered to represent 45 % of the whole dry matter weight; Vinogradov cited in Li et al., 1973).

On the other hand our data agree well, on a whole dry matter basis with those of Riley and Roth (1971) for the diatoms Asterionella japonica and Phaeodactylum tricornutum grown in culture:

- Asterionella j. : 75 µg Ba/g total dry matter
- Phaeodactymum t.: 95 µg Ba/g total dry matter (Nitzschia)

Our data further agree well with those of Martin and Knauer (1973) for composite, natural, diatom-enriched phytoplankton, collected by net-towing off the Oregon coast (Monterey Bay). Martin and Knauer classified their samples on a chemical basis; arithmetic mean Ba values are:

- samples with no detected Ti: 53 µg Ba/gr dry matter (group I)
- samples with Ti : 55 µg Ba/gr dry matter (group II)
- samples enriched in Sr :306 µg Ba/gr dry matter (group III)

Martin and Knauer suggested the Ti enriched samples to consist of older phytoplankton populations with slower turnover rates. As a result such populations might accumulate several elements up to a higher level. In this context we will not consider their values for samples enriched in Sr. These samples are reported to contain strontium sulphate secreting Radiolaria. This matter will be considered later (§ 5.2.3. in this part)when discussing the possible formation processes of suspended barite.

Martin and Knauer (1973) applied a more severe oxidation technique than we did to eliminate the organic matter, including a digestion with concentrated, hot nitric acid, heating to 400°C and a final digestion with H_2O_2. They observed Ba to be entirely associated with the oxidizable fraction.They supposed however that frustule adsorbed elements could have been dissolved during organic matter oxydation. This would explain the discrepency between their data and ours as concerns the fraction to which Ba is bound. To explain

the fact that we could have failed to extract the Ba during the organic matter combustion, we consider the possibility that Ba is concentrated in an organic fraction closely associated with the skeleton and resistant to the oxidation technique used here. Whether Ba is concentrated in the siliceous phase or in a resistant organic fraction associated with the siliceous phase, in both cases the skeleton will function as a Ba-carrier.

In the following, the effective contribution of diatoms to the total Ba_p content in suspended matter is estimated. As discussed above, our data on the Ba content of Rhizosolenia alata frustules agree well with data for natural phytoplankton from the open ocean. Further, numerous SEM-EMP analyses of diatom frustules in GEOSECS samples showed that these contained no Ba above the SEM-EMP detection limit (100 to 1000 ppm). Thus, high Ba concentrations such as observed for the Black Sea diatoms (4000 to 30 000 ppm) are not found in the open ocean. Therefore we will consider the Ba content of Rhizosolenia a. frustules to represent an upper limit of the Ba content of diatom frustules in the open ocean.

ii) Diatom frustules as Ba-carriers

The siliceous fraction of the diatoms is considered to contain 120 ppm of Ba (from Table II.11). Biogenic silica represents some 10 % of the TSM weight (Bishop et al., 1977; Martin and Knauer, 1973; Copin-Montegut and Copin-Montegut, 1972; 1978); see Table II.12.A. In the transition from surface

Table II.12: Concentrations of total suspended matter (TSM), siliceous and calcareous matter, particulate organic matter and aluminosilicates as potential barium carriers in the watercolumn

	A	B	C	D	E
Section of the watercolumn	TSM in the Atlantic µg/Kg sw	SiO_2 µg/Kg sw	$CaCO_3$ µg/Kg sw	POM µg/Kg sw	alumino-silicates µg/Kg sw
Surface water	(1)	[=10% of TSM (2)]	[=6% of TSM (3)]	[=60% of TSM (4)]	(5)
High latitudes	max: 200	max: 20	max: 12	max: 120	2.2
Low latitudes (between 45°N and 45°S)	max: 50	max: 5	max: 2	max: 30	
Intermediate and deep water		[=10% of TSM (2)]	[=6% of TSM (3)]	[=60% of TSM (4)]	
(High and low latitudes)	max: 25	max: 2.5	max: 1.5	max: 15	1.4
Bottom water	range:	(6)	(6)	(6)	
(nepheloid layer)	12 - 100	2.5	1.5	15	4.5

(1) from Brewer et al. (1976)
(2) from Bishop et al. (1977) Martin and Knauer (1973) Copin-Montegut and Copin-Montegut (1972;1978)
(3) from Aubey (1976) and CFR-GEOSECS shore based data
(4) from Bishop et al. (1977); Copin-Montegut and Copin-Montegut (1972;1978) Krishnaswami et al. (1976)
(5) from Al_p geometric means in Buat-Menard and Chesselet (1979) and CFR-GEOSECS shore based data
(6) the $CaCO_3$ concentration in bottom water is similar to that in intermediate and deep water (CFR-GEOSECS shore based data); this is assumed also for SiO_2 and POM.

to intermediate and deep water, we assume silica to decrease in the same proportion as TSM. For bottom water we consider the same absolute silica content as for intermediate and deep waters (Table II.12.B).

The contribution of silica to total Ba_p is given in Table II.13.B. It appears that in surface water, diatoms can carry a maximum of 9 % of the total Ba_p content of suspended matter. Unless our data would underestimate the effective Ba content of open ocean diatoms, it is evident that diatoms can not be the main Ba-carriers, even in very productive surface waters (= north of 45°N and south of 45°S). Below surface waters, diatoms contribute for a max. of 3 % of the total Ba_p content of suspended matter.

4.3.2. The contribution of Ba associated with carbonate skeletons

The biogenic $CaCO_3$ fraction is assumed to carry 200 ppm of Ba (Church, 1970; Goldberg and Arrhenius, 1958; Thompson and Bowen, 1969), although the analysis of the Ba content of sediments with varying $CaCO_3$ content, points to the fact that this value should not exceed 10 to 30 ppm (Turekian and Tausch, 1964; Turekian, 1965). We remind here that it is our intention to compute an upper limit value of the contribution of non-barite phases to total Ba_p and therefore this higher value (200 ppm) will be used in the following estimations.

Table II.13: Contribution of siliceous and calcareous tests, POM and aluminosilicates to the total barium content of suspended matter.

Section of the watercolumn	A Total Ba_p (1) ng/Kg sw	B Ba carried by SiO_2 tests (2) ng/kg sw	% of Ba_p tot.	C Ba carried by $CaCO_3$ tests (3) ng/Kg sw	% of Ba_p tot.	D Ba carried by POM (4) ng/Kg sw	% of Ba_p tot.	E Ba carried by aluminosilic. (5) ng/Kg sw	% of Ba_p tot.	F Fraction of total Ba_p carried by non-barite phases %
Surface water										
High latitudes	27	2.4	9	2.4	9	7.2	27	1.3	5	50
Low latitudes (between 45°N and 45°S)	11	0.6	5.5	0.6	5.5	1.8	16.5		12	39.5
Intermediate and deep water										
High latitudes	27		1		1		3.5		3	8.5
Low latitudes (between 45°N and 45°S)	10	0.3	3	0.3	3	0.9	9	0.8	8	23
Bottom water										
(nepheloid layer)	14	0.3	2	0.3	2	0.9	6.5	2.7	19	29.5

(1) from Table 2
(2) SiO_2 tests contain 120 ppm of Ba; this study (Table 4)
(3) $CaCO_3$ tests contain a max. of 200 ppm Ba; from Church (1970)
(4) POM contains 60 ppm of Ba; from Martin and Knauer (1973); Riley and Roth (1971)
(5) aluminosilicates contain 600 ppm of Ba; from Turekian (1968) and Turekian and Wedepohl (1961)

From our Ca_p data concerning Atlantic and Pacific samples (see appendix II ; Table A.II.1), we deduce for surface, intermediate and deep water (= 110 samples) a geometric mean Ca_p value of 3 % of the TSM weight. Although part of this Ca_p is present as gypsum (see § 1.1.3 and section 2.2 in this part) we do not take account of its contribution and consider particulate $CaCO_3$ to represent a max. of 6 % of the TSM weight (Table II .12.C). For bottom water our data (see appendix II) show a similar absolute Ca_p content as for intermediate and deep water (Table II.12.C).

Our $CaCO_3$ estimations are to the low side when compared with values of Krishnaswami et al. (1976; $CaCO_3$ max. = 50 % of TSM in surface waters of the South Atlantic and the Subtropical North Atlantic) and Bishop et al. (1977; $CaCO_3$ max. = 30 % of TSM, at 300 m in the Equatorial Atlantic). In both these cases the volumes of filtered sea water exceed by far the volumes filtered during the GEOSECS expeditions (~ 10 litre). Bishop et al. for instance filtered up to 23.7 m^3 of sea water. The filtration of such large volumes makes it possible to sample the large (> 100 µm) Foraminifera and Pteropod shells, which can not be sampled quantitatively with the small volume (30 litre) samplers of the type used here (McCave, 1975). The sampling of such large $CaCO_3$ tests can be responsible for the observed differences between our data and literature data concerning the $CaCO_3$ content of suspended matter. The role of these fast settling potential Ba-carriers is important and will be discussed later in section 2.4 of part III, when treating the problem of the Ba supply to the

sediments.

The contribution of calcium carbonate to total Ba_p is given in Table II.13.C . In surface waters particulate carbonate carries a maximum of 9% of the total Ba_p amount. Below surface waters no more than 3% of total Ba_p is carried by carbonate skeletons.

4.3.3. The contribution of Ba associated with particulate organic matter

Particulate organic matter (POM) represents the main fraction of TSM. In surface water it represents some 60 % (Bishop et al., 1977, 1979; Copin-Montegut and Copin-Montegut, 1972, 1978) Krishnaswami et al., 1976 ; Krishnaswami et al., 1977) and in subsurface water some 40% (Bishop et al., 1976; Copin-Montegut and Copin-Montegut, 1972; 1978) of the TSM weight. The POM amount is generally taken as twice the particulate organic carbon amount (Strickland, 1965). POM is likely to be constituted by the remains of skeleton-free phyto- and zooplankton. Data concerning the Ba accumulation by skeleton-free phyto- and zooplankton exist (Riley and Roth, 1971; Martin and Knauer, 1973). Riley and Roth analyzed pure strains of 14, in vitro grown, phytoplankton species for a series of elements, including Ba. For the 5 different taxonomic classes that are concerned the range of Ba concentrations is given in Table II. 14 . Martin and Knauer analyzed composite zooplankton samples collected in Monterey Bay (Califorina). The Ba content of their zooplankton samples enriched in Euphausiids and Copepods are also given in Table II .14 .

From these date we deduce an average Ba content of 60 ppm of dry matter. We assume this value to be valid for POM in general.

Table II.14 : Ba content of in vitro grown, skeleton-free phytoplankton and composite, natural zooplankton; literature data.

A. In vitro grown phytoplankton (Riley and Roth, 1971)					
classis:					
Chlorophyceae:	37.5	to	80	µg/gr	dry matter
Cryptophyceae:	67	to	262	"	"
Xanthophyceae:	34.5			"	"
Chrysophyceae:	70	to	85.5	"	"
Prasinophyceae:	128	to	145	"	"
B. Composite, natural zooplankton (Martin and Knauer, 1973)					
samples enriched in:					
Euphausiids:	33 µg/gr dry matter				
Copepods:	16 " " "				arithmetic mean values
Open sea zooplankton	32 " " "				

The POM content of suspended matter in surface, intermediate and deep water is given in Table II.12.D. For bottom water, we assume the same absolute POM content as for intermediate and deep water.

The fractions of total Ba_p carried by POM are given in Table II.13.D . In surface water a maximum of 27% of total Ba_p is carried by POM. Below surface waters, this contributions decreases to 9% and less.

4.3.4. The contribution of Ba associated with aluminosilicates

SEM-EMP and INAA analyses of suspended matter of GEOSECS samples revealed that Al can be used as an indicator of aluminosilicates in suspended matter and confirm that the Al content of suspended aluminosilicates is similar to the one of shales (see § 1.1.1; chapter 1 in this part). We will therefore consider the Ba concentration in shales (= 600 ppm; Turekian and Wedepohl, 1961; Turekian, 1968), to be representative of the Ba content of aluminosilicates suspended in sea water.

INAA data on particulate Al were obtained at the CFR (Chesselet and Lambert, 1977; this study: see appendix II, Table A.II.2).
From samples of the Atlantic and the Pacific Ocean we deduce the following geometric mean values:
- surface water: 180 ng/Kg sw (14 samples);
- intermediate and deep water: 110 ng/Kg sw (111 samples);
- bottom water: 356 ng/Kg sw (25 samples).

The corresponding aluminosilicate concentrations are deduced by considering Al to represent 8% of the aluminosilicate mass; surface water: 2.2 µg/Kg sw ; intermediate and deep water :

1.4 µg/Kg sw; bottom water ; 4.5 µg/Kg sw (see Table II.12.E).

The fraction of total Ba_p carried by aluminosilicates is presented in Table II.13.E. It appears that aluminosilicates are especially important as Ba-carriers in bottom water, where they can carry up to 19 % of the total Ba_p amount. This increased abundance of aluminosilicates in bottom waters is related to the presence of resuspended sedimental materials (Ewing et al., 1971; Biscaye and Eittreim, 1977).

The data in Table II.13 show that in the largest part of the watercolumn (= intermediate and deep water) non-barite phases account only for 8.5 to 23% of the total Ba_p content in suspended matter. This supports the conclusion we reached in section 4.2 (Table II. 8) that for these depths, barite is the main Ba-carrier. In surface water up to 50 % of total Ba_p is carried by phases other than barite; here biogenic phases are important contributors. In bottom water up to 30 % of total Ba_p is carried by non-barite phases; here aluminosilicates are the main contributors. In both, surface and bottom waters the remaining fraction of the particulate Ba, is probably carried by barite particles, which were indeed observed in these waters, but could not be assessed quantitatively.

From Table II.13 it appears that an important bio-utilization of Ba takes place in surface water. The data further suggest that between surface and intermediate water, part of the Ba originally associated to biogenic matter is precipitated

as barite.

The probable linkage between biological activity and barite formation is discussed in the following chapter.

CHAPTER 5

THE PROBLEM OF THE ORIGIN OF SUSPENDED BARITE IN SEA WATER

5.1. THE AUTHIGENIC FORMATION OF BARITE IN SEA WATER

5.1.1. Is sea water saturated with respect to pure barite ?

The first to consider the possibility of an authigenic barite formation in sea water and who verified the barite saturation conditions, were Chow and Goldberg (1960). Although they did not possess accurrate values of the different ion activities at stake, their approach was nevertheless original in that they considered the possibility of a complex formation between the Ba^{++} and SO_4^{2-} ions. However an overestimation of the Ba^{++} and SO_4^{--} ion activities made these authors conclude that barite saturation conditions were present in the deep oceans. Later studies (Garrels and Thompson, 1962; Hanor, 1969) based on model calculations of complex formation between the following cationic and anionic species: Na^+, K^+, Mg^{2+}, Ca^{2+}, Sr^{2+}, Ba^{2+} and SO_4^{2-}, HCO_3^-, CO_3^{2-}, Cl^-, proved that complex formation affects considerably the ion activities. Therefore the $BaSO_4$ ion activity product is written:

$$(a_{Ba^{2+}})(a_{SO_4^{2-}}) = \gamma_{Ba^{2+}} \cdot f_{Ba^{2+}} \cdot m_{Ba^{2+}} \cdot \gamma_{SO_4^{2-}} \cdot f_{SO_4^{2-}} \cdot m_{SO_4^{2-}}$$

with a = activity of each ionic species

γ_i = activity coefficient of the ion in the liquid

f_i = fraction of unassociated, free ions

m_i = molality (moles/Kg sea water)

Hanor calculated that 93 % of the dissolved Ba is in the form of free, uncomplexed ions, while the remaining 7% occur mainly as aqueous complexes of $BaSO_4^\circ$ and $Ba(HCO_3)_2^\circ$ (Hanor, 1969). These values are independent of pressure and temperature conditions (Hanor, 1969; Church, 1972). The experimental data of Kester and Pytkowics (1970) show that at 25°C and 1 atm. pressure, the fraction of free, uncomplexed sulphate ions is 39%, while it decrease to 28% at 1°C and 1 atm. The remaining sulphate fraction occurs mainly as $NaSO_4^-$, $MgSO_4^\circ$, $CaSO_4^\circ$. At 1°C, a pressure increase to 500 atm. results in an increase of the fraction of free sulphate ions from 28% (at 1°C and 1 atm. pressure) to 35% (at 1°C and 500 atm.), Millero, 1971; Church, 1970; 1972; 1979). This pressure increase results in a three-fold increase of the $BaSO_4$ solubility product (Church, 1972).

$BaSO_4$ solubility products, Ba^{++} and SO_4^{2-} activity coefficients, free-ion fractions and barium solubilities for sea water in equilibrium with pure barite are listed in Table II.15 , as given in Church (1970; 1972; 1979).

A close look will now be taken at the dissolved barium concentrations in the main oceans, reproduced in literature. Table II. 16 reproduces surface and deep water dissolved Barium concentrations measured during various GEOSECS and other expeditions. When comparing the solubility values of barium (Table II.15), with the dissolved barium concentration in the oceans (Table II.16) it appears that $BaSO_4$ saturation is

Table II.15 : $BaSO_4$ solubility product; barium and sulphate ion activity coefficients, free ion fractions and barium solubilities in surface- and deep-sea water (Data from Church, 1970, 1972)

Temperature and pressure conditions	Barite solubility product; Ksol	Ion activity products Ba^{2+}	Ion activity products $SO_4^{=}$	Fractions of free unassociation ions Ba^{2+}	Fractions of free unassociation ions $SO_4^{=}$	Ba concentration at saturation Molality	Ba concentration at saturation µg/Kg
25°C; 1 atm	$1,1 \times 10^{-10}$	0,24	0,17	0,93	0,39	$2,6 \times 10^{-7}$	35 ± 7
1°C ; 1 atm	$0,54 \times 10^{-10}$	0,24	0,17	0,93	0,28	18×10^{-7}	24
1°C ; 500 atm	$1,5 \times 10^{-10}$	0,24	0,19	0,93	0,35	$3,6 \times 10^{-7}$	49

The Sea water $SO_4^{=}$ concentration is taken as 28×10^{-3} moles/Kg sw.

Table II.16: Literature data of dissolved barium concentrations in Atlantic and Pacific Ocean . Only data obtained by isotope - dilution mass spectrometry are considered

Station and position	Surface-sea water depth range;in m	diss.Ba in µg/ Kg sw	Deep-sea water depth range;in m	diss. Ba in µg/ Kg sw
ATLANTIC OCEAN:				
Chan et al. (1977): GEOSECS expedition				
17(74°N-01°W)	0 - 600	5.6	1000 - 3800	6.3
18(70°N-)	0 - 1000	5.9	2000 - 3000	7.1
19(64°N-35°W)	0 - 800	5.8	3500	6.7
11(63°N-35°W)	0 - 500	5.9	1000 - 2300	6.6
23(6°N-15°W)	0 - 200	6.	1000 - 2000	6.6
			2500	7.3
3(51°N-45°W)	0 - 1000	6.2	3000 - 4000	7.3
29(35°N-47°W)	0 - 700	5.9	4000 - 5000	8.9
115(28°N-25°W)	0 - 600	5.7	4000 - 5000	10.7
33(1°N- 5°W)	0 - 600	6.2	2800 - 4200	9.6
37(12°N-47°W)	0 - 200	5.3	5000	11.6
40(00° -40°W)	0 - 100	5.5	4300	11.
107(12°S-01°W)	0 - 200	5.2	3300 - 5500	11.9
54(15°S-35°W)	0 - 300	5.8	1000 - 3500	9.3
			5000	14.7
103(20°S-05°E)	0 - 300	6.2	4500	14.4
60(32°S-42°W)	0 - 200	5.3	4300	14.4
93(45°S-16°E)	0 - 200	6.1	5000	14.4
91(50°S-10°E)	0 - 150	10.1	3000 - 4000	14.4
74(55°S-50°W)	0 - 200	9.6	2000 - 5000	13.7
82(56°S-24°W)	0 - 200	11.1	5000	13.1
76(57°S-66°W)	0 - 300	9.6	3600 - 4500	14.1
89(60°S-)	200	13.	700 - 5500	14.4
Li et al.(1973):				
EL 35- I(56°S-128°E)	5	10.3	4000 - 4500	14.2
EL 35-II(47°S-128°E)	5	7.4	3700	14.4

Table II.16 :continued

Station and position	Surface-sea water depth range; in m	diss. Ba in µg/Kg sw	Deep-sea water depth range in m	diss.Ba in µg/ Kg sw
PACIFIC OCEAN:				
Bacon and Edmon (1972): GEOSECS test cruise				
GEOSECS III	30	4.7	3000	18.4
(17°S-172°W)			5600	14.3
Chan et al. (1976): GEOSECS expedition				
204 (31°N-150°N)	10	4.8	4500	20.8
			5600	40.8
Bernat et al. (1972):				
(19°N-119°W)	0	4.9	4500	23.6
Church and Wolgemuth (1972)				
(9°N-119°W)	-	-	4177-4561	22.0
Wolgemuth and Broecker (1970):				
Between 39°N and 05°S ; N O° W				
	0	7.1	4000	23.6
	(average values)			
MEDITERRANEAN SEA:				
Bernat et al. (1972)				
(41°N-64°E)	0	10.0	1900	11.9

nowhere attained in the oceans. However, the deep waters in GEOSECS station 204 are close to saturation, they show a dissolved barium content of 41 µg/Kg sw, while barium solubility at 1°C and 500 atm. pressure is 49 µg/Kg (Table II.15). Further, according to Edmond (Church, pers. comm.) the surface waters in the Bering Sea (GEOSECS station 219) have a dissolved barium concentration of 22.6 µg/Kg what is close to the saturation value of 24 µg/Kg at 1°C and 1 atm. pressure. It appears also that Black Sea waters and estuaries of some major rivers (Amazon; Congo) are super-saturated with respect to pure barite (Church, 1979). Further, Table II.16 shows that the surface waters south of 50° latitude south are characterized by higher concentrations of dissolved Ba. These concentrations remain however well below the barium solubility value of 24 µg/Kg at 1°C and 1 atm. pressure.

Since the watercolumn is undersaturated with respect to pure barite, virtually over the whole of the World Ocean, precipitation of barite in sea water can not be the source function of the barite we observe in suspended matter.

5.1.2. Sea water in equilibrium with a $(Ba,Sr)SO_4$ solid solution: a possible precipitation model?

Hanor (1969) was the first to consider the influence of a substitution of Ba by Sr in the barite crystal lattice on the solubility of barite in sea water. Hanor calculated

that his model sea water at 25°C and 1 atm. pressure could exist in equilibrium with a non-ideal $(Ba,Sr)SO_4$ solid solution in which 33 mol % of Ba is substitued by Sr. Church's experimental data show that barite, when precipitated in vitro in conditions approaching those existing in sea water, contained only 2 to 3 mol % of Sr, what is similar to values obtained for natural sedimentary barite (Church, 1970; 1972). Such small Sr incorporations have practically no influence on the solubility of barite (Church 1972). This implies that such dilute solid solutions can not be formed authigenically in sea water. More recently, Church (1979) showed that the presence of traces of K and Ca in the barite lattice rather increase the solubility of barite. The presence of trace amounts of Sr is supposed to work in the same direction (Church, 1979).

Due to the lack of data on the solid activity coefficients of $BaSO_4$ and $SrSO_4$ for non-dilute solid solutions (Church, pers. comm.), it is not possible at this point to verify if the barites strongly enriched in Sr, we observe in surface waters (section 2.4 in this part) can form authigenically in sea water. In order for the "Hanor-type" barite (33 mol% Sr ; Hanor, 1969) to be in equilibrium with sea water, the solid solution must be a non-ideal, asymmetrical one and the solid activity coefficients must be larger than unity (Hanor, 1969; Church, 1979). Today it is not known if these conditions are indeed fulfilled in the marine environment.

A possible mechanism, explaining the presence of variable amounts of Ba in $SrSO_4$ particles and Sr in $BaSO_4$

particles was suggested by Church (pers. comm., 1979): $SrSO_4$ particles are formed biologically (= by Acantharia). After release of these particles in the sea water an equilibration process starts, with Ba substituting for Sr. The substitution process will tend towards the formation of a solid solution stable in sea water.

Unless we are observing such a post-mortem substitution of Sr by Ba in biogenic $SrSO_4$ debris, the widely varying Sr/Ba molar ratios we observe among the barite particles is inconsistent with an authigenic formation in a single parcel parcel of sea water, considered as a given physico-chemical environment. In any case, we observe Sr-free barites, and for these there is no disagreement between Church and Hanor concerning the impossibility of inorganic precipitation under natural oceanic conditions.

Other processes, rather than purely inorganic precipitation in the watercolumn, appear to control the production of suspended barite.

5.2 BARITE FORMATION AND BIOLOGICAL ACTIVITY

The existence of a positive relationship between the Ba_p content and organic productivity is suggested by the similarity of the Ba_p and TSM distributions in surface waters, the TSM concentration being mainly governed by the intensity of organic productivity (Brewer et al., 1976; see section 4.3 in this part).

In the first place, the Ba_p profiles, and more specifically the position of the Ba_p peaks in surface and subthermocline waters are studied in relation with the profile of Tpot and the position of the dissolved O_2 and PO_4 extrema.

5.2.1. Profiles of Ba_p, Tpot, dissolved O_2 and dissolved PO_4 in Atlantic surface and subthermocline waters

Ba_p profiles are compared with those of Tpot, O_2 and PO_4 for the first 1000 m of the watercolumn. These profiles are given in Figure II.15 for stations analyzed at the CFR (Gif-sur-Yvette, France) (GEOSECS stations 82, 67, 31, 3) and stations analyzed by P. Brewer at WHOI (GEOSECS stations 5, 11, 17, 18, 23, 27). The Pacific stations and Atlantic station 58 were omitted due to the scantiness, or the lack of data on the Ba_p content in the upper part of the watercolumn. For the stations visited during HARMATAN, MIDLANTE and TRANSAT cruises, no data were available on the profiles of dissolved O_2 and dissolved PO_4.

FIGURE II.15

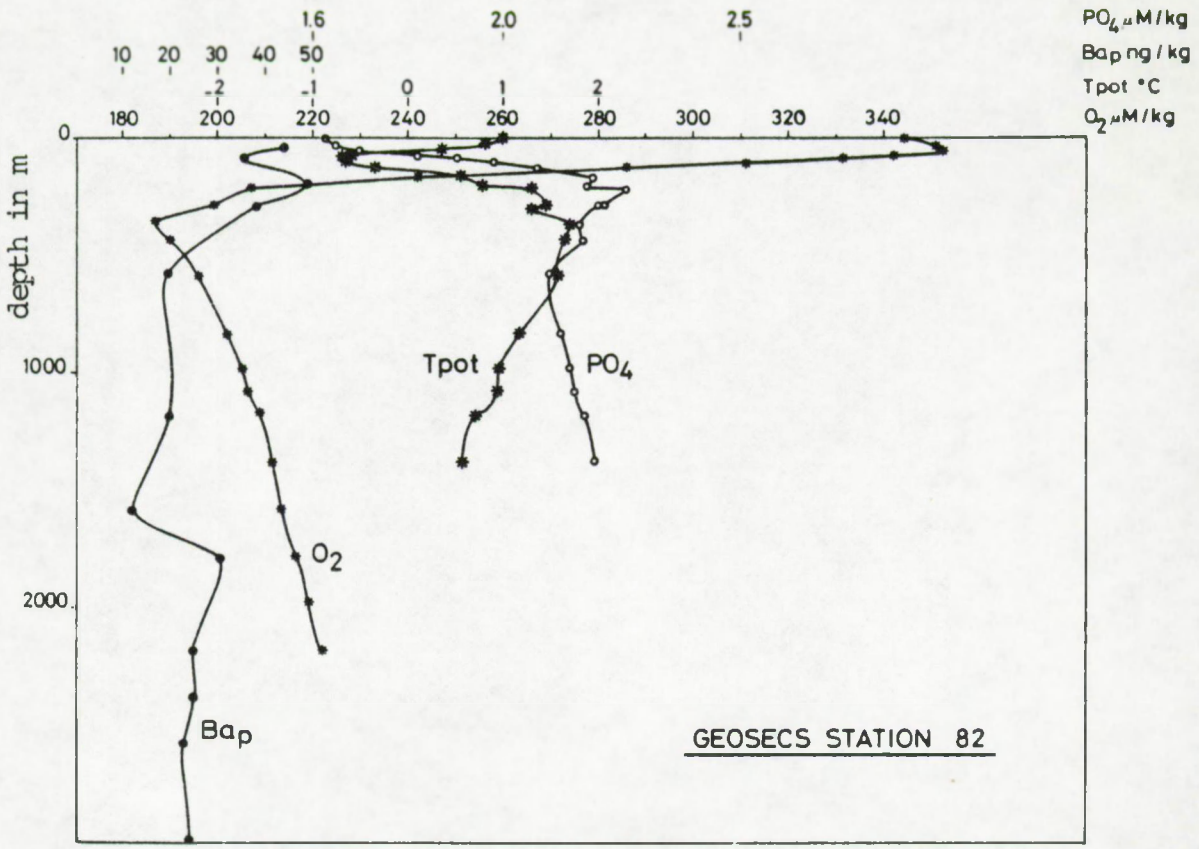

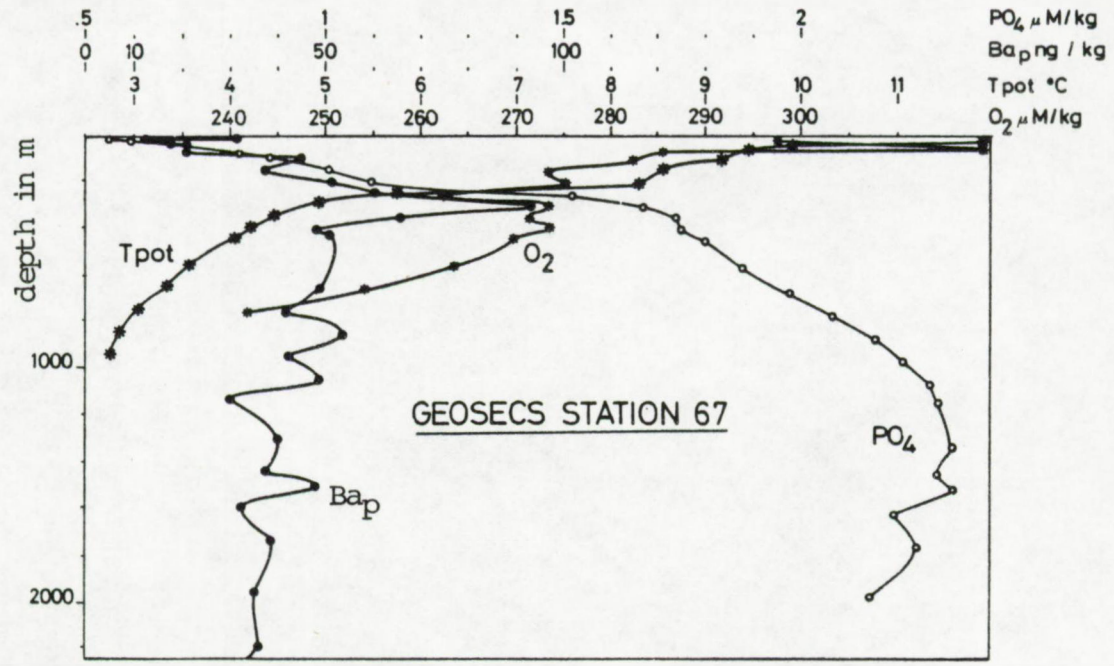

Profiles of total Ba_p, dissolved PO_4-P and O_2, Tpot in the first 2000 m of the watercolumn. Data for PO_4, O_2 and Tpot were collected on shipboard by GEOSECS participants. Values for total Ba_p for stations 27,5,11,17,18,23 are from P.Brewer; WHOI; GEOSECS shore-based data.

FIGURE II.15: continued

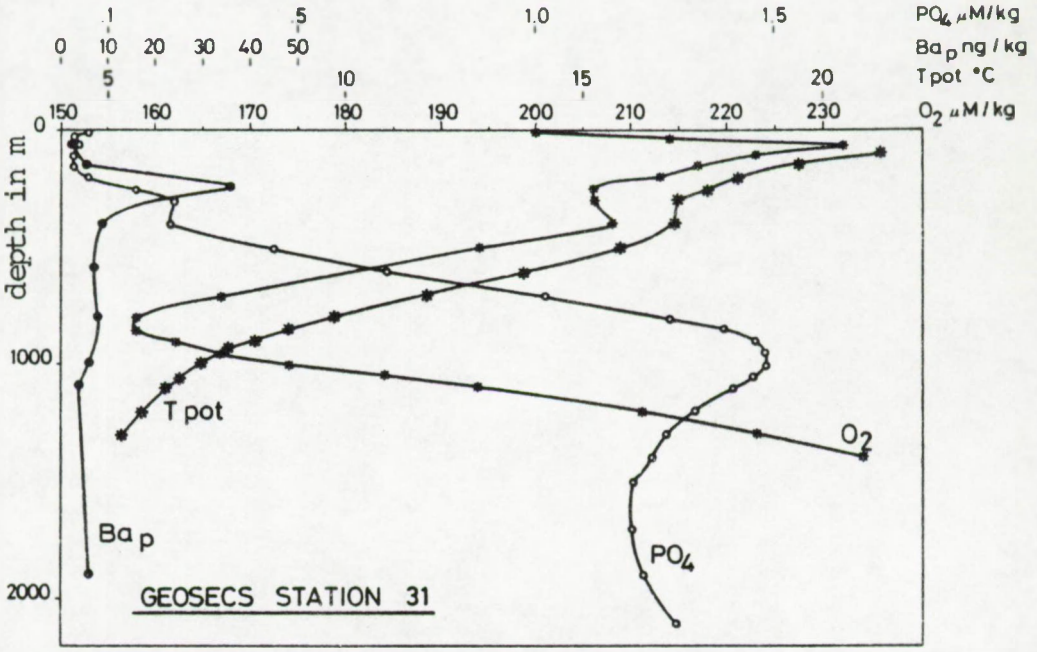

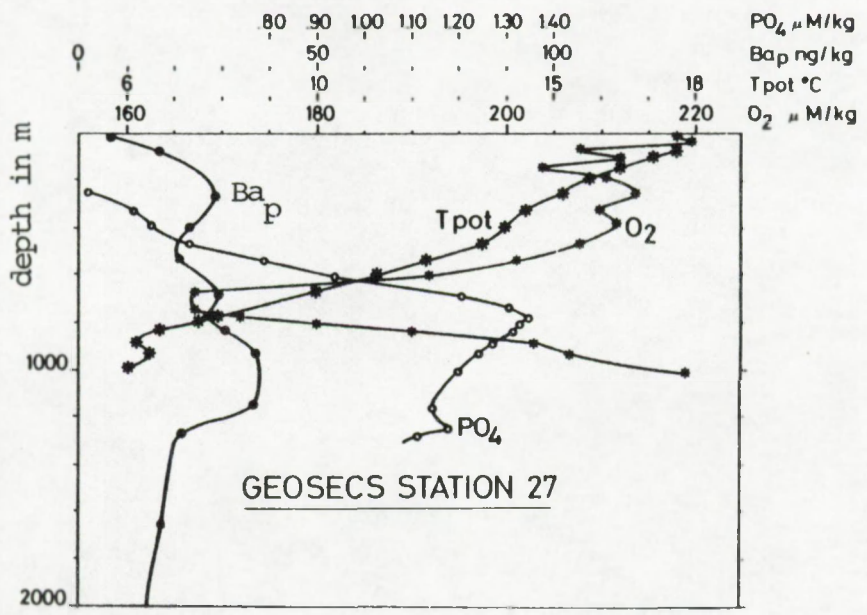

See page 182 for figure caption.

FIGURE II.15 : continued

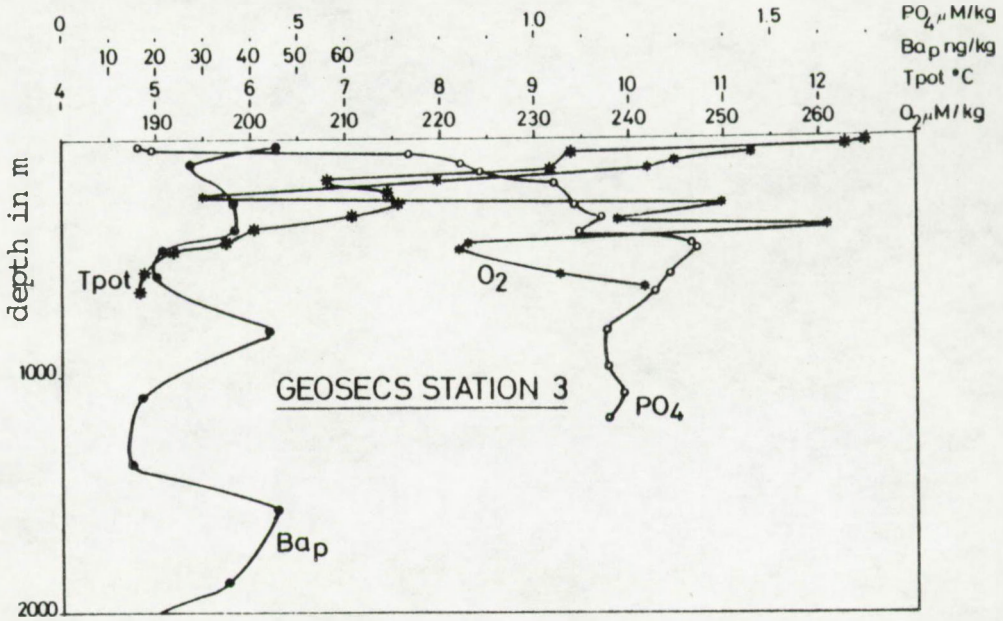

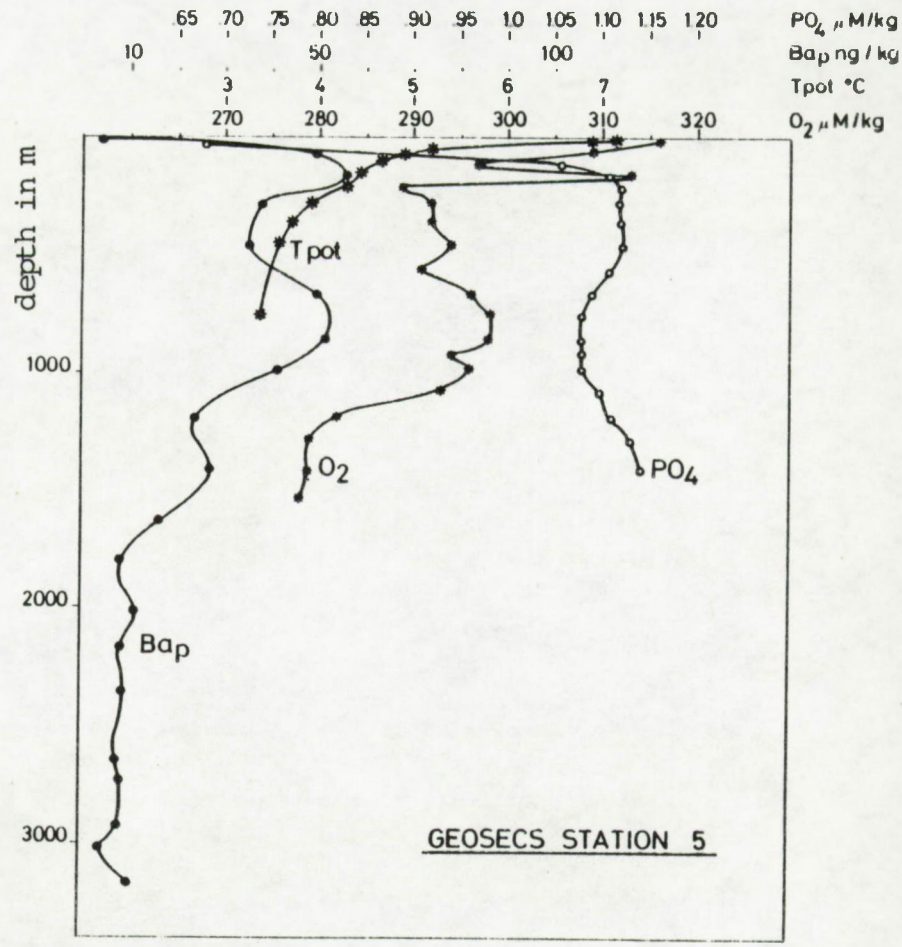

See page 182 for figure caption.

FIGURE II.15 : continued

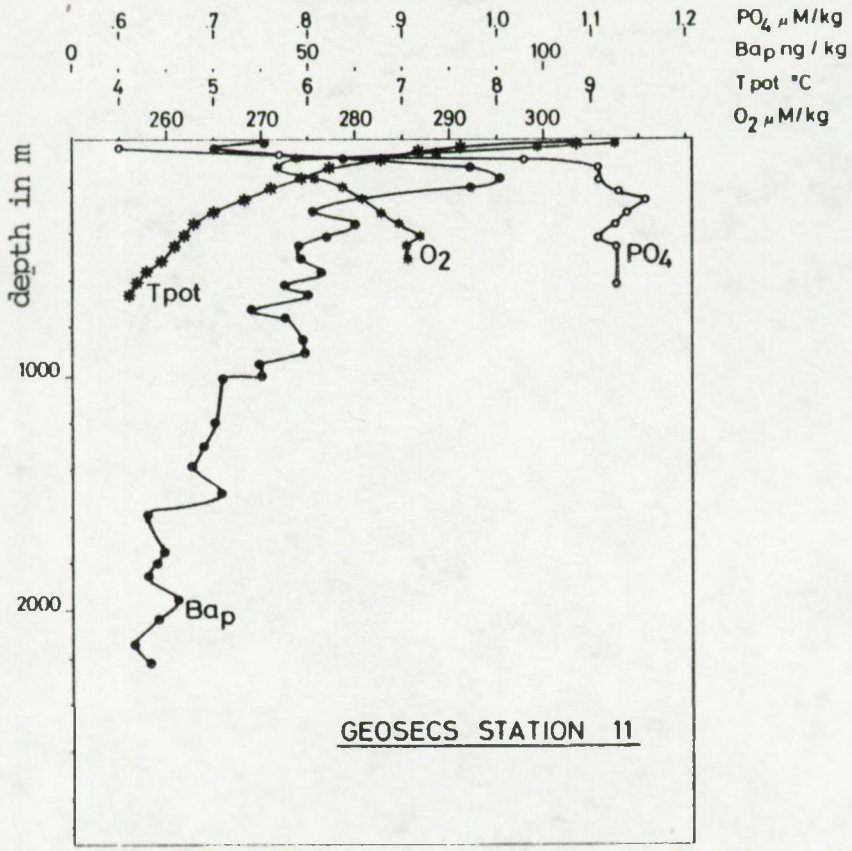

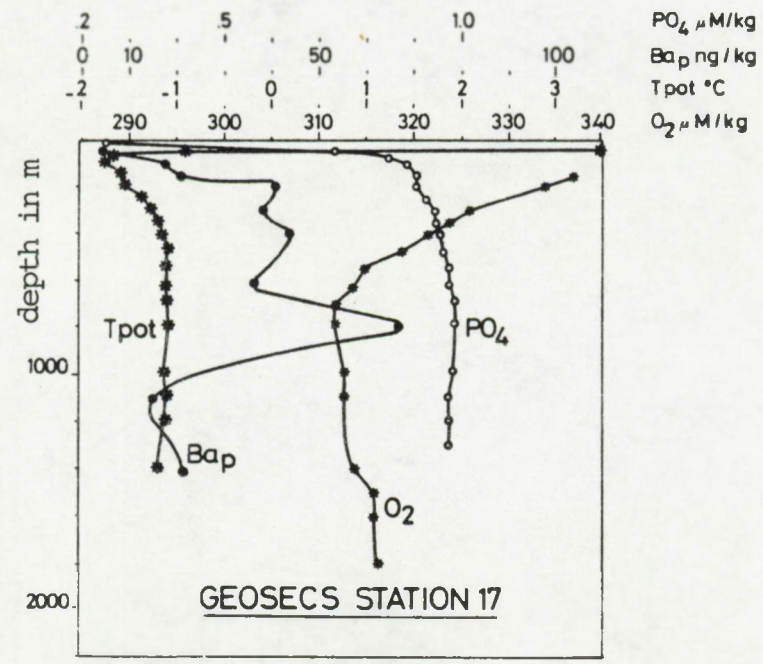

See page 182 for figure caption.

FIGURE II.15 : continued

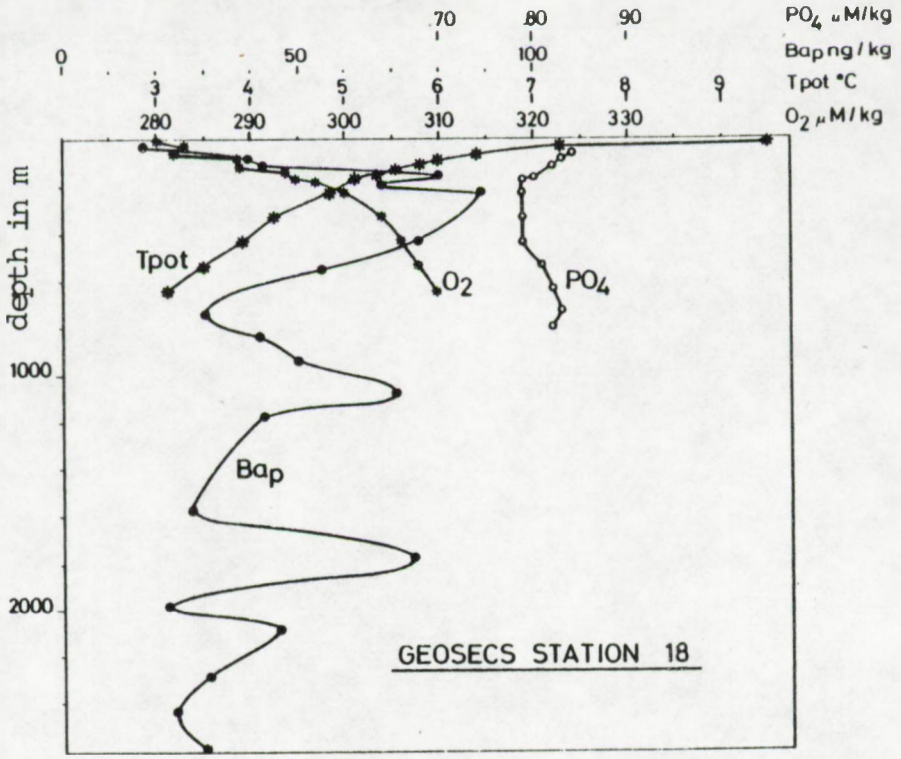

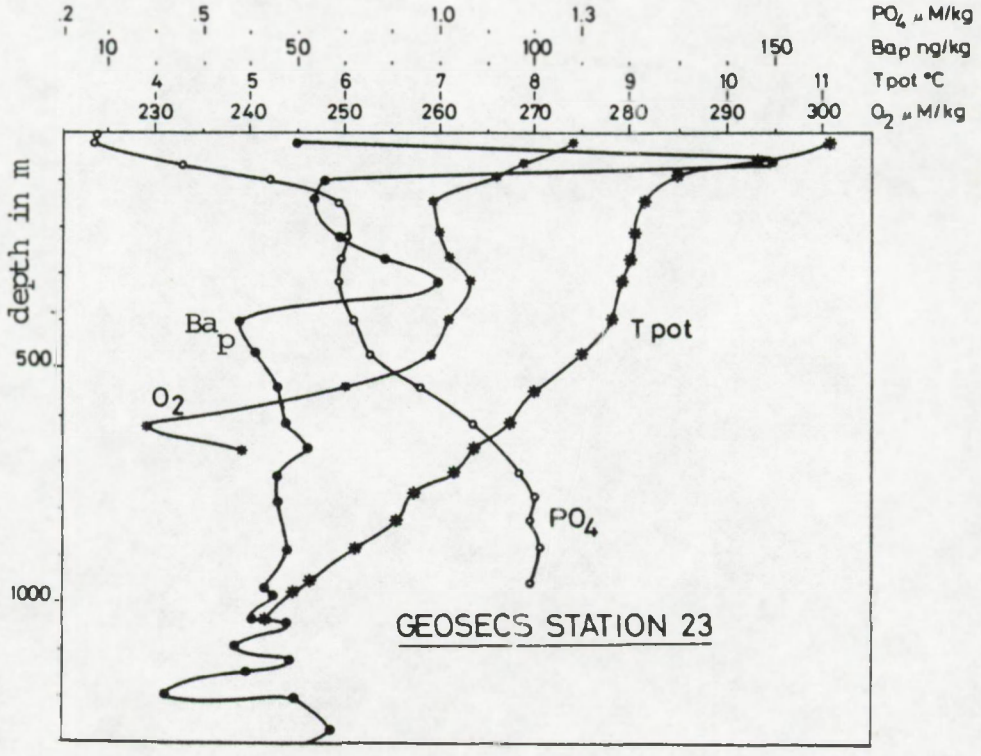

See page 182 for figure caption.

For GEOSECS stations 82, 67, 31, 27, 3, 5, 11, 17 the Ba_p maxima occur either within, or under O_2 minima. The latter occur in the region of the thermocline, or at greater depths. Literature offers evidence that O_2 minima in the watercolumn are the result of a biochemical oxidation of particulate organic matter:

- Profiles of dissolved oxygen, δC^{13}, δO^{18} in the North Atlantic, North and South Pacific and Antarctic Oceans (Kroopnick et al., 1972; Kroopnick and Craig, 1976), revealed that the O_2 minimum at 1000 m is due to biological consumption of oxygen. Indeed, the O_2 min. corresponds to a δC^{13} min. and a δO^{18} max., characteristic for a biological oxygen consumption, during which O^{16} is preferentially consumed and light $C^{12}O_2$ is produced, as compared to inorganic oxidation (Kroopnick et al., 1972).
- In order to establish a diffusion-advection model that successfully described the observed CO_2, C^{14}, C^{13}, O_2 and alkalinity extrema, Wyrtki (1962) and Craig (1969; 1971) had to consider the biochemical utilization of O_2 in deep water. Therefore Craig (1971) disagrees with the statements of Menzel and Ryther (1968, 1971) and Menzel (1970), that biochemical O_2 consumption does not occur below 200 to 300 m, and therefore that dissolved oxygen and dissolved organic carbon are conservative parameters in the deep ocean. This stands also in contrast to the sayings of Redfield et al. (1963), who observed, for a station in the N.W.-Atlantic, that the ratio of the difference in nitrate-N content between deep and surface water (= Δ N) to the difference in phosphate-P (= Δ P), and similarly that the $\Delta N/\Delta C$ is in

agreement with the N/P and N/C ratios of average phytoplankton. This is interpreted as a clear evidence of the primordial influence of plankton decomposition in determining the profiles of dissolved N,C and P.

- When calculating the O_2 consumption with depth at two Northeast Pacific stations, Miyake and Saruhashi (1956) observed that the increase in total dissolved CO_2 ($= \Sigma\ CO_2$) with depth can largely be ascribed to combustion of organic matter. From monthly observations, extending over one year, these authors further observed that variations of the biomass standing crop in the first 100 m of the watercolumn, coincided with variations in the integrated O_2 consumption in the first 1000 m.

Although evidence exists that the O_2 minimum is the result of biochemical O_2 consumption, the position itself of the minimum is thought to be induced by:

1) water circulation (advective and diffusive water movements; Wyrtki, 1962)
2) the fact that organic matter decomposes within a deep water body by which it is carried away from the deep water formation zone (Redfield et al., 1963)
3) the fact that organic matter accumulates and decomposes at specific density surfaces (Miyake and Saruhashi, 1956).

Thermoclines may represent density surfaces where organic matter accumulates.

Several studies show that the seasonal thermocline is indeed a region of organic matter accumulation and resulting biological activity (Bishop et al.,1977; Bishop and Edmond, 1976; Cahet et al., 1972; Minas, 1970). Measurement of productivity and chlorophyl-a in the seasonal thermocline regions of a few Mediterranean stations (Cahet et al., 1972) showed a high subthermocline biological activity. In a model approach this high productivity at the thermocline level is proposed to be sustained by the following processes (Cahet et al., op.cit.):

- passive accumulation of degraded phytoplankton (eventually outside the euphotic layer), due to a slowing down of its settling velocity. Such an accumulation favors a mineralization of these organic substances, itself favoring a "regenerated production".
- nutritive elements of the deep sea entering the surface waters through diffusion and upwelling, may accumulate in the under-thermocline region (as a result of a slowing down of diffusion), and may induce a "new production" if illumination conditions are favorable.

Such subthermocline high productivity niveaus in the Mediterranea are thought to induce the O_2 maximum which is generally observed at the same depths (Minas, 1970). Primary productivity characterized by a high photosynthetic activity, prevails in such a situation.

With the exception of GEOSECS station 11, the position of the thermocline observed the GEOSECS stations is deep (below 150 m). This will prevent any increased phytoplankton activity at the thermocline, such as observed in the Mediterranean Sea

(Cahet et al., 1972 and Minas, 1970). The supply of nutrients and the mineralization of organic matter might however sustain the development of other, heterotrophic organisms, what could explain the observed O_2 minimum in the case of the GEOSECS profiles.

At GEOSECS stations 82, 27 and 17, thermoclines are absent or only poorly developed. Ba_p maxima occur within (stations 82, 17) or under (station 27) an O_2 minimum. At stations 27 and 17 Ba_p maxima occur at relatively great depths; respectively at 1000 and 800 m.

At station 23 the Ba_p max. occurs at 70 m, within the thermocline; no O_2 extremum is observed at this depth. At station 18 the Ba_p max. occurs below 200 m and does not coincide with distinct events in the O_2 and Tpot profiles.

On two occasions (GEOSECS stations 82, 27) Ba_p maxima coincide also with maxima of dissolved PO_4. The latter probably result from the mineralization of accumulating organic matter.

To conclude, in nearly all cases Ba_p maxima coincide with O_2 minima present at the basis of the thermoclines or at relatively great depths, ~~but~~ outside the euphotic layer. The origin of the O_2 minimum appears to be biochemical. As a result their exists support for the argument that the production of particulate Ba is related with productivity, or more accurately with the presence of the decomposing products of biological activity.

5.2.2. The relationship between dissolved phosphorus and particulate barium in the first 1000m of the watercolumn

To trace the possible relationship between the particulate Ba content and biological activity we have compared the distribution of Ba_p with the one of organic productivity. We considered dissolved PO_4-P as a parameter of biological activity. This is justified since diss. phosphorus is generally regarded as an indicator of potential productivity in the euphotic layer (Steeman-Nielsen, 1954; Reid, 1962; Berger, 1970; Koblentz-Mishke et al., 1970) and since the concentration of this nutrient was measured* for the same stations for which Ba_p data are available (these are all the stations discussed in § 5.1.1).

From Figure II.15 it is apparent that the Ba_p maxima occur at different depths between the surfaces and 1000 m. Therefore we have computed the geometric means of both, Ba_p and diss. PO_4-P over this depth interval. In Figure II.16 the mean Ba_p values are plotted against the mean diss. PO_4-P values.

A linear relationship between Ba_p and dissolved PO_4 is apparent, when considering stations 31, 58, 27, 17, 3 and 5. For these stations a correlation coefficient of 0.95 (significant at the 0.05 level) is obtained. These results indicate a positive relationship between the production of particulate Ba and organic productivity.

---

* During the GEOSECS cruises the dissolved PO_4-P profiles were measured at each station. For GEOSECS station 67 the PO_4 data are given in appendix III.

FIGURE II.16

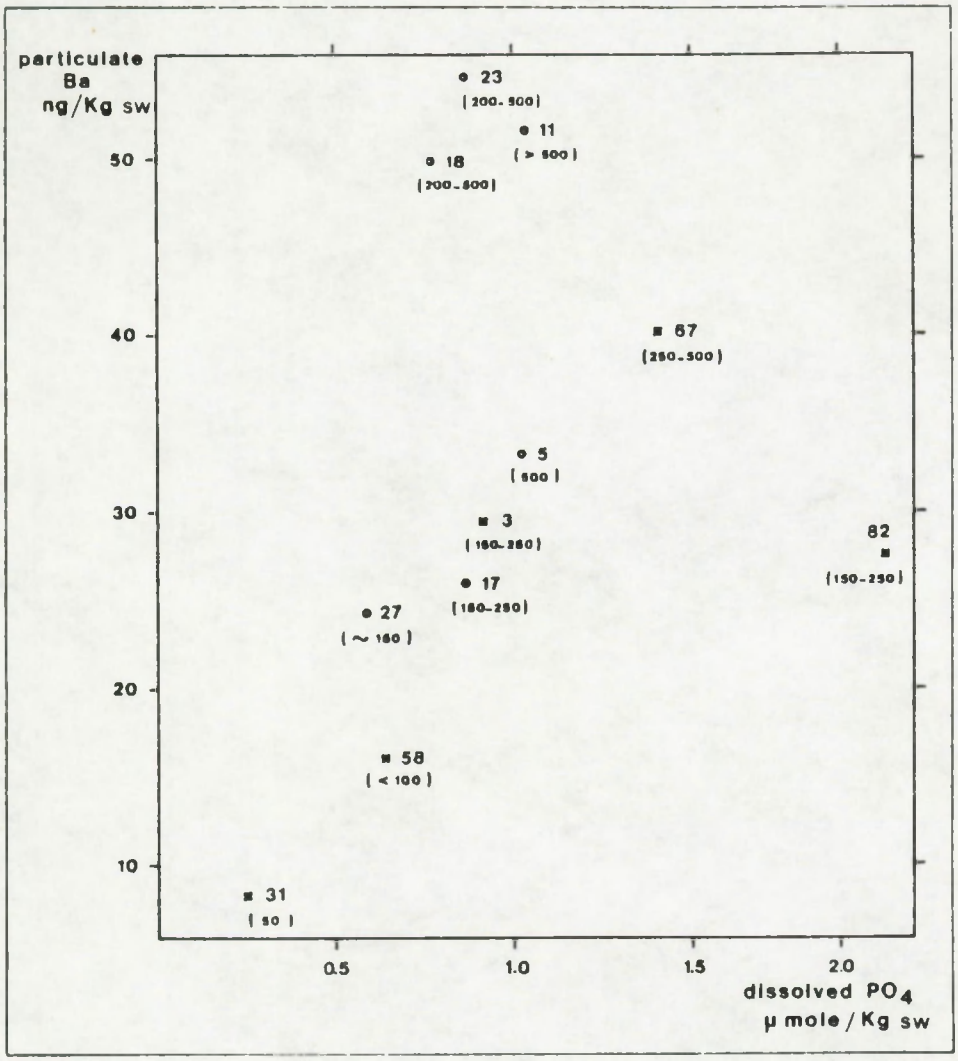

Total Ba_p versus dissolved PO_4. The geometric mean Ba_p value (in ng/Kg sw) observed between 150 and 1000 m, is plotted against the geometric mean dissolved PO_4 value (in µmole/Kg sw ; GEOSECS shipboard data) for the same depth interval. Crosses refer to Ba_p measurements performed by INAA at the CFR, open circles refer to INAA data obtained by P.Brewer at WHOI (GEOSECS shore-based data). Numbers refer to GEOSECS station numbers. Between brackets, values of organic C production rates (in mg $C.m^{-2}.day^{-1}$) from Koblentz-Mishke (1970); the value for station 31, from Steeman-Nielsen (1954).

Unfortunately, direct measurements of organic carbon production were not obtained at the same time as the collection of samples for Ba and PO_4. Carbon production data taken at a different period, but for the same general vicinity as these stations (Steeman-Nielsen, 1954; Koblentz-Mishke et al., 1970) are included in parentheses in Figure II.16. The stations from the Norwegian Sea (stations 11,18,23) and station 82, from the Antarctic fall much closer to the central line,when the relative intensity of organic carbon production is considered. For stations 11, 18, 23, this points towards high utilisation rates of PO_4 by the plankton,and for station 82 it appears that large supply in PO_4 does not result in a proportional rate of organic C production.

Since we have shown in section 4.2 of this part that, for the watercolumn extending between surface and bottom water, barite is the main Ba-carrier, the PO_4 - Ba_p relationship holds also for PO_4 - barite.

Strong evidence thus exists that the production of barite is related with biological activity. However, the arguments presented above leave the problem of the formation mechanism itself unresolved.

5.2.3 Two possible modes of biological formation of barite

The details of the apparent bond between the organic productivity and barite production are not known, but two complementary pathways of barite production can be consi-

dered:

a) Secretion of barite crystals by planktonic organisms.

Direct secretion of intracellular barite granules is known to occur in several species of the benthic protozoan Xenophyophora (Shulze und Thierfelder, 1905; Arrhenius and Bonatti, 1965; Tendal, 1972). In surface waters only $SrSO_4$ (celestite) secreting organisms, the acantharid Radiolaria, have as yet been reported (Botazzi and Schreiber, 1971). These organisms however, have a world wide distribution (Botazzi and Schreiber, op.cit.) and their spines contain up to 5400 ppm Ba (Arrhenius, 1963). However, our own SEM-EMP analyses of skeletal debris of acantharia, dis not reveal the presence of Ba, above the detection limit ($\sim$ 1000 ppm) (see section 2.3 in this part). Further, Martin and Knauer (1973) observed plankton, that was enriched in acantharid Radiolaria, to contain high levels of Ba.

A more precise indication on the role of microplankton in barite formation is found in Haeckel's monography on the Radiolaria (Haeckel, 1862). In the central capsuls of Radiolaria belonging to such families as the Collosphaera, the Sphaerzoida, the Coelodendrida, rhombic prisms were observed. These prisms were insoluble in boiling and cold water, in concentrated hot and cold sulphatic acid, in concentrated nitric acid and in concentrated chloridric acid (Haeckel, 1862). Haeckel tentatively identified these prisms as celestite and/or barite crystals. In Plate 10 some of Haeckel's original drawings, depicting the central-capsuls of different Radiolaria species with prisms enclosed within them, are reproduced. To our knowledge no other

PLATE 10

Collozoum coeroleum

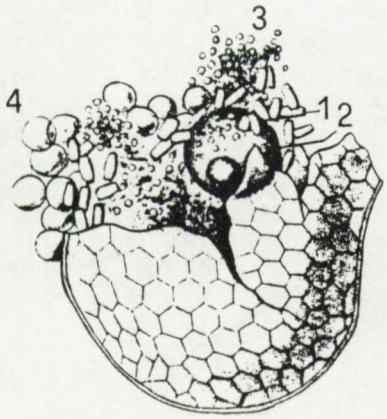

central capsules

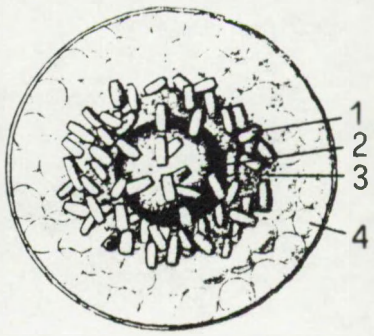

Collosphaera huxleyi

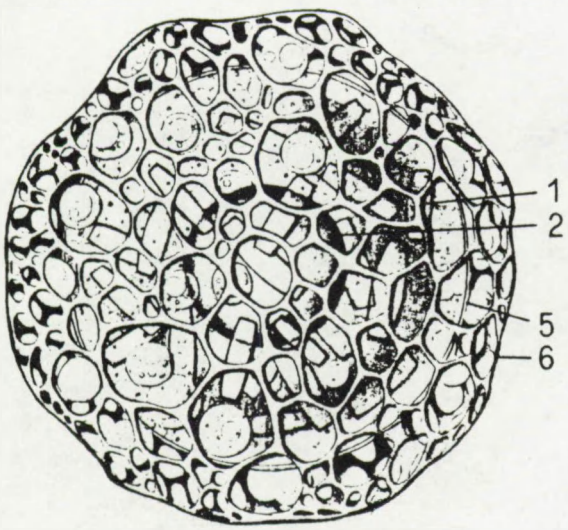

single individual

central capsule

1= Crystals ; 2= Fat droplet ; 3= Pigment grains ; 4= transparent vesicles ; 5= central capsule ; 6= silica skeleton

PLATE 11: Rhombic prisms inside the central capsula of Radiolaria. These prisms were tentatively identified by Haeckel as celestite and/or barite. Reproduced from Haeckel (1862).

information is available concerning the occurrence and the nature of such intra-capsular crystals in Radiolaria, since these early observations.

b) Decomposition of organic matter: As quoted in the introduction, Chow and Goldberg (1960) proposed that decaying organic matter, rich in sulphate, could form a micro-environment in which $BaSO_4$ saturation is attained. In fact,we observed sub-micron sized barite crystals and aggregates of barite prisms inside low density media, probably of organic composition (scetion 2.2 in this part, and Plate 11). These are likely to represent such micro-environments, with barite prisms having precipitated within them. Small aggregates of barite were observed at GEOSECS station 67 to occur down to 4424 m, suggesting that this mode of barite formation is not restricted solely to the surface waters.

Both of the discussed pathways could induce a maximum of suspended barite in the sub-surface waters, through disintegration of the carrier phase.

PLATE 11

BARITE GRAIN INSIDE AN ORGANIC PELLET

Location: GEOSECS Atlantic station 17 (74°56'N-01°07'W); 1860 m

Dark-field micrograph obtained with a 1 MeV transmission electron microscope of a barite grain (indicated by the arrow) inside an organic pellet.

From J.Klossa, Laboratoire R.Bernas, Orsay and Centre des Faibles Radioactivités, Gif-sur Yvette.

PLATE 11

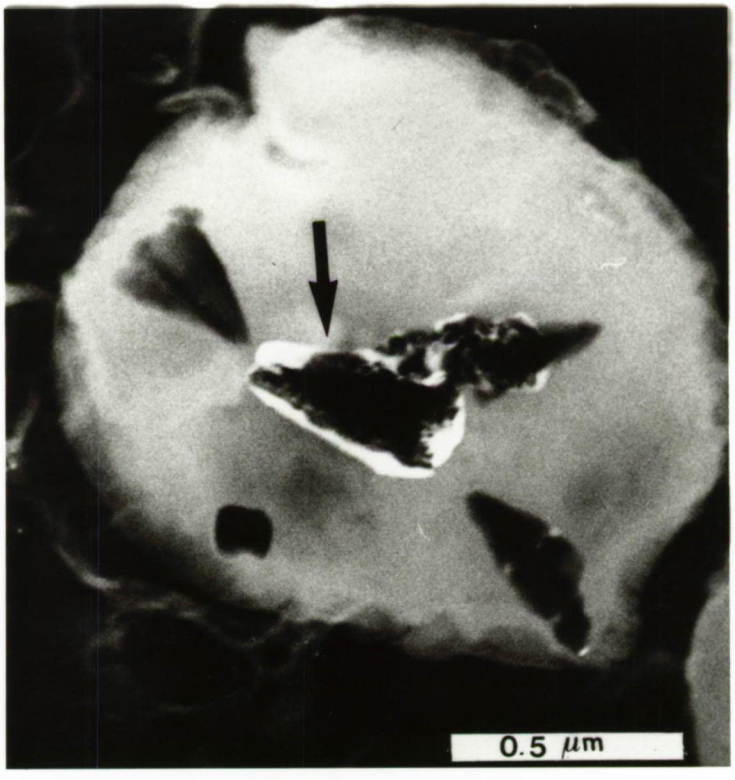

Discussion of chapters 2,3,4 and 5:

From the foregoing discussions it appears that barite crystals are an ubiquitous component of suspended matter. These crystals dissolve in the watercolumn, which is known to be undersaturated with respect to barium sulphate.

Suspended barite can occur as solid solutions with $SrSO_4$. The $SrSO_4$ content is in general less than 5 mol%, but in the sub-equatorial Atlantic surface waters, $SrSO_4$ fractions can exceed this value up to such level, that one can consider the complete substitution series,with $SrSO_4$ and $BaSO_4$ as end members,to be present. Fast dissolving $SrSO_4$ (celestite)debris of Acantharia occur only in the first 500 m of the watercolumn. Ba and Ca enriched discrete $SrSO_4$ particles, with no apparent biogenic morphology, do reach much greater depths, due to their occurrence as solid solutions,which reduces their rate of dissolution as compared to pure celestite.

Suspended barite is the major carrier of particulate Ba in intermediate and deep water. Particulate organic matter, siliceous and calcareous debris and aluminosilicates do contribute for between 8.5 and 23% of the total particulate Ba in this part of the watercolumn. In surface waters up to 50% of the total Ba_p amount is carried by non-barite particles, of which siliceous and calcareous debris and organic particulates constitute the main part. In bottom waters, up to 30% of the total Ba_p is carried by non-barite phases; here aluminosilicates,carrying 20% of the total Ba_p amount, are the main non-barite Ba-carriers.

for the total amount of particulate Ba in bottom waters. At GEOSECS stations 67 (Argentine Basin) and 282 (Antarctic) the resuspension of sediments appears to introduce excess barite in bottom waters.

The Ba_p maxima coincide often with O_2 minima, either in the region of the main thermocline, or at greater depth ($\sim$ 1000m). Thermoclines are regions where particulate matter accumulates, and therefore the O_2 minimum and the coinciding Ba_p maximum can be related with heterotrophic biological activity; the same can be said for O_2 and Ba_p extrema at greater depths, below the thermocline region. This supports the thesis that suspended barite is produced biologically. Since sea water is undersaturated for $BaSO_4$, this process must occur in suitable environments inside which saturation conditions are attained. The decomposing organic pellet or fecal pellet can be such microenvironment, and was in fact observed to contain barite crystals. Although biological activity is originally involved, in this case the formation itself of barite is probably a passive process. This mechanism of barite production is probably not the only possible one. The observed variation in Sr content of the surface-water barites suggests some biological control, which might be carried out by Acantharid or Collosphaerid Radiolaria. Although the exact pathway(s) of barite formation could not be unraveled here, we have shown that in any case barite formation stands in first order relation with organic productivity.

Conclusions of part II

1°. Suspended barite is a genuine and ubiquitous component of oceanic suspended matter.

2°. Suspended barite occurs often as a solid solution with $SrSO_4$. While below surface water, this substitution does not exceed a few mol%, the surface waters can contain the complete substitution series with $BaSO_4$ and $SrSO_4$ as end members. Besides Sr, K can be present in minor amounts.

3°. Factor analysis shows that above bottom waters the main particulate Ba phase, identified as barite, is a slowly dissolving component, sensitive to advective transport. This behaviour is shared in part with $CaCO_3$ (coccoliths) and dissolution resistive $SrSO_4$ particles having no biogenic habit. Morphological analyses indeed show the barite crystals to carry traces of a dissolution process. Further, influence of advective transport is emphasized by the presence of a greater fraction of barites altered by dissolution in the oldest watermass in place in the Argentine Basin profile (i.e. NADW), as compared with the younger watermasses below and above.

4°. Barite is the main carrier of Ba in suspended matter from intermediate and deep waters. In surface and bottom waters it is one of the major carriers of Ba.

5°. Barite production in the watercolumn is related with biological activity. The exact mechanism is not known.

PART III

A MASS BALANCE OF BARIUM IN THE OCEAN

INTRODUCTION

In part II of this work the importance of suspended barite, as the main carrier phase of Ba in the watercolumn, has been established. These biogenic barite particles sink through the watercolumn and are submitted to a dissolution process. In view of the discussion (see introduction page 1-10), pertaining to —— i) the importance of dissolving biogenic particles as the process explaining the enrichment of dissolved Ba in the deep sea and ii) the importance of settling biogenic particles as a source of sedimentary Ba, besides, or as opposed to volcanism —— the relative contributions of the suspended barite, we have detected, and of other biogenic particulates must be established.

Besides the dissolution of biogenic particles, the diffusive flux of dissolved Ba from the interstitial waters will contribute to the observed excess of dissolved Ba in deep versus surface water. Church (1970, 1972) and Li et al. (1973) observed that the dissolved Ba content of interstitial water is higher than in the watercolumn. For pore waters, the dissolved Ba concentrations exceed 40 µg/Kg SW, while the dissolved Ba concentrations in the deep sea attain only a World average of 16 µg/Kg sw (Li et al.,1973).
Li et al. estimated that the existing concentration gradient between pore waters and deep water resulted in an average diffusive flux of 0.1 µg Ba. $cm^{-2}.yr^{-1}$ to the deep ocean. Such a flux is insufficient to account for the dissolved Ba

enrichment in the deep sea, as shown in the following. Average deep water contains about 10 µg of diss. Ba/Kg SW more than surface water (see Table II . 16 in part II). Integrated over the deep part of the watercolumn, which has an average depth of 3500 m, this amounts to 3500 µg Ba. cm^{-2}. Since average deep waters have a residence time of about 1000 years (Broecker, 1963), the diffusive flux of dissolved Ba from the pore waters will contribute only for 100 µg. cm^{-2}, or 3% of the total amount of excess dissolved Ba in the deep watercolumn (3500 µg Ba.cm^{-2}). It is clear that other processes control the enrichment of dissolved Ba in deep water.

In the following we will show that it is the production, the settling and the dissolution of Ba enriched particles which control the dissolved Ba enrichment in the deep sea. When calculating the residence time of Ba in the watercolumn with the well known formula of Barth (1952) : $\tau = \frac{M}{R}$ with

τ = mean life; or residence-time of Ba in the ocean

M = standing crop of Ba ; M = 16 µg/Kg SW (average concentration of dissolved Ba in the deep sea; Li et al., 1973) X 350 litre (= volume of sea water in a column of deep water having a basis of 1 cm^2 and an average depth of 3500 m)

R = input or output rate ; the input rate of dissolved Ba by river discharge is 0.6* µg Ba.cm^2. yr^{-1} (Chan et al., 1976). This notation is preferred to dM/dt, which is mathematiccaly incorrect, since it is = 0 at steady state (see Carritt,1971 and Li, 1977).

We obtain for τ a value of 11000 years. Such a residence time, which is large compared to the age of deep-sea water (600 years in the Atlantic and 1200 years in the Pacific;

(*) note: this is a lower estimate, (see later section 1.1.)

Broecker, 1963), leads one to assume a homogenous vertical profile for dissolved Ba. The fact that the dissolved Ba profile is a heterogenous one , characterized by a biological scavenging in surface water and an enrichment in deep water, suggests that Ba is submitted in the watercolumn to a recycling process having a time constant that is smaller or equal to the deep water residence time. This recyling must then proceed between a particulate and a dissolved phase, such as it is known to occur for the nutrient elements.

The box-model analyses of Wolgemuth and Broecker (1970) and Li et al. (1973) see Figure III.1, indeed suggest that Ba is recycled in the watercolumn and that it is the dissolution of biologically produced particles that controls the enrichment of Ba in the deep sea.

In chapter 1 we will discuss a somewhat different box-model for Ba as those described in literature (see Figure III.1). This model will take into account the differences between the Atlantic and the Pacific Ocean as concerns the exchange rates between surface and deep reservoirs and between both deep reservoirs. The obtained input rates of dissolved Ba in the deep sea, which result from particle dissolution, will then be compared with estimated dissolution rates of the biogenic Ba carriers in suspension, which are : the barite crystals described in this study, and silica and carbonate debris.

In chapter 2 we will discuss the main mineralogical phases in which Ba occurs in the sediments, as well as their

possible sources. Further, sink and source of sedimentary Ba will be analyzed. The relative role of volcanism, of the settling of organic and skeletal debris and of the settling of suspended barite crystals, as sources of sedimentary barite will be discussed.

FIGURE III.1: Two-box model of the marine cycle of Ba; from Wolgemuth and Broecker (1970) and Li et al. (1973).

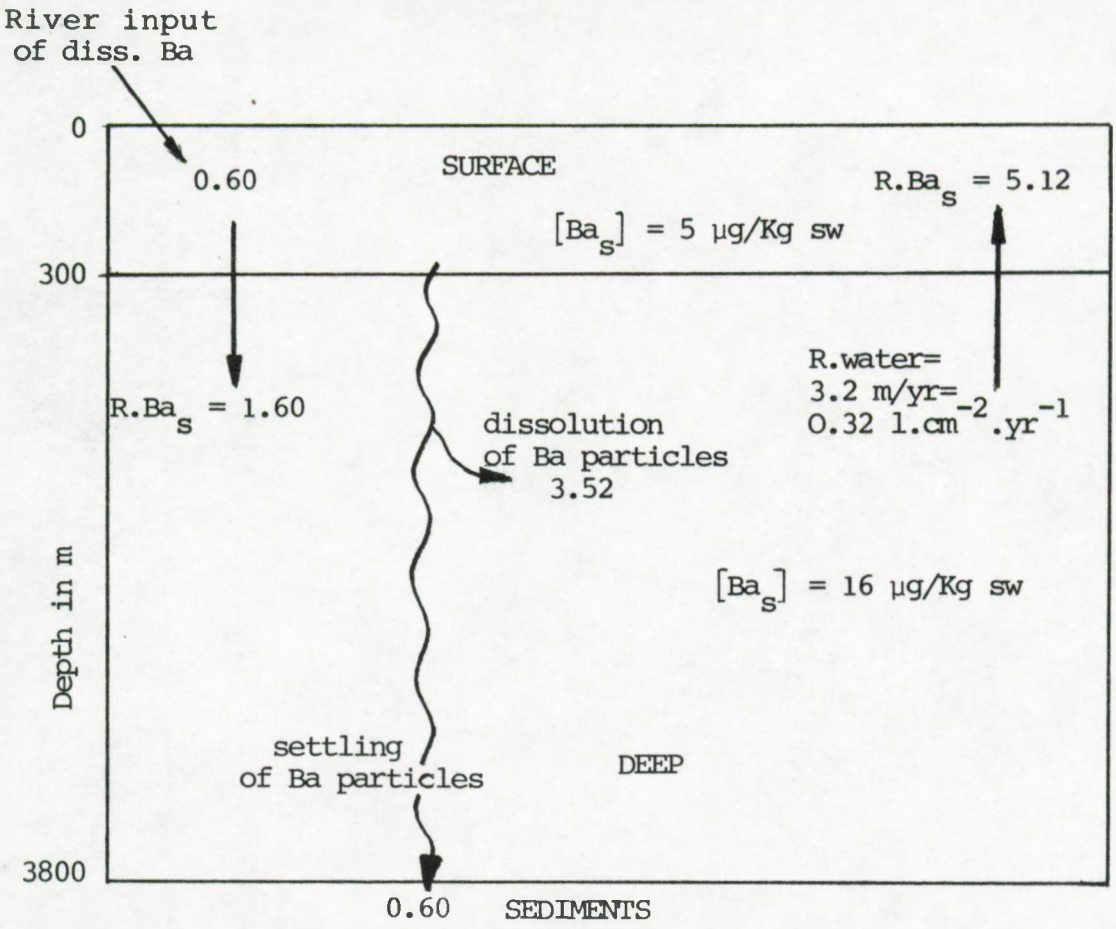

All values in µg.cm^{-2}.yr^{-1} , unless specified. R.Ba; R.water = exchange rates for dissolved Ba and water between surface and deep water box. Ba$_s$ = dissolved Ba.

CHAPTER I

THE CONTRIBUTION OF DISSOLVING SUSPENDED BARITE TO THE EXCESS OF DISSOLVED BARIUM IN DEEP WATER VERSUS SURFACE WATER

1.1. THE RECYCLING OF Ba IN THE OCEAN: THE BOX-MODEL APPROACH

In the ocean, profiles of dissolved barium resemble those of the main nutrients. They are characterized by a depletion in surface water and an enrichment in deep water. However, unlike Si, N,P that are extracted almost entirely from surface sea water and are therefore considered as "biolimiting" elements (Broecker, 1974), Ba such as C and Ca is never extracted completely from surface water. Therefore Ba, C and Ca are considered as "biointermediary" elements (Broecker, 1974). The general life cycle of such elements consists of:

- utilisation in the surface waters
- introduction, as dissolved species, in deep water through dissolution or oxidation of the carrier phase
- reintroduction, as dissolved species, in the surface waters through vertical advection of enriched deep-sea waters.

The use of two-box models by Wolgemuth and Broecker (1970) and Li et al. (1974) has lead to evaluations of the input rate of dissolved Ba in the deep-sea (J_{Ba}). These models were elaborated at the scale of the Pacific Ocean (Wolgemuth and Broecker, 1970) and the World Ocean (Li et al., 1973)

(see Figure III.1). They predict an average J_{Ba} of 3.5 $\mu g.cm^{-2}.yr^{-1}$. A more realistic approach however consists in considering the Atlantic and Pacific-Indian Oceans as two separate entities. This is necessary since residence times of Atlantic deep waters are about half the residence time of Pacific deep waters (Broecker 1963).

Broecker and Li (1970) have elaborated a three box-model for $\Sigma\ CO_2$, in which Pacific-Indian deep water and Atlantic deep water are considered as separate boxes; surface boxes are represented by a single common box. The sea water fluxes and particle fluxes between the boxes were calculated from mass-balance considerations for water, C^{14} and $\Sigma\ CO_2$. It was further assumed that the δO^{18}- salinity relationships observed in the ocean prevail. In the following a more detailed description is given of Broecker and Li's (1970) model. This model is reproduced in Figure III.2.

The three reservoirs are assumed to be homogenous; they are:

- warm surface water (WSW) that extends as a common, homogenous mass over both deep reservoirs. Indeed C^{14}/C^{12} and $\Sigma\ CO_2$ have nearly identical values in Pacific and Atlantic surface waters. This holds also for Ba_s (see Table II. 16).
- North Atlantic deep water (NADW), which is the main Atlantic water mass supplying the deep Pacific.
- Pacific-Indian deep water (PIDW).

FIGURE III.2

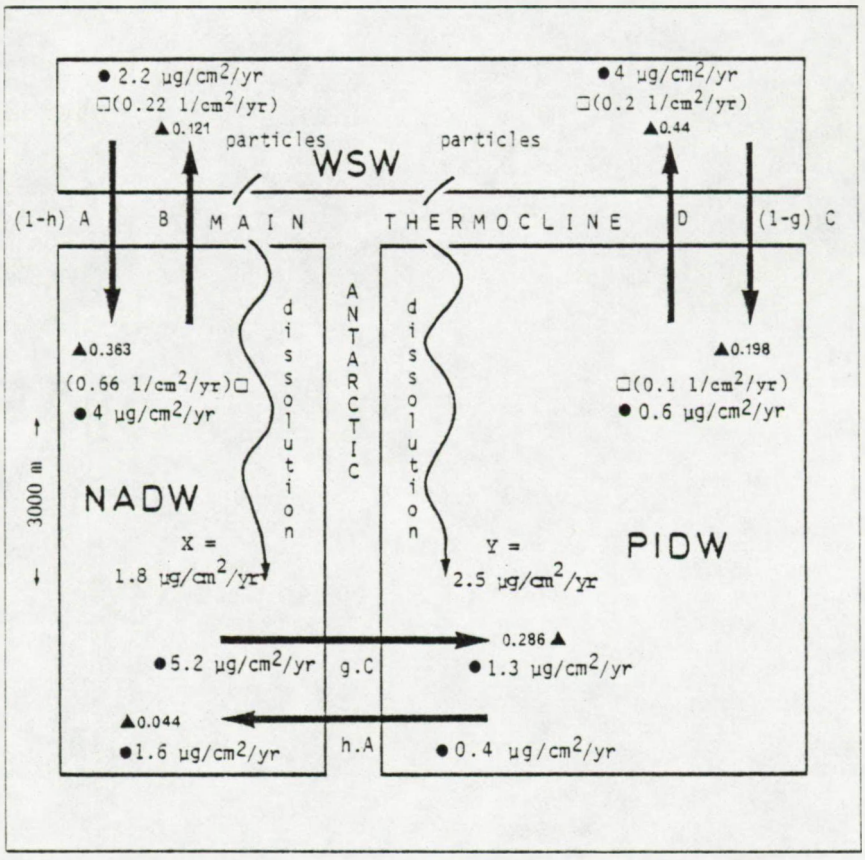

Box-model of the Ba cycle in the World Ocean. The model is based on a model of oceanic-water mixing of Broecker and Li (1970). Straight arrows indicate the directions of water fluxes between reservoirs. These flux values: ▲ in 10^{15} m^3/yr; □ in litre/cm^2/yr . A,C = rates of water supply from WSW to NADW and PIDW resp. . B,D = rates of water supply from NADW and PIDW to WSW. (1-h) and h = proportions resp. of WSW and PIDW required to generate NADW. (1-g) and g = proportions resp; of WSW and NADW required to generate PIDW . ● : fluxes of dissolved Ba resulting from water exchange between reservoirs. X and Y: fluxes of particulate Ba from WSW,resp. to NADW and PIDW, and dissolution rates of particulate Ba in NADW and PIDW. WSW = Warm Surface Water; NADW = North Atlantic Deep Water; PIDW = Pacific-Indian Deep Water.

These reservoirs are separated by zones of complex mixing called "mixing-cross" which are:

- the Antarctic Ocean, separating the Atlantic Ocean from the Pacific-Indian Ocean,
- the main-thermocline regions separating surface from deep water.

Transport of water between reservoirs takes place through the mixing cross. The proportions of WSW and PIDW (resp. 1-h and h) to generate NADW and of WSW and NADW (resp. 1-g and g) to generate PIDW, are derived from the positions of the different water types in a δO^{18}- salinity diagram (Fig. III.3). These data are from Craig and Gordon, cited in Broecker and Li (1970). In this diagram the waters of the northern Atlantic and the Weddell Sea, thought to be the main sources of deep water, fit straight lines. Since NADW falls along the mixing curve of North Atlantic surface waters it results that it must consist mainly of sinking North Atlantic surface water and that it can only be for a small part (not more than 20%) composed of Antarctic Bottom water (AABW). The diagram shows PIDW to have a δO^{18} and salinity composition which can result from a mixing of about equally important NADW (> 40%) and Antarctic water volumes.

The rates of water supply between reservoirs are calculated by considering conservation of water and of C^{14} in both deep reservoirs and the concentration of $\Sigma\ CO_2$ in each reservoir (Broecker and Li, 1970; page 3547):

- A,C are the rates of water supply from WSW to NADW and PIDW respectively.

FIGURE III.3

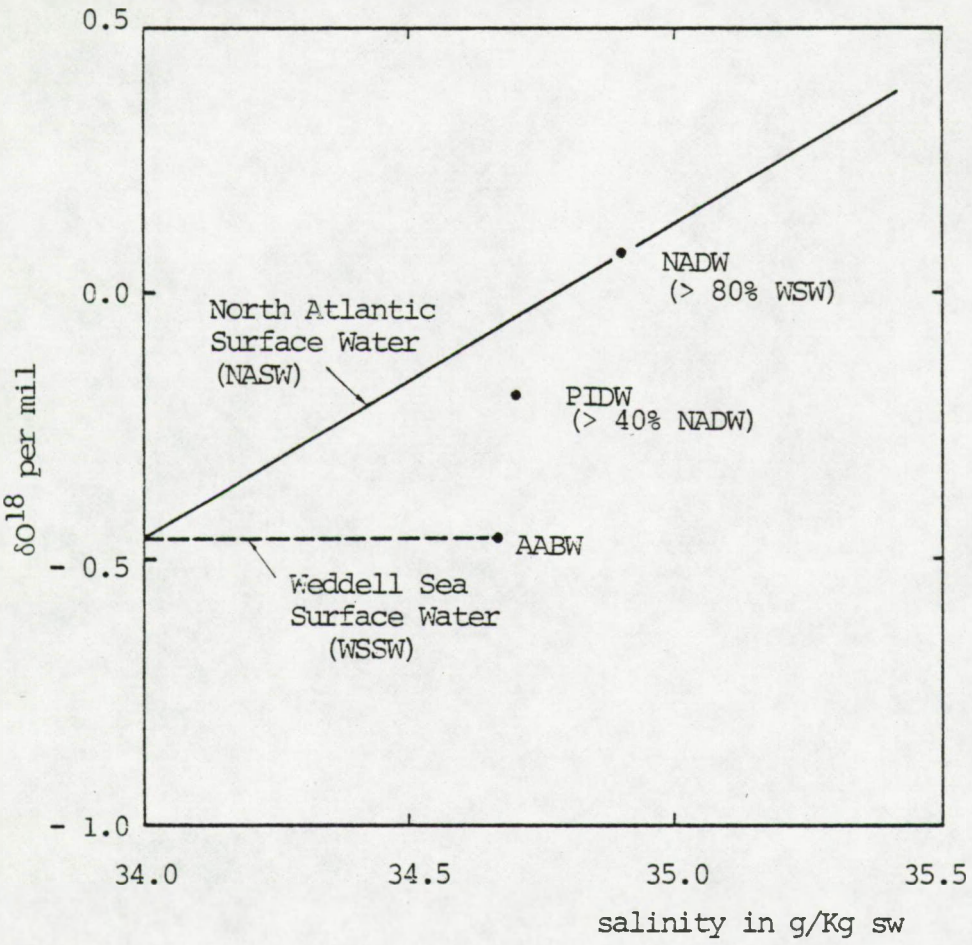

$\delta\ O^{18}$ - salinity diagram in which the main sources of oceanic deep water are plotted (NASW; WSSW). PIDW has an intermediary position between NADW and WSSW. Data are from Craig and Gordon (1970), cited Broecker and Li (1970).

- B,D are the rates of water supply to WSW, respectively from NADW and PIDW.

The reservoirs and the mixing zones have the following volumes:

- NADW : 0.15 x ocean volume = V_A
- PIDW : 0.60 x ocean volume = V_p
- WSW : 0.02 x ocean volume
- Antarctic : 0.23 x ocean volume
- ocean volume : 1.1×10^{18} m^3

The height of both deep water masses is taken as 3000 m.

Conservation of water in NADW and PIDW requires

$$A = B + gC \text{ and } C = D + hA$$

Conservation of dissolved barium concentration requires:

- in the NADW:

$$k_s(1 - h)A + k_p hA + X = k_a(B + gC) \qquad (3.1)$$

with X = particle flux from WSW to NADW

- in the PIDW:

$$k_s(1 - g)C + k_a gC + Y = k_p(D + hA) \qquad (3.2)$$

with Y = particle flux from WSW to PIDW

$k_s = Ba_s$ concentration in the surface water

$k_a = Ba_s$ concentration in the NADW

$k_p = Ba_s$ concentration in the PIDW

Broecker and Li give values of 0.10 and 0.60, as the best estimates of h and g resp. For these values of g and h they compute the following values for the different water fluxes (tranposed in units of $m^3.yr^{-1}$):

$$(1 - h)A = 0.363 \times 10^{15} \ m^3 \ . \ yr^{-1}$$

$$hA = 0.044 \quad "$$

$$B + gC = A = 0.407 \quad "$$

$$(1 - g)C = 0.198 \times 10^{15}\ m^3 \cdot yr^{-1}$$

$$gC = 0.286 \quad "$$

$$D + hA = C = 0.484 \quad "$$

$$B = 0.121 \quad "$$

$$D = 0.440 \quad "$$

From Table II.16 , the following average Ba_s concentrations are deduced: $k_s = 6\ \mu g.l^{-1} = 43\ \mu mole.m^{-3}$

$k_a = 10\ \mu g.l^{-1} = 73\ \mu mole.m^{-3}$

$k_p = 20\ \mu g.l^{-1} = 145\ \mu mole.m^{-3}$

By replacing these values in (3.1) and (3.2) particle fluxes X and Y are obtained:

$X = 7.7 \times 10^{15}\ \mu mole.\ yr^{-1}$

$X/A_a = 7.7 \times 10^{15}/5.5 \times 10^{13}\ \mu mole \cdot m^{-2} \cdot yr^{-1}$

$= 1.4 \times 10^{2}\ \mu mole \cdot m^{-2} \cdot yr^{-1}$

$= \underline{1.9\ \mu g \cdot cm^{-2} \cdot yr^{-1}}$

with A_a = area of surface ocean supplying particulate matter to the NADW; $A_a = V_a/3000 = 5.5 \times 10^{13}\ m^2$

$Y = 40.8 \times 10^{15}\ \mu mole \cdot yr^{-1}$

$Y/A_p = 40.8 \times 10^{15}/2.2 \times 10^{14}\ \mu mole \cdot m^{-2} \cdot yr^{-1}$

$= 1.85 \times 10^{2}\ \mu mole \cdot m^{-2} \cdot yr^{-1}$

$= \underline{2.5\ \mu g \cdot cm^{-2} \cdot yr^{-1}}$

with A_p = area of surface ocean supplying particulate matter to the PIDW; $A_p = V_p/3000 = 2.2 \times 10^{14}\ m^2$

The use of other estimations of h ang g in Broecker and Li, yields the following extreme values for X and Y:

h=0.2; g=0.6; X= 1.74 in $\mu g.cm^{-2}.yr^{-1}$ Y=4.4 in $\mu g.cm^{-2}.yr^{-1}$

h=0.0; g=0.4; X= 2.1 in $\mu g.cm^{-2}.yr^{-1}$ Y=2.47 in $\mu g.cm^{-2}.yr^{-1}$

The reliability of the model is discussed by Broecker and Li (1970). Two facts emphasize the important simplification implied by the model:

1°) No account is taken of decay processes in the mixing-cross (= thermocline + Antarctic waters), constituting 23 % of the ocean volume. This would lead to an underestimation of the particle fluxes. However Broecker and Li conclude that a proportional partitioning of the mixing-cross waters between NADW and PIDW has no influence on deep-sea residence times and on particles fluxes espressed per unit area.

2°) Exchange of CO_2 between the atmosphere and the mixing cross takes place, especially in the polar regions. Evidence exists that some of the C^{14} in the deep sea was not introduced through WSW, as assumed by the model but was taken up in the polar regions. If taken into account this process would result in an increase of the deep sea residence time (at least 10 %) and in a <u>decrease</u> of particle flux, which is however unlikely to exceed a factor 2. Broecker and Li suggest that the comparison between calculated and observed particle fluxes should resolve this question. Their comparison between the estimated particle -bound flux of $\Sigma\ CO_2$ and observed rates of $CaCO_3$ accumulation in sediments extending above the lysocline, indeed points towards an overestimation of the particles flux by a factor two, emphasizing the influence of exchange processes between atmosphere and cold surface water.

Discussion

The box-model, discussed here, takes only account of the watercolumn, which is considered as a closed system. It does not discuss the input of Ba to the ocean, since this is assumed, such as for any steady state model, to be counter-balanced by an equally important output to the sediments.

We will discuss briefly the estimated average input rate of dissolved Ba to the ocean, due to river discharge and atmospheric input. The study of several rivers, essentially of the North American continent, has shown that typical river water contains an average of 60 µg of dissolved Ba per litre (Wolgemuth and Broecker, 1970; Li et al. 1973 ; Chan et al., 1976; Hanor and Chan, 1977). Since rivers are considered to deliver some 10 litre of water per cm^2 of ocean floor every 1000 year (Turekian, 1968) it ensues that rivers supply 0.6 µg of dissolved Ba per cm^2 and per yr to the oceans. This amount is certainly supplemented by a Ba fraction, we call "labile-Ba", that is released from suspended clays by desorption and ion exchange processes during the mixing of river water with sea water (Kharkar et al., 1968; Hanor and Chan, 1977). This desorption process, on contact with sea water, is due to the very high concentrations in sea waters of Na^+, K^+, Mg^{++} and Ca^{++} which are the cations that will displace adsorbed elements from the clay particles, carried by the rivers. (Kharkar et al., 1968; Hanor and Chan, 1977). For the Mississippi river, Hanor and Chan calculated that as a result of desorption, the total input of dissolved Ba in the Gulf of

Mexico can be twice the input calculated when considering only the dissolved Ba load of typical river water. It is assumed further by Hanor and Chan that the total input of dissolved Ba is highly variable as a result of variations in river discharge. This makes it difficult to establish a statistically meaningful annual flux of Ba to the oceans (Hanor and Chan, 1977).

The Ba/Al ratio in atmospheric matter shows all Ba to be supported by aluminosilicate material, if this is assumed to have the average composition of shales. (Buat-Menard, 1979; Chester and Stoner, 1973). The average flux of atmospheric Al_p to the ocean surface is evaluated at 5 µg $Al.cm^{-2}.yr^{-1}$ (Buat-Menard and Chesselet, 1979). When taking the following composition for shales: Al = 80,000 ppm; Ba = 600 ppm (Turekian and Wedepohl, 1961), it follows that the flux of Ba in aluminosilicates to the ocean surface is: 0.034 µg.$Ba.cm^{-2}.yr^{-1}$. If we assume this entire quantity to become available as dissolved Ba, through ion exchange, (an unlikely assumption) it follows that this source can represent at most 6% of the river input of dissolved Ba.

Our box-model data suggest that the dissolution of biogenic particles in deep Indo-Pacific waters should liberate 30 % more Ba than in the deep Atlantic. This difference in dissolution rates is a direct result of the enrichment of Pacific deep waters in dissolved Ba (see Table II.16; part II). This enrichment itself is due to the fact that deep water leaves the Atlantic towards the Pacific at a higher rate than

deep Pacific water flows to the Atlantic, while steady state is maintained by a net flow of surface water from the Pacific to the Atlantic (Wolgemuth and Broecker, 1970). This higher dissolution rate in the Pacific implies of course also a higher particle production rate in Pacific surface water. Our data show that concentrations of particulate Ba in suspended matter from Pacific and Atlantic are similar. Therefore , suspended barite does not appear,at first sight, as the carrier of this excess Ba. However, a meaningful comparison between Atlantic and Pacific vertical fluxes of suspended barite requires that size, volume measurements be performed also on Pacific suspended barites, which is not the case today. Since a similar enrichment pattern is observed in the deep Pacific for dissolved silica (Broecker and Li, 1970), the larger productivity of particulate silica in Pacific surface water, predicted by the model, could be responsible for the higher consumption of dissolved Ba in the Pacific. Today, no data exists concerning this predicted greater productivity of SiO_2 in the Pacific.

In the following section we will compute the dissolution rate of the suspended barite crystals, observed during this work, as well as the one of other biogenic particles enriched in Ba. The latter evaluations will be based upon estimations of the rate of production and dissolution of the different carriers and upon the measured or estimated Ba content in each type of carrier. It is not our intention to enter here the debate upon the mechanisms that govern the predicted differences

in production and dissolution rates of Ba and Si between the Pacific and the Atlantic, but rather to verify if the magnitude of such dissolution rates for Ba can be accounted for by dissolving biogenic particulates, and most importantly to evaluate the contribution of suspended barite in this process.

1.2. THE ROLE OF THE BIOGENIC SUSPENDED PARTICLES, INCLUDING BARITE, IN THE IN-SITU FLUX OF DISSOLVED BARIUM IN THE DEEP-SEA

Several authors (Edmond, 1970; Ku et al., 1970; Bacon and Edmond, 1972; Li et al., 1973) have emphasized the role played by dissolution of diatom skeletons as a source of dissolved Ba in the deep sea.

If the dissolution of diatoms was the only way by which the deep waters become enriched in Ba_s, the Ba/Si ratio in diatoms should be equal to the ratio of "excess" dissolved Ba to "excess" dissolved Si in the deep ocean (Wolgemuth and Broecker, 1970; Ku et al., 1970):

$$(Ba/Si)_{diatoms} = \frac{(Ba_s)_{deep} - (Ba_s)_{surface}}{(Si_s)_{deep} - (Si_s)_{surface}} \qquad (3.3)$$

From the data of Chan et al. (1977) (for diss. Ba see Table II.16 in part II of this study) we deduce the following mean dissolved Ba and Si concentrations in the Atlantic Ocean:

- surface waters: Ba_s : 6 µg/Kg SW Si_s: 50 µg/Kg SW
- deep waters: Ba_s : 10 µg/Kg SW Si_s: 1500 µg/Kg SW

The ratio of excess Ba_s to excess Si_s then becomes:

$$\frac{10 - 6}{1500 - 50} = 2.8 \times 10^{-3}$$

Since Si accounts for 46.7 % of the SiO_2 weight, eq. (3.3) is written:

$\frac{Ba}{467,000} = 2.8 \times 10^{-3}$, with Ba = 1300 ppm, which is about 10 times larger than the value we measured for Rhizosolenia alata which was shown (§ 4.3.1., in part II) to be in agreement with data for diatom-enriched open ocean phytoplankton. This reflects the importance of the dissolution of other biogenic carriers of Ba in the deep sea. One of these is of course the suspended barite. Carbonate debris are the third carrier whose role will be investigated since, together with silica debris and particulate organic matter (POM), they represent the main biogenic constituents in suspended matter (Krishnaswani et al., 1977). The case of POM is not considered here since the Ba that is liberated during its decomposition can be assumed to become incorporated into barite (see part II, section 5.2). As a result, a barite production rate can be deduced from known rates of POM decomposition. This production rate will be calculated, before considering the dissolution of the three remaining Ba carriers.

The rate of POM decomposition is given by:

$$D = P - F \qquad (3.4)$$

with D = decomposition rate of POM

P = production rate of POM

F = vertical flux of the fraction of the total POM that is not remineralized

1°) The POM production rate:

POM = 2 x POC (particulate organic carbon) (Strickland, 1965), and the world average POC production rate is 7 $mgC.cm^{-2}.yr^{-1}$ as deduced from the data of Koblentz-Mishke et al. (1970)

on organic C production rates in the different regions of the World Ocean. This value is slightly higher than Ryther's estimation of 5.5 $mgC.cm^{-2}.yr^{-1}$.

If follows that the POM production rate is 14 $mg.cm^{-2}.yr^{-1}$.

2°) The POM flux:

Skopintsev (1972) considered an average World Ocean POC flux of 0.6 $mgC.cm^{-2}.yr^{-1}$, which is 5% of his estimation of the average organic C production rate: 12 $mgC.cm^{-2}.yr^{-1}$; that value is about twice the estimation of Koblentz-Mishke et al. (1970). From data on phytoplankton consumption by zooplankton and remineralization of the excreted matter, Menzel (1974) deduces that 4% of the annually produced amount of organic carbon will not be remineralized and remains as a refractory phase. As based on Ryther's 1969 value of organic carbon production rate in the World Ocean (5.5 mg $C.cm^{-2}.yr^{-1}$) Menzel computes an organic carbon flux of 0.2 $mgC.cm^{-2}.yr^{-1}$. Bishop et al. (1977) give a value of 1.1 $mgC.cm^{-2}.yr^{-1}$ for the downward flux of organic C in the Equatorial Atlantic, which is 6 to 12 % of the production rate in this region, estimated at 9 to 16 $mgC.cm^{-2}.yr^{-1}$. We will consider here that 5 % (= 0.3 mgC. $cm^{-2}.yr^{-1}$) of the organic C production, taken as 7 $mgC.cm^{-2}.yr^{-1}$ settles out from the surface waters. With POM being twice the POC content it follows that the POM production rate and downward flux are respectively 14 and 0.60 $mgC.cm^{-2}.yr^{-1}$. The POM decomposition rate is thus: 13.4 mg. $cm^{-2}.yr^{-1}$.

In § 4.3.3. of part II we considered the Ba content of POM to amount to 60 ppm. It follows that the barite production rate can be estimated at:

$$\frac{13.4 \times 60}{10^6} = 8 \times 10^{-4} \text{ mgBa.cm}^{-2}.\text{yr}^{-1}$$

$$= 0.8 \text{ µg Ba.cm}^{-2}.\text{yr}^{-1}$$

This value will be used later, whan discussing the gross budget of Ba in the ocean (see conclusion of part III).

We will now evaluate the contributions of dissolving suspended silica and carbonate debris and of dissolving suspended barite to the in -situ flux of dissolved Ba in the deep sea. The skeletal debris considered here, consist of slowly settling particles. They do not include the fast settling Foraminifera, Pteropod, Radiolaria shells and fecal matter, which will become important when disussing sedimentation rates.

1.2.1. The input of Ba by the dissolution of suspended silica skeletons

The SiO_2 production rate can be obtained from the following relation:

(SiO_2/POC) x POC production rate,

with SiO_2 representing the silica content of suspended matter and POC representing the particulate organic matter content of suspended matter.

We consider a SiO_2/POC ratio of 0.33 for suspended matter in surface water (see § 4.4.1. and 4.4.3. in part II). This value is based on observations in the Atlantic Ocean by Copin-Montegut and Copin-Montegut (1974) and Bishop et al., (1977)

and corroborates the former authors' data for the South-Indian Ocean (Copin-Montegut and Copin-Montegut, 1978). Antarctic waters can have higher SiO_2/POC ratios (about 1.3) as shown by Copin-Montegut and Copin-Montegut (1978) and Krishnaswami and Lal (1977). We will however, use the value of 0.33 as a good estimate of the average World Ocean SiO_2/POC ratio. We consider an average organic C production rate of 7 $mgC.cm^{-2}.yr^{-1}$ as deduced from the data of Koblentz-Mishke et al. (1970). By substituting these two values in (SiO_2/POC)x POC prod. rate. We obtain a value of 2.3 $mg.cm^{-2}.yr^{-1}$ for the production rate of SiO_2. Below we compare this value with literature values for average World Ocean rates:

- < 1.2 mg $SiO_2.cm^{-2}.yr^{-1}$ (Berger, 1970; deduced from data on deep water Si content and deep water residence times)
- 2.1 mg $SiO_2.cm^{-2}.yr^{-1}$ (Harriss, 1966; deduced from observed SiO_2/carbon ratios in marine plankton and organic C production rates)
- 5.1 to 9.6 mg $SiO_2.cm^{-2}.yr^{-1}$ (Heath, 1973; deduced from SiO_2/carbon ratios in diatoms, as observed by Lisitzin (1967), and World average organic C production rates).
- 24 to 48 mg $SiO_2.cm^{-2}.yr^{-1}$ (Lisitzin, 1967)

We will consider here neither the values of Lisitzin nor those of Heath, which are partially based on those of Lisitzin. Indeed, recent data of Copin-Montegut and Copin-Montegut (1978) show the SiO_2/POC ratios of Lisitzin for suspended matter to be overestimated. Therefore we take the value calculated above (2.3 mg $SiO_2.cm^{-2}.yr^{-1}$) as a reasonable estimate of the World average production rate of SiO_2. Of this quantity some 90% dissolves before reaching the sediment (Wollast, 1974). Of the

silica producers, diatoms are the most important ones (Lisitzin, 1967). If we take the Ba content of diatoms frustules as 120 ppm (see § 4.4.1.; part II), the following dissolution rate of Ba is deduced:

$$\frac{0.9 \times 2.3 \times 120}{10^6} = 2.5 \times 10^{-4} \text{ mg Ba. cm}^{-2}.\text{yr}^{-1}$$

$$= 0.25 \text{ µg Ba.cm}^{-2}.\text{yr}^{-1}$$

1.2.2. The input of Ba by the dissolution of suspended carbonate skeletons

Our INAA analyses show the GEOSECS samples to contain an average $CaCO_3$ content of 6% of the TSM weight (Table A.II.3). The $CaCO_3$ production rate can be obtained from: $(CaCO_3/POC) \times$ POC production rate (with POC, and POC production rate as used in § 1.2.1.). A $CaCO_3$ production rate of 1.4 $mg.cm^{-2}.yr^{-1}$ is obtained. Berger (1970) considers an average $CaCO_3$ accumulation rate of 0.34 $mg.cm^{-2}.yr^{-1}$. As a result about 80% (= 1.1 $mg.cm^{-2}.yr^{-1}$) of the amount produced, redissolves at depth.

These values are in good agreement with literature data:

production rate: - 2.0 $\pm$ 0.5 $mg.cm^{-2}.yr^{-1}$ (Li et al., 1969; Value deduced from alkalinity profiles and deep ocean residence times; World Ocean scale).

- 1 $mg.cm^{-2}.yr^{-1}$ (Honjo, 1976; 1977 coccolithal $CaCO_3$; Equatorial Pacific)

Dissolution rate: - 1.7 $mg.cm^{-2}.yr^{-1}$ (Li et al., 1969)

- 1.6 $mg.cm^{-2}.yr^{-1}$ (Berger, 1970; value deduced from mass-balance calculations; World Ocean scale)

Honjo further observed that the dissolution of coccolithal $CaCO_3$ was sufficient to account for estimated J_{CaCO_3} fluxes in the deep Pacific (Honjo, 1976, 1977).

Again, by taking the computed value of 1.1 $mg.cm^{-2}.yr^{-1}$, as a reasonable estimate of the World average $CaCO_3$ dissolution rate, and by taking $CaCO_3$ debris to contain 200 ppm of Ba (see § 4.3.2.) we obtain a dissolution rate for Ba of:

$$\frac{0.8 \times 1.4 \times 200}{10^6} = 2.2 \times 10^{-4} \text{ mg Ba.cm}^{-2}.\text{yr}^{-1}$$

$$= 0.22 \text{ µg Ba. cm}^{-2}.\text{yr}^{-1}$$

The combined dissolution of silica and carbonate debris produces an input rate of dissolved Ba in the deep-sea of 0.47 µg $Ba.cm^{-2}.yr^{-1}$.

1.2.3. The input of Ba by the dissolution of suspended barite

A. i) General formulation of the dissolution of a particulate phase in sea water

When particle size data are available it is possible to calculate the rate at which particulate matter dissolves, by considering the following formulation used by Lal and Lerman (1973):

$$\frac{\pi}{6} \cdot \rho \cdot \frac{d(N.D^3)}{dt} = J$$

with M = amount of matter that dissolves

N = number of particles

D = particle diameter

ρ = density of the particulate matter

In order to compute J we need more information on dD/dt, the rate of decrease of the particle radius. In Brun-Cottan (1976) the change in particle volume, as a result of dissolution, is written:

$$dV/dt = k \cdot D^2 \qquad (3.6)$$

with k = dissolution rate constant for a dissolution law which is proportional to the surface of the particle, assimilated to a compact sphere. Surface proportionality is also assumed in Lal and Lerman (1973, 1975) and Wollast (1974).

D = particle diameter

Since $dV/dt = (dV/dD).(dD/dt) = (\pi/2).D^2.(dD/dt)$

$$dD/dt = \frac{k \cdot D^2 \cdot 2}{D^2 \cdot \pi} = \frac{2}{\pi} \cdot k \qquad (3.7)$$

which is a constant, independent of particle size. Development of (3.5) and substitution of (3.7) in (3.5) results in:

$$J = \rho \cdot N \cdot D^2 \cdot k + \frac{\pi}{6} \cdot \rho \cdot D^3 \cdot \frac{dN}{dZ} \cdot \frac{dZ}{dt} \qquad (3.8)$$

with Z = depth.

In the following we will assume particles to settle trough the watercolumn, according to Stokes' settling law. Therefore dZ/dt, ther particle's settling velocity, is written

$$dZ/dt = C \cdot D^2, \text{ with } C = \text{constant} \qquad (3.9)$$

$$C = \frac{1 \cdot g \cdot (\rho_p - \rho_w)}{18 \cdot \nu}, \text{ (in } cm^{-1}.sec^{-1})$$

with $g = 981$ cm.sec^{-2} = gravitational acceleration

ρ_p = barite density = 4.5 gr.cm^{-3}

ρ_w = sea water density = 1.024 gr.cm^{-3} at 2°C and 34.8‰

ν = viscosity of sea water = 1.5×10^{-2} gr.cm^{-1}.sec^{-1}

The influence of vertical advection on the settling rate is not considered.

Substitution of (3.9) in (3.8) results in :

$$J = \rho \cdot N \cdot D^2 \cdot k + \frac{\pi}{6} \cdot \rho \, D^3 \cdot C \cdot D^2 \cdot \frac{dN}{dZ} \qquad (3.10)$$

The flux Ø of particles is $N.(C.D^2)$. At steady state the particle flux is constant with depth: $d\text{Ø}/dZ = 0$ and

$N \left(\frac{d(C.D^2)}{dZ}\right) = - C.D^2 \left(\frac{dN}{dZ}\right)$. It follows that

$$\frac{dN}{dZ} = - \frac{N}{C.D^2} \cdot \left(\frac{d(C.D^2)}{dZ}\right) = \frac{-2N}{D} \cdot \frac{dD}{dZ} \qquad (3.11)$$

Substitution of (3.11) in (3.10) gives:

$$J = \rho \cdot N \cdot D^2 \cdot k - \frac{2.\pi}{6} \cdot \rho \cdot D^4 \cdot N \cdot C \cdot \frac{dD}{dZ} \qquad (3.12)$$

Since $dD/dt = (dD/dZ).(dZ/dt)$, dD/dZ is easily obtained with the aid of (3.7) and (3.9). Subsequent substitution in (3.12) results in:

$$J = \frac{1}{3} \cdot \rho \cdot N \cdot D^2 \qquad (3.13)$$

For a sample with different size classes (3.13) is written:

$$J = \sum_i J_i = (\frac{1}{3} \cdot \rho \cdot k) \cdot \sum_i N_i \cdot D_i^2, \text{ in gr.cm}^{-3}\text{.year}^{-1} \qquad (3.14)$$

(see also Lal and Lerman, 1973).

Every term in (3.14) is known, with exception of the barite dissolution rate constant k. This constant will be deduced from our experimental data concerning the change of the size distribution of suspended barite with depth.

ii) Computation of the barite dissolution rate constant in sea water

In Brun-Cottan (1976[a]; 1976[b]) a model is described, based on particle size distributions, which formulates the vertical settling and dissolution of particles. Direct deduction of the dissolution rate constant k is possible. The model assumes the vertical transfer of particles to obey Stokes' settling law. From a comparative study of particle size distributions in the watercolumn it is possible to compute the settling time and dissolution rate of the particles transitting through a depth interval with chosen boundaries. The Brun-Cottan model enables a direct deduction of the dissolution rate constant, whereas in other contributions (Lal and Lerman, 1973; 1974; 1975) these constants are given values, experimentally determined by Peterson (1966) and Berger (1967) for silica and calcite tests and spheres.

Since the model postulates the presence of a stationary state, with constancy in time of physical and chemical parameters within the chosen boundaries, the following conditions and restrictions are imposed (Brun-Cottan, 1976a):

- the studied depth interval must be situated inside an identified watermass to minimize the effect of advective transport of particles
- the depth interval should be chosen below the surface layer which is influenced by rapidly variable processes such as productivity.

Further, calculation of the dissolution law coefficients requires that the following conditions be fulfilled within the chosen depth interval:

- the upper boundary of the depth interval is crossed by vertically settling particles characterized by the constancy of their flux and of their size distribution function
- the dissolution law is depth and time independent
- the dissolution law coefficients are independent of particle size
- particles have and preserve a spherical shape.

Further, particulate matter is considered to be chemically uniform . Brun-Cottan (1976a) states that although these conditions are probably not entirely fulfilled in the marine environment, they can be accepted for a first order approximation. In our case, the two last conditions are well fulfilled, since we are studying a specific mineralogical phase that consists to a large extend (50 %) of rounded and

spherical particles (see section 2.2 in part II), instead of a heterogenous collection of total particles as analyzed by Brun-Cottan (1976a).

The model calculations worked out by Brun-Cottan (1976a; 1976b) are resumed in appendix VII. The calculated dissolution rate constants k are:

Station 67 (2574m - 2982m)	0.5×10^{-5} cm/yr	=	0.05 µm/yr
Station 3 (1875m - 2479m)	1.0×10^{-5} cm/yr	=	0.1 µm/yr
Station 3 (2989m - 3267m)	4.0×10^{-5} cm/yr	=	0.4 µm/yr

The smallest and the largest k value are different by an order of magnitude, this is discussed below. In Figure III.4 A,B,C the evolution of the barite particle diameters is plotted against depth, as calculated with each of the three values for k. From Figure III.4.C it appears that if k = 0.4 µm/yr would be valid, particles occurring below 3000 m must have had an original diameter larger than 3.5 µm, at the moment of their production in surface water. The existence of this large k value is incompatible with the fact that the shape of our barite size distributions (§ 4.1.1 in part II) do not predict the important enrichment of the surface waters in large (> 3.5 µm) barite crystals. This enrichment would be required in order for the important numbers of suspended barite crystals occurring in the deep water (> 3000 m), to be compatible with such a large dissolution rate constant value.

Figure III.4.A

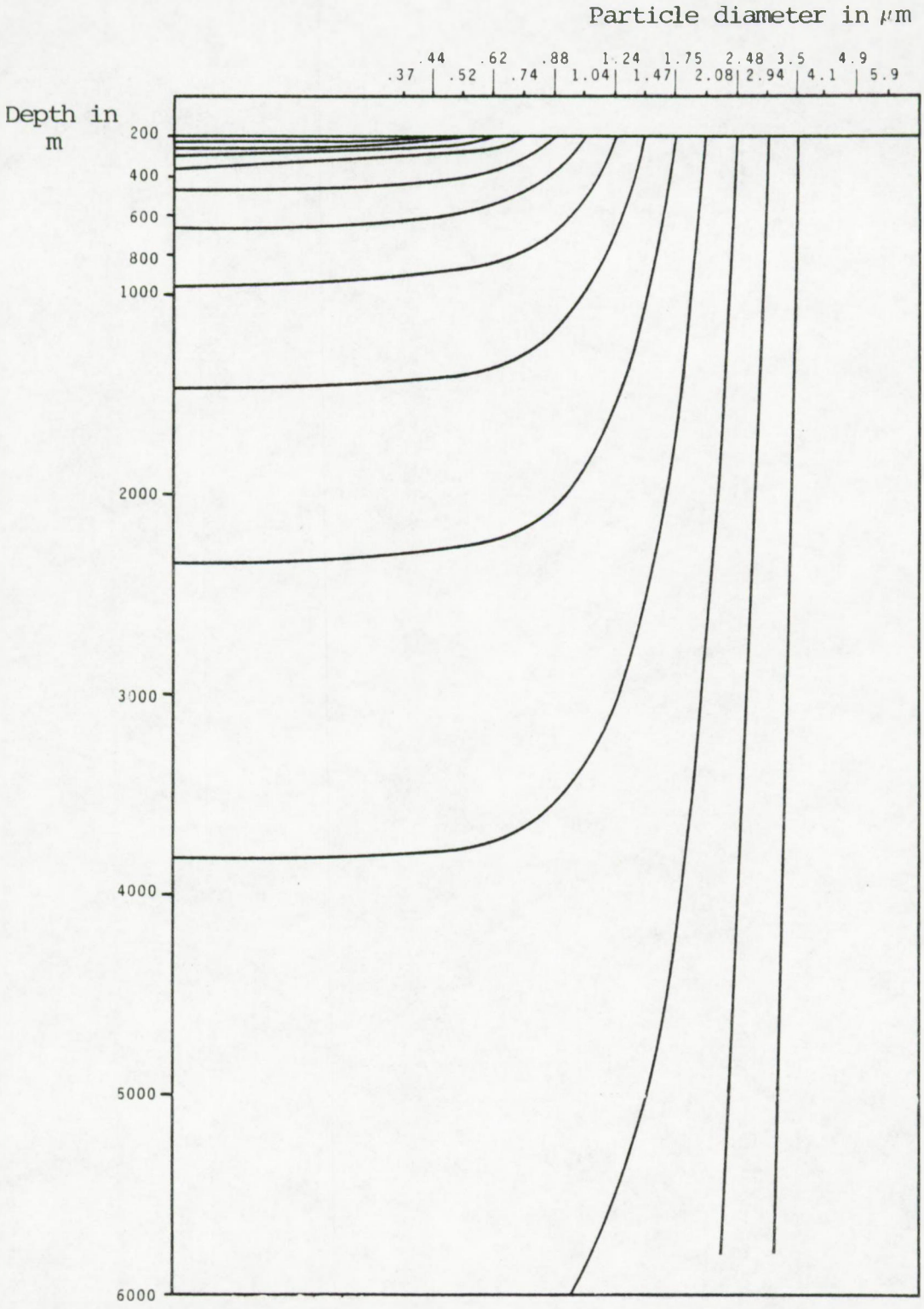

Calculated effect of the dissolution upon the decrease in diameter of suspended barite particles, which are produced in surface water (200 m) and which settle through the watercolumn, according to the Stokes settling law; for k, the barite dissolution rate constant, $= 0.5 \times 10^{-5}$ cm/yr.

Figure III.4.B

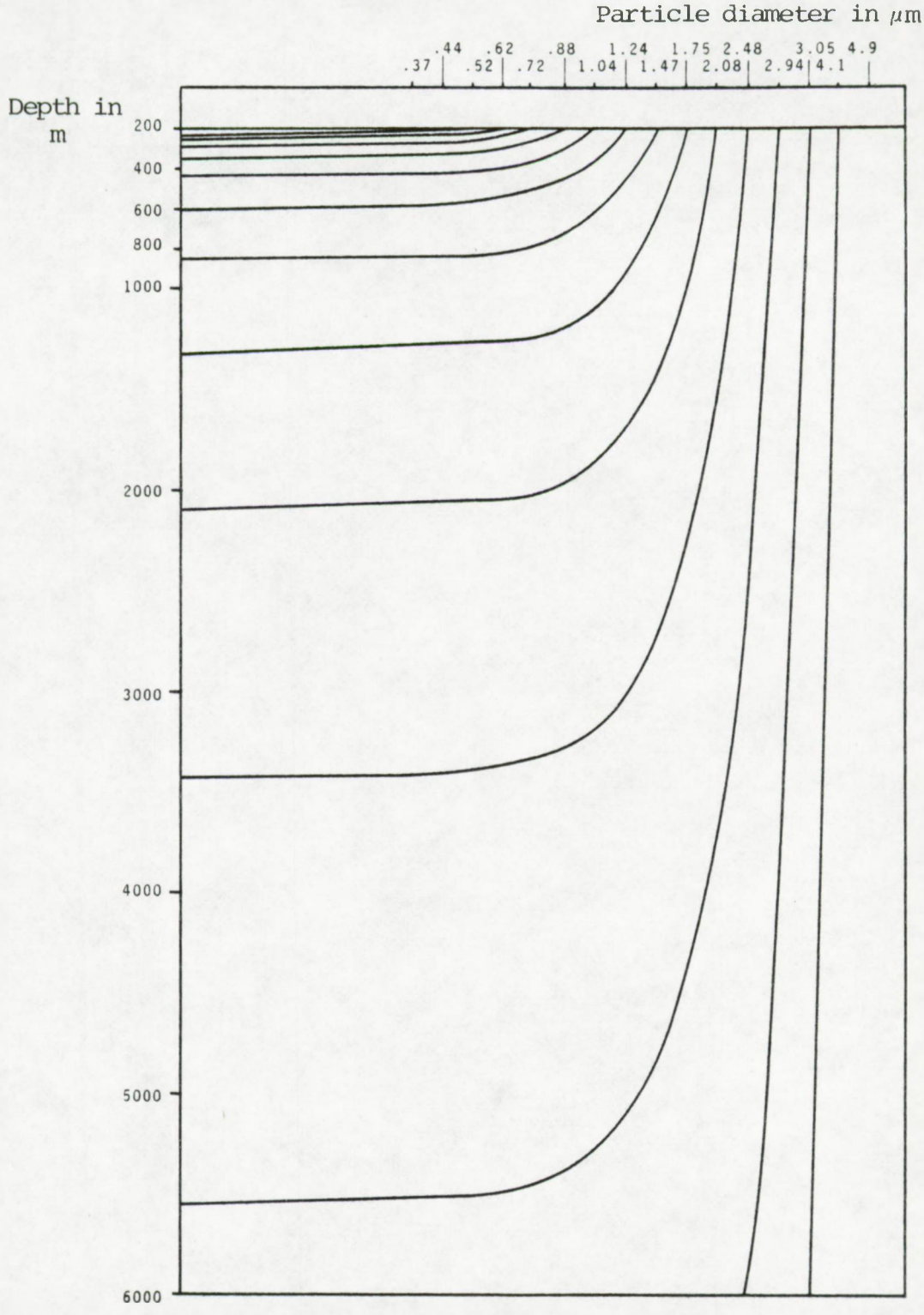

Calculated effect of the dissolution upon the decrease in diameter of suspended barite particles, which are produced in surface water (200 m) and which settle through the watercolumn according to the Stokes settling law; for k, the barite dissolution rate constant, = 1.0×10^{-5} cm/yr

Figure III.4.C

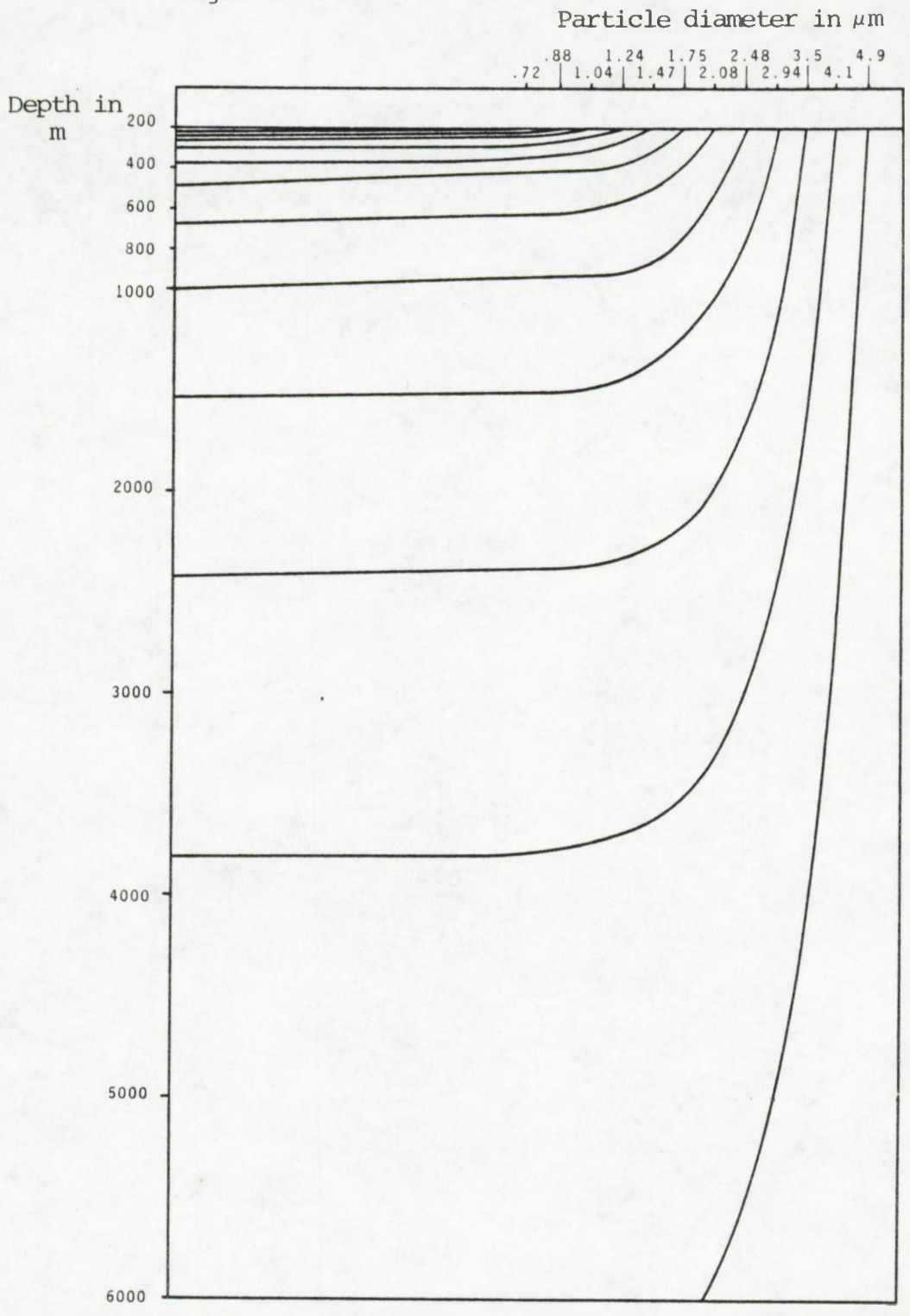

Calculated effect of the dissolution upon the decrease in diameter of suspended barite particles, which are produced in surface water (200 m) and which settle through the watercolumn, according to the Stokes settling law; for k, the barite dissolution rate constant, $= 4.0 \times 10^{-5}$ cm/yr

In the following, it is verified if the magnitude of the dissolution rate constants is compatible with conditions of undersaturation for barite, persisting in the deep-sea.

iii) Validity of the computed barite dissolution rate constants

We can verify which k value is consistent with the state of undersaturation of deep-sea water with respect to $BaSO_4$. The kinetics of $BaSO_4$ crystallization were shown experimentally to be surface controlled (Nancollas and Purdie, 1963; Nancollas, 1968; Nancollas, 1969). This was also observed for the kinetics of $SrSO_4$, $PbSO_4$ crystallization and dissolution (Campbell and Nancollas, 1969). For $BaSO_4$ the latter is extremely difficult to demonstrate, due to its very small solubility product. We will however assume that it has the same characteristics as both sulphate compounds analyzed by Campbell and Nancollas. The experimentally measured reaction rate is written by Nancollas as:

$$\frac{dC}{dt} = k' \cdot S \, (m - m_o)^2 \qquad (3.15)$$

- where the quadratic form of the right term reflects a surface controlled process
- $\frac{dC}{dt}$ is the concentration change with time
- $k'.S$ is the reaction rate constant in cm^3/year.mole

  with k' = constant in cm/year

  S = specific surface available for crystallization or dissolution, in cm^2/mole

- m is the concentration of the dissolved species in mole/cm^3
- m_o is the solubility in mole/cm^3
- the sign of the left term is - for a crystallization process, and + for a dissolution process.

When applied to the oceanic environment, which is assumed to be at steady state and which is an inhomogenous solution as concerns the Ba^{2+} and SO_4^{2-} species, eq. (3.15) can be written:

$$V=k'.S\{[Ba^{2+}]^{1/2}\ [SO_4^{2-}]^{1/2} - K_{sp\ BaSO_4}{}^{1/2}/\Gamma Ba^{1/2}.\Gamma\ SO_4{}^{1/2}\}^2 \quad (3.16)$$

The chosen numerical values of the different terms in eq. (3.16) are discussed below:

1° The solubility of $BaSO_4$ in sea water has been extensively studied by Church (Church, 1970; Church and Wolgemuth, 1972; Church, 1979) (see section 5.1 in part II). For deep water (1°C; 500 atm.) the following experimental values are reported by Church:

- $K_{sp} = 1.5 \times 10^{-10}$
- $\Gamma_{Ba} = \gamma_{Ba} \cdot f_{Ba} = 0.24 \times 0.93$

  with γ = activity coefficient

  f = fraction of free, unassociated ions
- $\Gamma_{SO_4} = \gamma_{SO_4} \cdot f_{SO_4} = 0.19 \times 0.35$

2° From the extensive data of Chan et al. (1977) on the dissolved Ba concentration in the Atlantic (see Table II in part II of this study), we deduce an average Ba_s concentration of 7×10^{-8} mole/litre for deep water. The $SO_4^=$ concentration is 28×10^{-3} mole/litre.

From 1° and 2° it follows that the $(m - m_o)^2$ term in eqs. (3.15) and (3.16) amounts to 3.2×10^{-9} mole^2/litre^2 or 3.2×10^{-15} mole^2/ cm^6

3° S, the specific surface of the suspended barite is deduced from our data on the barite particle size distributions in § 4.1.1., part II. Extreme values of 1.4×10^6 and 2.8×10^6 cm^2/ mole are observed.

4° V, the reaction rate, which is equivalent to the J_{Ba} of barite, can be deduced from our box-model value for the total J_{Ba} in the deep Atlantic. This total J_{Ba} amounts to 1.9 µg Ba.cm^{-2}.yr^{-1}, but we have seen that it might be overestimated by a factor two (section 1.1, part III). With dissolving silica and carbonate debris introducing dissolved Ba at a rate of 0.47 µg Ba cm^{-2}.yr^{-1} (see § 1.2.1 and 1.2.2 in part II), this leaves between 0.33 and 1.43 µg Ba.cm^{-2}.yr^{-1} to be accounted for by the dissolution of suspended barite.

These deduced range of barite dissolution rates, applies to a deep watercolumn of 3000 m. When expressed per Unit volume, these rates become:

8×10^{-12} mole Ba . litre^{-1}.yr^{-1} = V_{min}

34×10^{-12} mole Ba . litre^{-1}.yr^{-1} = V_{max}

By substituting all the values obtained in point 1° to 4° in eq. (3.16) and solving for k', one obtains :

$$k'_{min} = \frac{0.8 \times 10^{-14}}{3.2 \times 10^{-15} \times 2.8 \times 10^{6}} \text{ in } \frac{\text{mole}^2 \cdot \text{cm}^6}{\text{cm}^5 \cdot \text{mole}^2 \cdot \text{yr}}$$

$$\cong 1 \times 10^{-6} \text{ cm/yr} \quad \text{or} \quad 0.01 \text{ µm/yr}$$

$$k'_{max} = \frac{3.4 \times 10^{-14}}{3.2 \times 10^{-15} \times 1.4 \times 10^{6}}$$

$$\cong 7.5 \times 10^{-6} \text{ cm/yr} \quad \text{or} \quad 0.075 \text{ µm/yr}$$

These k' values are not directly comparable with the dissolution rate constants k, deduced from the settling and dissolution rate model above in point ii).
Since in eq. (3.7) $k = (dD/dt).(\pi/2)$, k' must multiplied by $\frac{\pi}{2}$ in order to be comparable with k :

$$k_{min} = k'_{min} \ (\pi/2) = 0.02 \text{ µm/yr}$$
$$k_{max} = k'_{max} \ (\pi/2) = 0.12 \text{ µm/yr}$$

It is clear from the foregoing that the dissolution rates we calculated for the 2574m, 2892m size distribution pair at station 67 (k = 0.05 µm/yr) and for the 1875m, 2479m size distribution pair at station 3 (k = 0.1 µm/yr) are consistent with the state of undersaturation of Atlantic deep water. The k value for the 2989m, 3267m size distribution pair at Station 3 is too high and will be neglected.

B. The in-situ flux of dissolved Ba from the dissolution of suspended barite

The magnitude of barite dissolution is now computed with eq. (3.14), in which an average k value of 0.075 µm/yr is used. This computation was done for every barite size distributions at stations 67, 3 and 5. The data are presented in Table III.1. It appears from this table that the average

input rate of dissolved Ba to the deep Atlantic, as a result of the dissolution of suspended barite, is about 0.4 µg $Ba.cm^{-2}.yr^{-1}$.

Table III.1: Depth-weighted values of J_{Ba}, resulting from the dissolution of suspended barite for 1 profile in the Argentine Basin and 2 profiles in the North American Basin. All data calculated by considering a barite dissolution rate constant k of 0.075 µm/yr.

Depth in m	Sea water volume litre/cm^2	J_{Ba} in 10^{-3} µg.$l^{-1}.yr^{-1}$
GEOSECS station 67 (Argentine Basin)		
151 --	25	0.8
353 --	25	1.7
658 --	35	1.1
1053 --	42	1.4
1499 --	57	1.1
2193 --	54	0.8
2574 --	40	0.7
2983 --	51	0.6
3601 --	47	0.6
4424 --	44	0.5
5304	100	0.6
5900 (sea floor)	Integrated J_{Ba} = 0.42 µg.$cm^{-2}.yr^{-1}$	
GEOSECS station 3 (North American Basin		
105 --	46	0.7
813 --	49	1.0
1083 --	53	0.4
1875 --	70	1.4
2479 --	40	0.4
2696 --	26	0.4
2989 --	29	1.4
3267	115	0.8
4280 (sea floor)	Integrated J_{Ba} = 0.36 µg.$cm^{-2}.yr^{-1}$	

Table III.1: continued

Depth in m	Sea water volume litre/cm^2	J_{Ba} in 10^{-3} µg.l^{-1}.yr^{-1}
GEOSECS station 5 (North American Basin)		
363 --	56	1.0
760 --	105	2.1
2464	178	0.9
3390 (sea floor)		Integrated J_{Ba} = 0.44 µg.cm^{-2}.yr^{-1}

Discussion

The contribution of each of the dissolving suspended biogenic carriers to the overall input of dissolved Ba to the deep watercolumn is reproduced in Tabel III.2. The resulting overall J_{Ba} is compared with the box-model value for the Atlantic Ocean.

Table III.2: Relative contribution of dissolving suspended barite, SiO_2 and $CaCO_3$ debris to the overall J_{Ba} in the deep Atlantic . All values expressed in µg Ba.cm^{-2}.yr^{-1}

Barite	0.4
SiO_2 skeletons	0.25
$CaCO_3$ skeletons	0.22
total :	0.87

Box-model overall J_{Ba} : 0.8 to 1.9 (in Atlantic ocean)

The value we deduced from particle dissolution estimations is in agreement with the lower box-model values for the deep-Atlantic. Our value is further very similar to the one obtained by Chan et al.(1976), by applying an advection-diffusion model to the dissolved Ba and Ra^{226} profiles in the deep Pacific at GEOSECS station 204: 0.7 µg $Ba.cm^{-2}.yr^{-1}$ (when considering a watercolumn of 4000 m). This leads one to suggest that box-models (Broecker and Wolgemuth,1970; Li et al.,1973 (see Figure III.1) and this work (Figure III.2)) systematically overestimate the J_{Ba} term. However, the general similitude of the three values considered here, validates the order of magnitude of the total J_{Ba} term.

The most important message resulting from this analysis is that the dissolution of suspended barite, which contributes for about 50% of the overall input of dissolved Ba in the deep sea by biogenic particle dissolution, is a major process controlling the excess of dissolved Ba in the deep-sea.

In the following chapter the role of suspended barite as a source of sedimentary barite is evaluated.

CHAPTER 2

THE ROLE OF SUSPENDED BARITE AS A SOURCE OF SEDIMENTARY BARITE

2.1. THE VARIOUS MINERALOGICAL PHASES OF SEDIMENTARY BARIUM: A REVIEW

Particulate Ba in the sediments is present mainly as authigenic barite (Church, 1970; Boström, 1973). The authigenic zeolites phillipsite and harmotome, common in slowly accumulating deep-sea sediments are also Ba-containing minerals (Church,1970; Arrhenius and Bonatti, 1965; Cronan, 1974). Besides these authigenic minerals, terrigenic, clay-type aluminosilicates represent an additional phase of sedimentary Ba. This Ba is introduced into the ocean, while incorporated in the lattice structures of clay particles. It is therefore considered as "inert Ba", which can not be redistributed into another mineralogical phase.

The authigenic character of sedimentary barite is emphasized by the following facts: 1°) The Th^{230}/Th^{232} isotopic composition of sedimentary barite (see introduction, page 8) shows them to be formed in the deep sea or at the sediment-water interface (Somayajulu and Goldberg, 1966; Church, 1970; Church and Bernat, 1972). Sedimentary barite is mainly

present as small (< 5 μm) crystals (Church, 1970). A rarer fraction consists of large (30-100 μm) crystals and is most often found in association with manganiferous deposits (Church, 1970). This concords with the recent observation of barite crystals occurring inside manganese modules in association with tests of planktonic organisms (Dugolinsky et al., 1977; Lalou, 1979). Plate 12, which was kindly procured by C. Lalou, shows a fringe of barite crystals deposited along the proloculus of a forminifera shell, inside a nodule. It is thought (C. Lalou) that these barite crystals have grown epigenetically on the proloculus wall, and have come eventually to replace the original wall.

Today, sedimentary barite has been reported to occur in the sediments of the Pacific and the Atlantic (Church , 1970; Arrhenius, 1963 : East Pacific sediments; Goldberg and Griffin, 1964 and Somayajulu and Goldberg, 1966: Mid-Atlantic-Ridge sediments).

PLATE 12

BARITE CRYSTALS INSIDE A MANGANESE NODULE

Location: Pacific Ocean 09°65'N-105°13'W

Depth: between 3214 and 3265 m

A. SEM picture of a Foraminifera proluculus wall, inside the manganese nodule, which has been substituted by barite crystals.

B. EMP picture of Ba

C. Magnified picture of A., showing individual barite crystals, some of which are pierced.

D. Elemental spectrum of the barite crystals: S K α at 2300 eV; Ba L α,β,γ at 4460 eV

Reproduced with permission of C.Lalou (Lalou et al., 1979)

PLATE 12

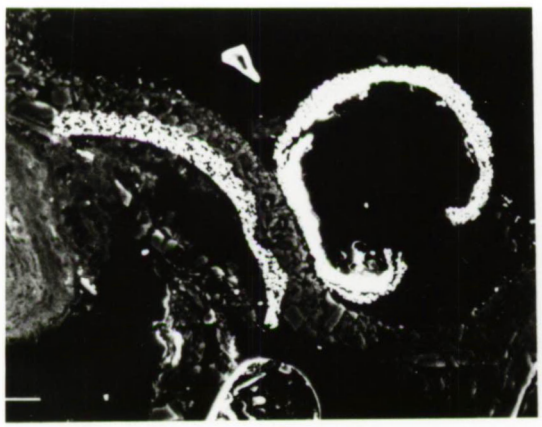

A

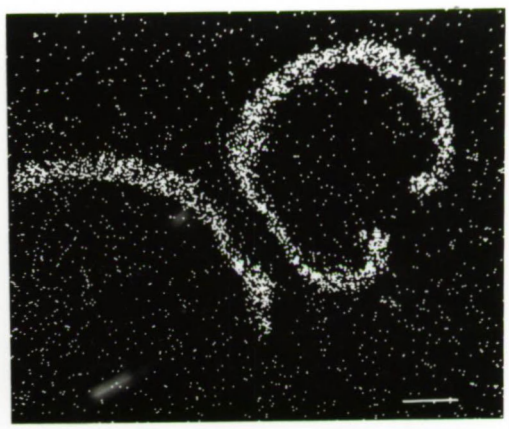

B

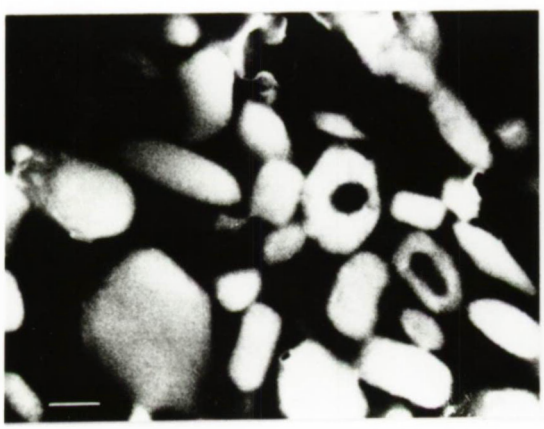

C

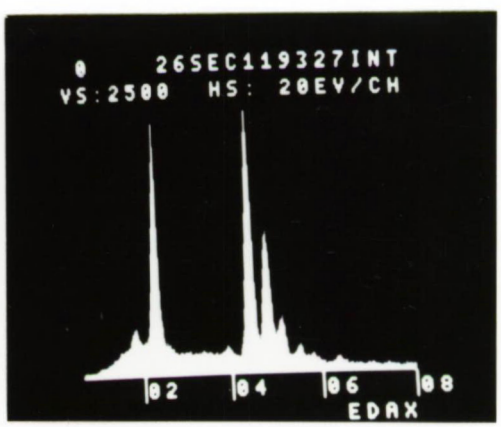

D

2.2. THE POSSIBLE SOURCES OF BARIUM IN THE AUTHIGENIC BARIUM-MINERALS OF THE DEEP-SEA SEDIMENTS : A REVIEW

Authigenic Ba- minerals in the deep-sea sediments derive their Ba from two possible sources:
1) volcanic processes, by which "juvenile " Ba is introduced to the sediments ; 2) biological processes in the surface waters, by which Ba of continental origin is consumed and which feed the sediments with biogenic particles enriched in Ba. As discussed in part II, suspended barite crystals are one of the products of this biological activity in surface water.

2.2.1. Volcanism as a source of sedimentary Ba

On a World Ocean scale, volcanism appears as a minor source of sedimentary Ba, since its influence is restricted to active ridge areas. Boström (1973) estimates that only about 1 % of the deep-sea sedimentary Ba in the World Ocean has its origin in volcanic processes. Of these, mantle degassing is believed to be the main process and not leaching of basalt (Boström, 1973). Even for the specific sediments of the East Pacific Rise (EPR), which cover the active ridge area, it is shown by Heath and Dymond (1977) that the biological source accounts for between 9 and 85 % of the total sedimentary Ba.

In specific sediments of active ridges the total Ba content, on a carbonate - free basis, can amount to 2 % (Heath and Dymond, 1977: metalliferous sediments of the EPR, Sayles and Bischoff, 1973: ferro-manganoan deposits in the Equatorial East Pacific) and even 6 % (on a total basis) for the Mn-rich deposits of the Afar Rift, which are very similar to the hot brine deposits of the Red sea (Bonatti et al., 1972). In general, this Ba is thought to be incorporated in authigenic barite (Boström and Peterson, 1966; Bischoff, 1969; Bonatti; et al., 1972; Bertine and Keene, 1975 ; Valette, 1978). Besides being incorporated in barite, Arrhenius and Bonatti (1965) suggest that volcanic Ba becomes also incoporated in harmotome, which is overgrown later by phillipsite.

2.2.2. Biological activity in surface water as a source of sedimentary Ba

The relationship between biological activity and accumulation of Ba in the sediments has been stressed by Goldberg and Arrhenius (1958), who observed an increase in the accumulation rate of Ba below the productive waters of the Equatorial Divergence. This Ba was assumed to occur as authigenic phillipsite and barite crystals inside excretion products of benthonic organisms. Church (1970) explains the observed accumulation rates of Ba as barite in the sediments of the East Pacific including the EPR region, by the flux of biogenic material to the sediments.

Several mechanisms of Ba incorporation by organisms are porposed: - Direct precipitation of $BaSO_4$ crystals by planktonic organisms (Chow and Goldberg 1960; Turekian, 1968)

- precipitation of $BaSO_4$ crystals in decaying organic matter (Chow and Goldberg, 1960)
- Concentration of Ba in organic matter and carbonate and Silica skeletons (Church, 1970; Ku et al., 1970; Edmond, 1970; Bacon and Edmond, 1972; Li et al., 1973; Chan et al., 1977).

This biogenic material sinks through the watercolumn and dissolves. However,part of it becomes incorporated into the sediments. Here, decay and dissolution of the carrier liberate Ba, which is redistributed into authigenic barite and possibly also into other authigenic minerals such as harmotome and phillipsite.

Besides biological scavenging processes in surface waters, biological activity at the sediment-water interface can control the production of sedimentary barite. The benthic protozoan Xenophyophora , which is ubiquitous in the deep-sea (Tendal, 1972) is known to secrete intracellular barite crystals (Arrhenius and Bonatti, 1963; Lowenstam, 1974; Tendal, 1972).

Boström et al. (1974) tried to reconstitute the composition of pelagic and active ridge sediments by considering variable contributions of typical biogenic, terrigenic and volcanic materials, and concluded that, as concerns the pelagic

sediments, it is biological material which controls the Ba supply to these sediments.

In Atlantic pelagic sediments the Ba concentrations were observed to vary between <1000 and >4000 ppm (on a $CaCO_3$-free basis),(Turekian and Tausch,1964). Goldberg and Arrhenius (1958) observed the Ba content of Pacific pelagic sediments to vary between 600 and 13000 ppm (on a $CaCO_3$-free basis). For equatorial Pacific sediments Boström et al. (1974) observe an average Ba content of 2900 ppm (on a SiO_2- and $CaCO_3$-free basis).

2.3. THE ACCUMULATION RATE OF BARIUM IN THE SEDIMENTS

2.3.1. The accumulation rate of total Ba

The accumulation rates of total Ba, given in literature are reproduced in Table III.3 .

Table III.3: Literature data concerning the accumulation rate of total Ba. All rates in $\mu g.cm^{-2}.yr^{-1}$

Rate	Location	Reference
0.3	Pacific, north of equator	Hanor (1972)
0.5	East Pacific Rise	Church (1970)
0.5	Mid Atlantic Ridge (south Atlantic)	Turekian (1968)
1.0	Antarctic	Turekian and Johnson (1964)
3.5	Pacific, at the equator	Hanor (1972)

2.3.2. The accumulation of Ba in terrigenic, aluminosilicate material

In order to compute the accumulation rate of Ba in terrigenic matter, we will analyze the available data on the accumulation in the sediments of particulate Al, which can be considered as a tracer of continental detritic matter (see discussion in § 1.1.1 of part II).

The accumulation rate of Al, over large sections of the open Pacific Ocean, is observed to vary between 2 and 50 $\mu g.cm^{-2}.yr^{-1}$ (Boström et al.,1973). For the Atlantic pelagic sediments extending between 30°N and 40°S, characterized by a $CaCO_3$-free sedimentation rate of 4 mm/10^3 yrs, Krishnaswami et al.(1976) evaluate the accumulation rate of Al at 16 $\mu g.cm^{-2}.yr^{-1}$. If we consider this latter value as an average rate for the World Ocean, we obtain from:

$(Ba/Al)^{\star}_{shale}$ x Al accumul. rate, (☆ see discussion p.62,65)

an average accumulation rate of Ba associated with aluminosilicates, of 0.12 $\mu g.cm^{-2}.yr^{-1}$. This amount is provided by two sources: the discharge from rivers and the input from the atmosphere. Since atmospheric input alone is shown to be sufficient to account for the suspended aluminosilicate load in sea water (Buat-Menard and Chesselet, 1979) the contribution of river discharge to the deep sea accumulation of terrigenic matter is probably controlled by erosion of the continental slope and transport of terrigenic matter by deep-sea currents (Buat-Menard, 1979).

2.3.3. The accumulation rate of barium in sedimentary barite

It is possible to estimate the sedimentary barite accumulation rate. Somayajulu and Goldberg (1964) and Church and Bernat (1972) observed that Io/Th geochronologies predicted similar sedimentation rates for the sedimentary barite as for the bulk sediment. Therefore, the knowledge of the sedimentation rate of the bulk sediment and of the barite concentration in the sediments is sufficient to calculate the barite accumulation rate (Somayajulu, pers. comm., 1979).

For those sediments characterized by a Ba content between 1000 and 4000 ppm ($CaCO_3$-free) and which cover the Mid Atlantic Ridge region and the East Atlantic, an average Ba value of 1100 ppm is observed north of 10°N and of 2000 ppm south of 10°N (Turekian and Tausch, 1964). In these average values are not considered the low concentrations in the East-Atlantic (Sargasso Sea) and the high values from the Walvis ridge. For the Pacific pelagic sediments an average of 3900 ppm is observed (Goldberg and Arrhenius, 1958). For Equatorial Pacific sediments an average Ba content of 2900 ppm (silica- and carbonate- free) was observed by Boström et al. (1974). The largest part of this sedimentary Ba is most likely comprised of barite, as observed by Church (1970) for carbonate sediments of the East Pacific Rise.
A minor fraction of the sedimentary Ba is carried by the aluminosilicate materials: max. 600 ppm, on a $CaCO_3$ free basis, if the aluminosilicate composition is taken as similar to the one of shales (Turekian, 1968; Turekian and Wedepohl, 1961). We will consider here an average value of 1800 ppm for sedimentary Ba that is supported by barite.

From the geochronological studies (66 cores analyzed) of the Atlantic-, Pacific- and Indian-Ocean sediments, by the Io/Th method, of Goldberg and Koide (1962) and Goldberg and Griffin (1964) (these data were revised by Ku et al., 1968), the following extreme bulk sedimentation rates are obtained:

minimum: 0.9 mm/1000 yrs (all rates on a carbonate free basis)

maximum: 23. mm/1000 yrs ,

with an average value of 4.5 mm/1000 yrs. By taking a sediment density of 2 g/cm^3 and a sediment weight porosity of 50 % (Somayajulu and Goldberg, 1964), the accumulation rate of Ba as barite is given by:

(sediment. rate in cm) x 2 x 0.5 x 1800 x 10^{-6}, in

$$\frac{cm \times g \times g}{yr \; c \; cm^3 \times g}$$

The following rates are obtained:

minimum: 0.16 µg $Ba.cm^{-2}.yr^{-1}$

maximum: 4 µg $Ba.cm^{-2}.yr^{-1}$

average: 0.8 µg $Ba.cm^{-2}.yr^{-1}$

This average is 10 times larger than the accumulation rate of Ba in continental, detritic matter (see above, § 2.3.2.). These estimated accumulation rates of Ba as barite closely encompass the observed accumulation rates of total Ba, given in literature (see Table III.3).

2.4. THE SUPPLY OF BARIUM TO THE SEDIMENTS BY THE SETTLING OF BIOGENIC PARTICLES, INCLUDING BARITE

As concerns pelagic sediments volcanic processes are outruled as a source of sedimentary Ba (see discussion in § 2.2.1., above). The alternative source of non-terrigenic Ba in the sediments is then biological activity in surface water.

2.4.1. The contribution of fast settling biological material

Evidence exists that the particulate biogenic matter in the sediments is conveyed to it, by fast settling fecal material (Schrader, 1971; Mc Cave, 1975; Krishnaswami et al., 1976; Bishop et al., 1977, 1979; Honjo, 1976; 1978). Bishop et al., (1977, 1979) have studied suspended matter obtained from large volume (up to 20 m^3) sea water filtrations in the upper 400 m in the Equatorial Atlantic and the Cape Basin. They observed fast settling fecal material* (estimated velocity: 300 m/day) to account for 99 % of the vertical flux of particulate matter. This very short time of transit through the watercolumn and the fact that they are protected by an organic coating, allow such particles to attain the sediments in an intact state (Schrader, 1971). This explains the presence of undissolved skeletal debris in sediments

---

* note: Such fast settling material represents a fraction of the suspended matter, which can not be sampled with the sampling equipment used here (i.e. 30 litre Niskin Bottles) (Mc Cave, 1975).

extending below deep watercolumns, which could not be crossed by individually settling tests, since these would have dissolved before reaching the sea floor. Besides this flux of fecal material, the vertical flux of the large Foraminifera and Pteroped shells and of the Radiolaria skeletons are other potential sources of carbonate and silica in the sediments. However, in the Equatorial Atlantic Bishop et al. (1977) show such fluxes to represent only a fraction (< 4 %) of the carbonate and silica fluxes resulting from fecal material settling. In the Cape Basin, on the contrary, Foraminifera and Pteropod fluxes can account for a significant fraction (up to 43 %) of the total $CaCO_3$ flux to the sediments (Bishop et al., 1979). In the following considerations of vertical fluxes of biogenic material, the contribution of Foraminifera is taken into account. Bishop et al. (1977; 1979) observed the following vertical fluxes of POM, SiO_2 and $CaCO_3$, resulting from fast settling material:

POM: 2.2 $mg.cm^{-2}.yr^{-1}$ (Equatorial Atlantic; Bishop et al. 1977)

0.05 to 1.1 $mg.cm^{-2}.yr^{-1}$ (Cape Basin; Bishop et al., 1979)

SiO_2: 0.85 $mg.cm^{-2}.yr^{-1}$ (Equatorial Atlantic)

0.02 to 0.65 $mg.cm^{-2}.yr^{-1}$ (Cape Basin)

$CaCO_3$: 1.31 $mg.cm^{-2}.yr^{-1}$ (Equatorial Atlantic)

0.14 to 2.36 $mg.cm^{-2}.yr^{-1}$ (Cape Basin)

The lowest values are from the open ocean in the Cape Basin; characterized by a low productivity (< 3.6 mg $C.cm^{-2}.yr^{-1}$; Bishop et al., 1979); the highest values are from regions

with a high productivity ($\geq$ 18 mg $C.cm^{-2}.\ yr^{-1}$; Bishop et al., 1977, 1979).

In Table III.4 these fluxes (A) of biogenic matter associated with fecal material are compared with: (B) estimations of world average deep-sea supply rates; (C) a deep sea fecal pellet flux; (D) observed accumulation rates in the sediments; (E) calculated world average accumulation rates in the sediments. From Table III.4 it is seen that the combined flux of fecal material and Foraminifera shells is able to account for the estimated supply and the estimated as well as the observed accumulation rates of POM, SiO_2 and $CaCO_3$.

We will now deduce the Ba flux that is associated with these fluxes of POM, SiO_2 and $CaCO_3$. Such as in section 4.3 of part II, we take 60, 120 and 200 ppm as the Ba content, respectively of the POM, SiO_2 and $CaCO_3$ phases. It follows that the flux of fecal material and Foraminifera to the sediments produces a Ba flux of <u>0.05 to 0.9 µg $Ba.cm^{-2}.yr^{-1}$</u>.

To this flux we must add the one that results from the settling of individual suspended barite crystals.

2.4.2. <u>The contribution of settling barite crystals</u>

We can calculate the vertical flux of barite in deep water and assume this amount to be a maximum value for <u>barite</u> settling on the sea floor. The vertical flux is obtained by working out:

Table III.4: Comparison of fecal-material associated fluxes of SiO_2, $CaCO_3$, POM with estimations of world average supply rates and accumulation rates, and with observed accumulation reates. All values in $mg.cm^{-2}.yr^{-1}$.

	Supply rates			Accumulation rates	
	A	B	C	D	E
	Surface sea fecal pellet flux (~ 300m) (1)	Calcul. world average supply rates to the deep-sea	Deep-sea fecal pellet flux (> 5000 m) (4)	Observed accumul. rates in shallow areas (<4000 m) extending above the carbonate compensation depth	Calcul. world average accum. rate
	SiO_2				
▲ 0.02≤	■ ≤ 0.85	0.72< <1.32 (2)			0.12 (2)
	$CaCO_3$				
0.14≤	≤2.36	1.3 (2)	0.14	2.0 (5); 1.5 (6) 1.2 (8)	0.34 (2)
	POM				
0.05≤	≤2.2	0.4 (3)	0.07		0.08 (7)

(1) From Bishop et al. (1977, 1979), Equatorial Atlantic and Cape Basin
(2) From Berger (1970) : World Ocean Average
(3) From Menzel (1974) : World Ocean
(4) From Spencer et al. (1978): low productivity Sargasso Sea
(5) From Church (1970) : East Pacific Rise
(6) From Turekian (1968) : Mid Atlantic Ridge
(7) From Romankevich (1968; cited in Church 1970)
(8) From Kolla et al. (1975) : Indian ocean.

▲ low productivity region
■ high productivity region

$$\phi = \Sigma\, m_D \cdot v_D \qquad (3.17)$$

with ϕ = flux of Ba as barite

m_D = mass of barite particles of diameter D (see eq. 1.7 in part I)

v_D = Stokes settling velocity of barites of diameter D (see eq. 3.9 in part III)

Equation (3.17) was worked out for the barite particle distributions of deep water samples at stations 67,3 and 5 (see Table III.5).

Table III.5: Vertical flux of particulate Ba, due to the settling of barite near the sea floor

Station and depth	Flux in µg Ba.cm^{-2}.yr^{-1}
Station 67 5305 m; (sea floor at 5900 m)	0.4
Station 3 3267 m; (sea floor at 4280 m)	0.4
Station 5 2464 m; (sea floor at 3390 m)	0.1

Adding these fluxes in Table III.5 to the Ba that is associated with the flux of fecal material (0.05 to 0.9 µg Ba.cm^{-2}.yr^{-1}) we deduce a total flux of Ba to the sediments of between 0.15 and 1.3 µg.Ba. cm^{-2}.yr^{-1}.

Discussion:

In Table III.6 the flux of biogenic Ba to the sediments is compared with the calculated accumulation rate of Ba as barite and with observed accumulation rates of total Ba. It follows that the combined flux of Ba in fecal material and in Foraminifera shells, and of Ba as suspended barite is sufficient to explain the observed accumulation rates of Ba in the Pacific, Atlantic and Antarctic Ocean. The very high accumulation rate of total Ba(3.5 $\mu g.cm^{-2}.yr^{-1}$) observed by Hanor (1972) in the Equatorial Pacific is only partially accounted for (30 %), suggesting a higher fall out in this region of biogenic matter from surface water.

It appears further from Table III.6 that the supply of fast settling biogenic material and of individual barite crystals, which contribute for up to 45%, can account in general for the calculated sedimentation rate of Ba as barite. This suggests that the Ba that is released from the decomposing biogenic carriers is precipitated as sedimentary barite. Such a process, if occurring at the sediment-water interface is not evident at first sight. Indeed, no evidence exists that barite saturation is obtained at the sediment-water interface. The concentration of dissolved Ba in bottom water, which attains a maximum of 22 µg/Kg SW (Pacific deep water) is a factor of two smaller than the solubility value for Ba in deep water (49 µg/Kg SW), obtained only in pore waters (Church and Wolgemuth, 1972). Further, as a result of the bioturbation of the first mm of pelagic sediments, which accumulate very slowly (1 tot 4 mm/1000 yrs),

Table III.6: Comparison between the supply of particulate Ba including barite, to the sediments and the accumulation rates in the sediments. All values in $\mu g.Ba.cm^{-2}.yr^{-1}$

SUPPLY			ACCUMULATION		
Ba associated with fecal material and Foraminifera at 400 m depth (1)	Ba associated with fecal pellets at 5581 m (2)	Ba in suspended barite (3)	Observed accumulation rates of total Ba (4)	Calculated accumulation rates of Ba as barite (5)	Calculated accumulation rates of Ba in detritic matter
from 0.05 to 0.9	0.05	from 0.1 to 0.4	0.3 0.5 1.0 3.5	from 0.16 to 4 average :0.8	0.08
Total : 0.15 to 1.3					

(1) From Table III.4A; SiO_2, $CaCO_3$ and POM are considered to contain respectively 120, 200 and 60 ppm of Ba.
(2) From Spencer et al. (1978) : Sargasso Sea.
(3) This study; Table III.5.
(4) See Table III.2, this study
(5) Calculated from existing data on sedimentation rates of bulk sediment and sedimentary barite content; see p. 246 of this study.

it is likely that the dissolved Ba in these first mm of the sediments becomes diluted by mixing with overlying bottom water. This should provent saturation conditions to be attained here. As a result inorganic precipitation of barite after release of the Ba from the carriers at the sediment-water interface is an unlikely process. Two possibilities remain:

1) The precipitation of barite occurs only deeper in the sediment, in saturated pore waters, as a result of a very slow release of the Ba from the carriers. The settled barite crystals, produced in surface waters, can operate as nuclei and accelerate the precipitation process.

2) The precipitation of barite occurs at the sediment-water interface, but inside microenvironments in which saturation conditions are obtained . The settled fecal pellet itself, as a closed system, may act as such. Goldberg and Arrhenius (1958) suggested that in sediments, fecal pellets observed to contain high amounts of Ba, could be the formation site of sedimentary barite. The benthic Xenophyophora, which secrete barite granules which are an ubiquitous component of the benthic fauna in the deep sea (Tendal, 1972), are a further example of such microenvironments. These organisms can be assumed to feed upon surface water derived biogenic matter that carries Ba. This Ba is than precipitated as cytoplasmatic barite granules.

Conclusion of part III

This in-situ flux of dissolved Ba in the deep sea (0.87 µg Ba. $cm^{-2}.yr^{-1}$), of which 46 % is due to the dissolution of suspended barite crystals, can again become available for biological consumption in the surface waters as a result of the upward directed advection of deep-sea water. When compared with the river input (min. 0.6 µg.Ba.$cm^{-2}.yr^{-1}$) it appears that 60 % of the total amount (A) of dissolved Ba that becomes available for consumption (1.4 µg Ba.$cm^{-2}.yr^{-1}$) is provided by the recycling of particulate Ba. In section 1.2 we have estimated the rate of barite production that can result from the decomposition of the POM, which is not lost in the deep sea, at 0.8 µg Ba. $cm^{-2}.yr^{-1}$. Adding the annual incorporation rate of Ba into skeletal material (= SiO_2 and $CaCO_3$ debris) —— 0.55 µg Ba.$cm^{-2}.yr^{-1}$ —— (see § 1.2.1. and 1.2.2.), a figure (B) of 1.35 µg Ba.$cm^{-2}.yr^{-1}$ is obtained for the annual "consumption" of Ba. The agreement between (A) and (B) ascertains the importance of biological activity and of the recycling of Ba in the watercolumn. Figure III.4 summarizes the gross budget of Ba in the ocean, as deduced from our data.

In pelagic sediments authigenic barite is the sink for the Ba that is scavengend in surface waters by biological activity. This barite represents the main Ba-mineral in the sediments and can consist for up to 45% of settled barite crystals, produced in surface water. The transfer mode of the biogenic Ba to sedimentary barite, at the sediment-water interface, is not yet clear.

FIGURE III.4

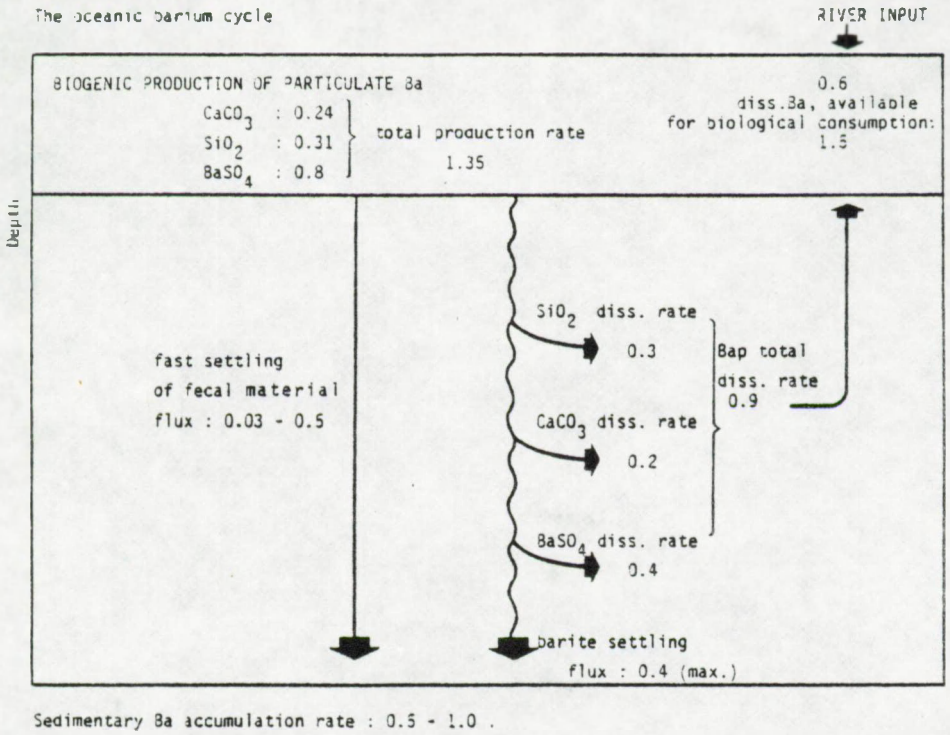

Numerical values for the components of the oceanic barium cycle. All values in μg $Ba.cm^{-2}.yr^{-1}$.

GENERAL CONCLUSIONS

Interpretation of particulate Ba and Al profiles, measured by neutron activation, shows that more than 90% of the total particulate Ba amount is supported by a non-terrigenic fraction. Further, the general shape of the particulate Ba profiles, which show maxima in surface water and minima in deep water, suggests a biological scavenging of Ba in surface waters and a dissolution of these particulates at depth. This is confirmed by other observations.

Electron microscope analyses show that particulate Ba in suspended matter is mainly present as small discrete particles of about one micron in diameter and containing S as other major constituent. They are observed in all inspected samples,which cover the North-, South-, Equatorial-Atlantic, the Antarctic and the South-Pacific. Electron microdiffraction analyses of these particles reveal a crystalline structure in agreement with barite. Systematic SEM-EMP analyses show that these suspended barite particles actually exist as solid solutions with Sr and K as minor constituents. When Sr is detected, these amounts do not exceed, in general, the 2% level (by weight). The K content is generally slightly larger than 1000 ppm.

In surface waters (first 500 m) of a particular station in the Equatorial Atlantic, a large fraction (33%) of the $BaSO_4$ particles are solid solutions with a $SrSO_4$ molar fraction

> 10%. In fact, the composition of the solid solutions can extend from $(Ba,Sr)SO_4$ and $(Sr,Ba)SO_4$ to nearly pure $BaSO_4$ and $SrSO_4$ end members. $SrSO_4$ particles occur essentially as Acantharia debris, which were not observed to contain Ba above the detection limit. Their occurrence is restricted to surface water. However, $(Sr,Ba)SO_4$ solid solutions, occurring as discrete particles, morphologically similar to barite particles, are observed also below 1000 m.

Some controversy exists in literature, on the possible authigenic origin of Sr-enriched barites. Although barites with a $SrSO_4$ molar fraction of 30% and more, such as we have observed in suspended matter from the surface waters, were proposed to exist in equilibrium with sea water (a fact which can be neither confirmed nor rejected at the moment, due to a lack of data on the solid activity coefficients of such solid solutions), more recent experimental data of Church point towards increased solubility of barites which contain minor amounts of substituting elements. In any case the possibility of an authigenic formation in sea water is difficult to reconcile with the occurrence, in a given parcel of sea water with a constant chemical composition, of solid solutions with varying Sr content. It is thought that this reflects rather the influence of a biological mediator.

The observed relationship between organic productivity and particulate Ba and barite content in the upper part of

the watercolumn emphasizes the control of biological activity upon the production of particulate Ba and barite. The detailed process leading to barite production is not known.

Several indications validate the idea that biological mediators represent suitable, restricted environments in which barite production is possible: 1) The ubiquitous presence of acantharid Radiolaria, secreting a $SrSO_4$ skeleton, and of collosphaerid Radiolaria, secreting intra-cellular crystals, assumed to consist of $SrSO_4$ and/or $BaSO_4$. Secretion of barite granules is known to occur in the benthic Xenophyphoria (Rhizopoda classis). The contribution of Acantharia to barite production might be indirect: during dissolution of Acantharia debris, Ba might substitute gradually for Sr, in a tendency to establish a compound stable in sea water. Such a process,as well, might result in the presence of a wide celestite-barite substitution series in surface waters, including barites with minor amounts of Sr.
2) Aggregates of barite prisms are observed inside pellet-like particles of small size (a few micron), which are assumed to consist of decaying organic matter, such as fecal pellets. In these pellets, the decomposition of proteine-rich matter can liberate sufficient sulphate to induce $BaSO_4$ precipitation. The sinking of such pellets and their bursting at depth can explain the coexistence in the same waters of non-corroded, euhedral and highly corroded barite particles. Indeed, decomposition of the protecting

organic membrane of the pellet can result in a local injection of "fresh", non-corroded barites to the watercolumn. This mechanism is similar to the one considered by Honjo to explain the presence of non-corroded coccoliths in the deep sea.

It is shown that for intermediate and deep waters barite particles account for more than 90% of the total particulate Ba in suspension. In surface waters (= first 150 to 300 m) up to 50% of the total particulate Ba amount can be carried by silica and carbonate skeletons and particulate organic matter, with the latter contributing the largest part (53%). Between surface and intermediate waters this pattern changes in favor of barite. It appears that POM decomposition must be an important process leading to barite formation. This is consistent with the fact that maxima of particulate Ba tend to occur in the vicinity of thermoclines and O_2 minima, i.e. regions coinciding with organic matter accumulation- and decomposition-sites, as shown by a comparative study of particulate Ba, Tpot and dissolved O_2 and PO_4 profiles in the Atlantic. In bottom water the contribution of resuspended aluminosilicates can account for up to 20% of the total particulate Ba amount. In areas characterized by the presence of a nepheloid layer, the increase of total particulate Ba in approach of the sea floor can be such, that the <u>barite</u> content itself exceeds the one in overlying waters. This points towards the introduction of sedimentary barite in the watercolumn.

Although the suspended aluminosilicate Ba-carriers appear to consist mainly of clay-type particles, Ba-minerals probably belonging to the zeolite and Ba-feldspar family are observed in suspension. Occasionally, iron-hydroxides (goethite) as well, are observed to contain minor amounts of Ba. Further, non-identified elongated Si,Al,Zn and Ba containing particles can occur.

Suspended barite particles are not solely submitted to the gravitational force. Their distribtuion in intermediate and deep water clearly shows influences of horizontal advective transport. This seems also to be the case for calcium carbonate and strontium sulphate particles, mainly accounted for by coccoliths and barite-like celestite particles with minor amounts of Ba.

Most of the suspended barite particles are corroded and only about 15% can be clearly recognized as euhedral particles. Further, a small but significant increase of the fraction of corroded particles is observed in the NADW core at a station in the Argentine Basin; in contrast to the situation in younger watermasses above and below the NADW core. This emphasizes the importance of advection and dissolution processes in determining the distribution of suspended barite at depth. This observed dissolution of barite, which is consistent with the fact that sea water is undersaturated with respect to $BaSO_4$, was evaluated.

Half of the overall input of dissolved Ba to the deep

sea, by dissolution of biogenic particles (= J_{Ba} flux), and estimated in this study at 0.9 $\mu g.cm^{-2}.yr^{-1}$, is accounted for by dissolving suspended barite. The other major contributors are calcareous and siliceous debris, which are each of about equal importance as a source of dissolved Ba. This overall J_{Ba} is in agreement with the lower estimate of our box-model deduced flux (0.8 to 1.9 $\mu g.cm^{-2}.yr^{-1}$) for the Atlantic Ocean. For the deep Pacific-Indian Ocean, this flux is predicted to be 30% larger, suggesting a greater production of particulate Ba in the surface waters of these oceans. The similarity of our data on total particulate Ba between the Atlantic and the Pacific Ocean, do not suggest differences to exist in the barite loads between these two oceans. A greater production of the calcareous and siliceous matter and/or a more efficient extraction of Ba by the plankton in the Pacific-Indian Ocean is then required. This is not verified yet by experimental data.

This deep-sea Ba-flux, which is finally re-introduced in the surface box by general upwelling, is as large or larger than the river input of dissolved Ba (min. 0.6 $\mu g.cm^{-2}.yr^{-1}$), what emphasizes the important role of this deep-sea recycled Ba in sustaining the observed consumption rates of Ba in the surface waters and of the control of biological activity upon the Ba-cycle in the ocean.

Together with the Ba associated with POM, SiO_2 and $CaCO_3$ within fast settling fecal material and Foraminifera shells, the settling of suspended barite particles is able to

account for calculated sedimentation rates of Ba as barite, and for observed global accumulation rates of Ba in the sediments. Of this Ba-flux to the sediments, suspended barite is calculated to account for between 30 and 60%.

The concordance between the flux of Ba to the sediments and the accumulation of Ba as barite, requires that Ba is released from the organic, siliceous and calcareous carriers, by oxydation and dissolution, and is precipitated as barite at the sediment-water interface. Since $BaSO_4$ saturation is probably not attained here, due to bioturbation and resulting dilution of the pore water dissolved Ba content, the barite formation is proposed to occur: 1) either in suitable micro-environments (= fecal pellet or bentic organism) at the sediment-water interface; 2) or deeper in the sediments (due to slow release of Ba from the carriers) in the saturated pore waters. In both cases the discrete barite crystals,settled from the watercolumn, could function as growth nuclei.

Volcanism appears only as an important source of Ba for sedimentary barite, in active ridge areas; but even in such regions surface-water derived biogenic Ba can contribute for a large part to the overall supply of Ba to the sediments.

The discussions in this study show that several terms in the bio-geochemical cycle of Ba in the ocean need more detailed information. These are:

1) The average World Ocean input of dissolved Ba by river

discharge, including the extent of the effect of Ba desorbtion from clays when river water mixes with sea water. Such studies should be extended to the major rivers.

2) The predicted differences in overall J_{Ba} between the deep Atlantic and Pacific waters needs verification. Investigations of the suspended barite load of Pacific waters is required. Further, more data should be collected on the Ba content of the skeletal and organic carriers in order to more accurately assess their specific role in the Ba cycle and to detect possible discrepancies between the Atlantic and the Pacific.

3) The mechanism of barite production, both directly (i.e. barite secretion by living organisms) and indirectly (i.e. barite precipitation in decaying organic matter) must be investigated and requires in-vitro experimentations to be done. In addition, such investigations could throw some light upon the possible role of the fecal pellet, as a suitable precipitation environment, in the production of barite at the sediment-water interface.

REFERENCES:

Activation Analysis: Principles and Applications, Proceedings of a NATO advanced study institute held in Glasgow, J.M.A. Lenihan and S.J. Thomson ed. (Acad. Press, London N.Y., 1965).

T. Allen, Particle size measurement (Chapman and Hall Ltd, London, 1968).

J.T. Armstrong and P.R. Buseck, Quantitative chemical analysis of individual microparticles using the electron microprobe: theoretical, Anal. Chem. 47 (1975) 2178.

J.R. Arnold, Trace elements and transport in the ocean, in: Proc. 2nd U.N. Int. Conf. on the Peaceful Uses of Atom. En., Geneva 18 (1958) 344.

G. Arrhenius, Pelagic sediments, in: The Sea, 3, M.N. Hill ed. (Wiley Interscience, N.Y., 1963) 655.

G. Arrhenius and E. Bonatti, Neptunism and vulcanism in the ocean, in: Progress in Oceanography, 3, M. Sears ed. (Pergamon, London, 1965) 7.

O. Aubey, Contribution à l'étude de la dissolution des particules de carbonate de calcium dans les eaux profondes océaniques, Thèse de Doctorat 3ème cycle, Paris 6, 1976.

M.P. Bacon and J.M. Edmond, Barium at GEOSECS III in the Southwest Pacific, Earth Planet. Sci. Letters 16 (1972) 66.

H. Bader, The hyperbolic distribution of particle sizes, J. Geophys. Res. 75 (1970) 2822.

T.F.W. Barth, Theoretical Petrology, 1st ed., (Wiley & Sons, N.Y., 1952).

M. Bender, T. Snead and L.H. Chan, Barium intercalibration at GEOSECS I and III, Earth Planet. Sci. Letters 16 (1972) 81.

W.H. Berger, Foraminiferal ooze: solution at depth, Science 156 (1967) 373.

W.H. Berger, Biogenous deep-sea sediments: fractionation by deep-sea circulation, Geol. Soc. Am. Bull. 84 (1970) 1385.

A. Bernard, Etude de la spéciation des métaux lourds présents dans quelques sublimés volcaniques, mémoire de licence, Université Libre de Bruxelles, 1976.

M. Bernat, T. Church and J.C. Allegre, Barium and strontium concentrations in Pacific and Mediterranean sea water profiles by direct isotope dilution mass spectrometry, Earth Planet. Sci. Letters 16 (1972) 75.

K.K. Bertine and J.B. Keene, submarine barite-opal rock of hydrothermal origin, Science 188 (1975) 150.

P.E. Biscaye and S.L. Eittreim, Variations in benthic boundary layer phenomena; nepheloid layers in the North American Basin, in: Suspended solids in sea water, R. Gibbs ed. (Plenum N.Y., 1974) 227.

P.E. Biscaye and S.L. Eittreim, Suspended particulate loads and transports in the nepheloid layer, Marine Geology 23 (1977) 155.

P.E. Biscaye, V. Kolla and K.K. Turekian, Distribution of calcium carbonate in surface sediments of the Atlantic Ocean, J. Geophys. Res. 81 (1976) 2595.

J.l. Bischoff, Red Sea geothermal brine deposits : their mineralogy, chemistry and genesis, in: brines and recent heavy metal deposits in the Red Sea, E.T. Degens and D.A. Ross eds. (Springer- Verlag, N.Y., 1969), 368.

J.K.B.Bishop and J.M.Edmond, A new large volume filtration system for the sampling of oceanic particulate matter, J. Mar. Res. 34 (1976) 181.

J.K. Bishop, J.M. Edmond, D.R. Ketten, M.P. Bacon and W.B. Silker, The chemistry, biology and vertical flux of particulate matter from the upper 400 m of the Equatorial Atlantic Ocean, Deep-Sea Res. 24 (1977) 511.

J.K.B. Bishop, D.R. Ketten and J.M. Edmond, The chemistry, biology and vertical flux of particulate matter from the upper 400 m of the Cape Basin in the southeast Atlantic Ocean, Deep-Sea Res. 25 (1979) 1121.

C.E. Bolze, P.G. Malone and M.J. Smith, microbial mobilization of barite, Chem. Geol. 13 (1974) 141.

E. Bonatti, D.E. Fisher, O. Joensuu, H.S. Rydell and H. Beyth, Iron-mangenese-barium deposits from the northern Afar Rift (Ethiopia). Econ. Geol. 67 (1972) 717.

K. Boström, B. Farquharson and W. Eyl, Submarine hot springs as a source of active ridge sediments, Chem. Geol. 10 (1972) 189.

K. Boström, O. Joensuu and I. Brohm, Plankton: its chemical composition and its significance as a source of pelagic sediments, Chem. Geol. 14 (1974) 255.

K. Boström, O. Joensuu, C. Moore, B. Boström, M. Dalziel and A. Horowitz, Geochemistry of barium in pelagic sediments, Lithos 6 (1973)159.

K. Boström and M.N.A. Peterson, Precipitates from hydrothermal exhalation on the East Pacific Rise, Econ. Geol. 61 (1966) 1258.

E.M. Botazzi and B. Schreiber, Acantharia in the Atlantic Ocean, their abundance and preservation, Limnol. Oceanogr. 16 (1971) 677.

E.A. Boyle, F.R. Sclater and J.M. Edmond, The distribution of dissolved copper in the Pacific, Earth Planet. Sci. Letters 37 (1977) 38.

G.W. Brass and K.K. Turekian, Strontium distribution in GEOSECS oceanic profiles, Earth Planet. Sci. Letters, 23 (1974) 141.

P.G.Brewer, D.W. Spencer, P.E. Biscaye, A. Hanley, P.L. Sachs, C.L. Smith, S. Kadar and J. Fredericks, The distribution of particulate matter in the Atlantic Ocean, Earth Planet. Sci. Letters 32 (1976) 393.

W.S. Broecker, Radioisotopes and large-scale oceanic mixing, in: The Sea, 2, M.N. Hill ed. Wiley-Interscience, N.Y., 1963).

W.S. Broecker, Chemical Oceanography, Deffeyes ed. (Harcourt-Brace-Jovanovich, N.Y., 1974).

W.S. Broecker, R. Gerard, M. Ewing and B. Heezen, Natural radiocarbon in the Atlantic Ocean, J. Geophys. Res. 65 (1960) 2903.

W.S. Broecker and Y.H. Li, Interchange of water between the major oceans, J. Geophys. Res. 75 (1970) 3545.

W.S. Broecker, Y.H. and J. Cromwell, Radium-266 and Radon-222: concentration in Atlantic and Pacific Oceans, Science 158 (1967).

M. Brongersma-Sanders, Barium in pelagic sediments and diatoms, Koninkl. Nederl. Akad. Wetensch. Proc. B 70 (1966) 93.

J.C. Brun-Cottan, Stokes settling and dissolution rate model for marine particles as a function of size distribution, J. Geophys. Res. 81 (1970) 2822.

J.C. Brun-Cottan, Contribution à l'étude de la granulométrie et de la cinétique des particules marines, Thèse de Doctorat Es-Sci. Phys., Paris 6 (1976).

P.Buat-Menard, Influence de la retombée atmosphérique sur la chimie des métaux en trace dans la matière en suspension dans l'Atlantique Nord, Thèse de Doctorat Es - Sciences, Paris 7, 1979.

P. Buat-Menard and R. Chesselet, Marine aerosols control on deep ocean heavy metals particulate chemistry, Proc. Intern. Conf. on Atm. Aerosols, Condens. and Ice Nuclei, Ireland, (Perg. Press, 1977).

P. Buat-Menard and R. Chesselet, Variable influence of the atmospheric flux on the trace metal chemistry of oceanic suspended matter, Earth Planet. Sci. Letters 42 (1979) 399.

G. Cahet, M. Fiala, G. Jacques and M. Panouse, Production primaire au niveau de la thermocline en zone néritique de Méditerranée Nord-Occidentale, Mar. Biol. 14 (1972) 32.

Y. Cameron, A computer program for factor analysis of geochemical and other data, Geol. Surv. Canada, paper 67-34 (1967) 41.

J.R. Campbell and G.H. Nancollas, The crystallization and dissolution of strontium sulfate in aqueous solution, J. Phys. Chem. 73 (1969) 1735.

D.E. Carritt, Oceanic residence time and geobiochimical interactions, in: Impingement of man on the oceans, D.W. Hood et. (Wiley-Interscience, N.Y., London, 1971) 191.

L.H. Chan, D. Drummond, J.M. Edmond and B. Grant, On the barium data from the Atlantic GEOSECS expedition, Deep-Sea Res. 24 (1977) 613.

L.H. Chan, J.M. Edmond, R.F. Stallard, W.S. Broecker, Y.C. Chung, R.F. Weiss and T.L. Ku, Radium and Barium at GEOSECS stations in the Atlantic and Pacific, Earth Planet. Sci. Letters 32 (1976) 258.

R. Chesselet, Deep ocean suspended matter chemistry, Thalassia Jugoslavica, 11 (1975) 135.

R. Chesselet, J. Jedwab, C. Darcourt and F. Dehairs, Barite as discrete suspended particles in Atlantic waters, Abstract 05, EOS, Trans. Am. Geophys. Un. 57 (1976) 255.

R. Chesselet, J. Jedwab, C. Darcourt, F. Dehairs and P. Kummert, Progress in particulate measurements; chemistry of particulate matter, 2nd GEOSECS Summer Instit. Woods Hole Oceanographic Institution, Woods Hole, Mass. U.S.A., April 1973.

R. Chesselet and C. Lambert, l'Aluminium, le fer et le manganese dans les particules en suspension à l'approche de l'interface eau- sédiment dans l'Atlantique et le Pacifique, Bull. Soc. Géol. France IXIX, 7 (1977) 235.

R. Chesselet, D.W. Spencer and P.E. Biscaye, Element transport by particles: the aluminium, manganese, iron system in Atlantic suspended matter, Geochim. and Ocean Mix. Symp., Joint Ocean. Ass. Edinburgh 1976, Book of Abstr. FAO Rome (1976).

R. Chester and R.G. Messiha-Hanna, Trace element partition patterns in North Atlantic deep-sea sediments, Geochim. Cosmoch. Acta 34 (1970) 1121.

R. Chester and J.M. Stoner, Average trace element composition of low level marine atmospheric particulates, Nature 246 (1973) 138.

R. Chester and J.H. Stoner, The distribution of particulate organic carbon and nitrogen in some surface waters of the World Ocean, Mar. Chem. 2 (1974) 263.

T.J. Chow, Barium in Southern California coastal waters: A potential indicator of marine drilling contamination, Science 193 (1976) 57.

T.J. Chow and E.D. Goldberg, On the marine geochemistry of barium Geochim. Cosmoch. Acta 20 (1960) 192.

Y. Chung, Radium-226 and Ra-Ba relationships in Antarctic and Pacific waters, Earth Planet. Sci. Letters 23 (1974) 192.

T.M. Church, Marine barite, Ph. D. Thesis, San Diego California (1970).

T.M. Church, Barium sulface solubility in sea water, Earth Planet. Sci. Letters ; in press. 1979.

T.M. Church and M. Bernat, Thorium and Uranium in marine barite, Earth Planet. Sci. Letters 14 (1972) 139.

T.M. Church and K. Wolgemuth, Marine barite saturation, Earth Planet. Sci. Letters 15 (1972) 35.

C. Copin-Montegut and G. Copin-Montegut, Chemical analyses of suspended particulate matter collected in the Northeast Atlantic, Deep-Sea Res. 19 (1972) 445.

C. Copin-Montegut and G. Copin-Montegut, The chemistry of particulate organic matter from the south Indian and Antarctic Ocean, Deep-Sea Res. 25 (1978) 911.

H. Craig, Abyssal carbon and radiocarbon in the Pacific, J. Geophys. Res. 74 (1969) 5491.

H. Craig, The deep metabolism: oxygen consumption in abyssal ocean water, J. Geophys. Res. 76 (1971) 5078.

H. Craig, The GEOSECS program: 1970-1971, Earth Planet. Sci. Letters 16 (1972) 47.

D.S. Cronan, Authigenic minerals in deep-sea sediments, in: The Sea, 5, E.D. Goldberg ed. (Wiley Interscience, N.Y., 1974).

C. Darcourt-Rieg, Etude des matières en suspension dans les eaux profondes Atlantiques; teneurs en éléments traces mesurés par activation neutronique; comparaisons avec le dédiment; Thèse de Doctorat 3ème cycle, Paris (1973).

W.A. Deer, R.A. Howie and J. Zussman, Rock- forming minerals (Longman ltd., London, 1975).

F. Dehairs, Le barium et la barytine: Résultats des campagnes GEOSECS, Léçons et séminaires, "Dynamique des océans", 4ème session E 4, Louvain la Neuve, 1 (1977) 319.

F.Fehairs, R.Chesselet and J.Jedwab, Discrete suspended particles of barite and the barium cycle in the open ocean, Earth Planet. Sci. Letters, GEOSECS collected papers volume, 1979, in press.

G.Dietrich, K.Kalle, W.Krauss and G. Siedler, Allgemeine Meereskunde (Gebr. Borntraeger, Berlin-Stuttgart, 1975).

B.K.Dugolinsky, S.V.Margolis and W.C.Dudley, Biogenic influence on growth of manganese nodules, J. Sedim. Petrol. 47 (1977) 428.

J.M. Edmond, Comments on the paper by T.L. Ku, Y.H. Li, G.G. Mathieu and H.K. Wong, "Radium in the Indian-Antarctic Ocean south of Australia", J. Geophys. Res. 75 (1970) 6878.

C. Emiliani, Mineralogical and chemical composition of the tests of certain pelagic foraminifera, Micropaleontology 1 (1955) 377.

M. Ewing, S.L. Eittreim, J. Ewing and X. Lepichon, Sediment transport and distribution in the Argentine Basin, in: Physics and Chemistry of the Earth, L.H. Ahrens ed. (F. Press, S.K. Runcorn, H.C. Urey) 8 (1971) 49.

R.M. Garrels and C.L. Christ, Solutions, Minerals and Equilibria (Harper and Row, N.Y., 1965).

R.M. Garrels and M.E. Thompson, A chemical model for sea water et 25°C and one atmosphere total pressure, Am. J. Science 260 (1962) 57.

E.D. Goldberg, Determination of opal in marine sediments, J. Mar. Res. 18 (1958) 178.

E.D. Goldberg and G. Arrhenius, Chemistry of pelagic sediments, Chemistry of pelagic sediments, Geochim. Cosmoch. Acta 13 (1958) 153.

E.D. Goldberg and J.J. Griffin, Sedimentation rates and mineralogy in the South Atlantic, J. Geophys. Res. 69 (1964) 4293.

E.D. Goldberg and M. Koide, Geochronological studies of deep sea sediments by the ionium/thorium method, Geochim. Cosmochim. Acta 26 (1962) 417.

E.D. Goldberg, B.L.K. Somayajulu, J. Galloway, I.R. Kaplan and G. Faure, Differences between barites of marine and continental origins, Geochim. Cosmoch. Acta 33 (1969) 287.

F. Guichard, T.H. Church, M.Treuil and H. Jaffrezic, Rare earths in barites: distribution and effects on aqueous partitioning, Geochim. Cosmochine. Acta, 1979, in press.

E. Haeckel, Radiolarien (Rhizopoda Radiolaria), Eine Monographie (G. Reimer Verlag, Berlin, 1862).

J.S. Hanor, Barite saturation in sea water, Geochim. Cosmoch. Acta 33 (1969) 894.

J.S. Hanor, Rates of barium accumulation in the Equatorial Pacific, Geol. Soc. Am., Abstracts with Programs 4 (1972) 526.

J.S. Hanor and L.H. Chan, Behavior of barium during mixing of Missisippi river and Gulf of Mexico waters, Geol. Soc. Am. Bull. Abstr. with Programs 7 (1975) 1098.

J.S. Hanor and L.H. Chan, Non-conservative behaviour of Ba during mixing of Mississippi river and Gulf of Mexico waters, Earth Planet. Sci. Letters 37 (1977) 242.

H.H. Harman, Modern Factor Analysis, (Univ. Chicago Press, 1967) 474.

R.C. Harriss, Biological buffering of oceanic silica, Nature 212 (1966) 275.

G.R. Heath, Dissolved silica and deep-sea sediments, in: Geologic History of the Oceans, W.W. Hay ed.,(S.E.P.M. Spec. Publ., 1974).

G.R. Heath and J. Dymond, Genesis and transformation of metalliferous sediments from the East Pacific Rise, Bauer Deep, and Central Basin, north west Nazca plate, Geol. Soc. Am. Bull. 88 (1977) 723.

A. Herbosch, Etude de la géochimie et de la metallogénie de l'uranium en milieu continental lacustre, Thèse de Doctorat Es-Sci. Université Libre de Bruxelles (1975).

A. Herbosch, Facteurs controlant la distribution des éléments dans les shales uranifères du bassin permien de Lodève (Herault, France), IAEA-SM-183/2 (1974) 359.

S. Honjo, Coccoliths: Production, transportation and sedimentation, Mar. Micropal. 1 (1976) 65.

S. Honjo, Biogenic particles in the ocean: Do they dissolve in the watercolumn ?, in: The fate of fossil fuel CO_2 in the oceans, N.R. Andersen and A. Malahoff ed. (Plenum Press, N.Y., London, 1977)269.

S. Honjo, Sedimentation of material in the Sargasso Sea at a 5367 m deep station, J. Mar. Chem. 36 (1978).

J. Jedwab, Copper, zinc and lead minerals suspended in ocean waters, Geoch. Cosmoch. Acta 43 (1979) 101.

H.F. Kaiser, The varimax criterion for analytic rotation in factor analysis, Psych. 23 (1958) 187.

D.R. Kester and R.M. Pytkowicz, Effect of temperature and pressure on sulphate ion association in sea water, Geochim. Cosmoch. Acta 34 (1970) 1039.

J. Klossa, Contribution à l'étude de la matière particulaire par une méthode d'analyses ponctuelles combinées, Thèse de Doctorat 3ème cycle, Paris 7, (1977).

O.J. Koblentz-Mishke, V.V. Volkovinsky and J.G. Kabanova, Plankton primary production of the World Ocean, in: Scientific Exploration of the South Pacific, W.S. Wooster ed. (U.S. Natl. Acad. Sci., Washington D.C., 1970) 183.

V. Kolla, A.W.H. Bé and P.E. Biscaye, Calcium carbonate distribution in the surface sediments of the Indian Ocean, J. Geophys. Res. 81 (1976) 2605.

S. Krishnaswami and D. Lal, Particulate organic carbon in Atlantic surface waters, Nature 266 (1977) 713.

S. Krishnaswami, D. Lal and B.L.K. Somayalulu, Investigations of gram quantities of Atlantic and Pacific surface particulates, Earth Planet. Sci. Letters 32 (1976) 403.

P. Kroopnick and H. Craig, Oxygen isotope fractionation in dissolved oxygen in the deep sea, Earth Planet Sci. Letters 32 (1976) 375.

P. Kroopnick, R.F. Weiss, and H. Craig, Total CO_2, ^{13}C and dissolved oxygen - ^{18}O at GEOSECS II in the North Atlantic, Earth Planet. Sci. Letters 16 (1972) 103.

T.L. Ku, Y.L. Li, G.G. Mathieu and H.K. Wong, Radium in the Indian-Antarctic Ocean south of Australia, J. Geophys. Res. 75 (1970) 5286.

T.L. Ku, W.S. Broecker and N. Opdyke, Comparison of sedimentation rates measured by paleo-magnetic and the ionium methods of age determination, Earth Planet. Sci. Letters 4 (1968).

D. Lal, The oceanic microcosm of particles; suspended particulate matter, about 1 gram in 100 tons of sea water, plays a vital role in ocean chemistry, Science 198 (1977) 997.

D. Lal and A. Lerman, Dissolution and behavior of particulate biogenic matter in the ocean: some theroretical considerations, J. Geophys. Res. 78 (1973) 7100.

D. Lal and A. Lerman, Size spectra of biogenic particles in ocean water and sediments, J. Geophys. Res. 80 (1975) 423.

C. Lalou, E. Brichet, G. Poupeau, P. Romary and C. Jehanno, Growth rates and possible age of a North Pacific manganese nodule, in: Marine geology and oceanography of the Central Pacific manganese nodule province, T.Bischoff and D.Piper eds. (U.S. Geol. Survey, 1979, in press).

C.E. Lambert, Contribution à l'étude du fer et de l'aluminium particulaires dans l'océan, Thèse de diplôme d'Etudes supérieures, Université de Picardie, France (1979).

C.E. Lambert, C. Jehanno, J.C. Brun-Cottan, N. Silverberg and R. Chesselet, size distribution of suspended aluminosilicates in deep South Atlantic waters (submitted to Deep-Sea Res.).

L. Lebart and J.P. Fenelon, Statistique et Informatique appliquée (Dunod Paris, 1972).

C.M. Lederer, J.M. Hollander and I. Perlman, Table of isotopes, 6th ed. (Wiley & sons, N.Y., London, Sydney, 1968).

Y.H. Li, Confusion of the mathematical notation for defining the residence time, Geochim. Cosmoch. Acta 41 (1977) 555.

Y.H. Li, T.L. Ku, G.G. Mathieu and K. Wolgemuth, Barium in the Antarctic Ocean and implications regarding the marine geochemistry of Ba and Ra-226, Earth Planet. Sci. Letters 19 (1973) 352.

Y.H. Li, T. Takahashi and W.S. Broecker, Degree of saturation of $CaCO_3$ in the oceans, J. Geophys. Res. 74 (1969) 5507.

A.P. Lisitzin, Basic relationship in distribution of modern siliceous sediments and their connection with climatic zonation, Intern. Geology Rev. 9 (1967) 631.

A.P. Lisitzin, Sedimentation in the World Ocean, Soc. of Econ. Paleon. and Miner. special publ. n° 17, 1972.

H.A. Lowenstam, Impact of life on chemical and physical processes, in: The Sea, E.D. Goldberg ed. (Wiley Interscience, N.Y., 1974) 715.

J. Martin and G.A. Knauer, The chemical composition of plankton, Geoch. Cosmoch. Acta 37 (1973) 1639.

I.N. McCave, Vertical flux of particles in the ocean, Deep-Sea Res. 22 (1975) 181.

W.L. McIntyre, Trace element partition coefficients: a review of theory and applications to geology, Geochim. Cosmoch. Acta 27 (1963) 1209.

D.W. Menzel, The role of in situ decomposition of organic matter on the concentration of non-conservative properties in the sea, Deep-Sea Res. 17 (1970) 751.

D.W. Menzel, Primary productivity, dissolved and particulate organic matter and the sites of oxidation of organic matter, in: The Sea, 5, E.D. Goldberg ed. (Wiley Interscience, N.Y., 1974) 659.

D.W. Menzel and J.H. Ryther, Organic carbon and oxygen minimum in the South Atlantic Ocean, Deep-Sea Res. 15 (1968) 327.

D.W. Menzel and J.H. Ryther, Distribution and cycling of organic matter in the oceans, in: 1968 Symposium on Organic Matter in Natural Waters, (University of Alaska, Alaska, 1971).

G. Michard, T.M. Church and M. Bernat, The pore water chemistry of recent sediments in the western Mediterranean Basin, J. Geophys. Res. 79 (1974) 817.

F.J. Millero, Effect of pressure on sulphate ion association in sea water, Geochim. Cosmoch. Acta 35 (1971) 1639.

H.J. Minas, La distribution de l'oxgène en relation avec la production primaire en Méditerranée Nord-Occidentale, Mar. Biol. 7 (1970) 181.

S. Miner, Air pollution aspects of barium and its compounds, (Litton Systems Inc., PB 188083, Bethesda Maryland, 1969).

Y. Miyake and K. Saruhashi, On the vertical distribution of the dissolved oxygen in the ocean, Deep-Sea Res. 3 (1956) 242.

W.H. Munk, Abyssal recipes, Deep-Sea Res. 13 (1966) 707.

G.H. Nancollas, Kinetics of crystal growth from solution, J. Cryst. Growth 3,4 (1968) 335.

G.H. Nancollas and N. Purdie, Crystallization of barium sulphate in aqueous solution, Trans. Far. Soc. 59 (1963) 735.

G.H. Nancollas and N. Purdie, The kinetics of crystal growth, Quart. Rev. 8 (1964) 1.

M.N.A. Peterson, Calcite: Rates of dissolution in a vertical profile in the Central Pacific, Science 154 (1966) 1542.

L. Provasoli, J.J. McLaughlin and M.R. Droop, The development of artificial media for marine algae, Arch. Mikrobiol. 25 (1957) 392.

A.P. Ratner, On the theory of the distribution of electrolytes between a solid crystalline and a liquid phase, J. Chem. Phys. 1 (1933) 789.

N.W. Rakestraw, Particulate matter in the oxygen minimum layer, J. Mar. Res. 17 (1958) 429.

A.C. Redfield, B.H. Ketchum and F.A. Richards, The influence of organisms on the composition of sea water, in: The Sea, 3, M.N. Hill ed. (Wiley Interscience, N.Y., 1963).

J.L. Reid, On circulation, phosphate-phosphorus content and zooplankton volumes in the upper part of the Pacific Ocean, Limnol. Oceanogr. 7 (1962) 287.

J.L. Reid, W.D. Nowlin and W.C. Patzert, On the characteristics and circulation of the Southwestern Atlantic Ocean, J. Phys. Ocean., 7 (1977) 62.

K. Revelle and K.O. Emery, Barite concretions from the ocean floor, Bull. Geol. Soc. Am. 62 (1961) 707.

J.P. Riley and I. Roth, The distribution of trace elements in some species of phytoplankton grown in culture, J. Mar. Biol. Ass. U.K. 51 (1971) 63.

J.H. Ryther, Photosynthesis and fish production in the sea, Science 166 (1969) 72.

A. Schmidt, Atlas der diatomaceen-kunde, Band III (O.R. Reisland, Leipzig; 1874-1959).

H.J. Schrader, Fecal pellets: Role in sedimentation of pelagic diatoms, Science 174 (1971) 55.

W. Schulze, Neutronenaktivierung als analytisches Hilfsmittel, (F. Enke verlag, Stuttgart, 1962).

F.E. Schulze and H. Thierfelder, Uber Baryumsulfat in Meerestieren (Xenophyophora F.E. Sch.), Sitzungsberichten der Gesellschaft Naturforschender Freunde zu Berlin, 2-4 (1905).

D.W. Skopintsev, On the age of stable organic matter: Aquatic humus in oceanic waters, in: The changing chemistry of the oceans, D. Dyrssen and D. Jagner ed. (Wiley, N.Y., 1972) 205.

B.L.K. Somayajulu and E.D. Goldberg, Thorium and uranium isotopes in seawater and sediments, Earth Planet. Sci. Letters 1 (1966) 102.

D.W. Spencer, P.G. Brewer, A. Fleer, S. Honjo, S. Krishnaswami and Y. Nozaki, Chemical fluxes from a sediment trap experiment in the deep Sargasso Sea, J. Mar. Res. 36 (1978) 493.

D.W. Spencer, E.T. Degens and G. Kulbicki, Factors affecting element distributions in sediments, in: Origin and Distribution of the Elements, L.H. Ahrens ed., Intern. Ser. Monogr. in Earth Sci. 30 (1968) 981.

E. Steeman-Nielsen, On organic production in the oceans, J. du Conseil 19 (1954) 309.

F.L. Sayles and J.L. Bischoff, Ferromanganoan deposits in the Equatorial East Pacific, Earth Planet. Sci. Letters 19 (1973) 330.

R.E. Stoiber and W.I. Rose, Fumarole incrustations at active Central American Volcanoes, Geoch. Cosmoch. Acta, 38 (1974) 495.

J.D.H. Strickland, Production of organic matter in the primary stages of the marine food chain, in: Chemical Oceanography, J.P. Riley and G. Skirrow ed. (1965) 477.

M. Stuiver, The C^{14} distribution in West Atlantic abyssal waters, Earth Planet. Sci. Letters 32 (1976) 322.

O.S. Tendal, A monograph of the Xenophyophoria (Rhizopoda, Protozoa), Galathea Report 12 (1972) 7.

C. Thompson and V.T. Bowen, Analyses of coccolith ooze from the deep tropical Atlantic, J. Mar. Res. 27 (1969) 32.

S. Tsonugai, H. Yamahata, S. Kudo and O. Saito, Calcium in the Pacific Ocean, Deep-Sea Res. 20 (1973) 717.

K.K. Turekian, Some aspects of the geochemistry of marine sediments, in: Chemical Oceanography, 2, J.P. Riley and G. Skirrow (Acad. Press, Lonson, N.Y., 1965).

K.K. Turekian, Deep-sea deposition of barium, cobalt and silver, Geochim. Cosmoch. Acta 32 (1968) 603.

K.K. Turekian and R.L. Armstrong, Magnesium, strontium and barium concentrations and calcite-aragonite ratios of some recent molluscan shells, J. Mar. Res. 18 (1960) 133.

K.K. Turekian and D.G. Johnson, The barium distribution in sea water, Geochim. Cosmoch. Acta 30 (1966) 1153.

K.K. Turekian and E.H. Tausch, Barium in deep-sea sediments of the Atlantic Ocean, Nature 201 (1964) 696.

K.K. Turekian and K.H. Wedepohl, Distribution of the elements in some major units of the earth's crust, Geol. Soc. Am. Bull. 72 (1961) 175.

J.S. Valette, Etude des processus sedimentaires et géochimiques en milieu volcanique marin: Le modèle de Vulcano (Italie) Thèse de Doctorat Es-Sci. Naturelles, Perpignan, France, 1978.

F. Vaslow and G.E. Boyd, Thermodynamics of coprecipitation: dilute solid solutions of AgBr in AgCl, J. Am. Chem. Soc. 74 (1952) 4691.

Z.A. Vinogradova and V.V. Koval'skiy, Elemental composition of the Black Sea plankton, Dokl. Akad. Nauk USSR, Earth Sci. Section 147 (1962) 217.

G.T. Wallace, G.L. Hoffman and R.A. Duce, The influence of organic matter atmospheric deposition on the particulate trace metal concentration of Northwest Atlantic surface water, Mar. Chem. 5 (1977) 143.

K. Wolgemuth, Barium analyses from the first GEOSECS test cruise, J. Geophys. Res. 75 (1970) 7686.

K. Wolgemuth and W.S. Broecker, Barium in sea water, Earth Planet. Sci. Letters 8 (1970) 372.

R. Wollast, The silica problem, in: The Sea, E.D. Goldberg ed. (Wiley Interscience, N.Y., 1974) 359.

K. Wyrtki, The oxygen minima in relation to ocean circulation, Deep-Sea Res. 9 (1962) 11.

VRIJE UNIVERSITEIT BRUSSEL

FAKULTEIT WETENSCHAPPEN

EENHEID ANALYTISCHE SCHEIKUNDE

DISCRETE SUSPENDED PARTICLES OF BARITE AND THE BARIUM CYCLE IN THE OPEN OCEAN

Proefschrift voorgelegd met het oog op het behalen van de graad van Doctor in de Wetenschappen

Promotor: I. ELSKENS

TOME II : APPENDIX

OKTOBER 1979

DEHAIRS FRANK

VRIJE UNIVERSITEIT BRUSSEL

FAKULTEIT WETENSCHAPPEN

EENHEID ANALYTISCHE SCHEIKUNDE

DISCRETE SUSPENDED PARTICLES OF BARITE AND THE BARIUM CYCLE IN THE OPEN OCEAN

Proefschrift voorgelegd met het oog op het behalen van de graad van Doctor in de Wetenschappen

Promotor: I. ELSKENS

TOME II : APPENDIX

OKTOBER 1979

DEHAIRS FRANK

TABLE OF CONTENTS

APPENDIX I

ELEMENTAL COMPOSITION OF THE WHOLE-CELL AND SILICEOUS FRACTION OF TWO DIATOM SPECIES GROWN IN CULTURE:Al,Cu,V,Mn,Sr,Ca,Mg

- Rhizosolenia alata
- Chaetoceros lauderi

The two diatom species, Rhizosolenia alata and Chaetoceros lauderi were grown in culture at the CERBOM laboratories (Nice, France). The method of diatom culturing and analysis of elemental composition is discussed in chapter 3 of part I. Four different types of growth media were used:

- type A: aged sea water, filtered on membranes of 0.45 µm pore size
- type B: artificial sea water, filtered on membranes of 0.45 µm pore size
- type C: aged sea water, unfiltered
- type D: artificial sea water, filtered on membranes of 0.45 µm pore size, and enriched in dissolved Ba, up to a concentration of 30 µg/Kg sea water.

In the following all concentration data are expressed in ppm of total dry weight.

Strontium (Tables A.I.1; A.I.2)

For Rhizosolenia a. the Sr content of the whole cells ranges from 643 to 1567 ppm of which about 40% is associated with the siliceous fraction. For Chaetoceros l. no Sr is detected, with exception of the diatoms grown in natural, unfiltered sea water. The Sr content measured for type C diatoms is therefore attributed to particulate Sr phases that were present in the culture medium before the culture was started.

The data for Rhizosolenia a. are larger by a factor 20 to 100 when compared with those of Riley and Roth (1970), which concern essentially non-siliceous phytoplankton: they observed a range of values from 1.5 to 39 ppm for cultured phytoplankton, and 70 ppm for sea plankton (see Table II.14.A, in part II, for the species composition of their phytoplankton). Our values are but slightly larger than those Martin and Knauer (1973) observed for open ocean phytoplankton: they observed a concentration range from 53 to 225 ppm for their groups I and II (see page 162 of this study, for the definition of these categories of phytoplankton samples). However, Martin and Knauer reported that only 3% of the Sr was associated with the silica fraction.

The uptake capacity of Sr is species dependent, in the same sense as it was observed for Ba (see § 4.4.1 in part II).

Calcium (Tables A.I.1 and A.I.2)

For the whole cells, concentrations range from 2577 to 6399 ppm in Rhizosolenia a. and from 279 to 5200 ppm in Chaetoceros l. . These values are one to two orders of magnitude larger than those observed by Martin and Knauer: 3 to 13 ppm, for their groups I,II and III. Riley and Roth did not analyze for Ca. The 10 times larger Ca values observed in both cases for type C diatoms are attributed to the presence of carbonate particles in the sea water before starting the cultures. For Rhizosolenia a., type D diatoms show 30% of

their Ca to be associated with the silica fraction, while for type B diatoms this quantity amounts to 90%. The latter value is probably overestimated due to the inefficient oxidation of the organic fraction for this sample (see Table II.10 in part II). The Ca fraction associated with siliceous matter is much smaller for Cheatoceros l. than for Rhizosolenia a. (Table A.I.2). From the data in this table for Chaetoceros type A diatoms, characterized by a poor elimination of the organic matter (see Table II.10 in part II), it appears that the Ca fraction associated with the siliceous matter exceeds probably not the 3% level for these diatoms.

Manganese (Tables A.I.1 and A.I.2)

For the whole cell fraction, concentrations range from 23 to 88 ppm for Rhizosolenia a. and from 91 to 437 ppm for Chaetocers l. . With the exception of both values observed for the Chaetoceros diatoms grown in artificial media (types B and D), our values are of the same order of magnitude as those of Riley and Roth; 4 to 73 ppm for their phytoplankton grown in culture and 118 ppm for their sea plankton. Martin and Knauer observe the follwong range of values: 5 to 32 ppm for their groups I,II and III. For both species it is evident that the uptake has been 3 times larger for the diatoms grown in artificial media. This shows the natural sea water media to be depleted with respect to Mn. Further, Chaetoceros l. appears to have concentrated 4 to 6 times more Mn than Rhizosolenia a. has. For Rhizosolenia a. Mn is entirely associated with the silica fraction, whereas for Chaetoceros l. this amounts only to 10%. Martin and Knauer's

data show 6% of the Mn to be associated with the silica fraction.

Magnesium (Tables A.I.1 and A.I.2)

As concerns the cultures of the natural sea water media, 2996 ppm is found for Rhizosolenia a. (type C) and 3105 to 3256 ppm for Chaetoceros l. Such values are an order of magnitude smaller than those of Martin and Knauer: 0.74 to 1.75%, for their groups I, II and III. Riley and Roth did not analyze for Mg. For the artificial sea water media, 12910 to 18932 ppm are detected in Rhizosolenia a. and 17822 to 79605 ppm in Chaetoceros l.. This shows the natural sea water samples to be depleted with respect to Mg. For Rhizosolenia a. 40 to 100% of the total Mg amount is bound to the silica fraction, while this is only 15% for Chaetoceros l.. Martin and Knauer's data show less than 3% of the Mg to be associated with the silica fraction.

Aluminium (Table A.I.1 and A.I.2)

For the whole cell fraction concentrations range from 247 to 4658 ppm for Rhizosolenia a. and from 345 to 851 ppm for Chaetoceros l.. With the exception of the Rhizosolenia type D sample, our values are similar to those of Riley and Roth, and Martin and Knauer; these authors observed the following ranges of concentrations:

- Riley and Roth: 118 to 1750 ppm for cultured phytoplankton
  and 5000 ppm for sea plankton
- Martin and Knauer: 7 to 2850 ppm for their groups I, II and III

As concerns Rhizosolenia a., 32 to 100% of the Al is associated with the silica fraction, while for Chaetoceros l. this amounts to a mean of 78%. Martin and Knauer's observed that this amount, in general remains below the 50% level.

Vanadium (Tables A.I.1 and A.I.2)

For both diatom species, V concentrations do not exceed the 2 ppm level and are similar to values observed by Riley and Roth: 1.2 to 5.7 ppm for their cultured phytoplankton and 3.1 ppm for their sea plankton. Martin and Knauer did not analyze for V.

40 to 44% of the total V amount appears to be associated with the silica fraction.

Copper (Tables A.I.1 and A.I.2)

Cu concentrations range from 9 to 40 ppm for both diatom species. Such values are similar to those of Riley and Roth and Martin and Knauer; these authors observed the following concentrations:

- Riley and Roth: 25 to 210 ppm for cultured phytoplankton
  and 36 ppm for sea plankton
- Martin and Knauer: 1 to 40 ppm for their groups I, II and III

It is probable that for Rhizosolenia a. all the Cu is associated with the silica fraction, while this is only 60% for Chaetoceros l.. Although Martin and Knauer, in a few cases, found relatively high amounts of Cu in association with the silica fraction (occasionally up to 80%), their values are generally lower than ours.

Table A.I.1: Sr, Ca, Mn, Mg, Al, V and Cu content of the whole cells and the siliceous fraction of the diatoms Rhizosolenia alata and Chaetoceros lauderi. All values in ppm of total dry matter.

	Sr		Ca		Mn		Mg		Al		V		Cu	
	whole cells	silica fract.	whole cells	silica fract.	whole cells	silica fract.	whole cells	silica fract.	whole cells	silica fract.	whole cells	silica fract.	whole cells	silica fract.
Rhizosolenia alata														
type A	N.A.	428 (10)	N.A.	1752 (17)	N.A.	35 (2)	N.A	3458 (14)	N.A.	619 (26)	N.A.	1.0 (75)	N.A.	28 (100)
type B	1567 (13)	691 (13)	2577 (19)	2384 (20)	88 (4)	144(?) (2)	12910 (11)	14460 (7)	247(?) (79)	1827 (4)	N.D.	N.D.	N.D.	14 (>100)
type C	926 (8)	327 (15)	22376 (3)	12892 (7)	23 (4)	23 (4)	2996 (7)	2169 (21)	543 (3)	741 (2)	1.5 (13)	1.0 (21)	9 (73)	23(?) (90)
type D	643 (25)	359 (19)	6369 (7)	1738 (15)	77 (3)	86 (2)	18932 (4)	7588 (7)	4568 (2)	1476 (2)	0.9 (27)	0.2 (80)	N.D.	19 (>100)
Chaetoceros lauderi														
type A	72 (97)	N.D.	5200 (6)	165 (50)	92 (2)	6 (6)	3256 (8)	659 (48)	345 (6)	339 (2)	0.9 (39)	0.3 (>100)	7 (>100)	17(?) (77)
type B	N.D.	N.D.	279 (18)	N.D.	261 (2)	14 (5)	17822 (7)	885 (58)	851 (4)	741 (5)	0.3 (>100)	2.0	40 (98)	20 (>100)
type C	495 (8)	760 (13)	31531 (3)	3621 (12)	91 (3)	16 (3)	3105 (17)	220 (80)	437 (1)	205 (2)	1.7 (11)	0.1 (>100)	15 (75)	5 (>100)
type D	N.D.	N.D.	N.A.	217 (79)	437 (2)	343 (1)	79605 (37)	23209 (4)	N.A.	571 (7)	N.A.	0.4 (>100)	N.A.	76 (53)

Numbers in brackets refer to 2σ% values.

N.A.: Not analyzed. For Chaetoceros 1. type D diatoms, the dead time for γ-spectrometry was too high, even after a delay of 1 hour. This is too long when measuring for short-life isotopes, such as those of Ca, Mg, Al, Cu and V.

N.D.: Not detected.

Table A.I.2: Average amounts of Sr, Ca, Mn, Mg, Al, V and Cu associated with the silica fractions of the diatoms Rhizosolenia alata and Chaetoceros lauderi; all values in %

Sr	Ca	Mn	Mg	Al	V	Cu
Rhizosolenia alata						
45	30 to 90	100	71	32 to 100	44	100
* C,D	B,D	C,D	B,C,D	C,D	C,D	C,D
Chaetoceros lauderi						
N.D.		10	15	78	40	60
*	A	A,B,C	A,B,C,D	A,B,C	A,B,C	A,B,C

* Letters refer to the samples which served to compute the average %.

APPENDIX II

INSTRUMENTAL NEUTRON ACTIVATION DATA FOR SUSPENDED MATTER: ELEMENTS OTHER THAN BARIUM

- Table A.II.1:Concentrations of particulate S, Sr, Ca, Al, V and Cu at GEOSECS station 67. For Sr, Ca, Mn, V and Cu the fractions associated with aluminosilicates are given, as computed with the Al-index method
- Tables A.II.2 and A.II.3: Concentrations of particulate Al and Ca at other Pacific and Atlantic Ocean stations

Table A.II.1: Profiles of particulate S, Sr, Ca, Al, Mn, V and Cu at GEOSECS station 67.

GEOSECS station 67: particulate S

Depth in m	%	ng/Kg	2σ %
10	14.40	15105	14
102	2.95	1879	3
300	5.10	1279	5
2392	6.75	731	7
4221	5.69	814	6
4633	4.97	302	5
5634	< 6	< 400	

Table A.II.1: continued

GEOSECS station 67, particulate Sr

Depth in m	ppm	ng/Kg	2σ %	Fraction assoc. with aluminos. %	Fraction assoc. with $CaCO_3$ %
10	143	15.0	73	9.5	25.6
42	1080	261.0	15	0.3	1.7
62	1557	197.8	8	0.4	2.5
102	2924	186.5	8	0.7	3.3
151	2239	55.5	13	0.6	1.0
199	1389	35.6	19	1.8	7.5
251	1341	41.3	15	2.0	7.2
300	1199	30.1	16	1.7	14.6
353	1395	35.4	25	1.9	12.7
405	1951	40.3	16	1.4	8.6
445	1282	23.6	25	1.8	13.6
445	1312	30.5	11	1.9	11.9
658	849	18.2	41	5.0	17.8
760	1639	17.6	44	3.2	6.7
857	1582	36.3	29	3.3	8.6
953	1272	17.9	27	3.2	10.8
1053	1048	20.3	30	2.7	10.3
1127	887	8.1	58	6.1	21.3
1316	1495	15.8	23	4.2	12.4
1438	404	8.0	70	10.8	24.0
1499	1333	18.5	16	5.1	14.4
1590	1430	19.1	59	3.4	10.8
1741	1175	16.0	29	2.0	4.1
1959	766	6.1	65	9.7	21.1
2193	866	10.7	17	9.0	33.1
2392	1140	12.3	39	4.9	15.1
2574	679	7.4	37	11.8	39.0
2758	501	9.0	61	6.4	21.8
2982	1288	12.1	26	5.4	16.4
3444	1500	9.8	43	5.0	12.9
3601	420	7.9	54	11.1	22.9

Table A.II.1: continued

GEOSECS station 67: particulate Sr, continued

Depth in m	ppm	ng/kg	2 %	Fraction assoc; with aluminos. %	Fraction assoc. with $CaCO_3$ %
3841	170	12.1	33	7.5	19.8
4035	1004	8.0	39	10.1	20.2
4221	838	12.0	68	7.9	17.2
4424	616	6.8	41	16.2	27.8
4633	813	4.9	28	14.7	25.4
4839	540	5.6	> 100	30.0	39.5
5051	1434	18.8	48	9.9	11.7
5304	312	5.3	> 100	77.5	81.2
5526	424	9.8	> 100	31.9	39.1
5599	360	17.1	43	60.7	65.0
5634	136	8.9	24	100.	100.
5894	16	2.5	> 100	100.	100.

The fraction of total Sr associated with $CaCO_3$ tests is calculated by taking 40% of the total Ca_p load to be in the carbonate form and by considering $CaCO_3$ skeletons to contain 1500 ppm of Sr. See text, § 1.1.3 in part II.

Table A.II.1: continued

GEOSECS station 67: particulate Ca

Depth in m	%	ng/Kg	2σ %	Fraction associated with aluminosilicates %
GEOSECS station 67 (44°58'S - 51°10'W); Watercolumn: 5902 m				
10	1.24	1298	19	5.0
42	1.85	2327	14	2.5
62	2.27	2839	12	1.8
102	5.04	3217	9	3.
151	5.96	1480	9	1.7
199	5.43	1391	11	3.4
251	4.63	1425	11	4.4
300	10.32	2588	10	1.5
353	10.06	2555	11	2.
405	9.33	1926	8	2.
445	8.21	1906	9	1.7
445	10.82	1992	8	2.0
658	7.17	1537	8	4.4
760	7.98	857	13	4.9
857	5.50	1264	9	6.9
953	6.50	915	9	4.6
1053	5.19	1007	9	4.0
1127	8.90	810	12	4.5
1316	8.21	871	12	5.6
1438	3.53	704	14	9.
1499	8.26	1148	9	6.2
1590	6.99	934	15	5.0
1741	1.64	224	32	10.8
1959	5.69	456	19	9.4
2193	8.42	1035	10	7.
2392	7.75	839	11	5.2
2574	7.36	801	10	7.6
2758	5.09	924	20	4.6
2982	9.41	883	10	5.4

Table A.II.1: continued

GEOSECS station 67: particulate Ca, continued

Depth in m	%	ng/Kg	2σ %	Fractions associated with aluminosilicates %
3192	7.84	951	15	6.3
3444	8.06	529	13	7.
3601	3.37	632	21	10.4
3841	1.38	985	10	6.7
4035	6.72	538	12	11.0
4221	5.23	747	20	9.4
4424	4.88	542	14	15.4
4633	5.85	355	20	15.3
4839	3.41	356	20	34.8
5051	1.79	234	32	59.7
5304	0.76	131	43	100.
5526	2.09	480	18	49.
5599	1.04	493	26	100.
5634	1.15	755	22	100.
5804	1.98	3072	32	100.

Table A.II.1: continued

GEOSECS station 67: particulate Al

Depth in m	ppm	ng/kg	2σ %	Fraction associated with aluminosilicates %
GEOSECS station 67 (44°58'S - 51°10'W); watercolumn: 5902 m				
10	0.37	395	4	100
42	0.17	218	3	"
62	1.50	190	8	"
102	0.55	354	2	"
151	0.38	93	5	"
199	0.68	173	5	"
251	0.74	227	4	"
300	0.55	138	3	"
353	0.70	179	7	"
405	0.73	150	2	"
445	0.50	115	8	"
445	0.82	150	3	
658	1.14	243	2	
760	1.42	153	2	
857	1.38	318	2	
953	1.08	153	9	
1053	0.74	144	2	
1127	1.44	131	2	
1316	1.68	178	2	
1438	1.16	230	5	
1499	1.86	258	2	
1590	1.28	170	5	
1741	0.64	87	10	
1959	1.97	155	19	
2193	2.14	263	2	
2392	1.46	158	2	
2574	2.02	210	2	
2758	0.84	153	8	
2982	1.85	174	2	

Table A.II.1: continued

GEOSECS station 67: particulate Al, continued

Depth in m	%	ng/Kg	2σ %	Fraction associated with aluminosilicates %
3192	1.75	212	2	100
3444	2.06	135	3	"
3601	1.26	237	5	"
2841	0.34	239	2	"
4035	2.69	215	2	"
4221	1.77	253	4	"
4424	2.70	303	2	
4633	3.22	196	3	
4839	4.32	448	3	
5051	3.87	506	3	
5304	6.00	1033	2	
5526	3.7	852	1	
5599	5.78	2754	11	
5634	4.85	3173	2	
5804	9.69	15031	4	

Table A.II.1: continued

GEOSECS station 67: particulate Mn

Depth in m	ppm	ng/Kg	2σ%	Fraction associated with aluminosilicates %
10	155	16.2	2	26.5
42	63	7.9	4	29.
62	60	7.5	1	28.8
102	117	7.5	2	53.7
151	199	5.3	1	19.8
199	211	5.4	1	36.8
251	253	7.8	1	30.
300	228	5.7	3	24.4
353	179	4.5	1	42.3
405	205	4.2	2	39.8
445	301	5.5	5	22.2
445	184	4.3	1	39.8
658	213	4.6	1	51.6
760	547	5.9	2	27.1
857	235	5.4	1	67.5
953	443	6.2	1	27.1
1053	182	3.5	1	43.7
1127	317	2.9	2	46.4
1316	291	3.1	1	63.0
1438	228	4.8	2	48.9
1499	296	4.1	1	68.5
1590	698	9.3	2	20.1
1741	215	2.9	1	30.8
1959	411	3.3	2	49.9
2193	406	5.0	1	55.9
2392	339	3.7	2	46.6
2574	387	4.2	1	58.4
2758	280	5.0	2	32.5
2982	494	4.1	1	46.2
3444	601	4.0	1	35.9

Table A.II.1: continued

GEOSECS station 67: particulate Mn, continued

Depth in m	ppm	ng/Kg	2σ%	Fraction associated with aluminosilicates %
3601	228	4.3	1	63.0
3841	66	4.7	1	54.0
4035	584	4.7	1	48.6
4221	516	7.4	2	36.3
4424	505	5.6	1	57.5
4633	959	5.8	1	34.7
4839	801	8.3	1	57.3
5051	897	11.7	1	44.8
5304	1059	18.2	1	61.0
5526	897	18.0	1	50.3
5599	563	26.8	1	100.
5634	1002	65.6	1	51.1
5804	911	141.3	1	100.

Table A.II.1: continued

GEOSECS station 67: particulate V

Depth in m	ppm	ng/Kg	2σ%	Fraction associated with aluminosilicates %
10	30	3.2	6	29.0
42	30	3.7	6	9.9
62	16	1.9	15	15.8
102	30	1.9	8	30.4
151	51	1.3	8	11.9
199	62	1.6	9	17.8
251	38	1.2	13	31.2
300	46	1.1	10	19.7
353	61	1.5	14	18.8
405	66	1.4	5	17.7
445	70	1.3	7	18.6
445	26	0.6	23	31.1
658	54	1.2	9	33.8
760	120	1.3	7	19.4
857	56	1.3	10	39.8
953	97	1.4	9	18.1
1053	33	0.6	10	36.0
1127	89	0.8	9	26.3
1316	60	0.6	13	48.2
1438	76	1.5	11	56.9
1499	56	0.8	11	53.8
1590	102	1.4	10	20.4
1741	21	0.3	99	50.8
1959	78	0.6	18	40.7
2193	73	0.9	12	47.5
2392	84	0.9	7	28.3
2574	81	0.9	10	39.7
2758	40	0.7	21	33.6
2982	91	0.9	8	32.8
3192	50	0.6	16	57.3
3444	140	0.9	9	23.9
3601	80	1.5	15	25.7

Table A.II.1: continued

GEOSECS station 67: particulate V, continued

Depth in m	ppm	ng/Kg	2σ%	Fraction associated with aluminosilicates %
3841	11	0.8	11	49.4
4035	11	0.6	80	54.6
4221	110	1.6	42	26.1
4424	93	1.0	10	47.9
4633	168	1.0	10	31.2
4839	100	1.0	13	70.0
5051	126	1.7	10	49.5
5304	138	2.4	10	70.5
5526	330	7.6	3	18.2
5599	190	13.8	7	32.4
5634	102	6.7	8	77.2
5804	183	18.3	12	86.2

Table A.II.1: continued

GEOSECS station 67: particulate Cu

Depth in m	ppm	ng/Kg	2σ%	Fraction associated with aluminosilicates %
10	190	20.0	55	1.
42	312	39.1	43	0.3
62	18	2.3	> 100	47.
102	112	7.2	37	2.8
151	833	20.7	15	0.3
199	1496	38.3	17	0.3
251	520	16.0	40	0.8
300	476	11.9	48	0.6
353	770	19.5	45	0.5
405	388	8.0	40	1.0
445	525	12.2	65	0.5
445	698	12.8	33	0.7
658	1059	22.7	24	0.6
760	684	7.3	50	1.2
857	969	22.3	27	0.8
953	716	10.1	31	0.8
1053	450	8.7	33	0.9
1127	1164	10.6	28	0.7
1316	920	9.7	35	1.0
1438	670	13.3	51	1.0
1499	327	4.5	88	3.2
1590	446	6.0	68	1.6
1741	322	4.4	100	1.1
1959	1042	8.3	59	1.1
2193	1432	17.6	26	1.1
2392	852	9.2	62	0.8
2574	1380	15.0	27	1.0
2578	630	11.4	65	0.7
2982	1399	13.1	32	0.7
3192	646	7.8 1	43	1.5
3444	766	5.0	25	1.5
3601	8735	163.7	8	0.1

Table A.II.1: continued

GEOSECS station 67: particulate Cu, continued

Depth in m	ppm	ng/Kg	2σ%	Fraction associated with aluminosilicates in %
3841	994	70.8	9	0.2
4035	8690	69.5	7	0.2
4221	1760	25.2	31	0.6
4424	2395	26.6	18	0.6
4633	1078	6.5	49	1.7
4839	3948	40.9	19	0.6
5051	1648	21.5	30	1.3
5304	855	14.7	44	3.9
5526	816	18.8	39	2.6
5599	702	33.4	57	4.6
5634	315	20.63	57	8.7
5804	539	83.5	100	10.1

The fractions associated with aluminosilicate material were estimated as follows : the composition of aluminosilicates is assumed to be at best approached by the one of shales, which contain (Turekian and Wedepohl, 1961):

shales:	Al:	80,000 ppm
	Sr:	300 "
	Ca:	22,000 "
	V:	130 "
	Cu:	45 "
	Mn:	850 "

The fraction of element X, carried by aluminosilicates is then given by:

$$\left[\frac{X_{shale}}{Al_{shale}} \cdot Al_{sample} \right] / X_{sample}$$

Table A.II.2: INAA data of particulate Al at GEOSECS stations 82; 58; 31; 27; 3; 17; 282; 310; 269; 257.

A. GEOSECS Atlantic Ocean cruises

Depth in m	%	ng/Kg	2σ%
GEOSECS station 82 (56°15'S - 24°55'W); Watercolumn: 7873 m			
1	0.08	66	5 %
28	0.16	156	5 %
47	0.10	88	5 %
82	*		
97	0.15	83	84 %
118	0.99	476	12 %
200	0.58	187	9 %
287	0.29	105	27 %
272	0.34	116	5 %
432	0.63		7 %
582	0.66	126	4 %
832	0.60	138	9 %
981	0.78	111	5 %
1180	0.83	75	10 %
1379	0.46	44	5 %
1577	0.71	70	8 %
1776	0.58	99	6 %
1986	1.36	320	13 %
2186	1.53	133	11 %
2386	1.55	170	7 %
2583	1.34	212	5 %
2789	1.65	192	4 %
3190	0.65	71	16 %
3390	0.76	156	10 %
3592	1.58	170	3 %
3783	2.38	158	7 %
3996	0.31	246	3 %

* Quantities within the blank error.

Table A.II.2: particulate Al, continued.

Depth in m	%	ng/kg	2σ %
GEOSECS station 82: continued			
4296	0.83	221	5
4598	1.82	211	3
4901	0.99	255	29
5202	1.02	207	6
5502	1.29	289	10
5797	1.60	255	4
6403	0.71	127	10
6502	2.12	408	5
GEOSECS station 58 (27°02'S - 37°00'W); Watercolumn: 4588 m			
197	1.22	115	5
278	0.97	84	8
1786	1.73	107	2
2085	1.12	140	5
3097	2.87	139	2
4422	4.27	1010	2

Table A.II.2: particulate Al, continued.

Depth in m	%	ng/Kg	2σ%
GEOSECS station 31 (27°00'N - 53°31'W); Watercolumn: 5979 m			
1	1.87	726	6
60	0.14	47	18
152	0.20	56	11
252	0.49	73	12
403	0.32	40	11
603	0.73	66	8
799	0.58	52	12
901	1.19	103	7
1003	1.11	80	10
1103	0.82	69	9
1303	0.61	71	6
1500	0.83	116	8
1900	0.82	108	10
2300	0.70	84	8
2700	1.04	150	7
3000	0.56	59	10
3500	0.65	58	13
3700	0.58	60	15
4100	0.07	15	26
4300	1.24	126	7
4701	4.25	155	8
5500	2.43	282	10
GEOSECS station 3 (51°01'N - 43°01'W); watercolumn: 4283 m			
28	0.19	280	11
105	1.43	290	10
274	2.10	234	10
377	0.86	130	11
464	3.00	470	11
575	2.10	365	10
813	4.45	280	11
1083	2.10	310	10
1376	1.10	200	10
1575	2.60	540	10

Table A.II.2: particulate Al, continued.

Depth in m	%	ng/Kg	2σ%
GEOSECS station 3, continued			
1875	2.20	290	10
2039	2.50	420	10
2356	2.50	320	9
2479	2.30	335	9
2696	2.60	340	9
2989	3.40	530	9
3267	2.40	350	10
3368	3.40	410	10
3630	3.60	840	10
4064	6.28	1220	5
4049	6.70	1990	8
4221	8.15	10300	5

Table A.II.2: particulate Al, continued.

B. GEOSECS Pacific Ocean Cruises

Depth in m	%	ng/Kg	2σ%
GEOSECS station 282 (57°35'S - 169°36'E); watercolumn: 5502 m			
2131	0.96	158	2
3034	1.14	155	5
3458	1.62	237	3
4134	1.77	207	4
5187	5.41	2264	10
GEOSECS station 310 (26°55'S - 157°11'W); watercolumn: 5454 m			
1557	0.76	85	6
2734	0.90	84	13
3049	0.57	61	10
3227	3.07	327	3
3310	0.43	58	25
3748	0.89	92	5
4489	0.71	109	9
4789	1.17	127	10
GEOSECS station 269 (23°59'S - 174°26'W); watercolumn: 6371 m			
1253	0.23	34	9
2897	0.67	65	6
3146	0.23	31	5
3342	0.58	76	5
3962	0.29	48	10
5172	1.72	662	9
5963	7.12	412	6
6193	6.66	453	1
6348	5.43	565	1

Table A.II.2: particulate Al, continued.

Depth in m	%	ng/Kg	2σ%
GEOSECS station 257 (10°10'S - 70°00'W); watercolumn: 5177 m			
1263	0.84	116	7
2464	0.62	41	5
2813	0.41	57	17
3486	0.42	76	36
3737	2.10	188	20
4234	0.73	118	1
4334	1.25	119	10
4480	1.05	175	10
4829	0.98	158	8
4999	-	153	4
5125	-	274	7
5158	0.89	159	5

Table A.II.3: INAA data of particulate Ca for GEOSECS stations 82, 58,27,3,17,282,310,269,257.

A. GEOSECS Atlantic Ocean Cruises

Depth in m	%	ng/Kg	2σ%
GEOSECS station 82 (56°15'S - 24°55'W); Watercolumn: 7873 m			
1	1.62	1292	24
28	1.36	1360	35
47	0.66	595	36
82	0.71	2975	15
97	< 1.41	< 800	
118	< 0.43	< 204	
200	2.31	765	34
287	< 0.51	< 187	
372	1.36	425	44
432	1.19	256	61
582	1.12	212	66
832	< 1.02	< 238	
981	< 0.34	< 238	
1180	*		
1379	< 0.39	< 39	
1577	< 0.20	< 20	
1776	*		
2186	1.80	170	67
2386	*		
2583	*		
2789	*		
3592	*		
3783	< 1.29	< 85	
3996	0.12	93	52
4296	< 0.37	< 102	
4598	< 0.51	< 76	
4901	2.81	731	58
5202	1.43	314	52
5502	*		

* Quantities within the blank error.

Table A.II.3: particulate Ca, continued.

Depth in m	%	ng/Kg sw	2σ %
GEOSECS station 82 (continued)			
5797	0.60	95	80
6502	1.19	230	60
GEOSECS station 58 (27°02'S - 37°00'W); Watercolumn: 4588 m			
197	12.30	1160	11
278	7.02	610	17
1786	7.33	450	15
2085	3.45	430	22
3097	7.63	370	18
4422	1.73	410	21
GEOSECS station 27 (42°00'N - 41°59'W); Watercolumn:			
801	3.6	527	22
1000	< 4.4	< 535	
1242	5.1	493	35
2630	8.2	722	23
3885	2.7	323	33
4678	5.4	654	27

Table A.II.3: particulate Ca, continued.

Depth in m	%	ng/Kg	2σ%
GEOSECS station 3 (51°01'N - 43°01'W); Watercolumn: 4283 m			
4191	12.97	6000	32
4150	14.33	5745	25
4111	11.19	4828	21
4064	9.91	1938	17
GEOSECS station 17 (74°56'W - 01°07'W); Watercolumn: 3740 m			
466	0.85	204	60
1198	0.5	153	74
1396	1.9	255	57
1497	1.2	255	65

Table A.II.3: particulate Ca, continued.

B. GEOSECS Pacific Ocean Cruises

Depth in m	%	ng/Kg	2σ%
GEOSECS station 282 (57°35'S - 169°36'E); Watercolumn: 5502 m			
2131	5.9	972	16
3034	6.1	833	22
3458	3.0	1333	15
4134	3.2	381	35
5187	4.1	1722	60
GEOSECS station 310 (26°55'S - 157°11'W); Watercolumn: 5454 m			
1557	12.8	1439	16
2734	4.0	376	42
3227	6.3	669	23
3310	5.1	690	31
3748	5.4	565	26
4489	2.2	336	40
GEOSECS station 269 (23°59'S - 174°26'W); Watercolumn: 6371 m			
1253	3.6	552	28
2897	3.1	302	47
3342	2.2	301	60
5172	0.8	318	34
5963	2.5	145	54
6193	1.5	102	50
6348	1.1	113	49

Table A.II.3: particulate Ca, continued.

Depth in m	%	ng/Kg	2σ%
GEOSECS station 257 (10°10'S - 170°00'W): Watercolumn: 5177 m			
1263	1.67	231.0	30
2464	2.59	171.8	32
2813	0.73	101.2	54
3486	1.23	220.9	30
3737	5.40	489.0	30
4234	1.70	276.3	29
4334	✖		
4480	< 0.53	< 161.0	
4829	✖		
4999	0.60	137.0	66
5125	0.65	165.0	53
5158	< 0.51	< 90.6	

✖ Quantities within the blank error.

APPENDIX III

GEOSECS shipboard and shore-based collected data for station 67: dissolved phosphate, silica, nitrate, oxygen; potential temperature; salinity; total carbon dioxide (titration and gas chromatography); alkalinity (titration); sea water density; argon, nitrogen (gas chromatography) and total suspended matter.

TABLE A.III.1

DATA REPORT

R/V KNORR — GEOSECS LEG VI — STATION NIS 67

POSITION 44 58.5S 51 0.0W — FIRST CAST 1942 9 DEC 72 — DEPTH 5902 CORR.M

STATION -CAST	BOTTLE NUMBER	DEPTH M	TEMP DEG C	POT TEMP DEG C	SALINITY 0/00	SIGMA THETA	SIGMA Z	SIGMA 4	OXYGEN µM/KG	SIL µM/KG	PO4 µM/KG	NO3 µM/KG	ALK(T) µ EQ/KG	CO2(T) µM/KG	CO2(GC) µM/KG	PRESS D.BAR
72 4	1	10	11.980	11.987	34.561	26.288	26.333	43.392	298	0.4	0.55	5.0	2300	2041	2020	10
72 4	2	42	9.956	9.951	34.593	26.602	26.873	43.949	320	0.4	0.60	6.3	2300	2017	2022	42
72 4	3	62	9.483	9.476	34.625	26.787	27.069	44.093	286	0.7	0.03	9.3	2301	2068	2051	62
72 4	4	102	9.269	9.258	34.631	26.828	27.291	44.152	283	2.5	0.89	10.5	2300	2068	2067	102
72 4	5	151	8.620	8.604	34.631	26.933	27.624	44.312	274	3.9	1.02	13.6	2297	2095	2075	152
72 4	6	199	7.871	7.851	34.579	27.006	27.920	44.454	276	4.5	1.11	15.1	2297	2091	2078	200
72 4	7	251	5.829	5.807	34.311	27.072	28.240	44.716	263	8.1	1.53	21.8	2280	2122	2111	253
72 4	8	300	5.058	5.034	34.223	27.095	28.494	44.816	274	10.1	1.68	24.1	2286	2130	2114	302
72 4	9	353	4.535	4.508	34.185	27.123	28.776	44.897	272	11.5	1.75	25.0	2282	2125		356
72 4	10	405	4.290	4.260	34.183	27.147	29.044	44.946	274	13.1	1.76	25.3	2285	2125	2126	408
72 4	11	445	4.139	4.106	34.178	27.159	29.247	44.974	270	14.6	1.81	26.2	2283	2143	2124	449
72 4	12	445	4.139	4.106	34.178	27.159	29.247	44.974	273	14.8	1.82	26.2	2282	2136	2119	449
72 4	15	559	3.692	3.652	34.184	27.209	29.835	45.070	264	19.6	1.89	27.4	2287	2159	2133	564
72 4	16	659	3.410	3.364	34.194	27.244	30.337	45.134	254	24.0	1.99	28.7	2297	2161	2147	664
72 4	17	760	3.154	3.102	34.229	27.296	30.869	45.212	242	30.8	2.08	30.1	2299	2186	2164	767
72 4	18	857	2.972	2.914	34.271	27.346	31.375	45.281	226	37.4	2.17	31.4	2310	2190	2181	865
72 4	19	953	2.871	2.806	34.311	27.388	31.870	45.332	216	42.9	2.23	32.3	2305	2213	2185	963
72 4	20	1053	2.620	2.549	34.337	27.430	32.383	45.401	213	48.3	2.28	32.9	2320	2204	2200	1064
72 4	21	1127	2.690	2.613	34.390	27.467	32.757	45.429	201	53.0	2.30	33.1	2318	2227	2206	1138
72 4	22	1316	2.579	2.488	34.461	27.550	33.722	45.523	188	63.2	2.33	33.6	2340	2235	2227	1330
72 4	23	1438	2.621	2.520	34.545	27.599	34.329	45.566	164	65.8	2.30	33.1	2335	2250	2224	1453
72 1	1	1499	2.578	2.472	34.565	27.619	34.632	45.590	183	69.5	2.33	33.4	2335	2248	2197	1515
72 4	24	1590	2.718	2.602	34.619	27.651	35.076	45.607	185	65.5	2.21	32.0	2339	2235		1607
72 1	2	1741	2.554	2.427	34.642	27.684	35.813	45.658	183	74.2	2.26	32.5	2357	2242	2211	1761
72 1	3	1959	2.554	2.408	34.699	27.731	36.856	45.705	169	74.0	2.13	31.2	2346	2247	2223	1982
72 1	4	2193	2.758	2.566	34.788	27.787	37.966	45.739	208	61.5	1.92	27.9	2341	2223	2202	2220
72 1	5	2392	2.767	2.576	34.825	27.818	38.699	45.770	220	56.6	1.80	26.1	2346	2219	2189	2423
72 1	6	2574	2.605	2.399	34.830	27.836	39.750	45.807	222	58.5	1.77	25.9	2340	2214	2183	2608
72 1	7	2759	2.486	2.263	34.829	27.847	40.600	45.832	226	61.3	1.76	25.9	2345	2221	2184	2796
72 1	8	2902	2.199	1.960	34.802	27.849	41.626	45.867	217	72.7	1.88	27.3	2349	2223	2213	3023
72 1	9	3192	1.925	1.671	34.779	27.852	42.597	45.903	213	83.9	1.96	28.5	2353	2243	2213	3238
72 1	10	3444	1.599	1.327	34.751	27.854	43.759	45.943	209	97.9	2.08	30.1	2356	2239	2222	3496
72 1	11	3601	1.303	1.100	34.729	27.852	44.476	45.966	211	106.8	2.16	31.2	2361	2260	2225	3656
72 1	12	3601	1.303	1.100	34.730	27.852	44.477	45.967	207	107.5	2.16	31.1	2364	2242	2243	3656
72 1	15	3841	1.167	0.865	34.717	27.857	45.575	45.998	207	115.6	2.20	31.6	2360	2267	2225	3902
72 1	16	4035	0.944	0.627	34.706	27.863	46.467	46.031	212	117.5	2.23	31.8	2365	2255	2246	4101
72 1	17	4221	0.755	0.424	34.696	27.866	47.323	46.058	215	120.4	2.24	32.1	2363	2271	2223	4293
72 1	18	4424	0.503	0.235	34.687	27.869	48.230	46.083	218	126.6	2.27	32.3	2365	2251	2240	4500
72 1	19	4633	0.422	0.056	34.676	27.870	49.182	46.104	221	126.2	2.28	32.5	2365	2275	2226	4715
72 1	20	4839	0.330	-0.057	34.673	27.873	50.104	46.120	224	126.4	2.29	32.6	2366	2258	2241	4927

TABLE A.III.1: continued

DATA REPORT

R/V KNORR — GEOSECS LEG VI — STATION NIS 67 (CONT)

POSITION 44 50.5S 51 0.0W — FIRST CAST 1942 9 DEC 72 — DEPTH 5902 CORR.M

STATION -CAST	BOTTLE NUMBER	DEPTH M	TEMP DEG C	POT TEMP DEG C	SALINITY 0/00	SIGMA THETA	SIGMA Z	SIGMA 4	OXYGEN µM/KG	SIL µM/KG	PO4 µM/KG	NO3 µM/KG	ALK(T) µ EQ/KG	CO2(T) µM/KG	CO2(GC) µM/KG	PRESS D.BAR
72 1	21	5051	0.273	-0.138	34.669	27.874	51.041	46.130	225	128.0	2.31	32.6	2364	2280	2231	5145
72 1	22	5304	0.273	-0.169	34.667	27.874	52.139	46.134	226	128.4	2.30	32.6	2367	2258	2223	5404
72 7	15	5526	0.259	-0.210	34.671	27.879	53.116	46.144	226	128.6	2.31	32.9				5634
72 7	16	5599	0.260	-0.219	34.667	27.876	53.428	46.142	226	128.6	2.33	33.2				5709
72 1	23	5634	0.261	-0.222	34.665	27.875	53.586	46.141	227	129.4	2.31	32.8	2366	2273	2233	5747
72 7	17	5666	0.259	-0.228	34.665	27.875	53.721	46.142	226	129.5	2.32	33.1				5779
72 7	18	5701	0.263	-0.229	34.668	27.878	53.873	46.145	226	128.8	2.32	33.2				5815
72 7	19	5733	0.260	-0.229	34.667	27.877	54.010	46.144	226	129.1	2.33	33.2				5848
72 7	20	5764	0.272	-0.229	34.660	27.878	54.144	46.145	218	127.5	2.31	33.3				5880
72 7	21	5780	0.275	-0.228	34.667	27.877	54.210	46.144	226	128.0	2.32	33.2				5896
72 7	22	5798	0.276	-0.229	34.666	27.876	54.288	46.143	226	127.8	2.33	33.2				5915
72 1	24	5804	0.271	-0.235	34.666	27.876	54.315	46.144	227	129.8	2.31	32.8	2369	2259	2234	5921
72 7	23	5810			34.669				226	127.3	2.32	33.2				5927
72 7	24	5821	0.279	-0.230	34.667	27.877	54.389	46.144	226	126.5	2.31	33.1				5939

TABLE A.III.2

SUPPLEMENTARY CARBONATE CHEMISTRY REPORT FOR STATION 67

CAST	SAMP	DEPTH M	MEASURED PARAMETERS TITALK EQ/KG (E-3)	TITCO2 M/KG (E-3)	PCO2 ATM (E-4)	CALCULATED PARAMETERS P=1 ATM, T=INSITU PCO2 ATM (E-4)	CO2 M/KG (E-5)	HCO3 M/KG (E-3)	CO3 M/KG (E-4)	CARBALK EQ/KG (E-3)	PH	CALCULATED PARAMETERS P AND T=INSITU CO2 M/KG (E-5)	HCO3 M/KG (E-3)	CO3 M/KG (E-4)	PH	SFC	SFA
4	1	9.	2.300	2.041		2.908	1.196	1.845	1.839	2.213	8.252	1.196	1.845	1.839	8.252	3.008	1.855
4	2	41.	2.300	2.017		2.360	1.035	1.807	1.987	2.205	8.318	1.035	1.808	1.986	8.317	3.165	1.962
4	3	61.	2.301	2.068		3.005	1.339	1.887	1.666	2.221	8.228	1.337	1.888	1.665	8.227	2.633	1.634
4	4	101.	2.300	2.068		2.991	1.342	1.888	1.659	2.220	8.229	1.340	1.888	1.656	8.226	2.598	1.614
4	5	150.	2.296	2.095		3.432	1.573	1.932	1.469	2.226	8.174	1.570	1.932	1.466	8.170	2.266	1.411
4	6	190.	2.296	2.091		3.243	1.525	1.926	1.492	2.224	8.191	1.520	1.926	1.487	8.186	2.266	1.414
4	7	250.	2.290	2.122		3.890	1.966	1.982	1.193	2.221	8.109	1.958	1.983	1.188	8.103	1.760	1.104
4	8	299.	2.286	2.130		3.819	1.944	1.991	1.182	2.228	8.113	1.974	1.992	1.176	8.105	1.715	1.078
4	9	353.	2.282	2.125		3.694	1.955	1.986	1.185	2.224	8.125	1.944	1.987	1.178	8.113	1.695	1.067
4	10	404.	2.285	2.125		3.593	1.918	1.985	1.203	2.226	8.132	1.905	1.986	1.195	8.121	1.701	1.072
4	11	445.	2.283	2.143		4.063	2.181	2.012	1.086	2.229	8.084	2.166	2.013	1.077	8.071	1.521	0.960
4	12	445.	2.282	2.136		3.501	2.094	2.002	1.120	2.227	8.099	2.079	2.004	1.111	8.087	1.570	0.990
4	15	559.	2.287	2.156		4.337	2.365	2.033	1.017	2.237	8.056	2.345	2.034	1.007	8.040	1.390	0.879
4	16	650.	2.296	2.161		4.085	2.250	2.031	1.044	2.244	8.079	2.227	2.033	1.032	8.061	1.426	0.903
4	17	759.	2.299	2.166		4.752	2.641	2.065	0.935	2.253	8.019	2.611	2.067	0.922	7.997	1.227	0.778
4	18	856.	2.305	2.190		4.524	2.530	2.067	0.976	2.262	8.039	2.498	2.068	0.960	8.014	1.256	0.798
4	19	953.	2.305	2.213		5.507	3.090	2.099	0.824	2.264	7.959	3.049	2.101	0.808	7.931	1.040	0.662
4	20	1053.	2.320	2.204		4.620	2.616	2.082	0.955	2.273	8.030	2.575	2.084	0.936	7.999	1.182	0.754
4	21	1126.	2.318	2.227		5.559	3.139	2.113	0.821	2.277	7.956	3.089	2.115	0.803	7.923	1.003	0.640
4	22	1316.	2.340	2.235		5.071	2.873	2.116	0.900	2.296	7.996	2.818	2.119	0.877	7.957	1.061	0.679
4	23	1437.	2.335	2.250		5.877	3.324	2.137	0.794	2.296	7.936	3.259	2.140	0.771	7.893	0.915	0.586
1	1	1490.	2.335	2.248		5.781	3.275	2.134	0.804	2.295	7.942	3.207	2.137	0.780	7.898	0.916	0.587
4	24	1589.	2.339	2.235		5.151	2.902	2.116	0.894	2.295	7.990	2.835	2.119	0.866	7.943	1.005	0.645
1	2	1741.	2.356	2.242		4.787	2.712	2.119	0.950	2.310	8.021	2.642	2.122	0.926	7.970	1.046	0.673
1	3	1958.	2.346	2.247		5.337	3.022	2.129	0.869	2.303	7.975	2.939	2.134	0.835	7.918	0.911	0.587
1	4	2192.	2.341	2.223		4.697	2.639	2.099	0.970	2.293	8.026	2.554	2.104	0.929	7.962	0.978	0.632
1	5	2392.	2.346	2.218		4.434	2.490	2.091	1.021	2.296	8.049	2.401	2.097	0.975	7.980	0.994	0.644
1	6	2574.	2.340	2.214		4.416	2.495	2.087	1.015	2.290	8.049	2.400	2.093	0.964	7.974	0.953	0.619
1	7	2758.	2.345	2.221		4.469	2.535	2.095	1.003	2.296	8.044	2.432	2.101	0.951	7.964	0.911	0.593
1	8	2961.	2.348	2.223		4.362	2.501	2.096	1.015	2.299	8.053	2.391	2.103	0.957	7.965	0.882	0.576
1	9	3191.	2.353	2.243		4.829	2.797	2.122	0.927	2.307	8.012	2.670	2.129	0.869	7.917	0.772	0.506
1	10	3444.	2.356	2.239		4.538	2.660	2.115	0.965	2.308	8.035	2.528	2.123	0.901	7.933	0.765	0.503
1	11	3600.	2.361	2.260		5.051	2.985	2.142	0.880	2.318	7.992	2.836	2.149	0.817	7.884	0.674	0.445
1	12	3600.	2.364	2.242		4.363	2.578	2.116	0.995	2.315	8.051	2.443	2.124	0.926	7.944	0.765	0.504
1	15	3840.	2.360	2.267		5.301	3.158	2.151	0.837	2.319	7.971	2.994	2.159	0.772	7.856	0.611	0.405
1	16	4034.	2.365	2.255		4.656	2.796	2.134	0.928	2.319	8.022	2.630	2.143	0.854	7.902	0.654	0.434
1	17	4222.	2.363	2.270		5.253	3.177	2.155	0.832	2.322	7.973	2.998	2.164	0.780	7.845	0.563	0.375
1	18	4423.	2.365	2.251		4.454	2.711	2.128	0.949	2.318	8.038	2.542	2.138	0.867	7.905	0.620	0.414
1	19	4633.	2.365	2.275		5.260	3.221	2.160	0.821	2.324	7.971	3.025	2.170	0.743	7.830	0.513	0.343
1	20	4839.	2.366	2.257		4.598	2.825	2.138	0.916	2.321	8.024	2.636	2.148	0.820	7.878	0.552	0.370
1	21	5050.	2.364	2.280		5.462	3.364	2.167	0.790	2.325	7.954	3.145	2.177	0.707	7.800	0.455	0.306
1	22	5302.	2.367	2.257		4.557	2.806	2.137	0.921	2.322	8.027	2.602	2.149	0.825	7.867	0.509	0.343
1	23	5634.	2.366	2.273		5.111	3.149	2.157	0.837	2.325	7.981	2.917	2.169	0.740	7.809	0.432	0.293
1	24	5803.	2.369	2.259		4.530	2.789	2.138	0.927	2.323	8.030	2.569	2.151	0.821	7.854	0.466	0.317

TABLE A.III.3

ARGON / NITROGEN SUMMARY FOR STATION 67

SAMPLE	DEPTH	SALINITY	POTENTIAL TEMPERATURE	ARGON CONCEN-TRATION ML/KG	ARGON SOLUBILITY ML/KG	ARGON PER CENT SUPER-SATURATION	NITROGEN CONCEN-TRATION ML/KG	NITROGEN SOLUBILITY ML/KG	NITROGEN PER CENT SUPER-SATURATION
401	10	34.561	11.906	0.3000	0.2889	3.82	11.34	10.72	5.63
402	42	34.593	9.951	0.3115	0.3015	3.30	11.71	11.14	5.09
404	102	34.631	9.257	0.3103	0.3060	1.40	11.73	11.29	3.86
405	151	34.631	8.603	0.3182	0.3104	2.51	11.86	11.44	3.81
406	199	34.579	7.850	0.3269	0.3157	3.53	12.31	11.63	5.89
407	251	34.311	5.807	0.3316	0.3314	0.05	12.50	12.16	2.79
408	300	34.225	5.033	0.3422	0.3376	1.33	12.73	12.37	2.87
410	405	34.183	4.259	0.3434	0.3440	-0.18	12.67	12.59	2.22
411	845	34.178	4.105	0.3513	0.3453	1.73	13.02	12.63	3.05
412	445	34.178	4.105	0.3602	0.3456	4.30	13.17	12.63	4.24
415	559	34.184	3.651	0.3492	0.3490	0.02	13.11	12.76	2.72
416	656	34.194	3.363	0.3571	0.3515	1.58	13.25	12.84	3.16
417	760	34.229	3.101	0.3612	0.3536	2.12	13.34	12.92	3.26
418	857	34.271	2.913	0.3624	0.3551	2.02	13.44	12.97	3.64
419	953	34.311	2.805	0.3615	0.3560	1.53	13.42	13.00	3.27
420	1053	34.337	2.549	0.3683	0.3582	2.81	13.54	13.07	3.60
421	1127	34.390	2.613	0.3620	0.3575	1.25	13.48	13.04	3.34
422	1316	34.481	2.468	0.3694	0.3583	3.07	13.63	13.07	4.26
423	1438	34.545	2.515	0.3665	0.3579	2.40	13.61	13.06	4.24
101	1499	34.565	2.471	0.3633	0.3562	1.40	13.56	13.07	3.91
102	1741	34.642	2.427	0.3643	0.3584	1.62	13.52	13.07	3.41
103	1959	34.699	2.407	0.3645	0.3584	1.67	13.54	13.07	3.57
104	2193	34.768	2.366	0.3620	0.3566	1.49	13.48	13.01	3.61
105	2392	34.825	2.575	0.3592	0.3566	0.71	13.47	13.01	3.53
106	2574	34.830	2.398	0.3636	0.3582	1.50	13.46	13.06	3.20
107	2758	34.829	2.263	0.3642	0.3594	1.33			
108	2962	34.802	1.959	0.3613	0.3622	-0.25	13.63	13.20	3.27
109	3192	34.779	1.670	0.3690	0.3649	1.12	13.73	13.29	3.31
110	3444	34.751	1.326	0.3716	0.3682	0.93	13.80	13.40	2.98
111	3601	34.729	1.100	0.3731	0.3703	0.74	13.86	13.47	2.86
112	3601	34.730	1.100	0.3708	0.3703	0.12	13.91	13.47	3.23
115	3841	34.717	0.864	0.3779	0.3725	1.42	13.94	13.55	2.87
116	4035	34.706	0.627	0.3732	0.3748	-0.44	14.02	13.63	2.87
117	4221	34.696	0.423	0.3793	0.3768	0.64	14.15	13.70	3.31
118	4424	34.687	0.234	0.3827	0.3787	1.04	14.18	13.76	3.05
119	4633	34.676	0.055	0.3806	0.3805	0.01	14.23	13.82	2.96
120	4839	34.673	-0.057	0.3758	0.3816	-1.53	14.22	13.86	2.60
121	5051	34.669	-0.157	0.3831	0.3824	0.16	14.25	13.89	2.62
122	5304	34.667	-0.168	0.3837	0.3827	0.23	14.27	13.90	2.68
123	5654	34.665	-0.222	0.3853	0.3833	0.51	14.33	13.91	2.96
124	5804	34.666	-0.265	0.3861	0.3834	0.69	14.36	13.92	3.31

Table A.III.4 : GEOSECS station 67 : Volumes of filtered sea water and weight of total suspended matter

Depth in m	Weight of filtered water volume : Kg	Suspended matter weight µg/ Kg sw
10	5669.7	104.9
42	4686.9	125.4
62	8438.4	125.3
102	9186.0	63.8
151	9219.5	24.8
199	9676.1	25.6
251	5846.2	31.9
300	9129.5	25.1
353	9383.8	25.4
405	9436.5	20.7
445	9672.9	18.4
445	9561.8	23.2
559	8926.3	18.1
658	8311.2	21.4
760	9126.6	10.7
857	9649.2	23.0
953	4795.7	14.1
1053	9642.3	19.4
1127	8020.7	9.1
1316	8395.0	10.6
1438	9080.6	19.9
1499	9643.7	13.9
1590	7780.3	13.4
1741	7393.0	13.7
1959	9724.1	8.0
2193	9509.9	12.3
2392	8859.3	10.8
2574	9911.0	10.9
2758	8758.4	18.2
2982	9478.3	9.4
3192	7005.7	12.1
3444	9745.2	6.6
3601	10113.8	6.4
3601	6777.5	18.7
3841	9125.7	71.2
4035	9127.7	8.00
4221	5455.4	14.3
4424	9550.9	11.1
4633	9878.1	6.6
4839	9714.9	10.4
5051	9325.8	13.1
5304	9472.5	17.2
5526	7657.1	23.0
5599	8486.4	47.6
5634	9858.9	65.4
5804	4501.3	155.0

APPENDIX IV

FACTOR ANALYSIS: Results for the GEOSECS station 67 profile

In this study factor analysis is performed with a somewhat hybrid method. It consists in the utilisation of a "truncated" principal factor solution (Herbosch, 1975). Although less rigorous it is the most usual method utilized by the geochemists (Spencer et.,1968; Cameron, 1967; Herbosch[☆], 1975). In practice the application of the method implies:

1° Log-transformation of the variables

2° Calculation of a correlation matrix of the reduced variables

3° Diagonalization of the correlation matrix and extraction of the eigenvalues and eigenvectors, to produce a matrix of principal components.

4° Arbitrary selection of the number of factors; the selected factors are those with eigenvalues larger than 0.8 (Herbosch, 1975; Cameron, 1968); this truncated principal components matrix gives a good estimation of the principal factor matrix.

5° The rotation of the principal factors, to achieve "simple structure" (Harman, 1967); in this case an orthogonal rotation by the VARIMAX criterion (Kaiser, 1958) was utilized.

6° The factor scores are calculated following the approximative method of the "ideal variables" (Harman, 1967). Factor scores are expressed in reduced values.

[☆] Herbosch compared this method with factor analysis sensu strictu an concluded that the results obtained by both methods are in agreement.

In total, 15 variables and 41 samples were considered (= complete profile). The correlation matrix and the principal components matrix are presented in Tables A.IV.1 and A.IV.2 . In the latter matrix, 4 factors have eigenvalues larger than 0.8 and were selected. They constitute the principal factor matrix. Rotation of these factors, following the VARIMAX criterion, produces a VARIMAX matrix (Table A.IV.3 and Table A.IV.4).

TABLE A.IV.1:

GEOSECS station 67 (Argentine Basin)

Complete profile: correlation matrix for 41 samples

(All data Log-transformed)

	mean	st. dev.	BA	SR	CA	AL	V	CU	TSM	MN	CALK	SAL	TPOT	SIL
BA	.157E+01	.220E+00	1.000	.155	.558	.314	.273	.008	.464	.277	-.415	-.537	.235	-.276
SR	.119E+01	.387E+00	.155	1.000	.587	-.364	-.118	-.384	.390	-.231	-.802	-.420	.749	-.879
CA	.295E+01	.315E+00	.558	.587	1.000	-.074	.180	-.058	.543	-.034	-.746	-.472	.653	-.706
AL	.242E+01	.431E+00	.314	-.364	-.074	1.000	.836	.442	.541	.887	.443	.249	-.665	.365
V	.123E+00	.393E+00	.273	-.118	.180	.836	1.000	.368	.582	.870	.140	.062	-.430	.077
CU	.118E+01	.374E+00	.008	-.384	-.058	.442	.368	1.000	.212	.320	.302	.170	-.427	.339
TSM	.128E+01	.323E+00	.464	.390	.543	.541	.582	.212	1.000	.558	-.267	-.098	.081	-.410
MN	.823E+00	.366E+00	.277	-.231	-.034	.887	.870	.320	.558	1.000	.320	.182	-.597	.228
CALK	.336E+01	.741E-02	-.415	-.802	-.746	.443	.140	.302	-.267	.320	1.000	.691	-.877	.921
SAL	.154E+01	.270E-02	-.537	-.420	-.472	.249	.062	.170	-.098	.182	.691	1.000	-.441	.432
TPOT	.456E+00	.333E+00	.235	.749	.653	-.665	-.430	-.427	.081	-.597	-.877	-.441	1.000	-.851
SIL	.162E+01	.550E+00	-.276	-.879	-.706	.365	.077	.339	-.410	.228	.921	.432	-.851	1.000
PO4	.286E+00	.114E+00	-.077	-.777	-.582	.267	.019	.231	-.414	.140	.725	.043	-.721	.909
NO3	.144E+01	.132E+00	-.057	-.783	-.563	.224	-.013	.240	-.449	.101	.693	.023	-.683	.900
O2	.236E+01	.573E-01	.298	-.633	.594	-.036	.242	.019	.460	.121	-.755	-.445	.433	-.760

	mean	st.dev.	PO4	NO3	O2
BA	.157E+01	.220E+00	-.077	-.057	.298
SR	.119E+01	.387E+00	-.777	-.783	.633
CA	.295E+01	.315E+00	-.582	-.563	.594
AL	.242E+01	.431E+00	.267	.224	-.036
V	.123E+00	.393E+00	.019	-.013	.242
CU	.118E+01	.374E+00	.231	.240	.019
TSM	.128E+01	.323E+00	-.414	-.449	.460
MN	.823E+00	.366E+00	.140	.101	.121
CALK	.336E+01	.741E-02	.725	.693	-.755
SAL	.154E+01	.270E-02	.043	.023	-.445
TPOT	.456E+00	.333E+00	-.721	-.683	.433
SIL	.162E+01	.550E+00	.909	.900	-.760
PO4	.286E+00	.114E+00	1.000	.995	-.716
NO3	.144E+01	.132E+00	.995	1.000	-.700
O2	.236E+01	.573E-01	-.716	-.700	1.000

TABLE A.IV.2:

GEOSECS station 67 (Argentine Basin)

Complete profile: Principal components matrix

factors	1	2	3	4	5	6	7	8	9	10	11	12
eigen-values	7.01	3.81	1.66	.82	.63	.35	.30	.16	.11	.08	.04	.03
% tot. var.	46.7	25.4	11.1	5.5	4.2	2.3	2.0	1.1	.7	.6	.2	.2
cumulated %	46.7	72.1	83.2	88.7	92.9	95.2	97.2	98.3	99.0	99.5	99.8	99.9
BA	.327	-.492	.655	.154	-.296	-.210	.238	-.047	.072	.006	-.051	-.033
SR	.890	.003	-.122	.118	.119	.325	.038	-.095	.220	.005	-.023	.006
CA	.765	-.326	.233	-.096	-.301	-.021	-.339	.169	.088	.017	.043	-.011
AL	-.429	-.866	-.026	.123	-.043	-.013	.059	-.046	.038	-.169	.097	.054
V	-.144	-.905	-.060	.066	.167	-.060	-.290	-.156	-.036	-.049	-.090	-.025
CU	-.353	-.439	-.016	-.805	-.111	.061	.065	-.107	.028	.037	.011	-.008
TSM	.369	-.800	-.098	.055	-.217	.336	.110	.126	-.144	-.002	-.048	.009
MN	-.304	-.881	-.086	.208	.159	-.049	.020	-.014	.011	.220	.053	.022
CALK	-.958	-.019	-.224	.075	-.103	.062	.013	.060	.050	-.006	-.006	-.067
SAL	-.508	.010	-.776	.054	-.322	-.145	.010	.030	.073	.015	-.054	.041
TPOT	.895	.331	.076	-.006	-.218	-.031	-.061	-.135	-.063	.033	-.013	.083
SIL	-.982	.054	.110	-.025	-.036	.014	-.031	.059	.077	.003	-.049	.049
PO4	-.864	.100	.469	.023	.054	.129	-.052	.032	.010	-.001	-.003	.014
NO3	-.845	.129	.500	-.016	.042	.081	-.052	.031	.015	.021	-.040	.057
O2	.752	-.377	-.054	-.233	.392	-.171	.096	.193	.040	-.035	-.047	.034

factors	13	14	15
eigen-values	.00	.00	.00
% tot. var.	.0	.0	.0
cumulated %	100.0	100.0	100.0
BA	.001	-.001	.000
SR	.003	-.000	-.000
CA	.001	-.001	-.000
AL	.001	.004	-.001
V	.000	.001	.000
CU	.002	.000	.000
TSM	-.003	-.002	.000
MN	-.002	.003	.000
CALK	-.001	.038	-.002
SAL	.023	-.008	.003
TPOT	-.006	.028	.001
SIL	-.053	-.005	.000
PO4	.018	.004	.013
NO3	.031	-.000	-.009
O2	.005	.014	.001

TABLE A.IV.3:

GEOSECS station 67 (Argentine Basin)

Complete profile

VARIMAX factor matrix contributing for 88.7 % of the total variance

	factors	1	2	3	4
sum of	squares	6.020	3.700	2.490	1.095
.801	BA	.090	-.371	.805	.080
.821	SR	.838	.123	.222	.233
.756	CA	.651	-.118	.560	-.066
.950	AL	-.255	-.930	-.029	-.140
.848	V	.025	-.904	.056	-.165
.966	CU	-.175	-.278	-.059	-.925
.789	TSM	.486	-.712	.195	-.084
.920	MN	-.124	-.949	-.035	-.045
.973	CALK	-.774	-.237	-.561	-.060
.863	SAL	-.149	-.183	-.899	-.015
.917	TPOT	.724	.486	.346	.190
.986	SIL	-.933	-.110	-.279	-.142
.976	PO4	-.982	-.018	.082	-.068
.981	NO3	-.979	.027	.113	-.096
.764	O2	.774	-.165	.305	-.212

Factors 2 and 4 in Table A.IV.3 are discussed below (see also Table II.2 and Figure II.2 in part II).

Factor 2 (24.7 % of the total variance) has high negative loadings for Al_p, V_p, Mn_p, TSM, a significant negative loading for Ba_p and a positive loading for Tpot.
Analyses of North Atlantic sediments revealed that the lithogenous fraction (= fraction of sediments that remains after removal of the ferro-manganese minerals, the carbonate minerals and the adsorbed elements) contributed for 71 %* of the total V concentration and for 32 %* of the total Mn concentration and has a continental, detritic origin (Chester and Messiha-Hanna, 1970). It appears that most of the V is of continental origin. Mn is known to precipitate in sea water in the oxide form (Spencer and Brewer, 1971; Chester and Messiha-Hanna, op.cit.), but it may also enter the oceans in the particulate oxide form by river discharge (Chester and Messiha-Hanna, op.cit.). At station 67 we observed, for the watercolumn above the nepheloid layer, that in the mean 44% of the total Mn_p content is accounted for by aluminosilicates (see Table A.II.1; appendix A.II). This is in accord with Chester and Messiha-Hanna's data for pelagic sediments. The distribution of the important non-detritic fraction of total Mn_p, has been documented by Chesselet and Lambert (1977). In regions characterized by the presence of a nepheloid layer, these authors observed lower Al/Mn ratios in suspended matter in in surface and

intermediate waters, as compared to bottom waters, where the Al_p/Mn_p ratios are close to those of shales. The non-detritic Mn-vectors were identified by SEM-EMP to consist of $CaCO_3$ debris, particulate organics and iron hydroxides (Chesselet and Lambert, op.cit.).

Our data show 32% of the total V_p content to be accounted for by aluminosilicates. This is lower than observed by Messiha-Hanna for the detritic fraction of pelagic sediments (see above). No information is available concerning the identity of the other V_p-vectors.The strong correlation between V and Al (Table A.IV.1, suggests some kind of association with the aluminosilicate materials ; scavenging of V-rich particulates, or adsorbtion of V from solution can be possible processes.

The significant factor loading for Ba_p is likely to result from the important part of the total Ba_p content that is carried by the aluminosilicates in the bottom waters.

The siginificant loading for TSM on factor 2, points to the fact that aluminosilicates and associated phases represent an important part of the TSM.

Factor 2 is proposed to represent the input of detritic, continental matter in the xatercolumn, as well as the resuspension of sediments.

Factor 4:(7.3% of the total variance) is a one element factor, with a high negative loading for Cu_p. Turekian and Imbrie (1966) analyzed deep-sea cores from the Atlantic Ocean and observed a correlation between carbonate and Cu. They assumed Cu to be extracted from sea water and to become associated and preserved with carbonate fraction. Buat-Menard and Chesselet (1979) observed an enrichment of Cu in oceanic suspended matter, relative to the earth crust, and an apparent independency of the Cu_p concentrations towards atmospheric input. These results suggest an involvement of Cu_p in the biological cycle. From the study of the dissolved Cu profile, Boyle et al. (1977) concluded that that Cu was scavenged in surface and deep water and was released again at the sediment-water interface. An additional process that influences the distribution of particulate Cu in the watercolumn is anthropogenic input of Cu to the oceans, as shown by Jedwab (1979). Jedwab showed , from an investigation of GEOSECS suspended matter samples, that Cu_p occurs as a series of mineralogical phases, distinct from the terrigenic and the biogenic suspended fractions: copper and copper-zinc (brass) particles, copper oxide (tenorite, paratenorite), copper carbonate (malachite) and copper enriched lead hydroxychloride (laurionite) . Metallic copper and especially brass can be assigned a technological origin; while the other compounds can be atmospheric and marine alteration products of copper artifacts (Jedwab, op.cit.). This possibility is emphasized by the higher frequencies of copper-compounds

in the North-Atlantic. Further, submarine erosion of basalt rocks and direct injection by aerial and submarine volcanism are other possible sources. Incrustations of biogenic debris in malachite suggest that in situ formation must also be considered (Jedwab, op.cit.). From our data we can conclude that the distribution of Cu_p is regulated by a process which is distinct from the input of terrigenic matter to the ocean, and also from the biological scavenging insofar this process is well represented by factor 1.

TABLE A.IV.4:

GEOSECS station 67 (Argentine Basin)

Reduced profile: Correlation matrix for 36 samples

(All data Log-transformed)

	mean	st.dev.	BA	SR	CA	AL	V	CU	TSM	MN	CALK	SAL	TPOT	SIL
BA	.155E+01	.199E+00	1.000	.612	.590	-.003	.019	-.297	.457	.004	-.671	-.690	.519	-.684
SR	.113E+01	.261E+00	.612	1.000	.686	-.244	-.041	-.194	.406	-.121	-.775	-.742	.614	-.782
CA	.289E+01	.289E+00	.590	.686	1.000	-.368	-.027	-.056	.324	-.298	-.805	-.635	.742	-.794
AL	.239E+01	.340E+00	-.003	-.244	-.368	1.000	.791	.394	.492	.838	.465	.278	-.738	.462
V	.759E-01	.349E+00	.019	-.041	-.027	.791	1.000	.318	.457	.816	.150	.006	-.503	.173
CU	.118E+01	.341E+00	-.297	-.194	-.056	.394	.318	1.000	.373	.229	.254	.193	-.388	.260
TSM	.121E+01	.249E+00	.457	.406	.324	.492	.457	.373	1.000	.466	-.191	-.259	-.049	-.214
MN	.789E+00	.317E+00	.004	-.121	-.298	.838	.816	.229	.466	1.000	.335	.163	-.677	.325
CALK	.336E+01	.670E-02	-.671	-.775	-.805	.465	.150	.254	-.191	.335	1.000	.870	-.830	.986
SAL	.154E+01	.285E-02	-.690	-.742	-.635	.278	.006	.193	-.259	.163	.870	1.000	-.590	.818
TPOT	.412E+00	.288E+00	.519	.614	.742	-.738	-.503	-.388	-.049	-.677	-.830	-.590	1.000	-.835
SIL	.175E+01	.363E+00	-.684	-.782	-.794	.462	.173	.260	-.214	.325	.986	.818	-.835	1.000
PO4	.318E+00	.517E-01	-.342	-.483	-.639	.396	.175	.106	-.122	.274	.712	.306	-.656	.775
NO3	.148E+01	.504E-01	-.349	-.495	-.629	.361	.146	.083	-.148	.237	.713	.319	-.625	.779
O2	.235E+01	.518E-01	.398	.521	.514	.012	.258	.133	.353	.163	-.679	-.596	.229	-.679

	mean	st.dev.	PO4	NO3	O2
BA	.155E+01	.199E+00	-.342	-.349	.398
SR	.113E+01	.261E+00	-.483	-.495	.521
CA	.289E+01	.289E+00	-.639	-.629	.514
AL	.239E+01	.340E+00	.396	.361	.012
V	.759E-01	.349E+00	.175	.146	.258
CU	.118E+01	.341E+00	.106	.083	.133
TSM	.121E+01	.249E+00	-.122	-.148	.353
MN	.789E+00	.317E+00	.274	.237	.163
CALK	.336E+01	.670E-02	.712	.713	-.679
SAL	.154E+01	.285E-02	.306	.319	-.596
TPOT	.412E+00	.288E+00	-.656	-.625	.229
SIL	.175E+01	.363E+00	.775	.779	-.679
PO4	.318E+00	.517E-01	1.000	.997	-.666
NO3	.148E+01	.504E-01	.997	1.000	-.698
O2	.235E+01	.518E-01	-.666	-.698	1.000

TABLE A.IV.5:

GEOSECS station 67 (Argentine Basin)

Reduced profile: Principal components matrix

factors	1	2	3	4	5	6	7	8	9	10	11	12
eigen-values	7.38	3.42	1.42	.89	.65	.41	.35	.16	.15	.11	.04	.01
% tot. var.	49.2	22.8	9.5	5.9	4.3	2.7	2.4	1.1	1.0	.7	.2	.1
cumulated %	49.2	72.0	81.5	87.4	91.7	94.5	96.8	97.9	98.9	99.6	99.9	100.0
BA	.668	-.329	.472	-.049	.268	-.150	-.315	-.060	.116	.058	-.075	.006
SR	.793	-.245	.245	.097	-.003	-.036	.447	-.156	.128	.000	-.026	.005
CA	.844	-.149	-.013	.225	.091	.380	-.053	.143	.189	.021	.057	-.013
AL	-.539	-.781	.056	-.086	.121	-.030	-.102	-.184	.043	-.123	.113	.002
V	-.261	-.842	-.005	-.177	-.129	.389	-.019	-.051	-.083	-.068	-.095	.000
CU	-.279	-.421	-.479	.671	-.165	-.043	-.103	-.122	.004	.100	-.018	.002
TSM	.190	-.786	.081	.342	.360	-.140	.116	.182	-.139	-.081	-.008	-.001
MN	-.416	-.807	.048	-.311	.018	-.005	.096	.056	-.035	.248	.041	.011
CALK	-.974	.080	-.071	.020	.154	-.019	.050	.026	.094	.003	-.046	-.018
SAL	-.776	.218	-.413	-.089	.395	.065	.056	-.025	.079	.003	-.022	.021
TPOT	.880	.364	.084	.097	.145	.146	-.030	-.084	-.141	.031	.020	.070
SIL	-.984	.081	-.016	.051	.061	.026	.031	.052	.093	-.025	-.011	.064
PO4	-.793	.023	.545	.194	-.186	.011	.003	.034	.021	-.003	.008	-.007
NO3	-.789	.065	.550	.199	-.165	.040	-.006	.041	.012	-.003	.006	.033
O2	.638	-.514	-.335	-.169	-.339	-.194	-.037	.118	.110	-.072	-.012	.046

factors	13	14	15
eigen-values	.00	.00	.00
% tot. var.	.0	.0	.0
cumulated %	100.0	100.0	100.0
BA	.003	.001	-.000
SR	.001	.000	.000
CA	-.002	.000	.000
AL	-.005	.000	.000
V	.001	-.000	-.000
CU	.001	-.000	.000
TSM	.001	-.000	-.000
MN	-.002	-.000	-.000
CALK	-.041	-.000	.000
SAL	.017	-.019	-.000
TPOT	-.018	-.005	-.004
SIL	.008	.022	-.003
PO4	.003	-.011	-.014
NO3	.001	-.009	.014
O2	-.007	-.010	-.002

TABLE A.IV.6:

GEOSECS station 67 (Argentine Basin)

Reduced profile

VARIMAX farctor matrix contributing for 87.4 % of the total variance

	factors	1	2	3	4
sum of squares		4.829	3.551	3.474	1.257
.780	RA	.852	-.121	-.114	-.165
.758	SR	.818	.054	-.292	.012
.785	CA	.705	.213	-.455	.187
.910	AL	-.147	-.897	.219	.191
.809	V	.024	-.888	-.028	.135
.935	CU	-.217	-.216	-.026	.917
.778	TSM	.493	-.530	-.054	.502
.923	MN	-.098	-.954	.063	-.001
.960	CALK	-.779	-.231	.540	.088
.828	SAL	-.891	-.060	.160	.066
.923	TPOT	.607	.632	-.374	-.126
.978	SIL	-.750	-.227	.596	.094
.963	PO4	-.243	-.204	.929	.009
.968	NO3	-.249	-.163	.938	-.002
.812	O2	.402	-.286	-.747	.100

Factors 2 and 4 in Table A.IV.6 are discussed below (see also Table II.3 and Figure II.4, in part II):

Factor 2: (23.7% of the total variance) remains unchanged, even in its contribution to the total variance. It represents the input of detritic, continental matter to the watercolumn, as well as the resuspension of the sediments (see also page A.41).

Factor 4 (8.4% of the total variance) has now a ratively high loading for TSM. It appears that outside the input zones of the watercolumn (i.e. surface and bottom waters) the distribution of Cu_p is related with the one of TSM. This emphasizes even more the dissimilar behaviour of Cu_p and the terrigenic matter in suspension. See also the discussion at page A.43 .

APPENDIX V

THE HYDROLOGICAL SITUATION IN THE ARGENTINE AND THE NORTH AMERICAN BASINS

GEOSECS station 67

The GEOSECS station 67 profile is characteristic of the hydrological situation in the Argentine Basin. Here water masses that originated in the Pacific and Indian Oceans, in the Weddell Sea and the North Atlantic Ocean, override each other. From the sea floor to the sea surface the following water-masses are present (from Dietrich et al., 1975; Reid et al., 1977) (see T-S diagram in Figure A.V.1):

- Weddell Sea Deep Water (WSDW) (Tpot $< 0°C$; salinity: $34.66‰ < < 34.70‰$). It originates in the Weddell Sea where it is found at a depth of ~ 1400 m, below the Circumpolar Water (CPW). In the Weddell Sea salinity and nutrient content decrease , while the O_2 content increases, on from CPW through WSDW to Weddell Sea Bottom Water (WSBW). WSBW flows eastward, south of 60° S; it does not enter the Argentine Basin.
- Circumpolar Water (CPW): It consist of Pacific Water having entered the Weddell Sea through the Drake Passage. This water is characterized by its high nutrient content, its salinity maximum and O_2 minimum. In the Argentine Basin North of 50°S ,CPW is split in an upper and lower mass (labelled as CPWu and CPWl) by the southward flowing of North Atlantic Deep Water (NADW). As a result two O_2 minima are observed, separated by O_2-rich NADW. At station 67, CPWl is recognized by its Tpot of ~ 2.5°C and its salinity of 35.50 ‰. The core of this watermass occurring at 3600 m, is indicated in the T-S diagram. CPWu is less well defined

in the T-S diagram, where it plots on the mixing curve between NADW and Antarctic Intermediate Water (AAIW) cores. It has a Tpot of ~ 2.6°C and a salinity between 34.30‰ and 34.70‰ .

- North Atlantic Deep Water (NADW): (Tpot ~ 2.6°C; salinity > 34.80 ‰). It originates in the North Atlantic and is characterized by its salinity and O_2 maxima and its nutrient minima. The NADW core is clearly visible in the T-S diagram. At station 67 we are observing the southern end of the NADW mass since it turns eastwards before reaching 50°S.
- Antarctic Intermediate Water (AAIW): It is a northward flowing low salinity (~ 34.10‰) watermass with a Tpot between 4 to 5°C that originates at 50°S, from the Antarctic Divergence. It overrides the CPW mass and underrides the waters of the Subtropical Anticyclonic Gyre. Its salinity minimum can be seen as far as 25°N. Its core, occurring at about 400 m, is not well defined in the T-S diagram, due to mixing with CPWu and overlying waters.
- Waters of the Subtropical Anticyclonic Gyre: surface waters.

GEOSECS stations 3 and 5

The GEOSECS station 3 and 5 in the North Atlantic have profiles characteristic of the hydrological situation of the North American Basin, where NADW is formed.

FIGURE A.V.1

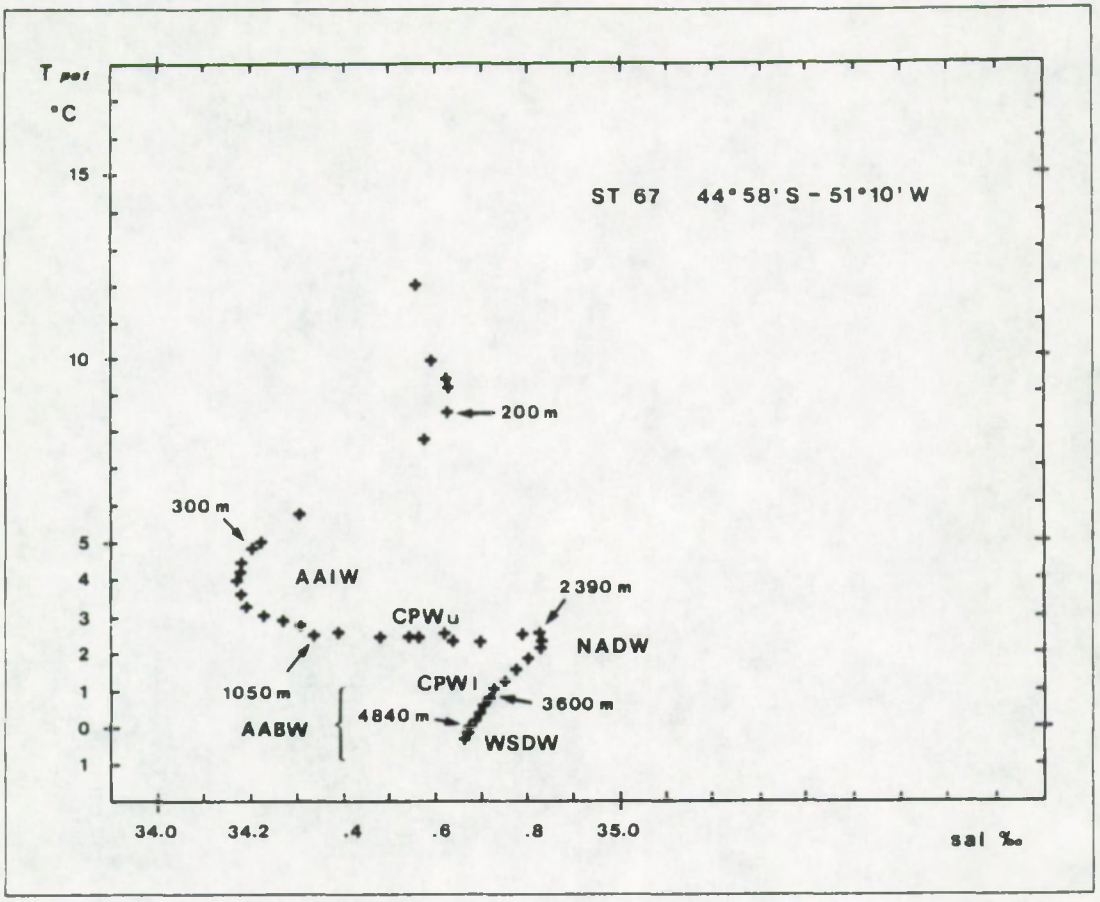

FIGURE A.V.2

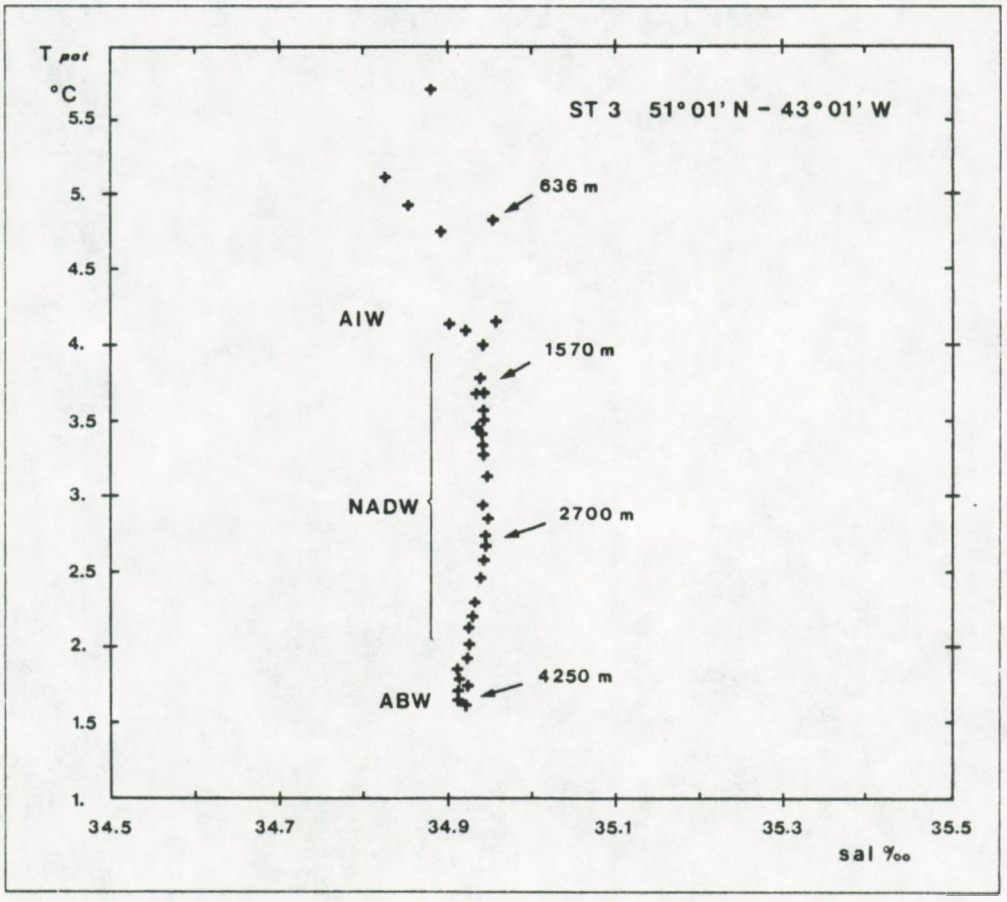

From the sea floor on, the following watermasses are observed (Dietrich et al., 1975, Chan et al., 1977) (see T-S diagram of station 3 in Figure A.V.2):

- A very dense watermass, Denmark Strait Water (DSW), that originates in the Greenland Sea, (sal. 34.91‰ ; Tpot 1.5°C). It flows over the Greenland-Iceland Ridge, through the Denmark Strait, into the western basin of the North Atlantic.
- A central composite watermass that is formed in these latitudes and extends between some 1500 m to 3500 m depth. It is the result of a mixing of waters of different origins and is characterized by salinities superior to 34.90 ‰ attaining some 34.92 ‰ between 1500 and 2700 m. Towards the bottom this watermass consists of a mixing of two arctic watermasses . The densest one is the already discussed DSW. The second Arctic watermass is formed in the Norwegian Sea and flows over the Iceland-Scotland Ridge into the eastern North Atlantic. It flows southwards and can enter the western basin through the Gibbs fracture in the Mid-Atlantic-Ridge at 53°N. In the western basin it mixes with part of the DSW. Towards the surface, NADW is formed by a partial mixing between both these arctic waters with Arctic Intermediate Water (AIW). Arctic Intermediate Water is formed in the Labrador Sea and spreads through the North Atlantic at a depth of 900 m (Dietrich et al. op.cit.) to 1500 m (Chan et al.,op.cit.). Its salinity is relatively low (34.90‰).

- A watermass at 500 m depth, characterized by a nutrient maximum and highly variable salinities. It represents the northernmost intrusion of Antarctic Intermediate Water (AAIW), (Chan et al.,op.cit.).
- Surface water (sal. 34.50‰; Tpot 12.5°C).

With exception of AAIW, the different watermasses at station 3 are all relatively young, since the respective source regions are relatively close. Further, the magnitude of the Greenland-Iceland-Scotland ridge overflows is regulated by the tidal rythms (Dietrich et al.,1975). Both, the young ages of the watermasses in presence and the discontinuous overflow of arctic waters, are factors that may contribute to the impediment of an equilibrium state.

APPENDIX VI

THEORY OF THE DISTRIBUTION OF A TRACER IN A CARRIER PHASE

In Mc Intyre (1963) the growth of a solid solution from an aqueous solution is expressed by the following reaction equation:

$$CrM_S + Tr_l^{z+} \gtrless TrM_s + Cr_l^{z+}$$

CrM_s and TrM_s are the tracer and carrier phase in the solid solution. Cr_l^{z+} and Tr_l^{z+} are the carrier and tracer ions in the liquid. M is the anion; it's concentration is unaffected by the substitution.

At equilibrium:

$$K = \frac{(TrM)_s \ (Cr^{z+})_l}{(CrM)_s \ (Tr^{z+})_l} = \frac{(TrM)_s \ / \ (CrM)_s}{(Tr^{z+})_l / \ (Cr^{z+})_l}$$

Values between parentheses represent <u>activities at equilibrium</u> and therefore K is a constant independent of phase compositions. For an ideal solution, where activities are equal to concentrations (activity coefficients = 1), K is equal to D_{ideal} the ideal distribution coefficient in the Henderson-Kracek homogenous distribution law:

$$K = D_{id} = \frac{(Tr/Cr)_s}{(Tr/Cr)_l}$$

Tr and Cr = concentrations of tracer and carrier

$(Tr/Cr)_s$ = ratio of tracer of carrier in the solid

$(Tr/Cr)_l$ = ratio of tracer to carrier in the liquid

Further, K is equal to the ratio of the solubility products of the pure carrier phase to the pure tracer phase:

$$K = \frac{K.CrM}{K.TrM} = D_{ideal}$$

In the case of Ba substitution by Sr in barite crystals, Church (1970) observed that D_{ideal} predicted higher values for Sr incorporation, than those found experimentally. For example at 25°C and 1 atm. pressure :

$$D_{ideal} = \frac{Ksol\ BaSO_4}{Ksol\ SrSO_4} = \frac{1.1 \times 10^{-10}}{2.6 \times 10^{-7}}$$

$$= \frac{a\ BaSO_4 / a\ SrSO_4}{a\ Sr^{2+} / a\ Ba^{2+}}$$

(with a = activities and a Ba^{++} = activity at saturation)

and $aSrSO_4 / aBaSO_4 = \frac{1.1 \times 10^{-10}}{2.6 \times 10^{-7}} \times \frac{2.1 \times 10^{-5}}{5.7 \times 10^{-8}} = 0.15$ *

Thus 15 mol% of Ba is substituted by Sr in the ideal case. This value is about five times higher than the one found experimentally by Church (see above). As a result $(Ba,Sr)SO_4$ solid solutions behave non-ideally.

Therefore, Church (1970) wrote the real or observed distribution coefficient as a function of thermodynamical factors including ideal and non-ideal terms. This thermodynamical approach was originally elaborated by Ratner (1933), Vaslow and Boyd (1962) and is further extensively described in Mc Intyre (1963).

This approach makes use of the chemical potentials of both, the tracer and carrier phase in the liquid and the solid. These chemical potentials represent the change in free energy due to

---

* For values of solubility products and activities or concentrations see Table II.15.

the transformation of the solution and the solute from a standard state to the actual solution with activity a.

At equilibrium, these chemical potentials are written:

for the tracer phase,

$$\mu_l \text{ TrM} = \mu_x \text{ TrM} + RT \ln a^l_{TrM} \qquad \text{(in the liquid)} \quad (1)$$

$$\mu_s \text{ TrM} = \mu_o \text{ TrM} + RT \ln a^s_{TrM} \qquad \text{(in the solid)}$$

with μ_x TrM and μ_o TrM = chemical potentials in the standard states

a^l and a^s = activities of tracer in liquid and solid phases

At equilibrium, μ_x TrM = μ_o TrM and

$$\frac{a^l_{TrM}}{a^s_{TrM}} = \exp\left[\frac{\mu_o \text{TrM} - \mu_x \text{TrM}}{RT}\right] = KTrM,$$

with K = solubility product

idem for the carrier phase:

$$\frac{a^l_{CrM}}{a^s_{CrM}} = KCrM$$

and

$$\frac{a^s_{TrM} \,/\, a^s_{CrM}}{a^l_{TrM} \,/\, a^l_{CrM}} = \frac{KCrM}{KTrM} \qquad (2)$$

a^s_i, the activity of the solid phase = $X_i \cdot \lambda_i$; with X_i = mole fraction in the solid solution and λ_i = solid activity coefficient. a^l_i = product of the activities of cations and anions in the liquid; $a^l_i = (m_{X^{z+}} \cdot \gamma_{X^{z+}}) \cdot (m_{y^{z-}} \cdot \gamma_{y^{z-}})$, X^{z+} = cation ,

(tracer or substituent) and y^{z-} = anion; m_i = molality and γ_i = activity coefficients.

(2) writes:

$$\frac{X_{TrM} \cdot \lambda_{TrM} \,/\, X_{CrM} \cdot \lambda_{CrM}}{m_{Tr}{}^{z+} \cdot \gamma_{Tr}{}^{z+} / m_{Cr}{}^{z+} \cdot \gamma_{Cr}{}^{z+}} = \frac{KCrM}{KTrM} = D_{id.} \qquad (3)$$

The observed values of the Sr substitution in natural, sedimentary and in precipitated barites, showed these solid $(Ba,Sr)SO_4$ solutions to be dilute (Church, 1970). Therefore λ_{CrM} the solid activity coefficient of the carrier phase is considered to be unity (see also Garrels and Christ, 1965). λ_{TrM}, the solid activity coefficient of the tracer phase is obtained from (1), by substituting a^s_{TrM} by $X_{TrM} \cdot \lambda_{TrM}$:

$$\mu_s TrM = \mu_o TrM + RT \ln X_{TrM} \cdot \lambda_{TrM}$$

$$= \mu_o TrM + RT \ln X_{TrM} + RT \ln \lambda_{TrM}$$

and since $\mu_o TrM + RT \ln X_{TrM} = \mu_s TrM$ (ideal)

it follows that $RT \ln \lambda_{TrM} = \mu_s TrM - \mu_s TrM(ideal)$

$$\lambda_{TrM} = \exp \left[\frac{\mu_s TrM - \mu_s TrM\ (ideal)}{RT} \right] \qquad (4)$$

with $\mu_s TrM - \mu_s TrM(ideal) = \Delta\mu_{TrM}$ = free energy change resulting from the transfer of one mole of TrM from an ideal solution with CrM to a non-ideal or observed solution, and this without change of the mole fractions (Mc Intyre, 1963).

The effectively observed distribution coefficient, Dobs, can be written as :

$$Dobs = \frac{(X_{TrM} \; / \; X_{CrM})}{(m^{1}_{Tr}z+ \; / \; m^{1}_{Cr}z+)}$$

From (3) and (4) and since λ_{CrM} was put = 1 we obtain:

$$D_{obs} = \frac{(X_{TrM} \; / \; X_{CrM})}{(m^{1}_{Tr}z+ \; / \; m^{1}_{Cr}z+)} = \frac{KCrM}{KTrM} \cdot \left(\frac{\gamma_{Tr}z+}{\gamma_{Cr}z+}\right) \cdot \exp\left[\frac{-\Delta\mu TrM}{RT}\right] \quad (5)$$

The observed distribution coefficient is thus function of the products of :

1. the ideal distribution coefficient, which is the ratio of the solubility products of the pure carrier to the pure tracer phase
2. a solution interaction factor, formulating the influence of the liquid composition on the distribution coefficient
3. a solid interaction factor, expressing the free energy change of the transfer from an ideal to a non-ideal situation (Mc Intyre, 1963; Church, 1970).

From (4) and (5) : $\lambda_{TrM} = \frac{D_i}{D_{obs}} \cdot \left(\frac{\gamma_{Tr}m+}{\gamma_{Cr}m+}\right)$ and since

$(\gamma_{Tr}m+ \; / \; \gamma_{Cr}m+)$ cancels in this specific case (Table II.15)

$$\lambda_{TrM} = D_i/D_{obs} \quad (6)$$

In the case of dilute solid solutions the activity coefficient of the tracer phase is thus obtained quite easily. For in vitro precipiated barite, Church (1970) observed:

	at 3°C; 1 atm	at 23°C; 1 atm
$\%SrSO_4$	2.0	2.7
D_{ideal}	2.1×10^{-4}	4.1×10^{-4}
D_{obs}	4.2×10^{-5}	8.2×10^{-5}
λ	5.2	5.0

It is stated that the magnitude of the solid activity coefficient (of the substituting phase) larger than unity is a measure of its rejection from the actual solid solution, relative to the ideal one.

If such dilute solid solutions effectively precipitate in the water-column, they must of course be in equilibrium with this liquid solution. Therefore activities of the solid and dissolved Ba^{2+} and SO_4^{2-} ionic species must be such that the solubility product of $BaSO_4$ at the local pressure and temperature conditions is satisfied.

Thus:

$$KsolBaSO_4 = \frac{\gamma_{Ba^{2+}} \cdot f_{Ba^{2+}} \cdot m_{Ba^{2+}} \cdot \gamma_{SO_4^{2-}} \cdot f_{SO_4^{2-}} \cdot m_{SO_4^{2-}}}{XBaSO_4 \cdot \lambda BaSO_4} \qquad (7)$$

It is easily seen, by substituting the activity coefficient, the fractions of unassociated ions and the molality in eq(7) by their values in Table II.5, that a 3 mol % subsitution such as observed by Church (1970) in vivo and in vitro will only bring

about a minor shift in the barium saturation concentration. For example, the Ba saturation concentration is (Church,1970):

a) for a cold surface sea water (3°C, 1 atm) in equilibrium with a pure barite phase:

$m_{Ba^{++}} = 1.8 \times 10^{-7}$ mole/Kg = 24 µg/Kg

b) for a cold surface sea water (3°C; 1 atm) in equilibrium with a dilute $(Ba_{0.97}, Sr_{0.03})SO_4$ solid solution ($\lambda_{BaSO_4} = 1$!):

$m_{Ba^{++}} = 1.75 \times 10^{-7}$ mole/Kg = 23 µg/Kg

the shift is less than 5%, while the actual Ba concentration in cold surface sea water is about 42% of the solubility value, or 10 µg/Kg sw.

However, as discussed in section 2.4 (part II) barites which have incorporated higher amounts of Sr than reported by Church, occur in sea water. One may wonder if such solid solutions form authigenically, for example in Antarctic surface waters where the $BaSO_4$ solubility product is smaller, due to the low temperatures and where the Ba^{++} concentrations are the highest of the Atlantic Ocean surface waters (Table II.16). Since data concerning the solid activity coefficients of carrier and substituent lack completely for non-dilute solid solutions, (Church pers. comm.) it is not possible in this case to verify if the $BaSO_4$ and $SrSO_4$ solubility products are satisfied in sea water. One may however consider a priori that a solid solution with for example a 10 mol % Sr substitution (see section 2.4 in part II) forms authigenically in Antarctic surface water (3°C; 1 atm.; 10 µg Ba_s/Kg or 7.3×10^{-8} mole Ba_s/Kg sw (see Table II.16).

From (3) and (5) we obtain:

$$D_{obs} = D_{ideal} \left(\frac{\gamma Sr^{++}}{\gamma Ba^{++}}\right) \cdot \frac{\lambda BaSO_4}{\lambda SrSO_4} \qquad (8)$$

$$D_{obs} = \frac{0.1 \;/\; 0.9}{9\times10^{-5}_{(*)} / 7.3\times10^{-8}_{(*)}} = 9 \times 10^{-5}$$

and $D_{ideal} = 0.54 \times 10^{-10}_{(*)} / 2.5 \times 10^{-7}_{(*)} = 2.16 \times 10^{-4}$

since $\gamma_{Ba}{}^{++} = \gamma_{Sr}{}^{++}$, (eq (8) gives $\frac{\lambda BaSO_4}{\lambda SrSO_4} = 0.42$ (9)

At equilibrium equation (7) must be fulfilled

$$0.54\times10^{-10} = \frac{0.24 \times 0.93 \times 7.3 \times 10^{-8} \times 0.17 \times 0.28 \times 28 \times 10^{-3}}{0.9 \times \lambda BaSO_4}$$

solving for $\lambda BaSO_4$ gives 0.45

and $\lambda SrSO_4 = 1.07$

However, we do not know if such solid activity coefficients are plausible.

Such solid solutions can not be regular or symmetrical solutions as supposed by Hanor (1969), since the following equations:

$$\ln \lambda BaSO_4 = B'(1-XBaSO_4)^2$$

$$\ln \lambda SrSO_4 = B'(1-XSrSO_4)^2$$

in which B' is a constant (Garrels and Christ, 1965) are not fulfilled for the present values of the solid activity coefficients and solid mole fractions.

(*) see Table II. 15. in part II

APPENDIX VII

APPLICATION OF THE STOKES SETTLING AND DISSOLUTION RATE MODEL

In the following, the theoretical aspects of the dissolution rate and Stokes settling rate model, described in Brun-Cottan (1976a - 1976b) will be resumed briefly. This theory is also described partly in Lal and Lerman (1973; 1974; 1975); Wollast (1974) and more recently as applied to GEOSECS data, in Lal (1977).

In the following, the eventual influence of vertical advection in the water column was not taken into account. Steady state conditions are assumed. The variation of particle diameter with depth (dD/dZ) is calculated with the aid of the dissolution rate (dD/dt) and the settling velocity (dZ/dt). By substituting dD/dt and dZ/dt in dD/dt = (dD/dZ). (dZ/dt) by their values in eq. 3.7 and 3.9 in §1.2.3 ;partII,we obtain:

$$\frac{dD}{dZ} = \frac{2.k}{\pi.C.D^2} \qquad (1)$$

Rearanging and integration results in :

$$\frac{C.D^3}{3} - \frac{C.D_o^3}{3} = \frac{2}{\pi} \cdot k. (Z - Z_o), \qquad (2)$$

with D_o = initial diameter at depth Z_o which is the upper boundary of the studied depth interval.

Rearanging of (2) gives :

$$D_o = D.\left[1 + \frac{k' \cdot (Z - Z_o)}{C.D^3}\right]^{1/3} \qquad (3)$$

with $k' = -(6/\pi).k$

eq (3) expresses the decrease of particle diameter in function of depth.

By formulating the flux constancy of the number of

particles it is possible to write any size distribution dN/dD at a depth Z as a function of dN/dD, the original size distribution at Z_o. Z_o being every depth shallower than Z from which on the settling and the dissolution processes are altering the original size distributions.

This flux constancy implies that the number of particles which at Z_o size for example between D and D + dD', have not decreased at Z, at least for those particles which have not dissolved. At depth Z, these particles will size between D and D + dD", with dD" > dD'. As a result the distribution function decreases for D at Z (Brun-Cottan ,1976).

Conservation of particle flux with depth is written :

$$d\phi_{D_o} = d\phi_D \qquad d\phi_{Z_o}(D\ ;\ D + dD') = d\phi_Z(D\ ;\ D+dD")$$

$$\int_{x_o}^{x_o+dx_o} CX_o^2 - \frac{dN}{dx_o}(x_o, z_o).dx_o = \int_{x}^{x+dx} CX^2.\frac{dN}{dx},(x,\ 2).dx$$

or,

$$\frac{dN}{dD_o}.C.D_o^2 \ .\ dD_o = \frac{dN}{dD}.C.D^2 \ .\ dD \qquad (4)$$

rearanging terms in (4) gives:

$$\frac{dN}{dD}(D,z) = \frac{dN}{dD_o}(D_o,\ z_o)\ .\ \left(\frac{D_o}{D}\right)^2\ .\ \frac{dD_o}{dD} \qquad (5)$$

equation (6) writes a size distribution dN/dD at a depth Z as a function of the original size distribution dN/dD_o at any depth Z_o, shallower than Z.

Derivation of (3) with respect to D gives :

$$\frac{dD_o}{dD} = \left(1 + \frac{k'.(Z - Z_o)}{C.D^3}\right)^{-2/3} \qquad (6)$$

and,

$$\left(\frac{D_o}{D}\right)^2 = \left(1 + \frac{k'.(Z - Z_o)}{C.D^3}\right)^{2/3} \qquad (7)$$

equations (6) and (7) may now be introduced in (5),

$$\frac{dN}{dD}(D,z) = \frac{DN}{dD_o}(D_o, z_o).\left(1 + \frac{k'.(Z-Z_o)}{C.D^3}\right)^{-2/3.2/3}$$

$$= \frac{dN}{dD_o}(D_o, z_o) \qquad (8)$$

For many natural collections of small particles, cumulated number distributions in function of particle diameter obey the hyperbolic distribution law (Bader, 1971). This law is shown (Lal and Lerman, 1975 ; Brun-Cottan, 1976), to apply also to marine suspensions. The cumulated particle number distribution writes :

$N = A.\ (D/D')^{-M}$ with D = particle diameter

D' = smallest diameter considered

if $D = D' \rightarrow N = A$, with A = number of particles with diameters $\geq D'$.

Derivation of this cumulated function with respect to D gives the particle number distribution in function of particle diameter :

$$\frac{dN}{dD} = \frac{-M.A}{D'}\left(\frac{D}{D'}\right)^{-(M+1)} = \frac{a}{D'}\left(\frac{D}{D'}\right)^{-m} \quad \text{with } a = -M.A \text{ and } -m = -(M+1)$$

(9)

which is also a hyperbolic function.

From (8) and (9) we obtain :

$$\frac{dN}{dD}(D,z) = \frac{a}{D'}\left(\frac{D_o}{D'}\right)^{-m} \qquad (10)$$

Do is now substituted by its value in (3) :

$$\frac{dN}{dD} = \frac{a}{D'} \left(\frac{D}{D'}\right)^{-m} \cdot \left[1 + \frac{k'.(Z - Z_o)}{C.D^3}\right]^{-m/3} \qquad (11)$$

$$= \frac{a}{D'} \left(\frac{D}{D'}\right)^{-m} \cdot G(D,z)$$

In (11), $\frac{a}{D'} \cdot \left(\frac{D}{D'}\right)^{-m}$ is substituted by $\frac{dN}{dD}(D,z_o)$; which is the distribution of D at initial depth Z_o.

$$\frac{dN}{dD}(D,z) = \frac{dN}{dD}(D,z_o) \cdot G(D, z) \qquad (12)$$

$$\text{with } G(D,Z) = \frac{dN(D,Z)}{dN(D_o,Z_o)} = \left[1 + \frac{k'(Z - Z_o)}{C \quad D^3}\right] \qquad (13)$$

From eq. (13) k' is deduced :

$$k' = -(6/\Pi)k = C.[G(D,Z)^{-3/m} - 1] \cdot \frac{D^3}{(Z - Z_o)} \qquad (14)$$

It is seen from (14) that in order to calculate the dissolution rate constant k, it is sufficient to know the power coefficient m of the size distribution at the upper boundary of the depth interval and the ratio G(D,Z) of the size distribution functions between the lower (Z) and the upper (Z_o) boundary of the depth interval. In practice the dissolution rate constant k is calculated for a specific size class. The validity of k is then verified for example by calculating the theoretical distribution $dN(D,Z)_{calc.}$ for the other size classes of the distribution at the lower boundary Z, with use of eq. (14) :

$dN(D,Z)_{calc.} = dN(D,Z_o)_{calc.}$ and $dN(D,Z)_{obs.}$ validates the value of k.

The model worked out by Brun-Cottan (1976a, b) and Lal and Lerman (1975) uses a power curve for fitting of the size distributions :

$dN/dD = a/D_o \ (D/D_o)^{-m}$,

with D being the particle diameter ; D_o being the smallest diameter measured ; a and m being dimensionless coefficients (see above). We remind that the size distribution of suspended barite do fit the log-normal law (§ 4.1.1 in part II). The fitting problem was overcome by describing the log-normal size distribution partly with a power curve. This was done by plotting the cumulated size distributions in log-log graphs. One or two linear segments obeying the power law :

$N = A - A(D/D_o)^{-M}$, with A and M dimensionless coefficients

and $M = m - 1$

are generally observed.

The model calculations were applied to each pair of consecutive size distributions at GEOSECS stations 67 and 3. At station 67 the good concordance between $dN(D,Z)_{calc.}$ and $dN(D,Z)_{obs.}$ was observed only for the samples collected at 2574 m - 2982 m (Figure II.10.A). At station 3 the size distribution pairs at 1875 m- 2479 m and 2989 m- 3267 m fit well to the model (Figure II.10.B). However the size distribution at station 67 (2574 - 2982m) is the only one which can be shown to reside inside a well identified watermass, as required by the model conditions. This watermass is the low salinity North Atlantic Deep Water (NADW) core (see T-S diagram in Figure A.V.1.).

A comparison between the pairs of size distributions at both stations (see Figure II.10.A,B) reveals at once that important differences between the dissolution rates will be found.

Indeed, the variation between successive size distributions is more important at station 3 than at station 67.

The computation of the dissolution rate constant k is considered now for each of these three cases separately. The variables which have to be known in order to compute k are given in Table A.VII.1 for each of the three cases. These variables are : the slope coefficient m of the size distribution at the upper boundary Z_o the ratio of the size distribution functions between Z and Z_o and the depth intervals $Z-Z_o$:

1) Station 67 (2574 m - 2982 m) (Table A.VII.1 and Figure A.VII.1a) the cumulated size distribution at 2574 m is shown ; it is seen that for diameters $\geq$ 1μ m a hyperbolic function can be applied, with a slope value M of 2. Therefore, m is 3 since m = M + 1). G(D,Z), the ratio ot the size distribution between 2982 m and 2574 m is calculated for the 1.04 to 1.47μm size class. This class contains the highest particle number (see Figure IV.1.A.) and the particles have a relatively high Stokes settling rate (60 m/yr). Further, G(D,Z) = 1066/1560 = 0.68 and $Z-Z_o$ is 408 m. Therefore, k' in eq. (14) becomes

$$k' = C(0.68^{-3/3}-1)\ \frac{1.24\times10^{-4}\ ^3}{40.800} = 2 \times 10^{-17}\ cm^2$$

$$\text{since } C = \frac{1 \times 981 \times 3{,}5 \times 3.15 \times 10^{7}}{18 \times 1{,}5 \times 10^{-2}} \text{ in } cm^{-1}.yr^{-1}$$ (see eq. 3.9 § 1.2.3 in part II)

$$= 4 \times 10^{11}\ cm^{-1}.yr^{-1}$$

k' becomes :

TABLE A.VII.1 : Values of m, = power coefficient of the barite particle size distributions at Z_o
G(D,Z) = ratio of the size distribution functions between Z and Z_o ; $Z - Z_o$
= depth interval ; k, = barite dissolution rate constant, for samples of
GEOSECS stations 67 and 3.

	Station 67 2574m - 2982 m	Station 3 1875m - 2479 m		Station 67 2989m - 3267m	
m	~ 3 (for Ø > 1µm)	~ 3 (for Ø < 1.13 µm)	~ 6.3 (for Ø > 1.13 µm)	~ 3.7 (for Ø < 1.13 µm)	~ 5.2 (for Ø > 1.13 µm)
G(D,Z)	0.68 (Ø 1.24 µm)	0.23 (Ø 1.04 µm)	0.29 (Ø 1.47 µm)	0.07 (Ø 0.9 µm)	0.09 (Ø 1.24 µm)
$Z - Z_o$	40800 cm	60400 cm		27800 cm	
k	0.5×10^{-5} cm/yr	1.0×10^{-5} cm/yr		4.0×10^{-5} cm/yr	

Note : particle size values correspond to class midpoints.

TABLE A.VII.2 : Comparison between observed and calculated size distributions of barite particles, settling and dissolving in the watercolumn.

Particle diameter in μm	Observed particle numbers per l at Z_o	Observed particle numbers per l at Z	Calculated particle numbers per l at Z	Nobs/NCalc. at Z
A. GEOSECS station 67 (Z_o = 2574 m ; Z = 2982 m)				
2.48	150	246	142	1.7
2.08	940	410	857	0.5
1.75	470	574	404	1.4
1.47	470	410	368	1.1
1.24	1560	1066	1066	1.0
1.04	620	328	348	1.0
0.88	310	162	133	1.2
0.74	1250	410	400	1.1
0.62	620	328	139	2.6
0.52	470	82	71	1.4
0.44	150	0	15	-
0.37	150	82	10	9.
B. GEOSECS station 3 (Z_o = 1875 m ; Z = 2479 m)				
2.95	0	40	0	-
2.48	0	160	0	-
2.08	0	200	0	-
1.75	750	400	269	1.5
1.47	1250	360	313	1.1
1.24	2250	240	315	0.7
1.04	3250	750	750	1.0
0.88	4250	500	630	0.8
0.74	4750	460	434	1.1
0.62	4500	360	245	1.5
0.52	3000	240	100	2.4
0.44	750	120	14	8.6
C. GEOSECS station 3 (Z_o = 2989 m ; Z = 3267 m)				
2.48	300	0	188	0
2.08	300	75	145	0.5

TABLE A.VII.2 : Continued

Particle diameter in μm	Observed particle numbers per l at Z_o	Observed particle numbers per l at Z	Calculated particle numbers per l at Z	Nobs/NCalc. at Z
1.75	590	225	200	1.1
1.47	590	150	123	1.2
1.24	3250	300	300	1.0
1.04	3250	375	417	0.9
0.88	4140	300	300	1.0
0.74	5320	225	221	1.0
0.62	3850	750	90	9.5
0.52	2370	75	28	3.0
0.44	300	225	2	83.0
0.37	590	0	2	0

FIGURE A.VII.1a

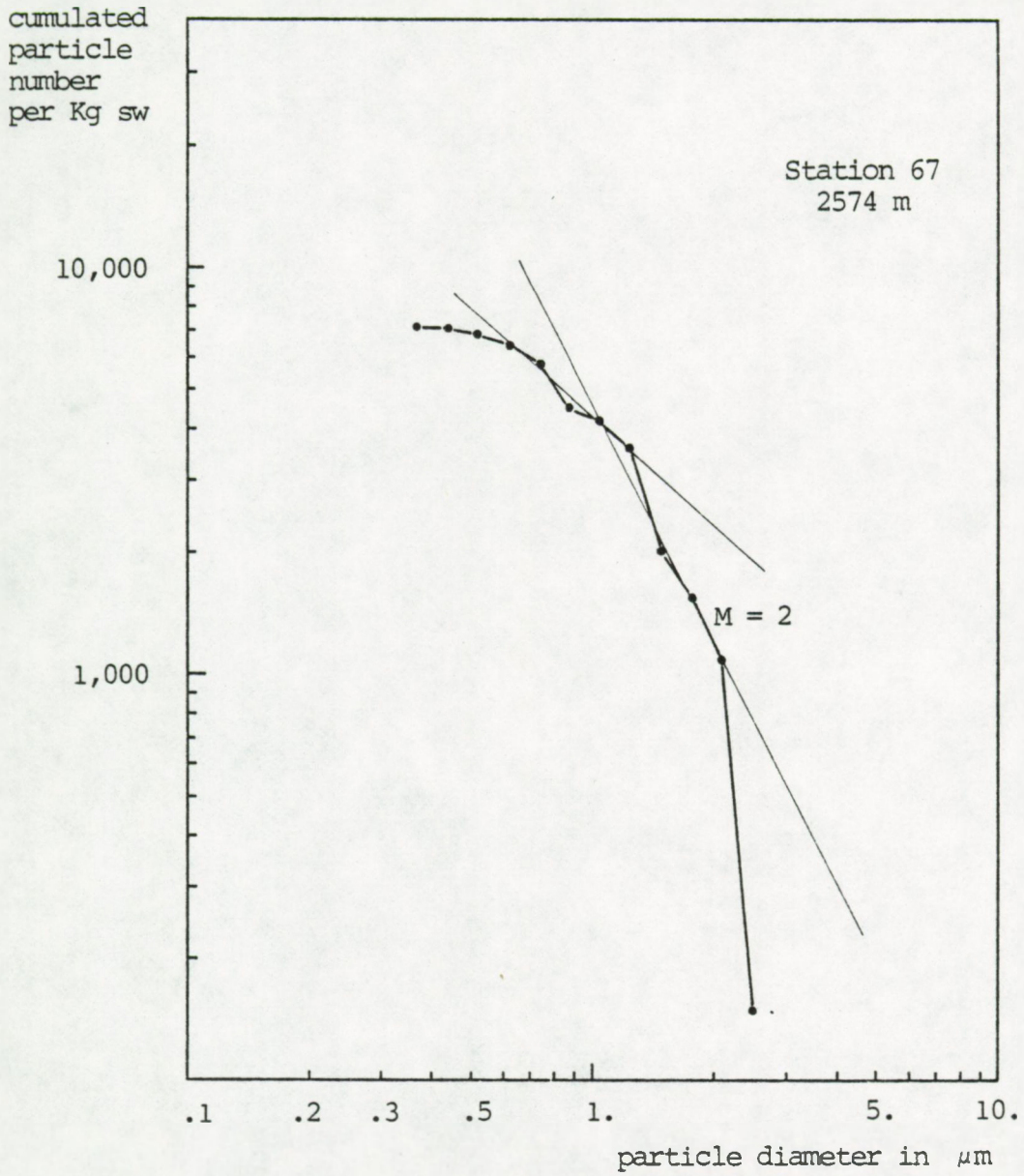

GEOSECS station 67: cumulative size distribution of the barite particles at 2574 m. M, the slope of the segment which covers diameters > 1 μm = 2.

$k' = 8 \times 10^{-6}$ cm. yr^{-1} and since $k = \Pi/6.k'$,

$k = 0,5 \times 10^{-5}$cm. yr^{-1} or 0.05 µm.yr^{-1}

With k, any G(D,Z) for any other diameter at 2982 m can be computed by using eq. (13). Multiplication of the calculated G(D,Z) values with $N(D,Z_o)$, the observed particle number of size D, at depth Z_o (2574 m) gives $N(D,Z)_{calc.}$, the calculated number of particles at depth Z (2982 m). These numbers are compared with the effectively observed numbers at 2982 m (Table A.VII.2,A and Figure A.VII.2). The goodness of the fit is expressed as R, the ratio of the calculated number to the observed number of barites in each size class (Table A.VII.2,A). The calculated and observed distribution fit well for diameters between 1.47 and 0.47 µm, with R values close to unity This is interpreted as a validation of the dissolution rate and Stokes settling model for this case.

2) Station 3 (1875 m - 2479 m)(Table A.VII.1) : From Figure A.VII.1b, it is seen that the cumulated size distribution can be fit by two hyperbolic functions. For diameters < 1.13 µm, the hyperbolic function has a slope value M of ∿ 2 (m = 3; since m = M+1) and for diameters >1.13 µm a slope value M of ∿ 5.3 (thus m = 6,3). For diameters > 1.13 µm, G(D,Z) was calculated for the 1.34 µm to 1.60 m size class : G(D,Z) = 360/1250 = 0.29. For diameters <1.13 µm G(D,Z) was calculated for the 0.95 to 1.13 µm size class : G(D,Z) = 750/3250 = 0.23. Further $Z-Z_o$ is 604 m. The resulting k values, computed by using eq. (14) are : for diameters > 1.13 µm, 0.9×10^{-5}cm/yr and for diameters <1.13 µm, 1.1×10^{-5}cm/yr. A mean value of 1.0×10^{-5} cm/yr is considered. The calculated and

FIGURE A.VII.1b

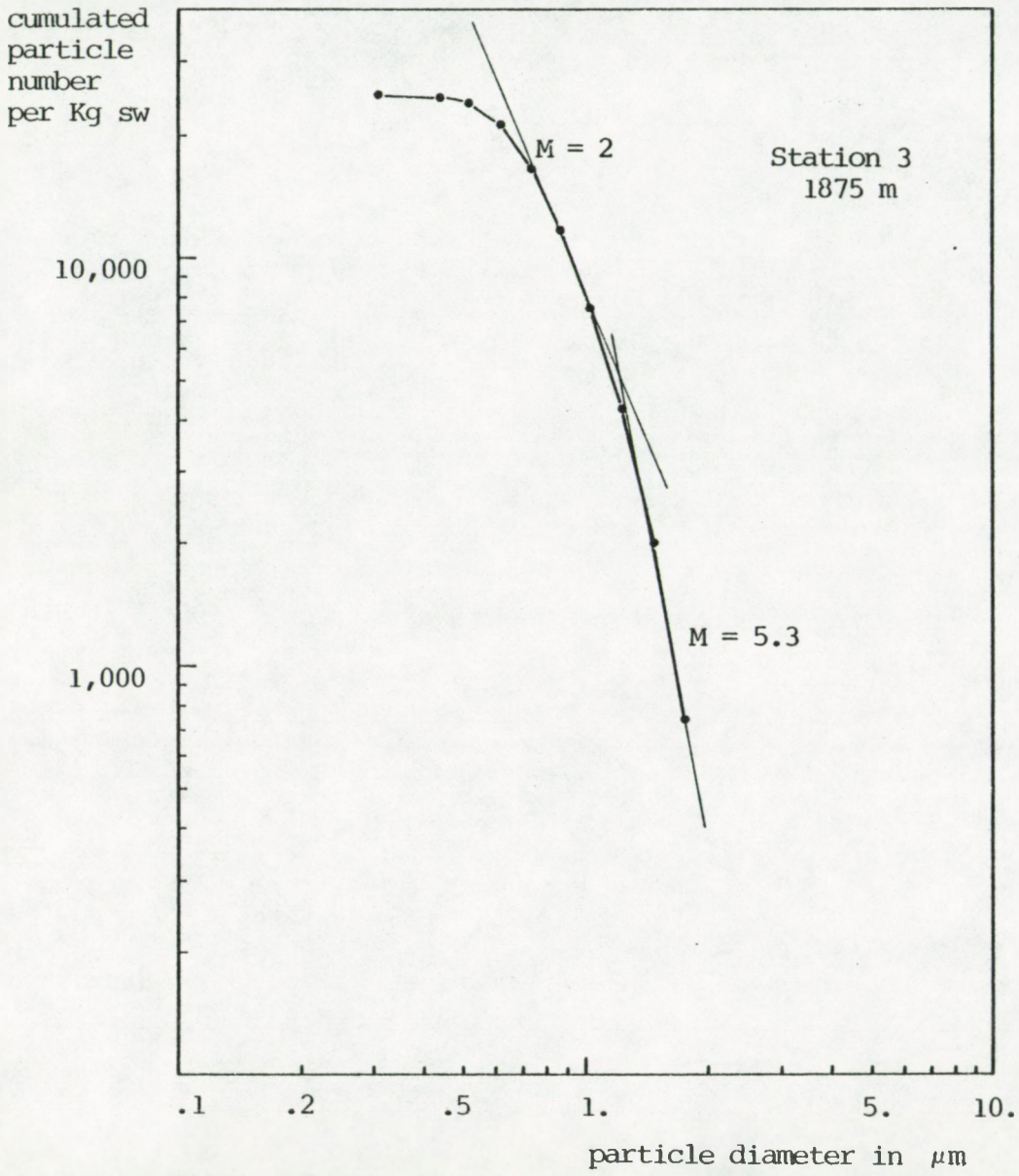

FIGURE A.VII.1c

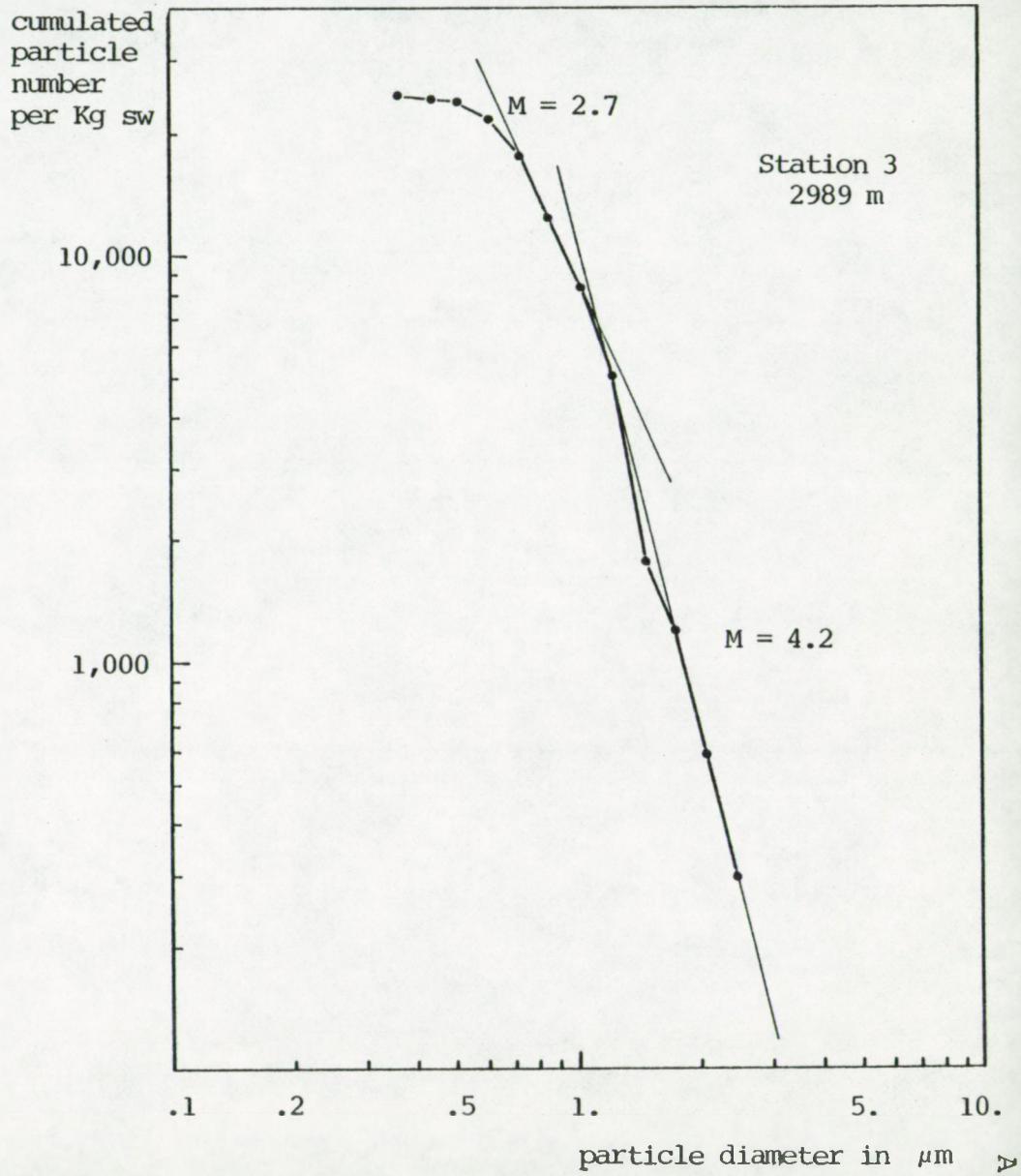

GEOSECS station 3: cumulative size distributions of the suspended barites at 1875 m and 2989 m. M = slope values.

observed distributions fit relatively well, for diameters between 0.6 and 1.75 μm (Figure A.VII.2). In this size range, R values reach extremes of 0.76 at 1.24 μm and 1.5 at 1.75 μm (Table A.VII. 2B).

3) Station 3 (2989 - 3267) (Table A.VII.1) : From Figure A.VII.1,c it is seen that the cumulated size distribution can be fit by two hyperbolic functions. For diameters >1.13 m the hyperbolic function has a slope value M of 4.2 (thus m = 5.2), and for diameters < 1.13 μm the hyperbolic function has a slope value M of 2.7 (thus m = 3.7).

For diameters >1.13 μm, G(D,Z) was calculated for the 1.13 to 1.34 μm size class : G(D,Z) = 0.09. For diameters <1.13 μm, G(D,Z) was calculated for the 0.8 to 0.95 μm size class : G(D,Z)= 300/4140 = 0.07. Further $Z-Z_o$ is 278 m. The resulting k values computed by using eq. (14) are : for diameters >1.13 μm, 4.2×10^{-5} cm. yr^{-1} and for diameters <1.13μm, 3.8×10^{-5} cm. yr^{-1}. A mean value of 4.0×10^{-5} cm/yr is considered. The calculated and observed distribution fit well for diameters between 0.74 and 1.75 μm, with R values close to unity (Table A.VII.2 C; Figure A.VII.2).

FIGURE A.VII.2

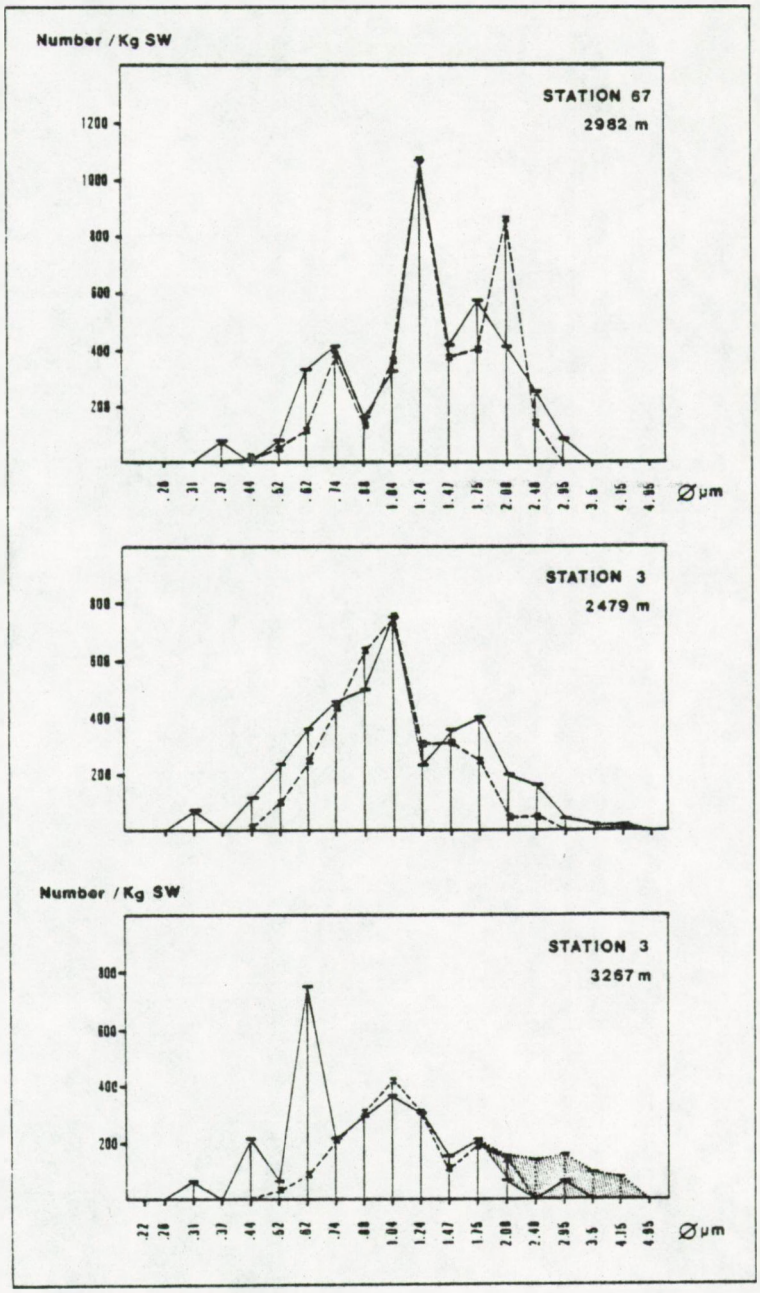

Comparison between observed and calculated barite particle size distributions. Solid line = observed distributions; broken line = calculated distributions (by application of a Stokes settling and dissolution rate model; see text). The hatched area to the right of the "observed" distribution, in the 3267 m sample of St. 3, represents hypothetical large barite particles which should be present in order for barite to account for 100% of the total Ba_p measured by INAA. Diameter values correspond to class midpoints.